

1-1-1994

Investigations of the miscibility, crystallization, melting, and deformation behavior of poly(ether ether ketone)/poly(ether imide) blends/

Hsin-Lung, Chen

University of Massachusetts Amherst

Follow this and additional works at: https://scholarworks.umass.edu/dissertations_1

Recommended Citation

Chen, Hsin-Lung,, "Investigations of the miscibility, crystallization, melting, and deformation behavior of poly(ether ether ketone)/poly(ether imide) blends/" (1994). *Doctoral Dissertations 1896 - February 2014*. 830.
https://scholarworks.umass.edu/dissertations_1/830

This Open Access Dissertation is brought to you for free and open access by ScholarWorks@UMass Amherst. It has been accepted for inclusion in Doctoral Dissertations 1896 - February 2014 by an authorized administrator of ScholarWorks@UMass Amherst. For more information, please contact scholarworks@library.umass.edu.

UMASS/AMHERST



312066011059908

INVESTIGATIONS OF THE MISCIBILITY, CRYSTALLIZATION, MELTING,
AND DEFORMATION BEHAVIOR OF POLY(ETHER ETHER
KETONE)/POLY(ETHER IMIDE) BLENDS

A Dissertation Presented

by

HSIN-LUNG CHEN

Submitted to the Graduate School of the
University of Massachusetts Amherst in partial fulfillment
of the requirements for the degree of

DOCTOR OF PHILOSOPHY

May 1994

Polymer Science and Engineering

© Copyright by Hsin-Lung Chen 1994

All Rights Reserved

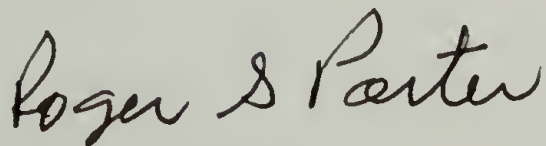
INVESTIGATIONS OF THE MISCIBILITY, CRYSTALLIZATION, MELTING,
AND DEFORMATION BEHAVIOR OF POLY(ETHER ETHER
KETONE)/POLY(ETHER IMIDE) BLENDS

A Dissertation Presented

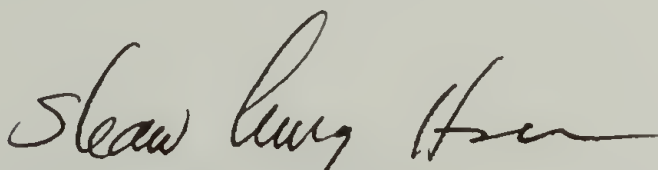
by

HSIN-LUNG CHEN


Approved as to style and content by:



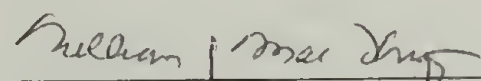
Roger S. Porter, Chairman



Shaw Ling Hsu, Member



James A. Donovan, Member



William J. MacKnight, Department Head
Polymer Science and Engineering

To

My late grandfather, Mr. Chin-Shi D. Chen,
my grandmother and my parents

ACKNOWLEDGMENTS

I am deeply indebted to my advisor, Professor Roger S. Porter. As a teacher, he always encourages his students to explore, and provides freedom for a scientific mind to flourish. He has never hesitated to show his caring and support to his students. I wish to express my deepest appreciation for his endless guidance, patience, support, and encouragement in the past four and half years. I would like to thank Professor Shaw Ling Hsu and Professor James A. Donovan for serving in my committee and for their constant interests and advice on this project.

I would like to thank the members in Prof. Porter's group: Dr. Li Hui Wang for his friendship and comments on this project, Dr. Jeff Kollodge for his assistance in the early stage of preparing this project, Mr. Nobuhiro Shibuya and Dr. Satoshi Osawa for their friendships, and Dr. Y. H. Lee for his help in the solid-state coextrusion experiment. I would like to express a very deep appreciation to my classmate, Yunwa Wilson Cheung, for his friendship and many technical discussions throughout the research of this dissertation. Thanks also go to Mario Perez for providing important references and comments for the infrared spectroscopic study, to John Domian, Norm Page, and Jay Conway for their assistance on the technical problems of the lab equipment, to Eleanor Thorpe for her friendship and helps.

I wish to thank all my classmates for their friendships which brought a fruitful and unforgettable first-year study in PSE. Thanks also go to my other friends in Amherst: Huiyong, Wencui, Yu-Ping, Dr. Ying-Chu Hsu, Weming, Tao, Chao-Cheng, and Mei-Wan. I wish to thank a special friend, Li-Ju, who always brings a lot of happiness. I am also deeply indebted to my family in Taiwan, who has been giving me the strongest support: my grandmother and my parents who always encourage me

with their love; my sisters and brother: Ya-Lin, for writing me so many letters in the past four and half years, Ya-Ping and Fong-Yih, for being such good friends of mine in the family.

Finally I thank Kuan Shi Yin Bodhisattva for blessing me with the strength and perseverance to overcome all the obstacles in research and life.

ABSTRACT

INVESTIGATIONS OF THE MISCIBILITY, CRYSTALLIZATION, MELTING, AND DEFORMATION BEHAVIOR OF POLY(ETHER ETHER KETONE)/POLY(ETHER IMIDE) BLENDS

MAY 1994

HSIN-LUNG CHEN, B.Ch.E., MING-CHI INSTITUTE OF TECHNOLOGY

M.S., UNIVERSITY OF MASSACHUSETTS AMHERST

Ph.D., UNIVERSITY OF MASSACHUSETTS AMHERST

Directed by : Professor Roger S. Porter

This dissertation reports the studies of the blends of poly(ether ether ketone) (PEEK) and poly(ether imide) (PEI). The investigations reported encompass both the thermodynamic and kinetic aspects of this binary blend.

The phase behavior of PEEK/PEI blends in the amorphous states was investigated by differential scanning calorimetry (DSC), density measurement, and Fourier-Transform Infrared (FTIR) spectroscopy. Amorphous PEEK/PEI blends were miscible over the whole composition range. The specific volume measurement and the equilibrium melting point depression analysis showed the existence of favorable interaction between PEEK and PEI. The FTIR study suggested that the oxygen lone-pair electrons of the ether groups in PEEK interact favorably with the electron-deficient imide rings in PEI. The coplanarity of the two nearest imide rings in PEI was changed by blending to accommodate the favorable interaction with PEEK.

The two-stage crystallization behavior of PEEK and PEEK/PEI blends was studied by thermal mechanical analysis (TMA) and DSC. The two crystallization stages of PEEK were first time distinguished clearly by measuring the thickness change of PEEK films during isothermal crystallization. A crystallization kinetics

model considering both primary and secondary crystallization was applied to extract the respective rate constants of the two crystallization stages. The results were discussed in terms of the diffusion mechanisms during PEEK crystallization.

The growth of PEEK spherulites from the pure melt and from the blends with PEI was studied by hot stage optical microscopy. The spherulite growth kinetics was analyzed using a modified Lauritzen-Hoffman theory which considers the diluent effect of PEI. The regime III-II transition was observed for PEEK and PEEK/PEI blends. The side surface free energy, fold surface free energy, and the work of chain folding were calculated, and were discussed in terms of the stiffness and bulkiness of PEEK molecules.

The semicrystalline morphology and the melting behavior of PEEK/PEI blends were studied by optical microscopy and DSC, respectively. The optical micrographs of PEEK spherulites grown from the blends showed that a significant amount of PEI was rejected to the interfibrillar regions of the PEEK spherulites. The melting study indicated that PEEK crystal reorganization on heating was hindered by blending with PEI, and this was attributed to the incorporation of PEI in the PEEK crystalline interlamellar regions.

The amorphous and the crystalline PEEK/PEI blend films were drawn uniaxially by solid-state coextrusion. The glass transition, density, crystallization behavior, and the respective orientations were studied. The T_g s of amorphous PEEK/PEI blends were depressed by drawing. The kinetics of crystallization of drawn PEEK/PEI blends was also reported. The orientation studies by IR dichroism showed that the orientations of both PEEK and PEI were decreased by increasing PEI content in the blends.

TABLE OF CONTENTS

ACKNOWLEDGMENTS	v
ABSTRACT.....	vii
LIST OF TABLES.....	xii
LIST OF FIGURES.....	xiii
CHAPTER	
1. INTRODUCTION	1
1.1 Background	1
1.2 Overview of Dissertation	5
References	9
2. PHASE BEHAVIOR OF PEEK/PEI BLENDS IN THE AMORPHOUS STATE	11
2.1 Introduction	11
2.2 Experimental	13
2.2.1 Materials and Blend Preparation	13
2.2.2 Thermal Analysis	15
2.2.3 Density Measurement	15
2.2.4 FTIR Study.....	16
2.3 Results and Discussion	17
2.3.1 Glass Transition Behavior.....	17
2.3.2 Strength of Intermolecular Interaction Between PEEK and PEI ...	23
2.3.3 Conformational Change and Nature of Specific Interaction	34
2.3.3.1 Blending Effect on the Imide Ring Conformation.....	34
2.3.3.2 Specific Interaction Between PEEK and PEI.....	46
2.4 Conclusions	52
References.....	55
3. TWO-STAGE CRYSTALLIZATION BEHAVIOR OF PEEK AND PEEK/PEI BLENDS	57
3.1 Introduction	57
3.2 Experimental	59
3.2.1 Materials and Sample Preparation	59
3.2.2 Thermal Mechanical Analysis and DSC Measurement	59

3.3 Results and Discussion	61
3.3.1 Two-Stage Crystallization of PEEK.....	61
3.3.2 Two-Stage Crystallization of PEEK in PEEK/PEI Blends	66
3.3.3 Two-Stage Crystallization Kinetics.....	73
3.4 Conclusions	85
References.....	86
4. SPHERULITE GROWTH KINETICS IN PEEK/PEI BLENDS	87
4.1 Introduction	87
4.2 Background	87
4.2.1 General Considerations	87
4.2.2 Crystal Growth Rate and Growth Regimes	90
4.3 Experimental	93
4.4 Results and Discussion	93
4.4.1 Nucleation Density	95
4.4.2 Regimes of Growth	101
4.4.3 Crystal Surface Free Energies.....	103
4.5 Conclusions	110
References.....	112
5. MELTING BEHAVIOR AND MORPHOLOGY OF PEEK AND PEEK/PEI BLENDS	114
5.1 Introduction	114
5.2 Background	115
5.3 Experimental	118
5.3.1 Solution Crystallization of PEEK.....	118
5.3.2 Optical Microscopy Study	119
5.3.3 Thermal Analysis	119
5.4 Results and Discussion	119
5.4.1 Melting Behavior of Solution-Crystallized PEEK	119
5.4.2 Morphology of Semicrystalline PEEK/PEI Blends.....	127
5.4.3 Melting Behavior of PEEK in PEEK/PEI Blends	130
5.5 Conclusions	138
References.....	139
6. UNIAXIAL DEFORMATION OF PEEK/PEI BLENDS BY SOLID-STATE COEXTRUSION	140
6.1 Introduction	140

6.2 Experimental	141
6.2.1 Sample Preparation.....	141
6.2.2 Thermal Analysis	142
6.2.3 Density Measurement	142
6.2.4 Infrared Dichroism	142
6.3 Results and Discussion	143
6.3.1 Uniaxial Draw of Amorphous PEEK/PEI Blends	143
6.3.2 Density Changes of Crystalline Drawn PEEK/PEI Blends.....	151
6.3.3 Crystallization Behavior	161
6.3.4 Orientations of PEEK and PEI in Drawn PEEK/PEI Blends.....	171
6.4 Conclusions	176
References.....	179
7. SUGGESTIONS FOR FUTURE WORK.....	181
APPENDIX: DERIVATION OF THE PEI C=O STRETCHING INTENSITIES BY VALENCE-OPTICAL THEORY	185
BIBLIOGRAPHY	187

LIST OF TABLES

Table

2.1 Elemental analysis of PEEK/PEI blends prepared by solution-blending from dichloroacetic acid.....	14
4.1 K_g , σ_e and work of chain folding q determined from Fig. 4.7	105

LIST OF FIGURES

Figure	
1.1	The chemical structures of PEEK and PEI.....2
1.2	The areas studied in this dissertation.....6
2.1	DSC traces of amorphous PEEK/PEI blends quenched after annealing at 400 °C for 3 mins. Heating rate was 20 °C/min..... 18
2.2	Composition variations of T_g , T_c , and T_m of PEEK/PEI blends after annealing at different conditions. The annealing conditions are indicated in the figure 19
2.3	The glass transition regions of amorphous PEEK/PEI blends quenched after annealing at 400 °C for 3 mins. Heating rate was 20 °C/min..... 21
2.4	Composition variation of the T_g width of amorphous PEEK/PEI blends 22
2.5	Specific volume vs. composition of amorphous PEEK/PEI blends 24
2.6	Melting points of PEEK vs. the crystallization temperature. T_{m1} is the peak temperature of the lower-melting endotherm and T_{m2} is that of the higher melting endotherm 27
2.7	Hoffman-Weeks plot of PEEK/PEI blends 30
2.8	The extrapolated equilibrium M.P. vs. composition plot of PEEK/PEI blends..... 31
2.9	The plot for obtaining the χ of PEEK/PEI blends..... 33
2.10	The FTIR spectra of amorphous PEEK, 50/50 blend, and PEI 35
2.11	The two C=O stretching modes of PEI: (a) in-phase mode (1778 cm^{-1}), and (b) out-of-phase mode (1725 cm^{-1})..... 36
2.12	The C=O bands of PEI in amorphous PEEK/PEI blends 38
2.13	The composition variations of the intensity ratio (R) and the widths at half-height (WHH) of the two PEI C=O bands 39
2.14	The effect of blending on the imide ring vibrations (1380 and 1357 cm^{-1}) of PEI..... 41
2.15	The conformations of the imide rings in PEI. The coplanarity of the two imide rings are determined by the rotational angles ϕ_1 and ϕ_2 43
2.16	The coplanarity variation of the PEI C=O out-of-phase stretching intensity 45

2.17	The C=O stretchings of PEEK in amorphous PEEK/PEI blends	47
2.18	The interaction spectra of PEEK/PEI 75/25 and 50/50 blends along with the spectra of pure PEEK and PEI	49
2.19	The interaction spectra of PEEK/PEI 30/70 blend along with the spectra of pure PEEK and PEI.....	51
2.20	The proposed specific interaction between PEEK and PEI. The oxygen lone-pair electrons of the ether groups in PEEK interact favorably with the electron-deficient imide rings in PEI.....	53
3.1	Schematic plot of the thermal mechanical analyzer for studying the isothermal crystallization of PEEK/PEI blends.....	60
3.2	Direct recorded TMA traces of PEEK during isothermal crystallization at T_c indicated. In the crystallization curves, the primary crystallization is denoted by "P", and the secondary crystallization is denoted by "S"	62
3.3	DSC isothermal crystallization exotherms of PEEK at 163, 165, and 168 °C.....	65
3.4	DSC scans of PEEK/PEI 90/10 blend after crystallization at 270 °C for different times indicated	67
3.5	DSC scans of PEEK/PEI 50/50 blend after crystallization at 270 °C for different times indicated	68
3.6	Direct recorded TMA traces of PEEK/PEI blends during isothermal crystallization at 191 °C	69
3.7	The optical micrographs of PEEK spherulites grown from (a) pure melt and (b) PEEK/PEI 75/25 blend.....	71
3.8	The simulated TMA curves depicting the crystallization of PEEK in the pure melt and in its blends with PEI	72
3.9	Relative degree of crystallinity vs. time plot of PEEK/PEI blends. The composition and the T_c are indicated in the figure. The solid lines are the results obtained by Price model fit. For PEEK at $T_c = 300$ °C, the dash line is the fit by the Avrami equation.....	76
3.10	Variations of k_s with T_c for PEEK/PEI blends in the temperature range between 162 and 225 °C	77
3.11	Variations of k_i with T_c for PEEK/PEI blends in the temperature range between 162 and 225 °C	78
3.12	Variations of k_s with T_c for PEEK/PEI blends in the temperature range between 290 and 310 °C	79

3.13	Variations of k_i with T_c of PEEK/PEI blends in the temperature range between 290 and 310 °C	80
3.14	Overlay plot of logarithmic rate constants vs. T_c of PEEK/PEI blends.....	81
3.15	Schematic descriptions of the two-stage crystallization behavior of PEEK in (a) the pure state, and in (b) the blends with PEI.....	83
4.1	Crystal growth in crystalline/amorphous polymer blends.....	89
4.2	Three regimes of crystal growth.....	92
4.3	The plot for distinguishing the three growth regimes.....	94
4.4	Optical micrographs of PEEK spherulites grown from (a) pure PEEK and (b) PEEK/PEI 75/25 blend at 250 °C.....	96
4.5	Radii of PEEK spherulites vs. time plot for growth rate determination; $T_c = 270$ °C.....	98
4.6	Composition variation of PEEK spherulite growth rate at 270 °C	99
4.7	The modified Lauritzen-Hoffman plot (Eq. (4.7)) for PEEK/PEI blends.....	104
4.8	Logarithmic growth rate vs. the crystallization temperature plot for PEEK/PEI blends. The lines are the results calculated by Eq. (4.5).....	106
4.9	Composition variation of regime III-II transition temperature of PEEK/PEI blends.....	107
5.1	Three possible morphologies for crystalline/amorphous polymer blends: (a) interlamellar segregation, (b) interfibrillar segregation, and (c) interspherulitic segregation.....	117
5.2	The DSC traces of PEEK after a stepwise annealing. The annealing temperatures are indicated in the figure.....	121
5.3	DSC traces of solution-crystallized PEEK and melt-crystallized PEEK at 300 °C.....	122
5.4	The WAXD patterns of (a) melt-crystallized PEEK, and (b) solution-crystallized PEEK.....	123
5.5	Heating rate dependence of the melting onset temperature (T_b), melting peak temperature (T_p), and melting end temperature (T_e) of solution-crystallized PEEK.....	125
5.6	Heating rate dependence of the melting onset temperature (T_b), melting peak temperatures (T_{p1} and T_{p2}), and melting end temperature (T_e) of melt-crystallized PEEK ($T_c = 300$ °C).....	126
5.7	Optical micrographs of PEEK spherulites grown from pure melt and PEEK/PEI blends	129

5.8	The DSC traces of PEEK/PEI blends crystallized at 297 °C for 12 hrs	131
5.9	The DSC traces of PEEK/PEI blends crystallized at 320 °C for 12 hrs	132
5.10	The DSC traces of PEEK crystallized at different temperatures for 12 hrs.....	134
5.11	The DSC traces of PEEK/PEI 75/25 blend crystallized at different temperatures for 12 hrs.....	135
5.12	T_{m1} vs. T_c plot of PEEK/PEI blends.....	136
5.13	T_{m2} vs. T_c plot of PEEK/PEI blends.....	137
6.1	The DSC traces of amorphous PEEK drawn at 125 °C	144
6.2	The DSC traces of amorphous 50/50 blend drawn at 125 °C.....	145
6.3	The variations of T_g with EDR for amorphous PEEK/PEI blends drawn at 125 °C.....	146
6.4	T_g and ΔC_p vs. EDR of amorphous PEEK drawn at 125 °C.....	148
6.5	T_g and ΔC_p vs. EDR of amorphous 50/50 blend drawn at 125 °C	149
6.6	The densities of amorphous PEEK/PEI blends drawn at 125 °C	150
6.7	The DSC traces of amorphous PEEK drawn at 125 °C. The cold crystallization exotherm is not observed at EDR = 4.0, indicating a strain-induced crystallization	152
6.8	The densities of crystalline PEEK drawn at 225 and 125 °C	153
6.9	The densities of crystalline 75/25 blend drawn at 225 and 125 °C.....	155
6.10	The DSC traces of crystalline PEEK drawn at 125 °C	157
6.11	The DSC traces of crystalline PEEK/PEI 75/25 blend drawn at 125 °C	158
6.12	The fractional crystallinity measured by DSC vs. EDR of crystalline PEEK/PEI blends drawn at 125 °C.....	159
6.13	The density of the amorphous phase calculated by the two-phase model for crystalline drawn PEEK/PEI blends; $T_{dr} = 125$ °C	160
6.14	The peak temperature of the cold crystallization exotherm vs. EDR plot of amorphous PEEK/PEI blends drawn at 125 °C.....	162
6.15	Directed recorded TMA traces of the isothermal crystallization of amorphous drawn PEEK (EDR = 2.0, $T_{dr} = 125$ °C). The crystallization temperatures are indicated in the figure.....	163

6.16	The DSC cooling curves of amorphous drawn PEEK after annealing at 370 °C for 5 mins.....	165
6.17	The peak temperature of the crystallization exotherm during cooling vs. EDR of crystalline and amorphous drawn PEEK.....	166
6.18	The DSC cooling curves of amorphous drawn PEEK/PEI 75/25 blend after annealing at 370 °C for 5 mins.....	168
6.19	The peak temperature of the crystallization exotherm during cooling vs. EDR of crystalline and amorphous drawn PEEK/PEI 75/25 blend.....	169
6.20	The peak temperature of the crystallization exotherm during cooling vs. annealing time at 370 °C of undrawn and drawn PEEK.....	170
6.21	Polarized infrared spectra of PEEK drawn from the amorphous state at 125 °C (EDR = 4.0).....	172
6.22	Dichroic ratios of various IR bands of amorphous drawn PEEK vs. EDR.....	173
6.23	The 2426 cm ⁻¹ band of PEEK. It can be seen that this band overlaps weakly with the bands of PEI.....	174
6.24	The 2965 cm ⁻¹ band of PEI. It can be seen that this band overlaps weakly with the bands of PEEK.....	175
6.25	The orientations of PEEK and PEI in amorphous drawn PEEK/PEI blends.....	177

CHAPTER 1

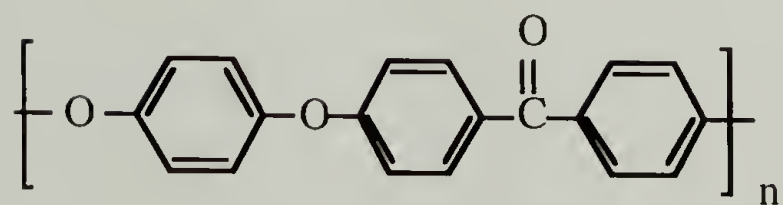
INTRODUCTION

1.1 Background

Due to their wide applications, high temperature polymers have become more commercially and technologically important. Consequently, their studies have been developed rapidly in recent years. These polymers normally have good mechanical properties and can sustain high temperature environment. Poly(ether ether ketone) (PEEK) and poly(ether imide) (PEI) are both members of this polymer family.

PEEK was commercialized by the Imperial Chemical Industries (ICI) under the commercial name of Victrex PEEK. The chemical structure of PEEK is shown in Fig. 1.1. PEEK is semicrystalline with good mechanical properties and solvent resistance. The maximum reported crystallinity of PEEK is about 48%.¹ The normally observed melting temperature of PEEK is 335 to 340 °C.²⁻³ This implies a high temperature performance and high temperature processing (typically 370 to 400 °C).¹ PEEK can be quenched from the melt to an amorphous glassy state without crystals. The T_g of amorphous PEEK is 145 °C.² Because of its excellent properties, PEEK has been specified for injection molded parts for use at high temperature and in aggressive environments. In addition, thermoplastic PEEK is an alternative to the thermosetting resins used as the matrix for fiber composites.⁴ The relatively low T_g is however a disadvantage of PEEK. This results in one order decrease in modulus at temperatures between T_g and T_m which limits the use of PEEK in some applications.

Poly(ether ether ketone) (PEEK)



Poly(ether imide) (PEI)

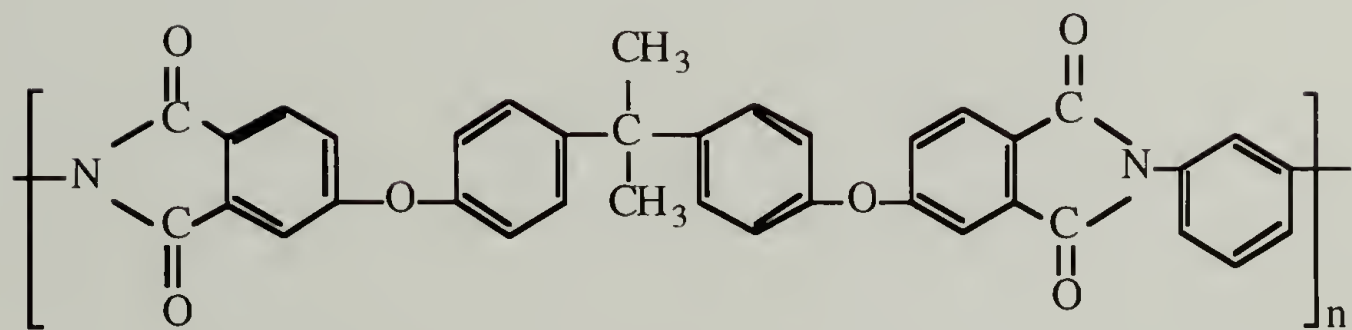


Fig. 1.1 The chemical structures of PEEK and PEI.

Due to the technological importance of PEEK, extensive fundamental research has been carried out over the past decade to establish the structure/property relationship for PEEK. These studies include crystal structures,⁵⁻⁹ crystallization and melting behavior,^{2-3,10-15} crystalline morphology,¹⁶⁻¹⁹ and chemical modifications.²¹⁻²⁴

PEI is a product of General Electric (GE), and is known by the commercial name of Ultem 1000. The chemical structure of PEI is also shown in Fig. 1.1. Unlike the conventional thermosetting polyimides, which are difficult to process, PEI is a linear and amorphous polymer with a high T_g of 215 °C.²⁵ Although PEI has the advantages of good mechanical properties and thermal stability, its use, particularly for aerospace applications, has been limited by the low solvent resistance.²⁵

Although the studies of high performance polymers are quite extensive, the investigations of the blends in this polymer family have just emerged. It is known that blending is a powerful method to tailor polymer properties. Through the control of blend composition and morphology, the desired material properties may be obtained. Blending PEEK with PEI thus appears to be an interesting method to balance the properties of these two polymers. As these two polymers exhibit miscibility in the amorphous phase, the miscibility may be used to increase the T_g of PEEK and improve the solvent resistance of PEI. In addition, the miscibility may affect the crystallization kinetics of PEEK, and hence provides a method to systematically alter PEEK crystallization rate. From the scientific viewpoint, blends of PEEK and PEI offer another binary pair containing one crystallizable component. Due to the aromatic moieties in the backbones, the chains of these two polymers are stiffer than the conventional aliphatic polymers. Therefore, it is of high interest to compare the phase behavior, crystallization phenomena, and morphology of PEEK/PEI blends with that

of the conventional crystalline/amorphous polymer blends such as poly(ethylene oxide) (PEO)/poly(methyl methacrylate) (PMMA).

It is known that the control of properties greatly relies on the understandings of the material behavior at the molecular level. These understandings for polymer blends encompass both the thermodynamic and kinetic aspects, since the interplay of these two determines the morphology and hence the properties of the blends. The thermodynamic aspect includes miscibility window, intermolecular interaction, and crystallization thermodynamics. The kinetic aspect contains the liquid-liquid phase separation kinetics, crystallization kinetics, and diffusion mechanism. The studies of PEEK/PEI blends are still limited.²⁶⁻³¹ The first study of this binary pair was reported in 1988 by Harris and Robeson.²⁶ They found that PEEK and PEI were miscible over the whole composition range in the melt, and the solvent resistance of PEI was improved upon blending with PEEK. In addition, the crystallization rate of PEEK was found to be decreased by blending with PEI.²⁶ Several investigations for this blend have followed including semicrystalline morphology,^{28,30-31} and brief studies on the miscibility and crystallization kinetics^{28,31}. These investigations are however still not sufficient to provide the structure/property relationships for this binary blend. The required knowledge including intermolecular interaction, detailed crystallization behavior and the deformation behavior of this binary blend is still lacking. Further studies are therefore necessary .

This dissertation is devoted to the studies of PEEK/PEI blends. The objective of this dissertation is to lay down the foundation for the structure/property relationship of this miscible binary pair. In addition, it is hoped that the experimental results obtained in this research can contribute to the development of the universal principles for the behavior of crystalline/amorphous polymer blends. The studies reported in this

dissertation include phase behavior, crystallization kinetics, morphology, and uniaxial deformation.

1.2 Overview of Dissertation

Both the thermodynamic and kinetic aspects of PEEK/PEI blends are studied in this dissertation. Fig. 1.2 shows the plot of the glass transition temperature (T_g) and equilibrium melting point (T_m^0) vs. the weight fraction of PEEK in the blend. The studies carried out in this dissertation are based on the different physical states of PEEK/PEI blends prepared by varying the thermal history. Above the T_m^0 of the blends, the amorphous states are obtained, and hence the phase behavior in the amorphous states can be investigated. When the blends are treated at temperatures between T_g and T_m^0 , PEEK may undergo crystallization; therefore, the crystallization kinetics and semicrystalline morphology can be studied. Finally, amorphous and crystalline PEEK/PEI blends may be uniaxially deformed at temperatures below T_g and above T_g , the uniaxial deformation of this binary blend can be studied.

Chapter 2 describes the phase behavior of PEEK/PEI blends in the amorphous state. The main objective of this study is to provide the knowledge of the strength and the nature of interaction that contribute to the miscibility. Previous studies of PEEK/PEI blends were derived from melt blending, since there are few solvent for PEEK.^{26-28,31} To avoid the disadvantages of melting blending such as possible thermal degradation, a solution blending method is used in this study. The glass transition behavior studied by differential scanning calorimetry (DSC) for this solution-blended binary pair is discussed. The specific volume of this binary pair is measured by the density gradient column to provide a glance of the strength of

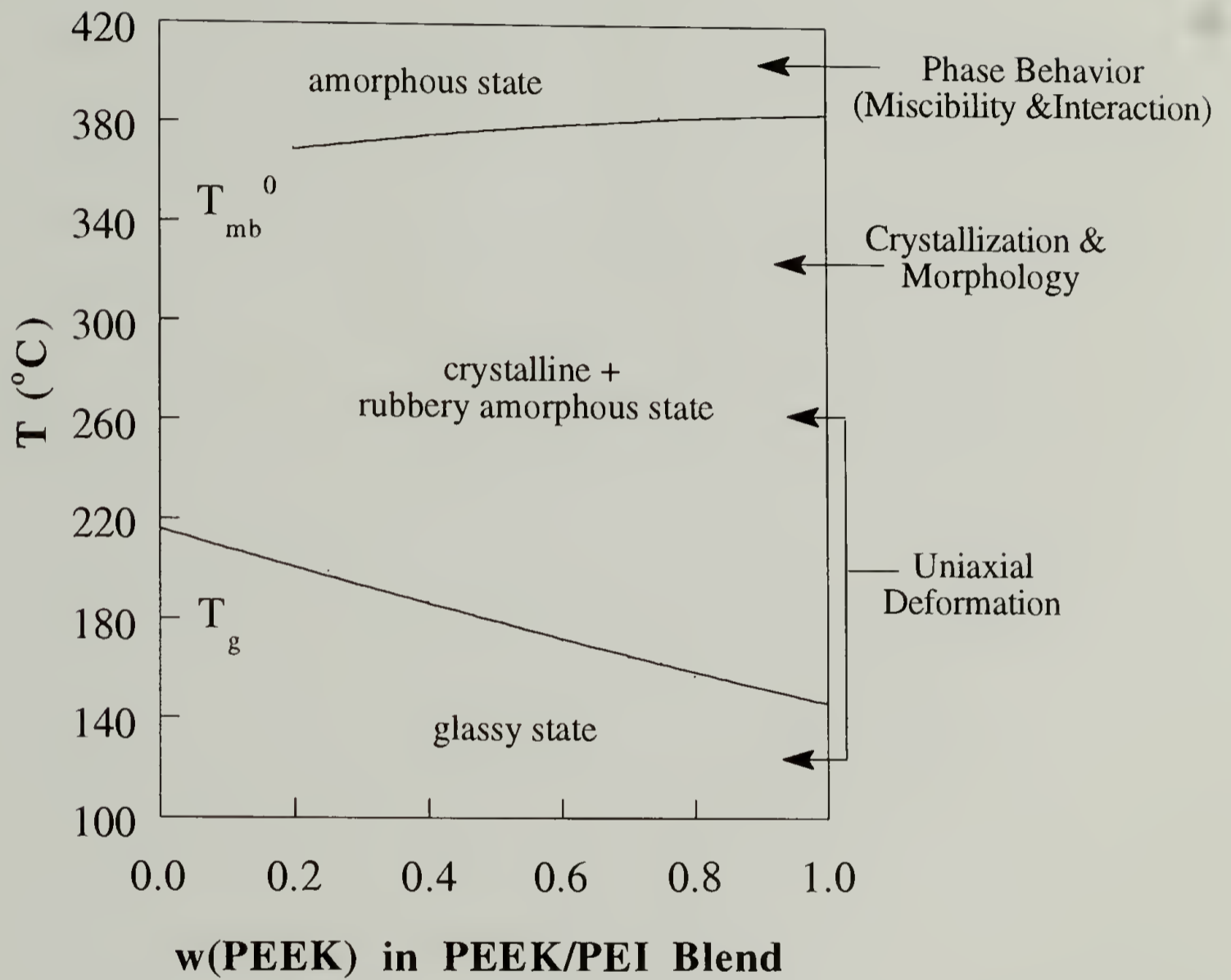


Fig. 1.2 The areas studied in this dissertation.

interaction. The equilibrium melting points of PEEK/PEI blends as extrapolated by the Hoffman-Weeks plot are employed to obtain the interaction parameter (χ) of this binary blend from the melting point depression analysis. The functional groups contributing to the specific interaction between PEEK and PEI are explored by Fourier-Transform Infrared (FTIR) spectroscopy. The effect of PEEK on the conformation of the imide rings in PEI is also discussed.

Although previous morphological studies for PEEK have identified two crystal populations of different thickness, there has been no real-time observation and quantitative study of the kinetics for these two PEEK crystallization stages. In Chapter 3, the crystallization behavior of PEEK and PEEK/PEI blends is described. The two-stage crystallization behavior of PEEK and PEEK/PEI blends is studied by thermal mechanical analysis (TMA) which is equivalent to a one-dimensional dilatometry. The two crystallization stages, which correspond to the formations of the two crystal populations, are clearly distinguished by measuring the variation of film thickness with time during isothermal crystallization. These two stages are however not distinguishable by DSC under comparable conditions. The effect of PEI on the distinction of these two PEEK crystallization stages is also discussed. The kinetic behavior of these two stages is studied by a crystallization kinetics model considering both the primary and the secondary crystallization. The features associated with these two crystallization stages in PEEK and PEEK/PEI blends are discussed.

The crystallization kinetics addressed in Chapter 3 is the macroscopic kinetics. The crystallization rate constants obtained in this study contain the information of both the nucleation rate and the crystal growth rate. The study of the crystal growth kinetics alone is of great interest, because the molecular parameters such as the crystal surface free energies and the work of chain folding can be determined. In Chapter 4,

the studies of PEEK crystal growth from both pure melt and PEEK/PEI blends are reported. The crystal growth rate is monitored by the cross-polarized optical microscopy. The growth rate is then analyzed by a modified Lauritzen-Hoffman theory considering the diluent effect, and the growth regime behavior is discussed. The fold surface free energy and the work of chain folding of PEEK are determined and are compared with that of several semicrystalline polymers of different chain flexibility.

Chapter 5 describes the melting behavior and the semicrystalline morphology of PEEK/PEI blends. In the previous studies on the melting of PEEK, only bulk-crystallized PEEK has been investigated.^{2-3,12} There has been no prior study on the melting behavior of solution-crystallized PEEK. In this chapter, the melting behavior of PEEK crystallized from its solution with dichloroacetic acid is reported and is compared with that of the melt-crystallized PEEK. The morphology of PEEK/PEI blends is observed by the optical microscopy. There is a controversy over the existence of interlamellar incorporation of PEI in the literature.^{28,31} In this chapter, a new method based on the study of PEEK crystal melting is established to resolve the existence of interlamellar incorporation.

There have been extensive studies on the uniaxial deformation of homopolymers, but such studies for polymer blends are rare. No study has been reported on the uniaxially oriented PEEK/PEI blends. In Chapter 6, the studies of uniaxially drawn PEEK/PEI blends are described. Films of amorphous and crystalline PEEK/PEI blends are drawn at 125 °C (which is below T_g) and 225 °C (which is above T_g) by solid-state coextrusion. The glass transition behavior, density, crystallization, and orientations of the drawn blends are reported and discussed.

References

1. Jones, J. P.; Leach, D. C.; Moore, D. R. *Polymer* **1985**, 26, 1385.
2. Blundell, D. J.; Osborn, B. N. *Polymer* **1983**, 24, 953.
3. Lee, Y., Ph.D. Thesis, Univ. of Mass., Amherst, Mass., **1988**.
4. Rose, J. B. *Am. Chem. Soc., Polym. Prepr.* **1986**, 27(1), 480.
5. Dawson, P. C.; Blundell, D. J. *Polymer* **1980**, 21, 577.
6. Hay, J. N.; Langford, J. I.; Lloyd, J. R. *Polymer* **1989**, 30, 489.
7. Hay, J. N.; Kemmish, D. J. *Polymer Commun.* **1989**, 30, 77.
8. Blundell, D. J.; D'Mello, J. *Polymer* **1991**, 32, 304.
9. Blundell, D. J.; Newton, A. B. *Polymer* **1991**, 32, 308.
10. Kumar, S.; Anderson, D. D.; Adams, W. W. *Polymer* **1986**, 27, 329.
11. Cebe, P.; Hong, S.-D. *Polymer* **1986**, 27, 1183.
12. Cheng, S. Z. D.; Cao, M.-Y.; Wunderlich, B. *Macromolecules* **1986**, 19, 1868.
13. Day, M.; Deslandes, Y.; Roovers, J.; Suprunchuk, T. *Polymer* **1991**, 32, 1258.
14. Deslandes, Y.; Sabir, F-N; Roovers, J. *Polymer* **1991**, 32, 1267.
15. Jonas, A.; Legras, R.; Issi, J.-P. *Polymer* **1991**, 32, 3364.
16. Lovinger, A. J.; Davis, D. D. *J. Appl. Phys.* **1985**, 58, 2843.
17. Bassett, D. C.; Olley, R. H.; Al Raheil, I. A. M. *Polymer* **1988**, 29, 1745.
18. Marand, H.; Prasad, A. *Macromolecules* **1992**, 25, 1731.
19. Lovinger, A. J.; Hudson, S. D.; Davis, D. D. *Macromolecules* **1992**, 25, 1752.
20. Jones, D. P.; Leach, D. C.; Moore, D. R. *Polymer* **1985**, 26, 1385.
21. Bishop, M. T.; Karasz, F. E.; Russo, P. S.; Langley, K. H. *Macromolecules* **1985**, 18, 86.
22. Bailly, C.; Williams, D. J.; Karasz, F. E.; MacKnight, W. J. *Polymer* **1987**, 28, 1009.
23. Karcha, R. J., Ph. D. Thesis, Univ. of Mass., Amherst, Mass., **1990**.
24. Franchina, N. L.; McCarthy, T. J. *Macromolecules* **1991**, 24, 3045.

25. Mittal, M. L., *Polyimides*, Vol.1, Plenum Press: New York , **1984**.
26. Harris, J. E.; Robeson, L. M. *J. Appl. Polym. Sci.* **1989**, 35, 1877.
27. Hedrick, J. C.; Arnold, C. A.; Zumbur, M. A.; Ward, Y. C.; McGrath, J. E. *35th Int. SAMPE Symp.* **1990**, 382.
28. Grevecoeur, G.; Groeninckx, G. *Macromolecules* **1991**, 24, 1190.
29. Prasad, A.; Marand, H. *Bull. Amer. Phys. Soc.* **1991**, 36(3), 632.
30. Hudson, S. D.; Davis, D. D.; Lovinger, A. J. *Macromolecules* **1992**, 25, 1759.
31. Hsiao, B. S.; Sauer, B. B. *J. Polym. Sci. Polym. Phys. Ed.* **1993**, 31, 901.

CHAPTER 2

PHASE BEHAVIOR OF PEEK/PEI BLENDS IN THE AMORPHOUS STATE

2.1 Introduction

The miscibility window is an important index for the processing and use of polymer blends. Therefore, phase behavior has been one of the most important studies for polymer blends. Due to the extremely small combinatorial entropy of mixing, the miscibility of two polymers relies almost exclusively on the existence of favorable intermolecular interaction.¹ Thus, extensive efforts have been made to investigate the specific interactions in polymer blends. The strength and the nature of the specific interaction have been the main focuses of these studies.¹

The strength of interaction in polymer blends can be characterized by the Flory-Huggins interaction parameter (χ).¹ There are several methods for measuring χ . These include small-angle neutron scattering (SANS), inverse gas chromatography (IGC), and thermal analysis.¹ Among these techniques, SANS is the most accurate for χ measurement. However, it requires deuterated polymers which are difficult to obtain. Thermal analysis is perhaps the most convenient method for measuring χ . This method is based on the equilibrium melting point (M.P.) depression and can be applied to the crystalline/amorphous blends.² In spite of its large uncertainties,³ the χ determined by the M.P. depression can be used as an approximation for the strength of interaction in polymer blends.

Although the interaction parameter can provide a measure of the magnitude of interaction, it does not give much insight on the nature of specific interactions. The specific interactions in polymer blends include dipole-dipole interaction, hydrogen bonding, etc.¹ The study of the nature of specific interaction in polymer blends is of great importance, since it can help polymer scientists design miscibility among various polymers and compatibilize immiscible polymer blends by introducing specific functional groups. Several spectroscopic techniques such as Infrared (IR) spectroscopy,⁴ Nuclear Magnetic Resonance (NMR) spectroscopy,⁵ and UV-Vis spectroscopy⁶ are useful for exploring the nature of specific interaction in polymer blends.

Although PEEK and PEI have been found to be miscible in the melt,⁷⁻⁹ the magnitude of intermolecular interaction and the nature of the specific interaction have not been explored. In addition, previous studies of this binary blend were based on the samples prepared by the melt blending in extruders.⁷⁻⁹ This method normally requires large sample amount, and thermally and mechanically induced degradation may occur.¹ Solution blending is normally more preferred since it can avoid these problems and can also provide better segmental mixing. Therefore, it is the first priority of this study to seek a solvent that can blend PEEK and PEI without introducing any chemical reaction. In this chapter, the studies of the phase behavior of solution-blended PEEK/PEI blends are reported. The glass transition behavior of amorphous PEEK/PEI blends is discussed. The strength of intermolecular interaction is evaluated by obtaining the interaction parameter from the equilibrium M.P. depression. The functional groups contributing to the specific interaction between PEEK and PEI are explored by the Fourier-Transform Infrared (FTIR) spectroscopy. The effect of blending on the conformation of PEI is also discussed.

2.2 Experimental

2.2.1 Materials and Blend Preparation

PEEK powder was acquired from Imperial Chemical Industries (ICI), Wilton, U.K. The molecular weights are $M_n = 16,800$, $M_w = 39,800$. PEI, was obtained from General Electric (GE, Ultem 1000). The molecular weights are $M_n = 12,000$, $M_w = 30,000$.

Blends of PEEK and PEI were prepared by solution-precipitation from dichloroacetic acid (boiling point = 194 °C). The concentration of polymers in the solvent was 4% (w/v). The mixtures were heated with stirring to 150 °C and were held at this temperature until homogeneous solutions were observed. After cooling to room temperature, the solutions were poured into a ten-fold excess volume of methanol and water mixture (50/50 (v/v)). The precipitates were filtered, washed with a large amount of water, and then dried in a vacuum oven at 95 °C to constant weight. The compositions of the resulting blends were determined by elemental analysis (performed by the Microanalysis Lab. at Univ. of Mass. at Amherst). The results of elemental analysis are shown in Table 2.1. It can be seen that the analyses agree well with the calculated values and the analyses of the as-received samples. In addition, it will be shown in 2.3.3 that the infrared spectra of the solution-recovered PEEK and PEI agree with that reported in the literature.¹⁰⁻¹¹ Therefore, it was concluded that no reaction took place during the blend preparation.

Table 2.1 Elemental analysis of PEEK/PEI blends prepared by solution-blending from dichloroacetic acid.

Sample	C(wt%)		H(wt%)		N(wt%)		Cl(wt%)
	Ana.	Cal.	Ana.	Cal.	Ana.	Cal.	Ana.
PEEK(a)	78.89	79.10	4.16	4.17	<0.1	0.00	<0.1
PEI (a)	74.09	75.00	4.20	4.00	4.72	4.73	<0.1
PEEK(s)	78.48	79.10	4.59	4.17	<0.1	0.00	0.29
PEI (s)	74.24	75.00	4.29	4.00	4.69	4.73	0.70
PEEK/PEI(s)							
75/25	77.82	78.07	4.08	4.13	1.14	1.18	<0.1
50/50	76.53	77.05	4.20	4.09	2.34	2.37	0.57
25/75	75.31	76.03	3.98	4.04	3.51	3.55	1.26

(a): as-received sample

(s): solution-recovered sample

2.2.2 Thermal Analysis

The T_g s of PEEK and PEEK/PEI blends were investigated as a function of melt annealing conditions. T_g s of the blends of PEEK and PEI were determined by a Perkin-Elmer DSC4. The blend powder was first heated at 100 °C/min to a melt annealing temperature. Three annealing temperatures were investigated: 370, 400 and 450 °C. After isothermal annealing for different times at each of these temperatures, the samples were quenched into liquid nitrogen to obtain the amorphous glassy states. The T_g s were then determined by DSC scans at a heating rate of 20 °C/min. T_g was taken as the midpoint of the heat capacity increment. The reported DSC thermograms were normalized to 1 mg of sample.

The interaction parameter of PEEK/PEI blends was evaluated by the equilibrium M.P. depression. The equilibrium M.P. of the blends were obtained by the Hoffman-Weeks plot. The blend was heated at 100 °C/min to 400 °C and was annealed for 3 mins at this temperature. The sample was subsequently cooled at ~ 200 °C/min to the desired crystallization temperature (T_c) and was crystallized for 12 hrs. After this crystallization, the sample was quickly quenched into liquid nitrogen. The crystalline PEEK/PEI blends were then scanned in the Perkin-Elmer DSC4 at 20 °C/min to determine the melting point of the PEEK crystals. The peak temperatures of the melting endotherms were taken as the melting points of PEEK crystals formed at T_c .

2.2.3 Density Measurement

Fully amorphous films of PEEK and PEEK/PEI blends for density measurement were prepared by compression molding at 400 °C for 3 mins under vacuum followed

by quenching in cold water. Densities of these blend films were measured by a density gradient column at 23 °C. Calcium nitrate aqueous solution was used to establish the density gradient ranging from 1.2400 to 1.4000 g/cm³. The sensitivity of the column was about 0.0001 g/cm³. The amorphous PEEK film used in this study exhibited a density of 1.2639 ± 0.0005 g/cm³ at 23°C, in agreement with the reported value.¹²

2.2.4 FTIR study

The thin films of amorphous PEEK/PEI blends for the FTIR studies were prepared by solution casting. PEEK and PEI homopolymers of different weight fractions were dissolved in dichloroacetic acid at 150 °C and the solution concentration was 1(w/v)%. The solution was then casted onto an aluminum foil on a Thomas Model 40 Micro hot stage at 400 °C. At this temperature, the dichloroacetic acid evaporated very quickly. The remaining blend film on the aluminum foil surface was annealed at 400 °C for 2 mins followed by quenching into cold water to obtain the amorphous state. The aluminum foil was then removed by etching with 5% NaOH aqueous solution at room temperature. Finally, the obtained blend films were washed with water and then dried in vacuo at 60 °C for 12 hrs. The IR spectra of the resulting blend samples were recorded in an IBM IR/32 Infrared spectrometer. The resolution was 2 cm⁻¹ after computer-averaging a total of 256 scans. The IR spectra of all solution-casted films showed no -OH absorption near 3500 cm⁻¹, indicating nearly complete removal of the solvent .

2.3 Results and Discussion

2.3.1 Glass Transition Behavior

The glass transitions of the solution-blended amorphous PEEK/PEI blends have been studied. Figure 2.1 shows the DSC scans of PEEK/PEI blends quenched from the melt after annealing at 400 °C for 3 mins. A single T_g is observed over the whole composition range, indicating the miscibility between PEEK and PEI at 400 °C. In addition, the cold crystallization exotherm, signifying the crystallization of PEEK from the blend upon heating, moves to higher temperature as the PEI content in the blend is increased. For the blends with PEEK wt% < 50%, the cold crystallization exotherm is not observed, indicating that PEEK is unable to crystallize from the miscible amorphous matrix in this composition range at the heating rate of 20 °C/min. This shows that PEEK crystallization is hindered by PEI, which is also an indication of segmental miscibility between these two polymers. The melt annealing conditions before quench may somewhat affect the crystallization and the T_g behavior of the blends. The effect of the melt-annealing condition on the crystallization behavior of PEEK has been investigated.¹² Figure 2.2 shows the composition variations of T_g s, cold crystallization peak temperature during heating (T_c), and the observed melting peak temperature (T_m) for the samples quenched after annealing at different conditions. It is seen that T_g , T_c , and T_m do not vary notably with the melt-annealing temperature (from 370 to 450 °C) and the annealing time (from 3 to 30 mins). Even though 370 °C is below the equilibrium melting point of PEEK, a homogeneous miscible melt can still be readily formed at this temperature.

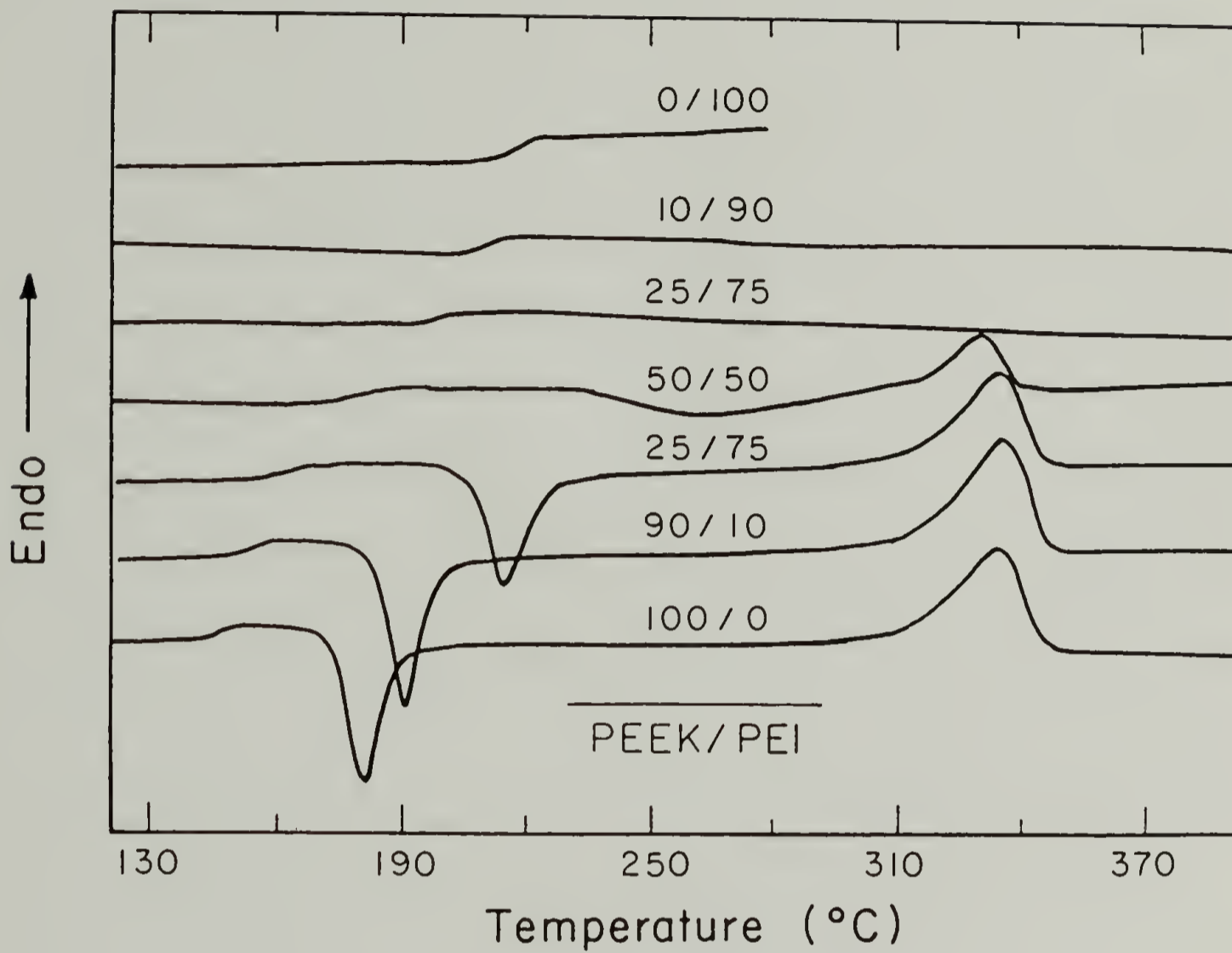


Fig. 2.1 DSC traces of amorphous PEEK/PEI blends quenched after annealing at 400 °C for 3 mins. Heating rate was 20 °C/min.

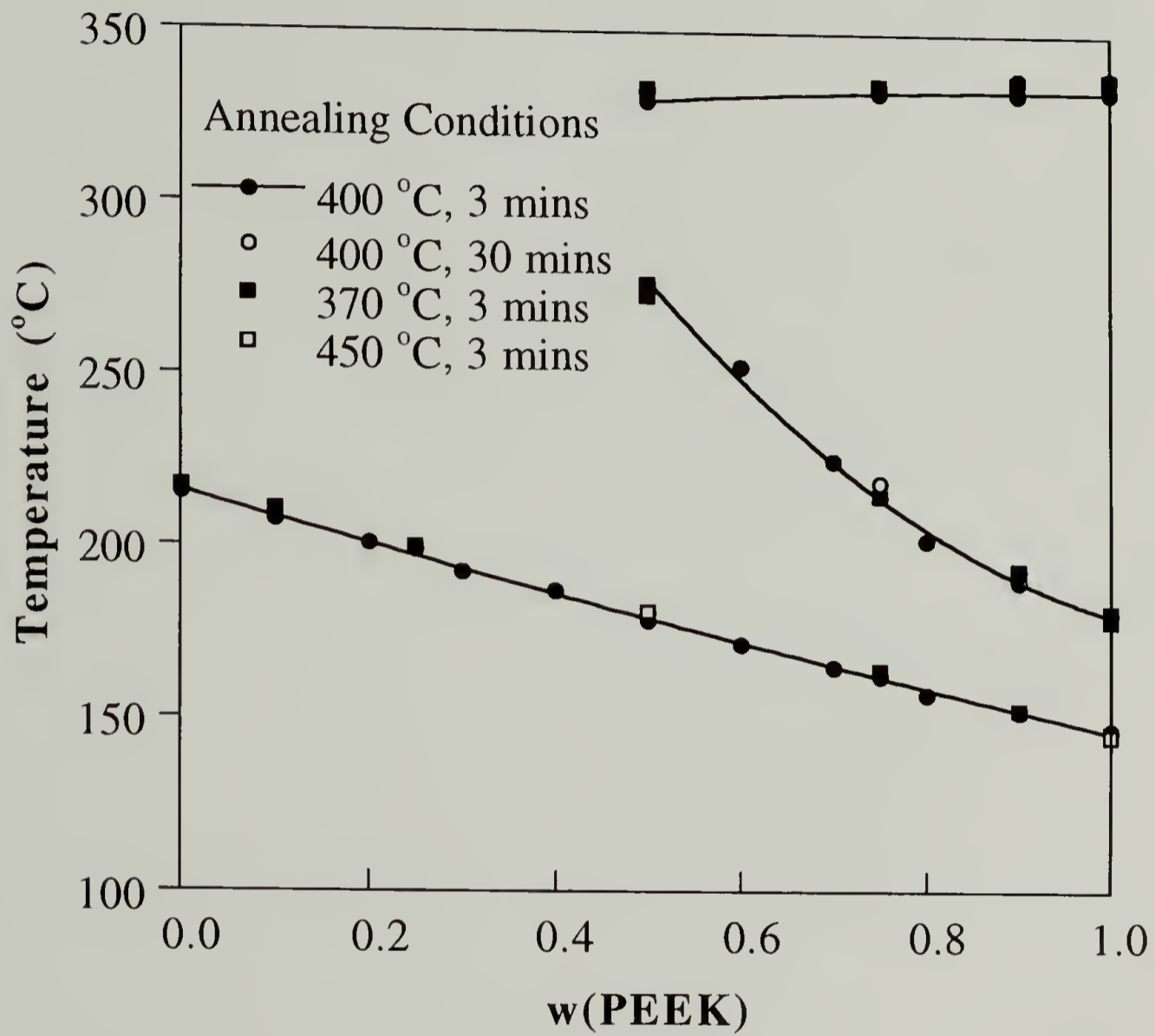


Fig. 2.2 Composition variations of T_g , T_c , and T_m of PEEK/PEI blends after annealing at different conditions. The annealing conditions are indicated in the figure.

The composition variation of T_g shown in Fig. 2.2 can be described satisfactorily by the simple Fox equation:¹³

$$\frac{1}{T_g} = \frac{w_1}{T_{g1}} + \frac{w_2}{T_{g2}} \quad (2.1)$$

or by the Gordon-Taylor equation:¹⁴

$$T_g = \frac{w_1 T_{g1} + k w_2 T_{g2}}{w_1 + k w_2} \quad (2.2)$$

with $k = 0.86$. This is in agreement with that found for the melt-blended blends.⁷ It is generally believed that if the T_g behavior of a blend can be described well by Eq. (2.1) and (2.2), the interaction between the components is not strong.¹³ Therefore, this may imply that the interaction between PEEK and PEI is not strong. The intermolecular interactions of the blends of sulfonated PEEK (SPEEK) and PEI have been studied.⁶ The composition variation of T_g of this binary pair deviates positively from that predicted by Eq. (2.1) and (2.2). The UV-Vis spectra of this binary pair have suggested an electron-donor interaction between the rings possessing electrophilic substituents in the SPEEK and the diamine aromatic moieties in the PEI. Such strong intermolecular interaction may not be present in PEEK/PEI blends judged from the difference in the T_g behavior between this binary pair and SPEEK/PEI blends.

It is also of interest to examine the width of the glass transition as a function of blend composition. The DSC thermograms of the glass transition of amorphous PEEK/PEI blends are shown in Fig. 2.3. It can be seen that T_g widths of the blends are broader than that of pure PEEK and PEI. The T_g width is plotted against the blend

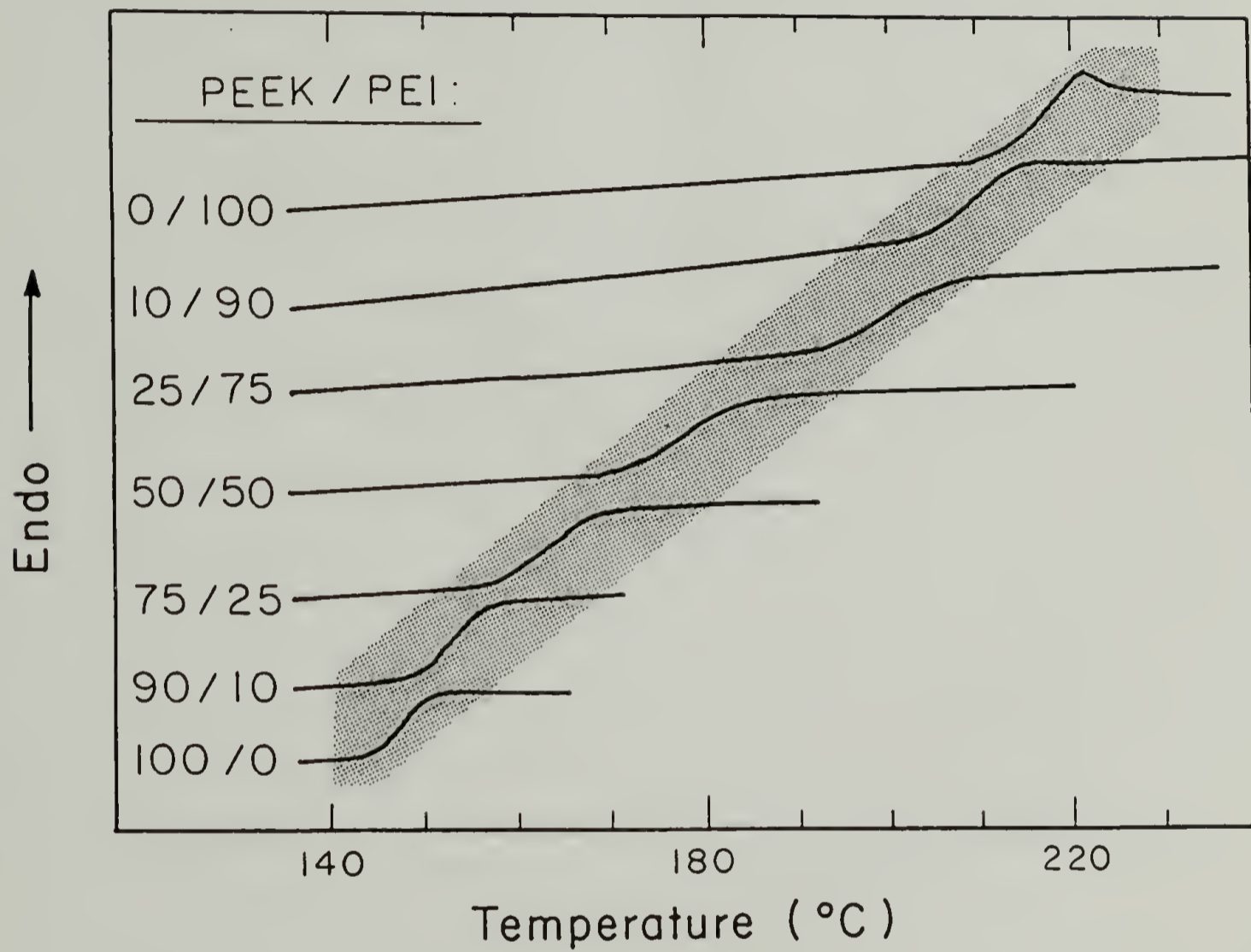


Fig. 2.3 The glass transition regions of amorphous PEEK/PEI blends quenched after annealing at 400 °C for 3 mins. Heating rate was 20 °C/min.

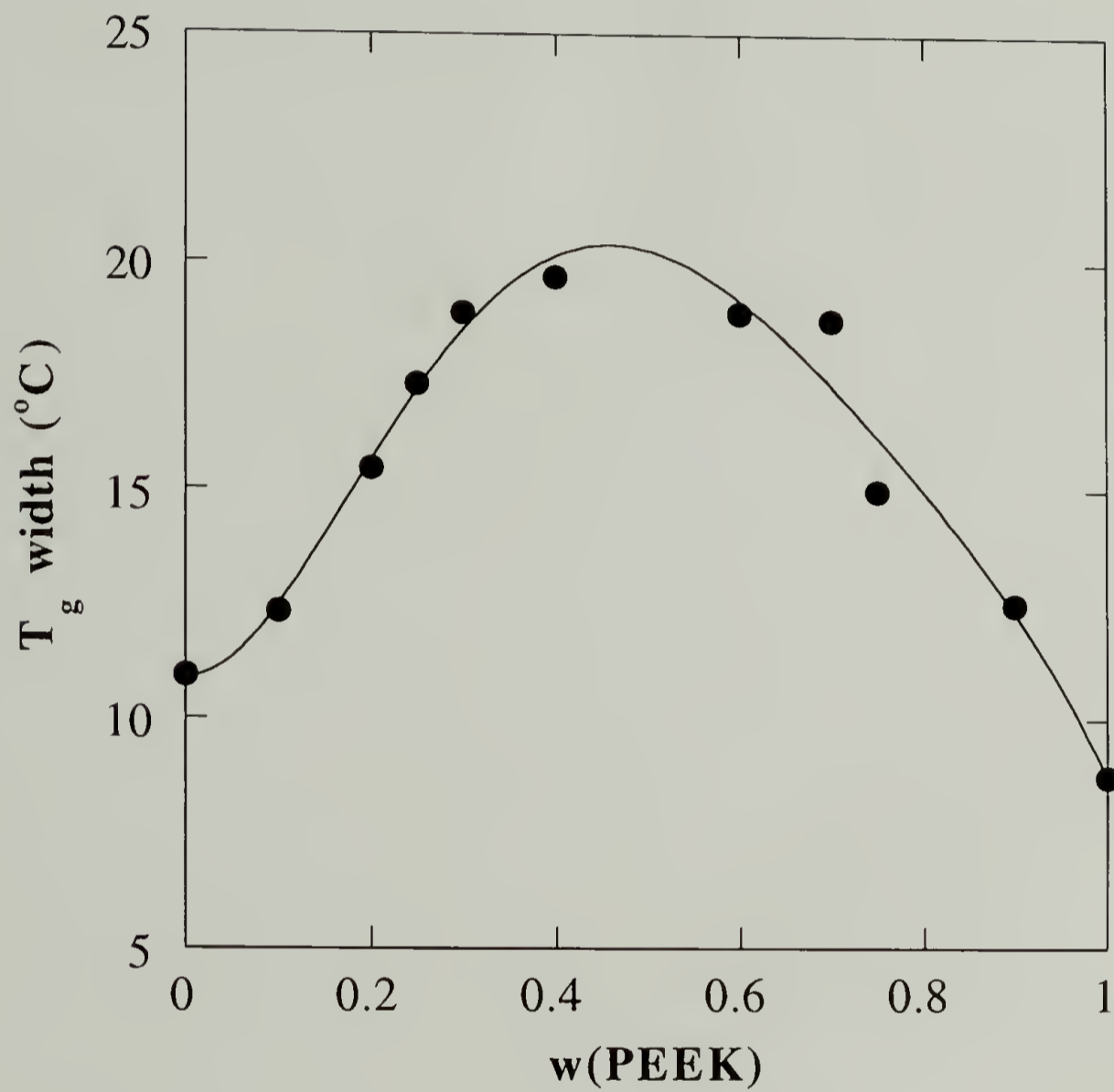


Fig. 2.4 Composition variation of the T_g width of amorphous PEEK/PEI blends.

composition in Fig. 2.4. It can be seen that the T_g width reaches maximum at ca. 50 wt% PEI. The T_g width broadening of this composition is about 10°C. The T_g broadenings have also been observed for binary blends of poly(vinyl chloride) (PVC)/poly(α -methyl- α -n-propyl- β -propiolactone) (MPPL),¹⁵ poly(methyl methacrylate) (PMMA)/PVC,⁵ and poly(styrene phosphonate ester)/cellulose acetate.¹⁶ Such broadening has been interpreted as an indicative of local composition fluctuation or the presence of microheterogeneity.¹⁷⁻¹⁸ However, these explanations are qualitative and have not been rigorously confirmed. It is possible that such broadening is just due to the increase in the width of the relaxation spectrum (a kinetic argument) rather than the presence of heterogeneity in the blends (a thermodynamic argument).

2.3.2 Strength of Intermolecular Interaction Between PEEK and PEI

The T_g behavior of PEEK/PEI blends indicated that the intermolecular interaction in this binary pair may not be strong. However, this does not preclude the presence of favorable interaction between PEEK and PEI. To gain further insight in the intermolecular interaction, the densities of amorphous PEEK/PEI blends are determined. This measurement is able to provide a glance on the intermolecular packing (which is related to the strength of interaction) between PEEK and PEI. The measured specific volume (inverse of the density) of amorphous PEEK/PEI blends is plotted against the blend composition in Figure 2.5. It can be seen that the specific volume of the blends shows a slight negative deviation from the linear additivity. This shows that the intermolecular packing between PEEK and PEI is closer than that in the ideal solution. Therefore, a favorable intermolecular interaction is present in PEEK/PEI blends.

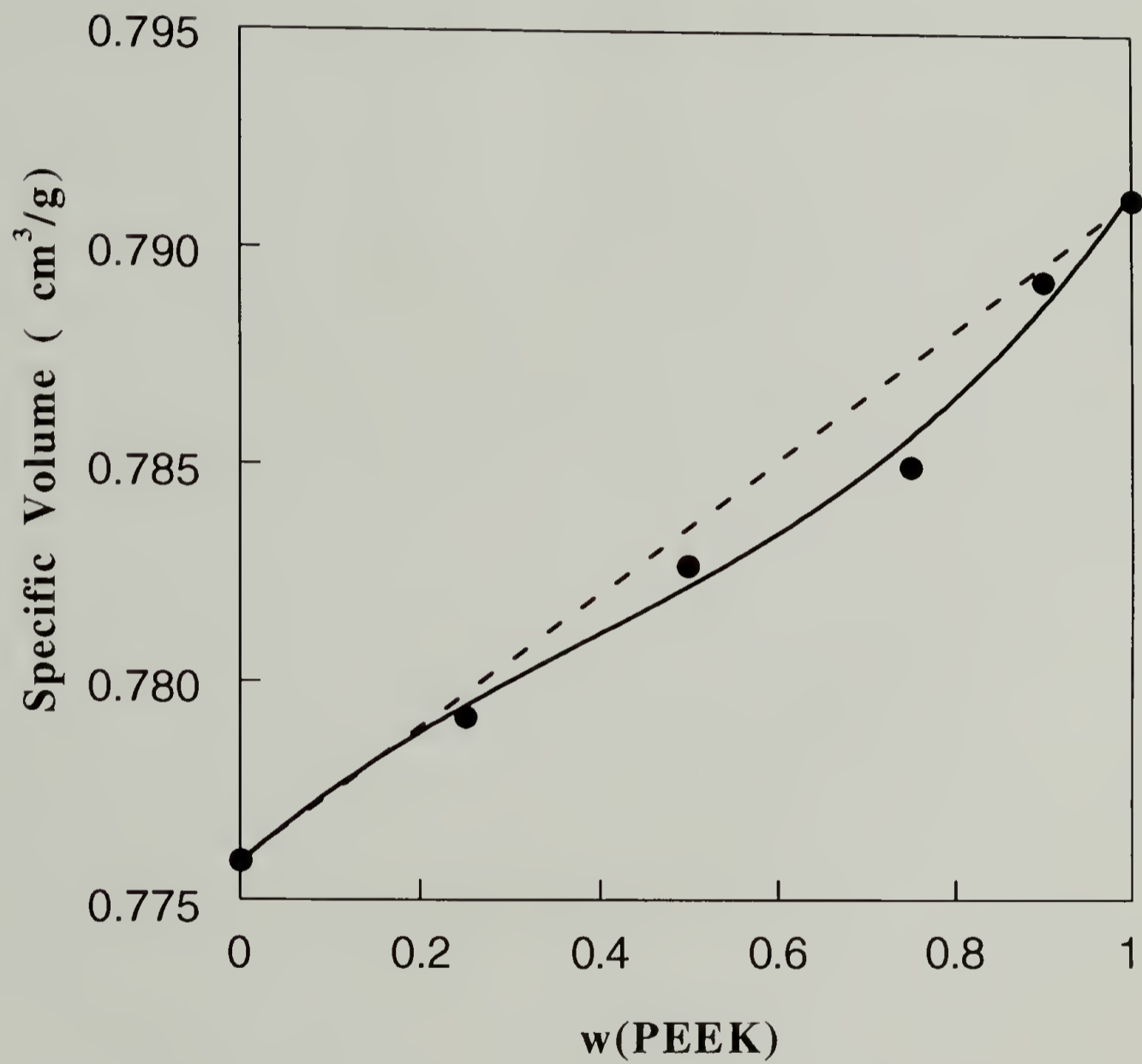


Fig. 2.5 Specific volume vs. composition of amorphous PEEK/PEI blends.

The equilibrium M.P. depression analysis is employed to obtain χ for PEEK/PEI blends. The equilibrium M.P. is defined as the melting point of the infinitely thick crystals.¹⁹ It is known that the polymer crystals are metastable and the M.P. of which depends on the prior crystallization history. Therefore, extrapolation is the only way to obtain the equilibrium M.P. of polymer crystals. There are several extrapolation methods for obtaining the equilibrium M.P. The most convenient and perhaps the most widely used method is the Hoffman-Weeks plot.¹⁹ This plot is based on the following equation:

$$T_m = T_m^0 \left(1 - \frac{1}{\gamma} \right) + \frac{T_c}{\gamma} \quad (2.3)$$

where T_m is the observed M.P., T_m^0 is the equilibrium M.P., and γ is the lamellar thickening factor signifying the ratio of final lamellar thickness to the critical lamellar thickness. From Eq. (2.3), T_m^0 is obtained by the intersection of T_m vs. T_c line with $T_m = T_c$ line.

The determination of the equilibrium M.P. by Eq. (2.3) for PEEK is further complicated by its double melting behavior. It is known that isothermally crystallized PEEK exhibits two melting endotherms.^{12, 20-21} These two endotherms have been ascribed to the meltings of two crystal populations of different thickness. One question should thus be answered before the use of Hoffman-Weeks plot to extrapolate T_m^0 for PEEK and PEEK/PEI blends; namely, "which melting point should be used for this extrapolation?". Although several values of the equilibrium M.P. have been reported for PEEK,^{12,20} these were obtained without considering the complications arising from the inhomogeneous morphology of PEEK. It is therefore necessary to redetermine the equilibrium M.P. by including this inhomogeneous morphology in the analysis.

Fig. 2.6 shows the T_m vs. T_c plot of PEEK. This plot has been reported previously by Lee and Porter,¹² who studied the as-received PEEK powders. PEEK powders used in this study have been recovered from the solvent to remove residual catalysts and impurities remained after polymerization. When the peak temperature of the first melting endotherm (T_{m1}) is used to extrapolate T_m^0 , an unreasonable negative value of T_m^0 is obtained. This can be ascribed to two complications. The first is associated with the nature of the morphology of PEEK. Since the lower-melting crystals are located in a region between the higher-melting crystals. Upon melting of the lower-melting crystals, the melted PEEK molecules are actually confined in a restricted environment, which as a result have a lower entropy compared to the amorphous PEEK molecules in the bulk. As a consequence, a reduction in the entropy of melting leading to an increase in the observed melting point is expected. The observed T_{m1} thus can not be used as the true melting point of the crystals. The second complication is associated with the possible error in the method of thermal analysis. The observed value of T_{m1} might be shifted due to the occurrence of recrystallization after melting of the lower-melting crystals. A melting model which accounts for the recrystallization after initial melting has been proposed by Rim and Runt,²² and by Lee and Porter.¹² The subsequent recrystallization after melting gives rise to a negative exotherm which overlaps with the melting endotherm corresponding to the melting of the initial crystals. The position of the endothermic maximum, which is taken as T_{m1} , can be shifted depending upon the magnitude and position of the recrystallization exotherm. Therefore, the observed T_{m1} may not be the melting point of the lower-melting crystals. From this discussion, it is concluded that T_{m1} cannot be used for T_m^0 extrapolation.

When T_{m2} is used for the extrapolation, the long extrapolation gives $T_m^0 = 384$ °C, somewhat lower than the 389 °C obtained by Lee and Porter.¹² The imprecision

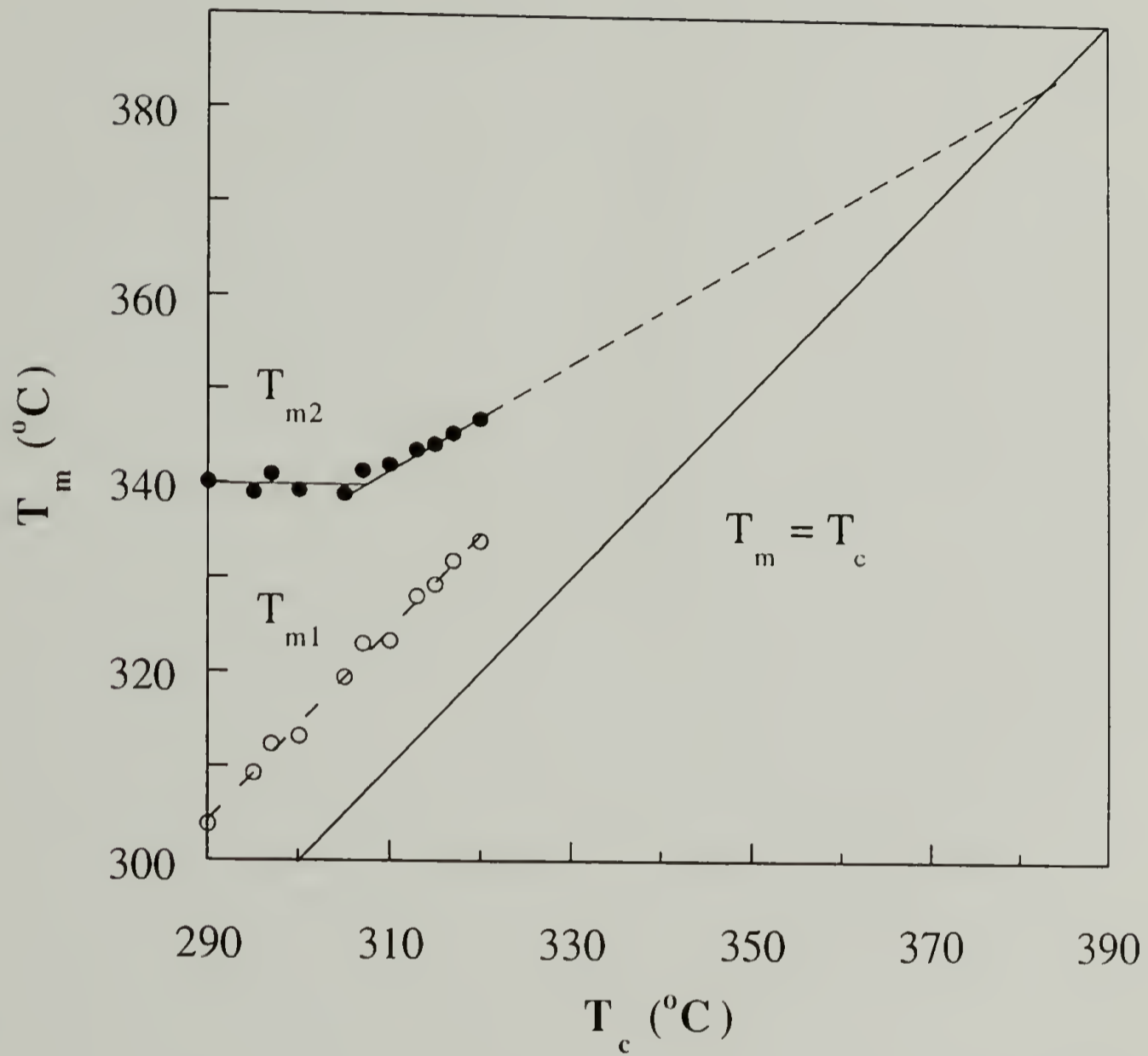


Fig. 2.6 Melting points of PEEK vs. the crystallization temperature. T_{m1} is the peak temperature of the lower-melting endotherm and T_{m2} is that of the higher melting endotherm.

arising from the long extrapolation in the Hoffman-Weeks plot of PEEK can likely account for this difference in T_m^0 . Attempt was made to crystallize PEEK at T_c higher than 330 °C to shorten the extrapolation distance; however, PEEK did not crystallize to its ultimate crystallinity for 12 hrs (as manifested by a cold crystallization exotherm in the subsequent DSC scan).

A major uncertainty in Hoffman-Weeks extrapolation arises from the possibility of crystal reorganization or recrystallization upon heating for melting point measurement.¹⁹ These processes thicken the initial crystals and hence the observed melting point does not correspond to that of the initial crystals. The slope of Hoffman-Weeks plot is given by the inverse of the lamellar thickening factor, namely, $1/\gamma$, as shown in Eq. (2.3). In the theory it was assumed that γ is independent of T_c and hence T_m vs. T_c plot is a straight line.¹⁹ If crystal reorganization or recrystallization takes place, the value of γ will increase and hence a decrease in slope will be observed in the Hoffman-Weeks plot. Therefore, in Fig. 2.6 the $T_c < 305$ °C region in which T_{m2} is approximately independent of T_c is an indication of the occurrence of crystal reorganization on heating. However, the $T_c > 305$ °C region in which T_{m2} increases linearly with T_c indicates that Hoffman-Weeks theory holds well and crystal reorganization is not important in this T_c region. Indeed, the study of the heating rate dependence of PEEK melting point has been reported.¹² For a lower T_c of 220 °C, T_{m2} was found to decrease with increasing heating rate, which clearly indicated the reorganization upon heating of crystals formed at this T_c . For higher T_c s of 318.6 and 322.8 °C, T_{m2} was independent of heating rate, which indicated that crystal reorganization did not occur during heating. These observations agree with the two distinct regions observed in Fig. 2.6. Therefore, although the extrapolation distance of T_m^0 shown in Fig. 2.6 is large, crystal reorganization does not affect the

measured melting point in the extrapolation region, and hence the extrapolation shown in Fig.2.6 is meaningful from the physical basis of Hoffman-Weeks equation.

Crystal reorganization on heating giving rise to constant melting point with increasing T_c has also been observed for other melt-crystallized polymers such as polyethylene.²³ The poorer crystals formed at lower T_c reorganize extensively on heating and lead to an almost constant T_m with changing T_c .

From the above discussions, it is shown that the T_m^0 of PEEK should be obtained from the extrapolation by T_{m2} . The T_m^0 s of PEEK/PEI blends are thus also extrapolated by T_{m2} , as shown in Fig. 2.7. The extrapolated equilibrium M.P.s of the blends (T_{mb}^0) are plotted against the composition in Fig. 2.8.

The relation between the equilibrium M.P. depression and χ is given by²

$$\frac{1}{T_{mb}^0} = \frac{1}{T_m^0} - \frac{R}{\Delta h_f^0 V_{1u}} \left[\frac{\ln \phi_2}{N_2} + \left(\frac{1}{N_2} - \frac{1}{N_1} \right) \phi_1 + \chi (T_{mb}^0) \phi_1^2 \right] \quad (2.4)$$

where N_1 and N_2 are the degree of polymerization of the amorphous and crystalline component, respectively. χ is given by

$$\chi = \frac{BV_{1u}}{RT} \quad (2.5)$$

where B is the interaction density. Substituting Eq. (2.5) into (2.4) we have

$$-\left\{ \frac{\Delta h_f^0 V_{1u}}{R} \left(1 - \frac{T_{mb}^0}{T_m^0} \right) + T_{mb}^0 \left[\frac{\ln(1 - \phi_1)}{N_2} + \left(\frac{1}{N_2} - \frac{1}{N_1} \right) \phi_1 \right] \right\} = \frac{BV_{1u}}{R} \phi_1^2 \quad (2.6)$$

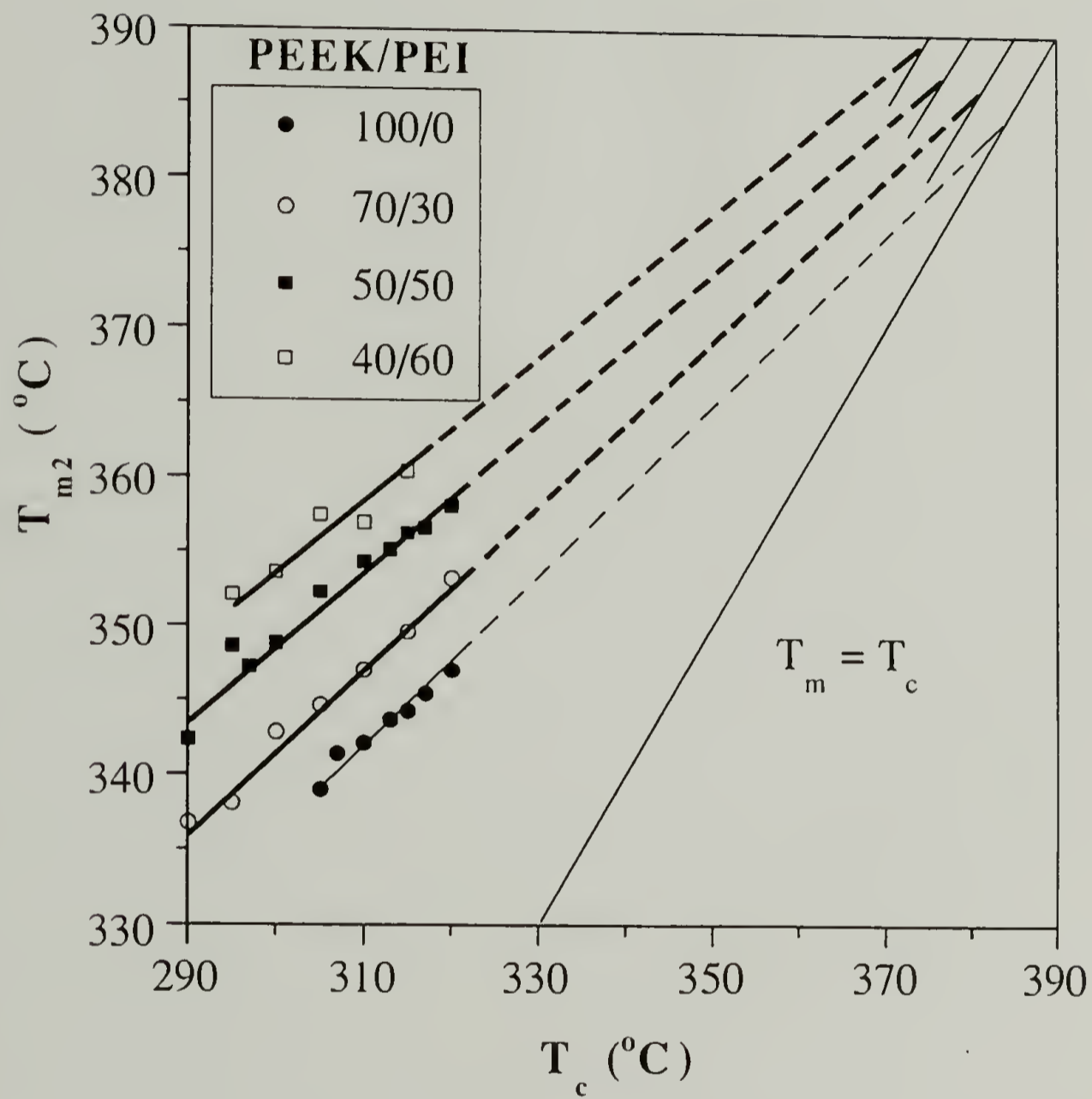


Fig. 2.7 Hoffman-Weeks plot of PEEK/PEI blends. The data are displaced by 5 $^{\circ}\text{C}$ to be able to discern the different compositions.

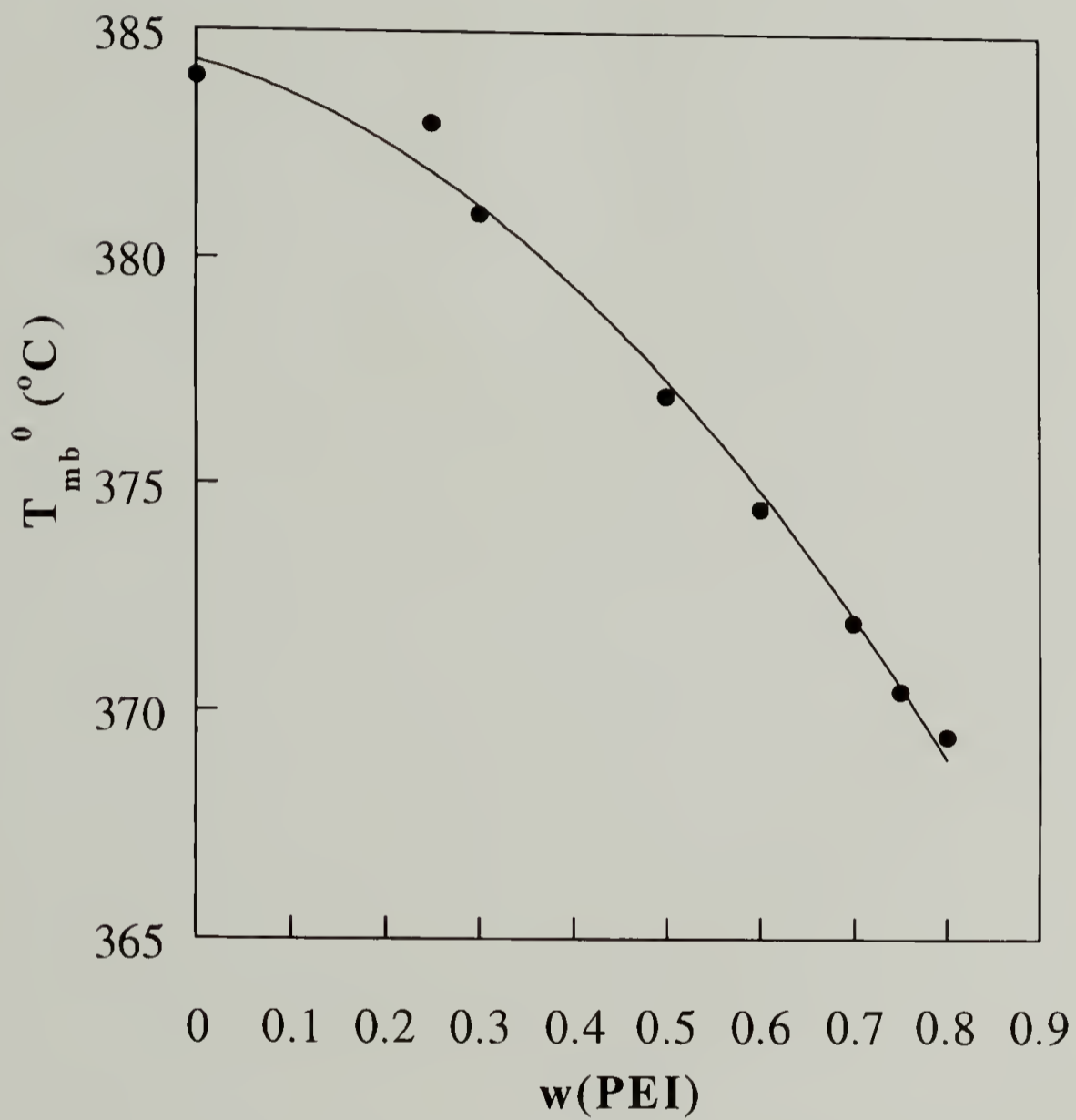


Fig. 2.8 The extrapolated equilibrium M.P. vs. composition plot of PEEK/PEI blends.

B can thus be obtained by plotting the left-side terms of Eq. (2.6) against ϕ_1^2 . χ at temperature T can then be calculated by Eq. (2.5). The parameters of PEEK/PEI blends required for χ determination by Eq. (2.6) are : $\Delta h_f^0 = 39.27 \text{ cal/cm}^3$,²⁰ $V_{1u} = 459.31 \text{ cm}^3/\text{mol}$, $V_{2u} = 227.87 \text{ cm}^3/\text{mol}$ (obtained from the density measurement). Fig. 2.9 shows the plot of Eq. (2.6). This plot gives $B = -1.2 \text{ cal/cm}^3$. Therefore, the calculated χ at 400 °C is -0.4.

Negative χ for PEEK/PEI blends confirms the miscibility between PEEK and PEI in the melt, and is consistent with the specific volume result in Fig. 2.5. Normally, for polymer blends with weak interaction, χ is larger than -0.1. For PEEK/PEI blends, $\chi = -0.4$ seems to imply pretty strong interaction between PEEK and PEI. Nevertheless, it has to be noted that χ determined by the equilibrium M.P. depression is subject to larger error than other methods such as SANS. Koningsveld has shown that even if the error of the extrapolated equilibrium M.P. is only $\pm 0.5 \text{ }^\circ\text{C}$, the χ obtained by the equilibrium M.P. depression is not able to distinguish between three essentially different thermodynamic phase behavior of the melt : (a) complete miscibility, (b) partial miscibility with a UCST, and (c) a stable LCST miscibility gap with a UCST one.³ In addition, the melting behavior of semicrystalline polymers is sometimes very complicated, which may consequently lead to large error in T_m^0 extrapolation. However, the χ determined from the M.P. depression can serve as the first approximation for the strength of interaction in polymer blends.

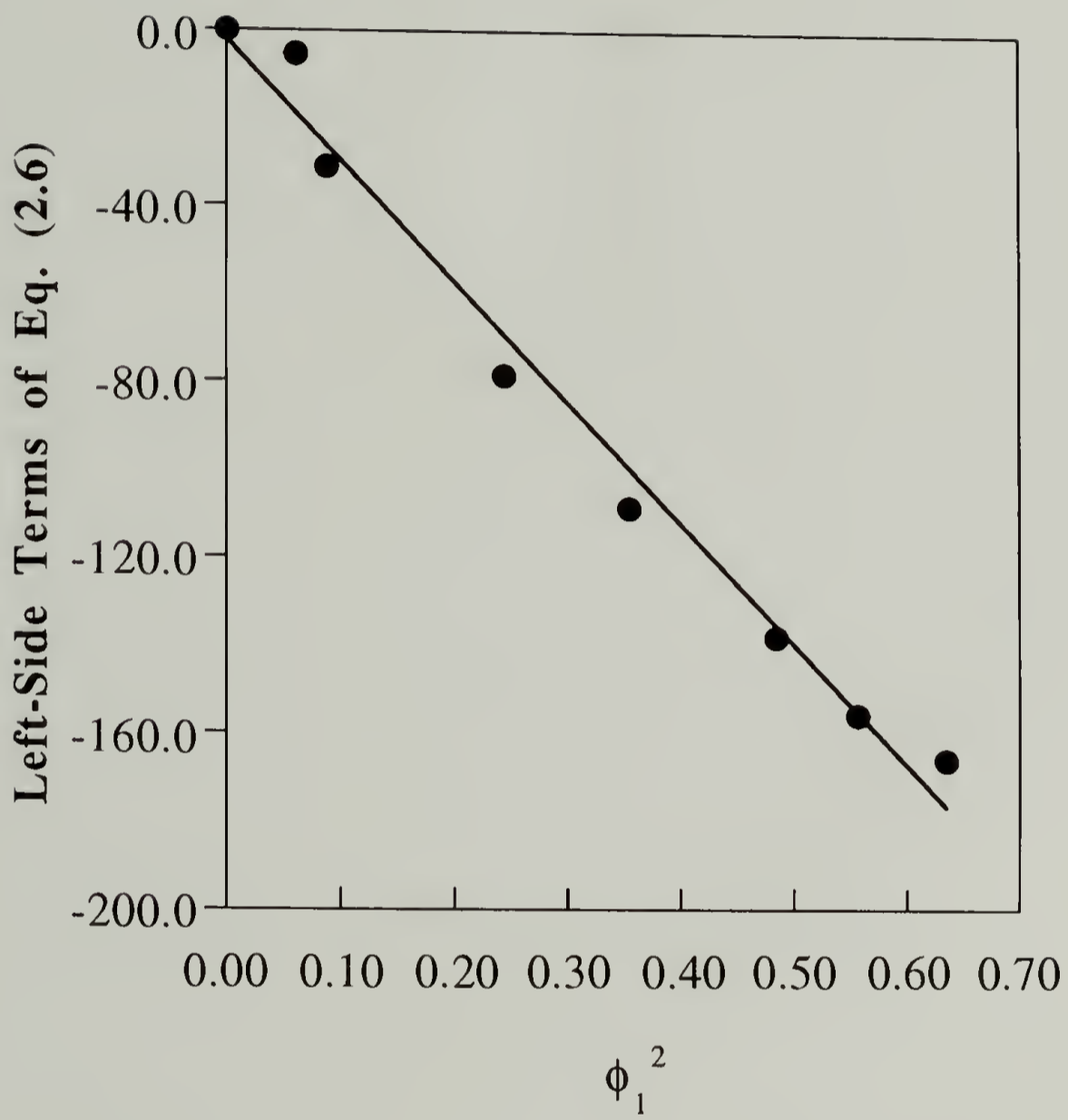


Fig. 2.9 The plot for obtaining the χ of PEEK/PEI blends.

2.3.3 Conformational Change and Nature of Specific Interaction

The nature of specific interaction between PEEK and PEI is explored by FTIR spectroscopy. Fig. 2.10 shows the FTIR spectra of amorphous PEEK, 50/50 blend, and PEI in the frequency region of 1850 to 450 cm^{-1} . There are several bands of PEEK and PEI that do not or only slightly overlap with each other, and hence the effects of blending on these bands can be examined directly. These bands are 1778, 1725, 1380, and 1357 cm^{-1} which are associated with PEI, and 1655 cm^{-1} which is associated with PEEK.

2.3.3.1 Blending Effect on the Imide Ring Conformation

The effect of blending on the C=O stretching bands of PEI is examined first. It is known that cyclic imides normally exhibit two carbonyl stretching bands.²⁴⁻²⁷ The first band located at higher frequency but with lower intensity has been attributed to the C=O in-phase stretching.²⁴⁻²⁷ The other C=O stretching band located at lower frequency but with higher intensity has been attributed to the out-of-phase stretching.²⁴⁻²⁷ It can be seen in Fig.2.10 that this feature is also observed for PEI, where the in-phase stretching is located at 1778 cm^{-1} and the out-of-phase stretching is located at 1725 cm^{-1} . The C=O stretching modes of pyromellitic dianhydride (PMDA) polyimides have been calculated by Silverman.²⁷ The C=O in-phase and out-of-phase stretchings of this polyimide have been found at 1779 and 1725 cm^{-1} , respectively.²⁷ Based on the calculated modes by Silverman, the two C=O stretching modes of PEI are shown in Fig. 2.11. It can be seen that the transition moment induced by the in-phase stretching aligns along the x axis defined by the Ph-N bond, whereas that

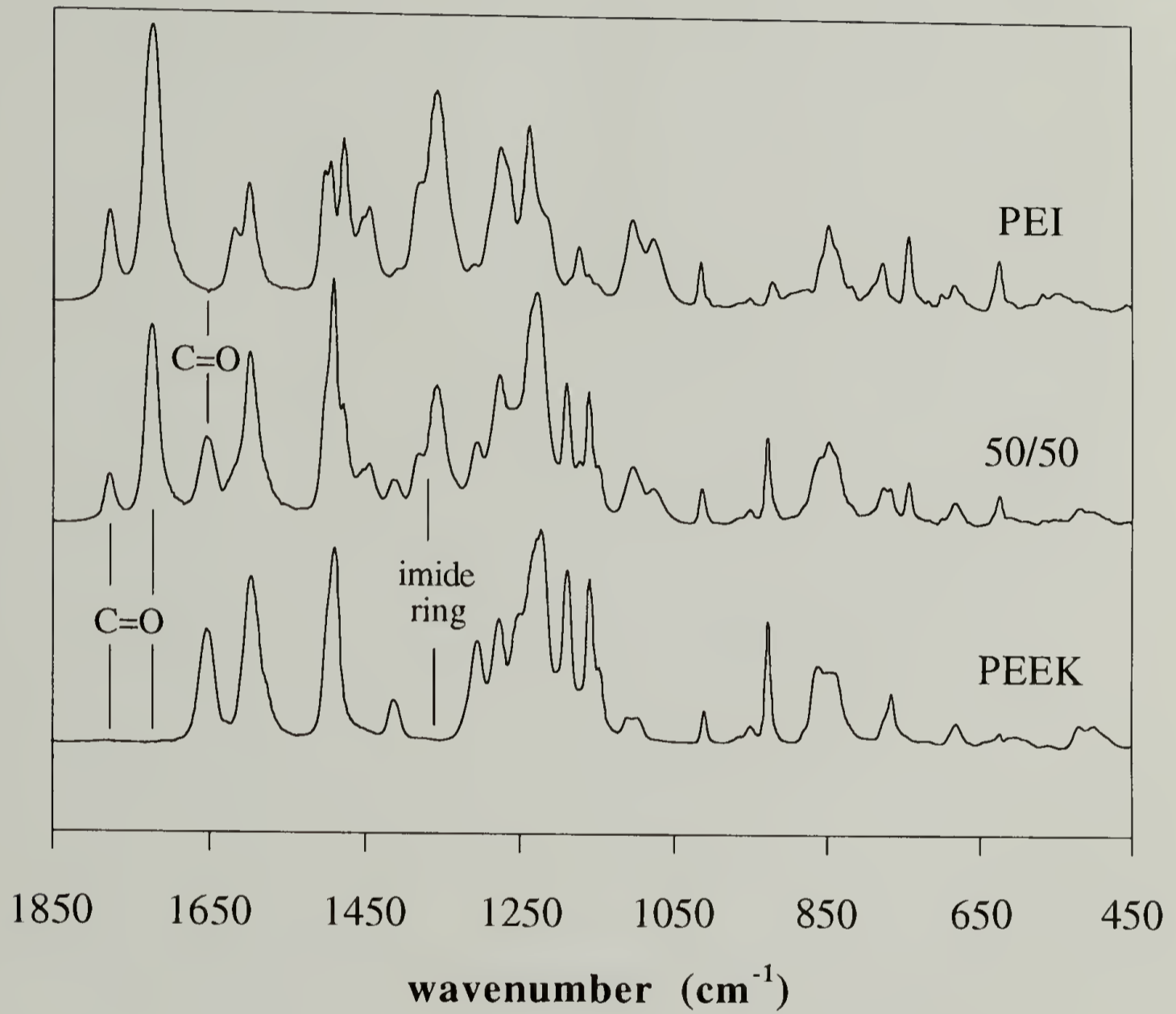
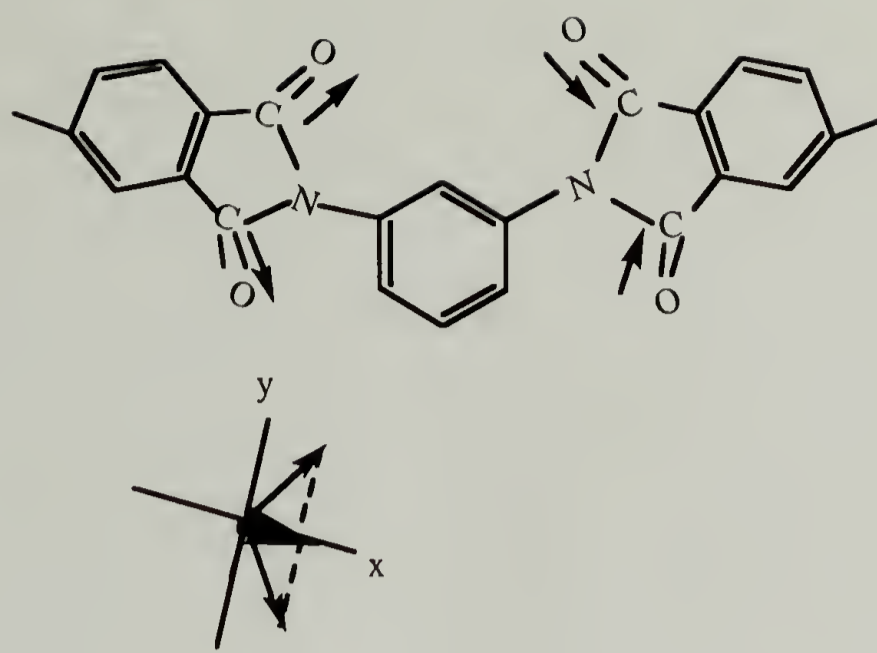
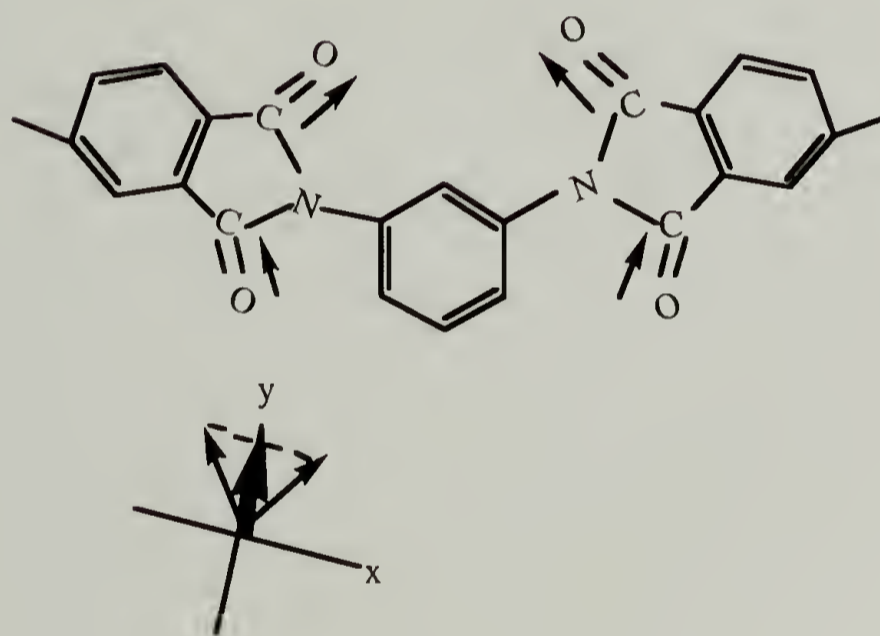


Fig. 2.10 The FTIR spectra of amorphous PEEK, 50/50 blend, and PEI.



(a)



(b)

Fig. 2.11 The two C=O stretching modes of PEI: (a) in-phase mode (1778 cm^{-1}), and (b) out-of-phase mode (1725 cm^{-1}).

induced by the out-of-phase stretching aligns along the y axis (the xy plane is defined by the plane of the imide ring).

Fig. 2.12 displays the C=O stretching bands of PEI in PEEK/PEI blends. Both the intensity and the frequency of the in-phase stretching are not affected by blending. However, the intensity of the out-of-phase stretching is strongly affected, and the frequency of this band is increased slightly by 2 cm^{-1} from pure PEI to PEEK/PEI 75/25 blend. Fig. 2.12 shows that blending with PEEK has an effect that is able to perturb the intensity of PEI C=O out-of-phase stretching significantly, but it only exerts a small influence on the frequency of this band.

The intensity ratio ($R = I_{\text{oop}}/I_{\text{ip}}$) of these two C=O stretching bands (since there is a little overlap between these two bands, curve fitting is used for deconvolution) and the respective width at half-height (WHH) are plotted against the blend composition in Fig. 2.13. Because the intensity of the C=O in-phase stretching is not perturbed, the value of R is proportional to the intensity of the out-of-phase stretching. In Fig. 2.13, it can be seen that the composition variations of both R and WHH are not monotonic. The composition variation of R shows a minimum at ca. 70 wt% of PEI. On the other hand, the composition variation of WHH of the out-of-phase stretching exhibits a maximum at this composition, and the WHH of this composition is 78% larger than that of the 75/25 blend. Blending only imposes a small effect on the WHH of the in-phase stretching. The WHH of this band of 30/70 blend is only 18% larger than that of the 75/25 blend.

The significant effect of blending on the intensity of C=O out-of-phase stretching may imply that some groups in PEEK interact favorably with the C=O groups in PEI. However, since the C=O groups in PEI are attached on the five-member imide rings, it

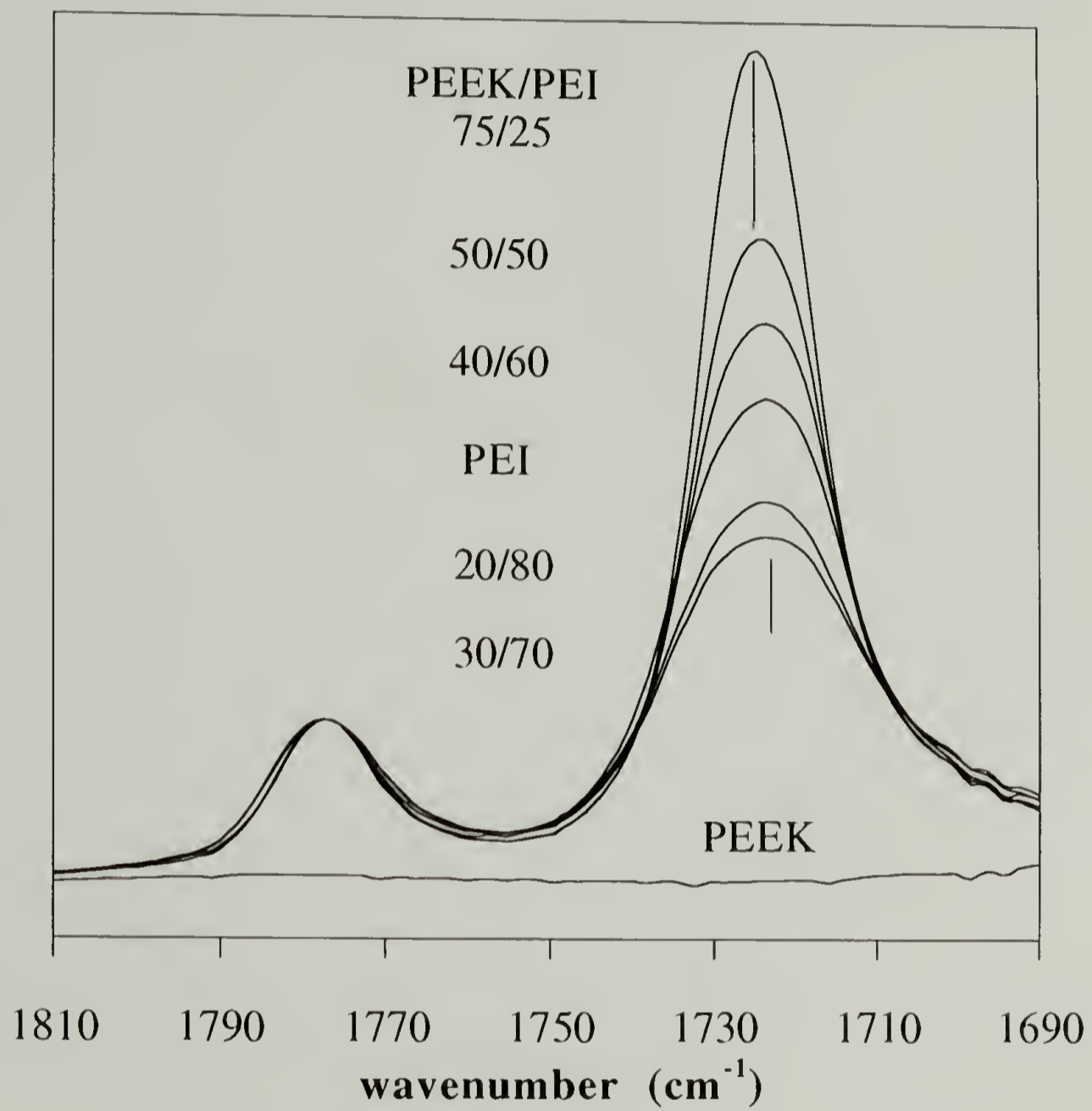


Fig. 2.12 The C=O bands of PEI in amorphous PEEK/PEI blends.

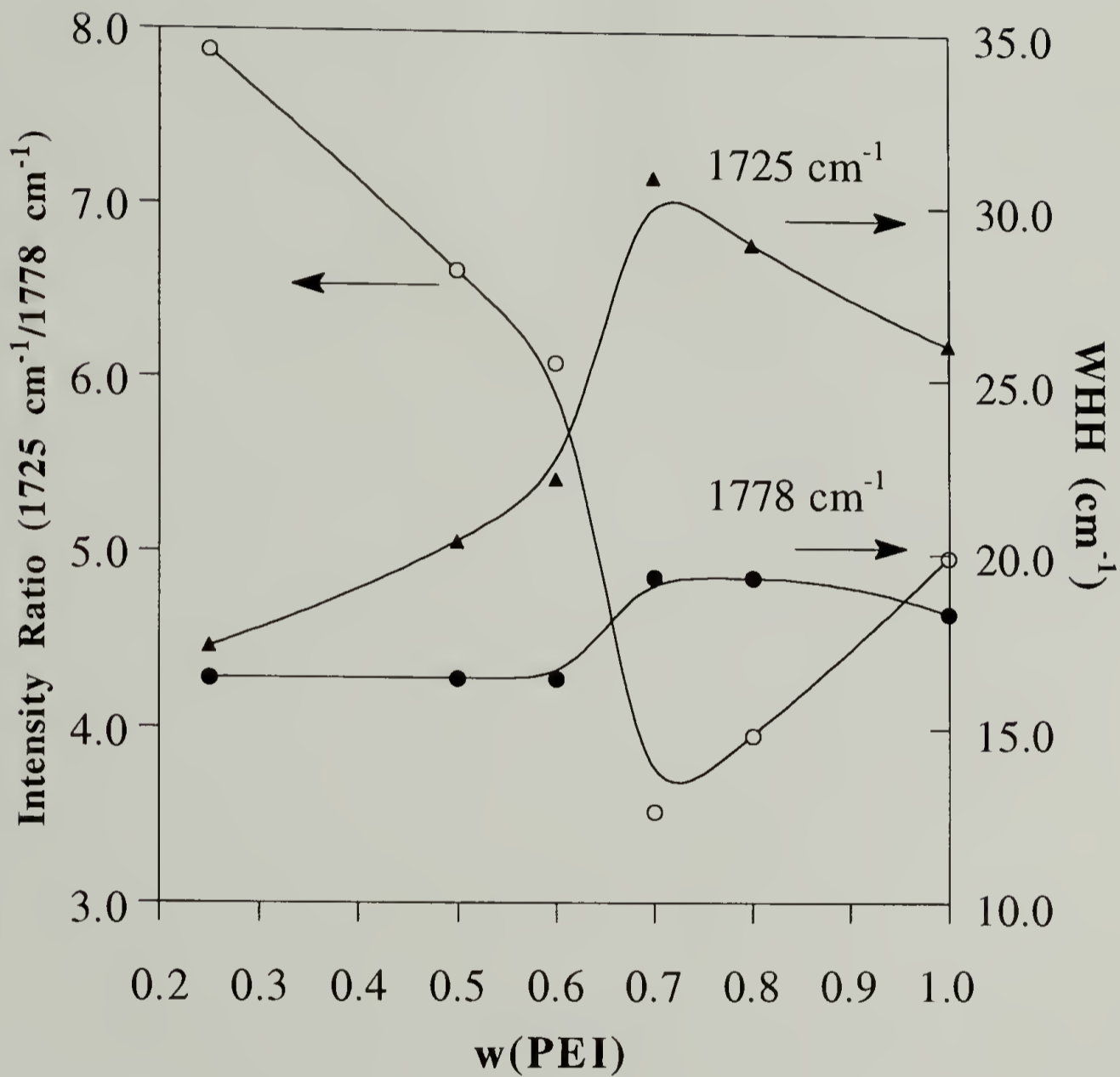


Fig. 2.13 The composition variations of the intensity ratio (R) and the widths at half-height (WHH) of the two PEI C=O bands.

is also possible that the change in C=O stretching intensity is due to the change in the conformation of the whole imide ring. Thus, it is instructive to examine if the bands associated with the imide ring vibrations are also affected by blending. There are two bands associated with the vibrations of the imide rings in PEI, they are the shoulder located at 1380 cm^{-1} and the band located at 1357 cm^{-1} . The precise vibration modes of these two bands have not been assigned. It has been suggested in other polyimides that the bands located in this frequency region are associated with the vibrations involving the C,C>N- bonds in the imide rings.²⁵⁻²⁷ For PMDA polyimides, the vibrations occurred in this frequency region involved significant deformation of the imide rings.²⁷ Fortunately, the 1380 and 1357 cm^{-1} bands of PEI overlap very weakly with the bands of PEEK, and hence they can be examined directly.

Fig. 2.14 displays the effect of blending on these two vibration bands. Like the C=O in-phase stretching, the intensity and the frequency of the shoulder at 1380 cm^{-1} are not affected by blending. On the other hand, just like the C=O out-of-phase stretching, the intensity of 1357 cm^{-1} is strongly modified by blending. The frequency of this band is increased slightly by 1 cm^{-1} from pure PEI to 75/25 blend. Interestingly, it can also be seen from Fig. 2.14 that the intensity of 1357 cm^{-1} shows identical composition variation to that of the C=O out-of-phase stretching. Since the intensities of both the C=O stretching and the C,C>N- vibration of the imide rings are affected by blending, it is likely that blending with PEEK has affected the conformation of the PEI imide rings.

A model considering the conformation of the imide rings in PEI is proposed here to explain the observed intensity variations. The consideration is centered on the effect of the coplanarity of the two nearest imide rings on the coupling of the individual transition moment induced by the C=O stretchings in each imide ring. Fig. 2.15

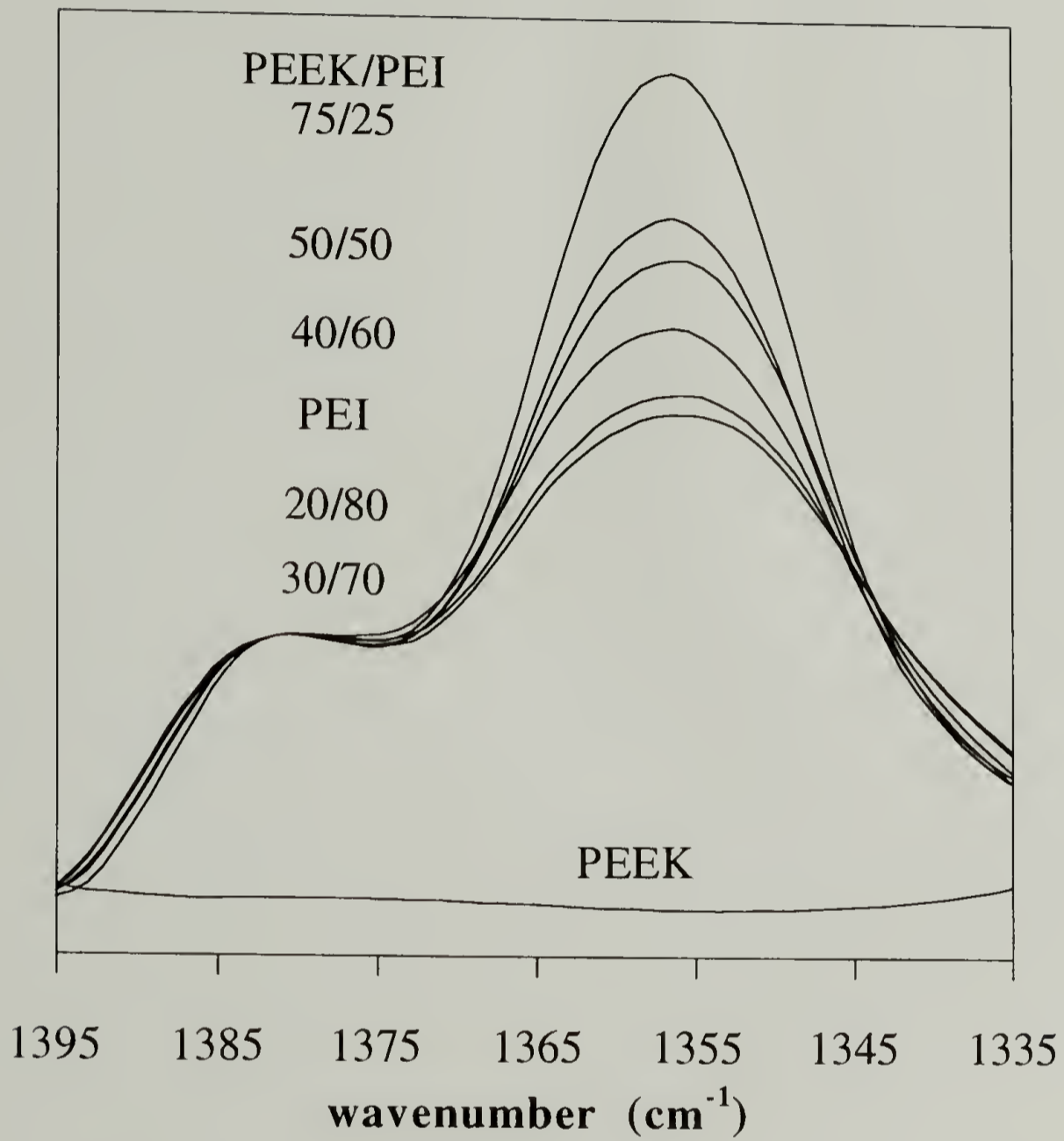


Fig. 2.14 The effect of blending on the imide ring vibrations (1380 and 1357 cm^{-1}) of PEI.

displays the imide groups in a PEI repeating unit. It can be seen that the coplanarity of the two imide rings is determined by the rotational angles ϕ_1 and ϕ_2 of the imide rings about the Ph-N axis. These two imid rings are coplanar when $\phi_1 = \phi_2 = 0$.

The Valence-Optical theory derived by Gribov for the IR absorption intensity of molecules containing identical groups can be used to examine the proposed model.²⁸ This theory has also been applied to $(\text{Ph})_2\text{X}$ and $(\text{Ph})_3\text{X}$ compounds to examine the effect of the rotational angles of the phenyl groups on the IR absorption intensities of the out-of-plane C-H bendings.²⁹⁻³¹ From the Valence-Optical theory, the infrared absorption intensity of a vibration mode in a molecule containing n identical groups is given by²⁸

$$A = \left(\frac{A_0}{\nu_0^2} \right) \left(\nu^2 / \sum_{k=1}^n \alpha_k^2 \right) \left(\sum_{k=1}^n \alpha_k \mathbf{h}_k \right)^2 \quad (2.7)$$

where A and ν are the observed intensity and frequency, respectively; A_0 and ν_0 are the intensity and frequency of a single group, respectively; α_k is the factor expressing the relative phase and amplitude of the groups; and \mathbf{h}_k is the unit vector of vibrational transition moment. Simply speaking, Eq. (2.7) is just a formula expressing the addition of n transition moment vectors in the space resulting from the vibrations of n identical groups.

From Eq. (2.7) and the vibration modes in Fig. 2.11, the intensity of the C=O in-phase stretching is derived as (see Appendix)

$$A_i = 1.5A_{0,i} \left(\frac{\nu_i}{\nu_{0,i}} \right)^2 \quad (2.8)$$

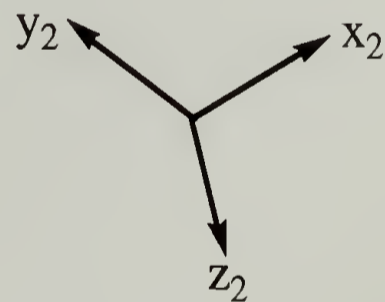
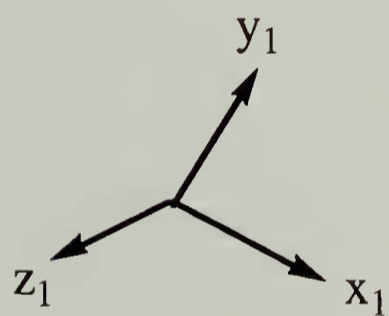
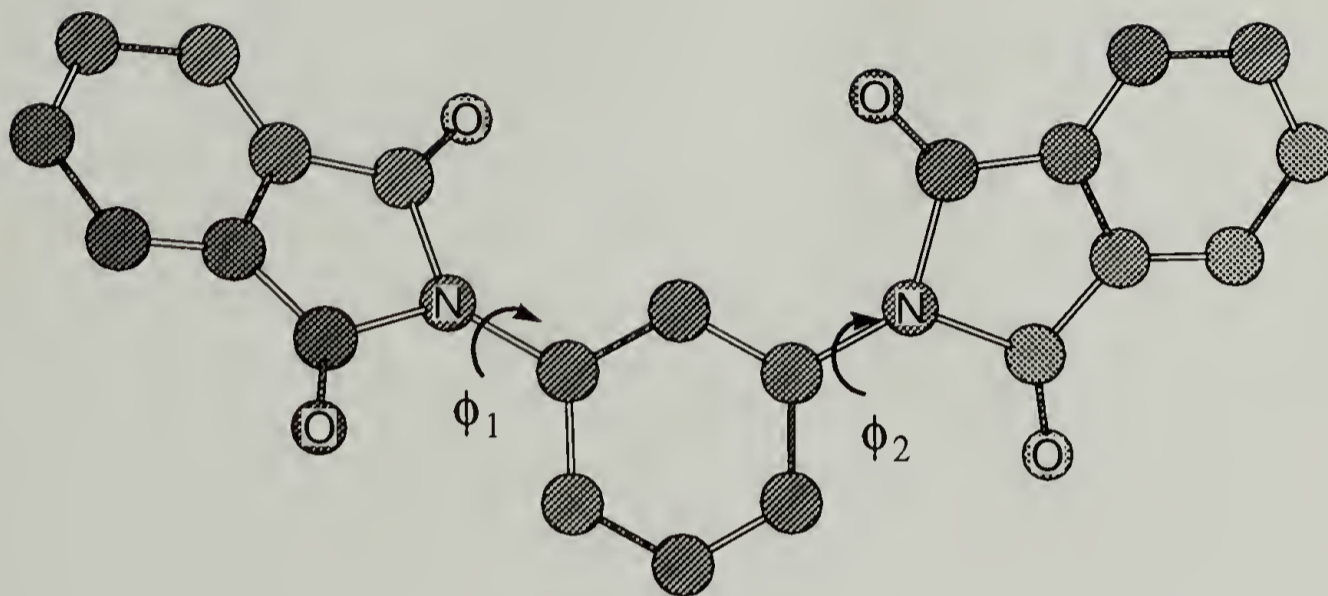


Fig. 2.15 The conformations of the imide rings in PEI. The coplanarity of the two imide rings are determined by the rotational angles ϕ_1 and ϕ_2 .

and the intensity of the C=O out-of-phase stretching is given by

$$A_{\text{oop}} = 0.5A_{0,\text{oop}}\left(\frac{\nu_{\text{oop}}}{\nu_{0,\text{oop}}}\right)^2 [2 + |\cos(\phi_1 - \phi_2)|] \quad (2.9)$$

The rotational angle difference, $(\phi_1 - \phi_2)$, signifies the coplanarity of the two imide rings. Since A_{oop} should increase with increasing coplanarity of the imide rings, the absolute value of $\cos(\phi_1 - \phi_2)$ is considered in Eq. (2.9); because when $(\phi_1 - \phi_2) < 90^\circ$ the coplanarity of the two imide rings decreases with increasing $(\phi_1 - \phi_2)$, but when $(\phi_1 - \phi_2) > 90^\circ$, the coplanarity increases with increasing $(\phi_1 - \phi_2)$.

Eq. (2.8) and (2.9) indicate that the intensity of the C=O out-of-phase stretching is dependent on $(\phi_1 - \phi_2)$ or the coplanarity of the imide rings, but on the other hand, the intensity of the in-phase stretching is not. It is thus suggested that blending with PEEK has affected the coplanarity of the imide rings, and this in turn leads to the change of the intensity of the C=O out-of-phase stretching. However, the change in coplanarity of the two imide rings can not affect the intensity of the in-phase stretching. The observations in Fig. 2.12 are consistent with the prediction of this model.

From Eq. (2.9), the expected variation of the C=O out-of-phase stretching intensity with $(\phi_1 - \phi_2)$ is schematically shown in Fig. 2.16. It is seen that a minimum is observed at $(\phi_1 - \phi_2) = 90^\circ$, i.e., when the two imide rings are perpendicular to each other. The minimum behavior observed at the 30/70 composition in Fig. 2.13 may be due to that the two imide rings at this composition are perpendicular to each other.

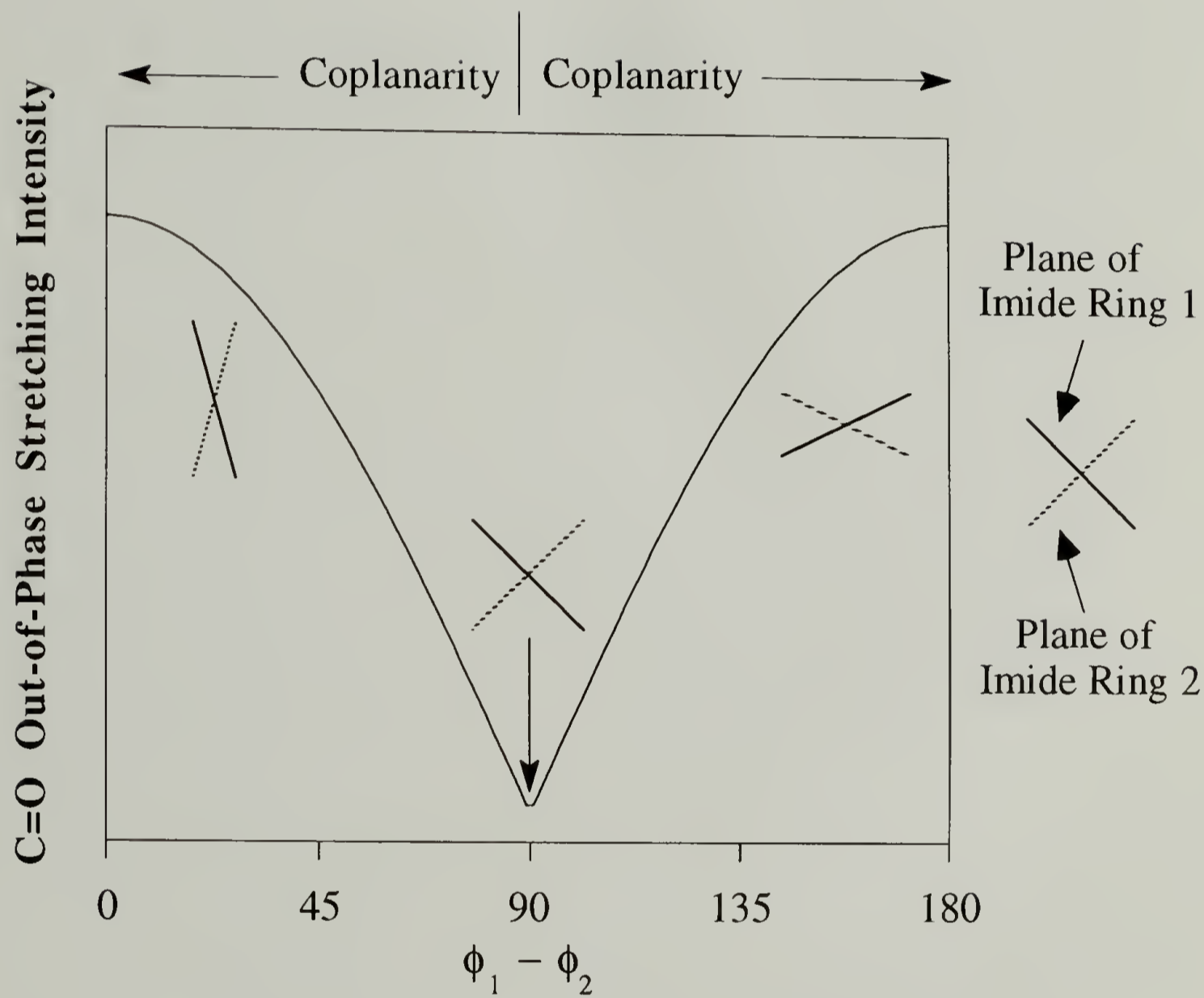


Fig. 2.16 The coplanarity variation of the PEI C=O out-of-phase stretching intensity.

It is seen that the model proposed here has offered reasonable explanations for the observed intensity changes of the PEI C=O stretchings. Similarly, the composition variations of the intensities of 1380 and 1357 cm^{-1} may also be due to the change in the coplanarity of the imide rings upon blending. The vibration mode of 1380 cm^{-1} may thus give a transition moment aligned along the Ph-N axis, just like the C=O in-phase stretching. On the other hand, the transition moment resulted from the vibration mode of 1357 cm^{-1} may not align along the Ph-N axis, and consequently the intensity of which depends on the coplanarity of the imide rings, just like the C=O out-of-phase stretching.

2.3.3.2 Specific Interaction Between PEEK and PEI

From the above discussions, it is suggested that the imide rings in PEI interact favorably with some groups in PEEK. The change in coplanarity of the two imide rings upon blending may be due to the necessity of maximizing the favorable intermolecular interaction between PEEK and PEI. Now the question is "What are the groups in PEEK that interact favorably with the imide rings in PEI?".

The C=O stretching frequency of PEEK is observed at 1655 cm^{-1} , due to the conjugation of the C=O group with the neighboring -Ph- groups.³² This C=O stretching band overlaps very weakly with the bands of PEI. Therefore, it is interesting to examine the blending effect on this band first. The C=O stretching bands of PEEK in PEEK/PEI blends are shown in Fig. 2.17. It can be seen that blending has very little effect on this band. Therefore, the C=O group in PEEK does not contribute to the specific interaction between PEEK and PEI.

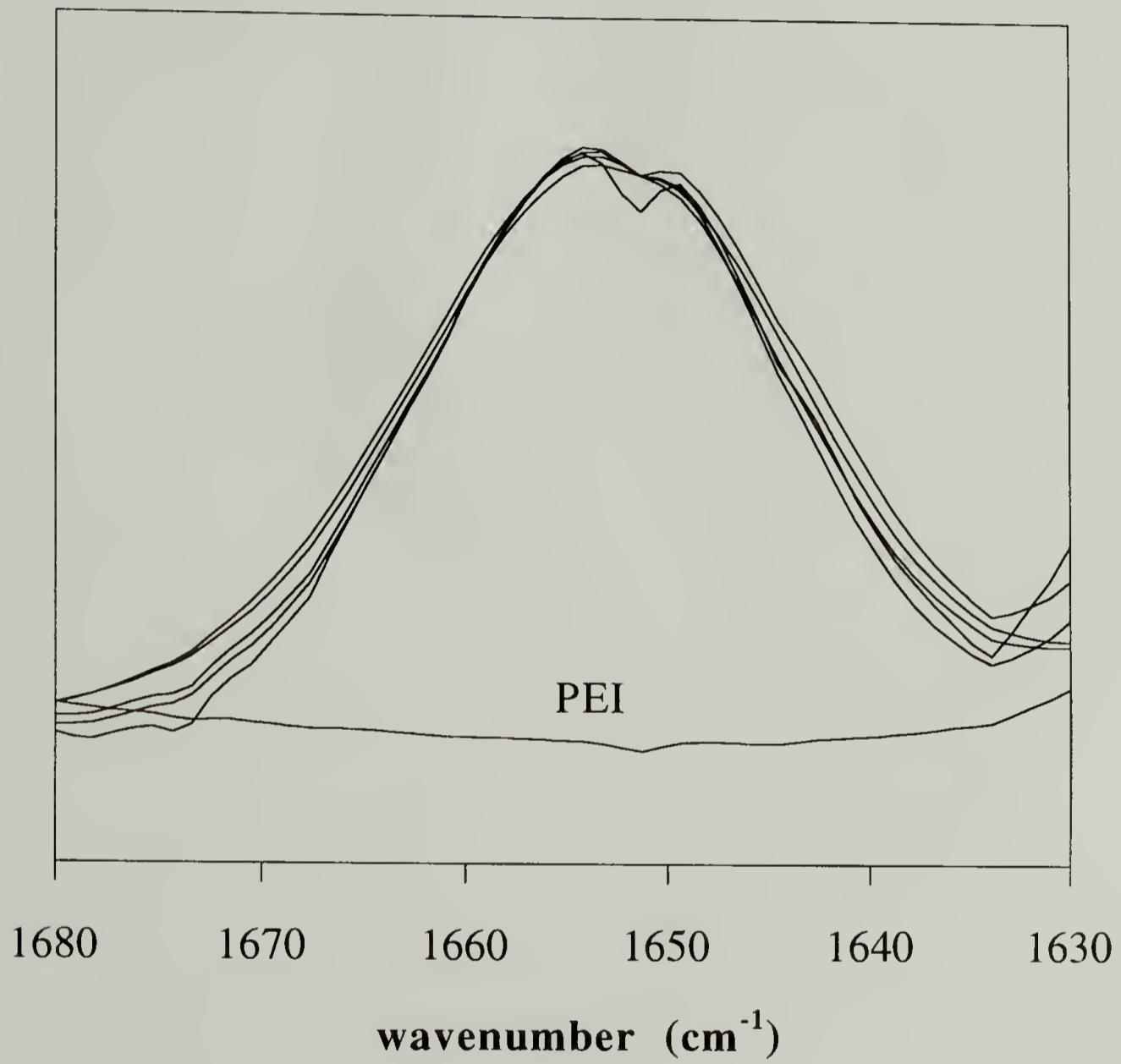


Fig. 2.17 The C=O stretchings of PEEK in amorphous PEEK/PEI blends.

The calculations of the charge distribution for N-substituted Maleimides have been reported.³³ The positive charge distribution was found in the imide rings, due to the delocalization of the nitrogen lone-pair electrons to the C=O groups and the substituted Ph groups. Therefore, the imide rings in PEI are electron deficient. If the imide rings interact favorably with some groups in PEEK, the interacting groups in PEEK should thus be electron-donating in nature. One of the groups in PEEK having this kind of nature is the ether group which contains the lone-pair electrons.

Unfortunately, other bands of PEEK overlap significantly with those of PEI. Therefore, the spectral subtraction was used to obtain the difference spectra of PEEK/PEI blends. The difference spectra or the interaction spectra were obtained by subtracting the pure PEEK and PEI spectra from the blend spectra. When the blend spectra were subtracted by the pure PEI spectra, the PEI C=O in-phase stretching was used as the reference to determine the scaling factor for the subtraction. The difference spectra were obtained as the 1778 cm⁻¹ band was completely removed. The resulting spectra were subsequently subtracted by the pure PEEK spectra. The C=O stretching (1655 cm⁻¹) of PEEK was used as the reference, and the final interaction spectra were resulted after this band was almost removed. To be certain that the resulting interaction spectra were not due to the artifact introduced by subtraction, the difference spectra of a PEEK/PEI composite were also obtained. A PEEK and a PEI film were stacked together forming a composite, and the IR spectra of this composite were recorded. The difference spectra of this composite were obtained by the same fashion as that of the blends.

The difference spectra of PEEK/PEI 75/25, 50/50, and the composite are shown in Fig. 2.18 along with the spectra of pure PEEK and PEI. It can be seen that the

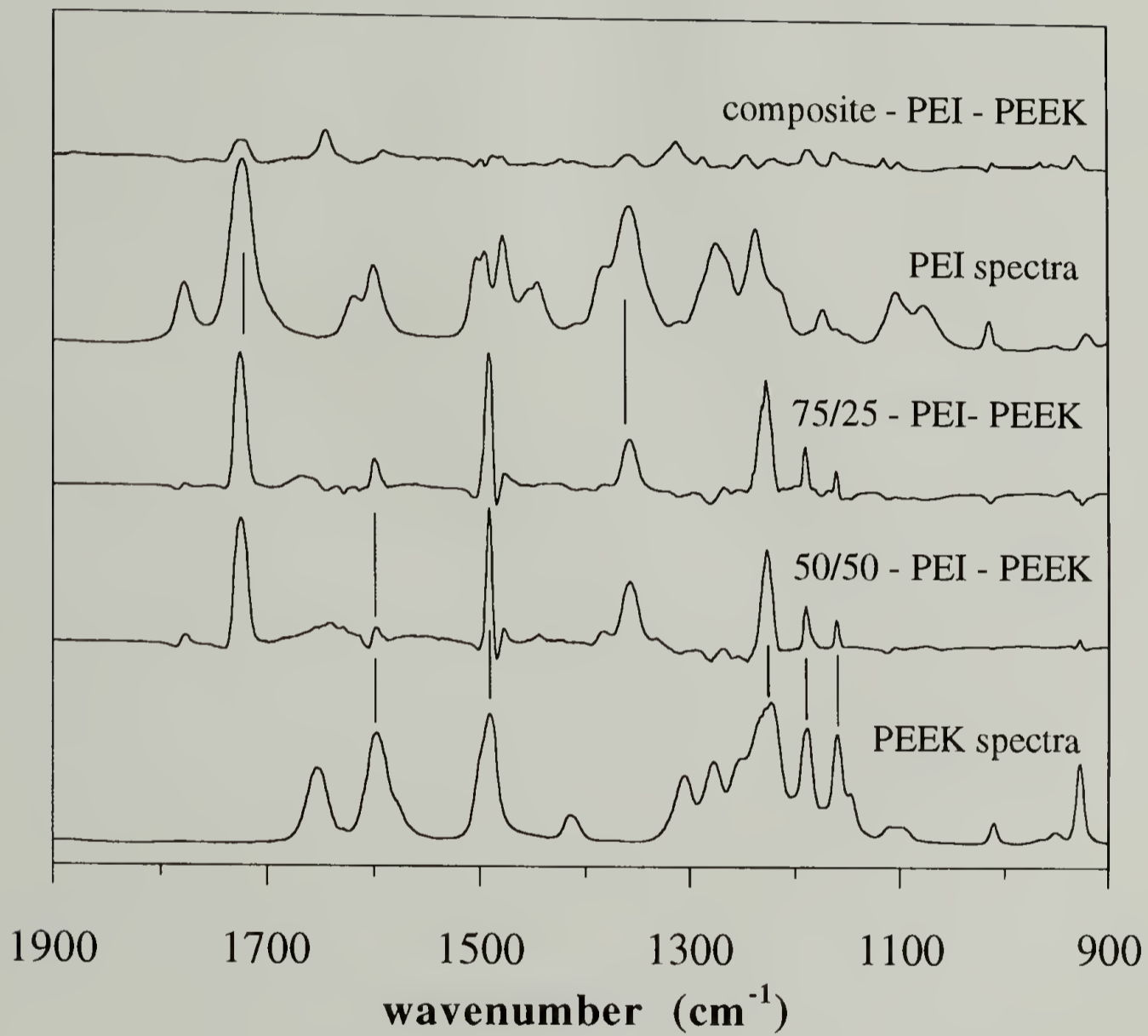


Fig. 2.18 The interaction spectra of PEEK/PEI 75/25 and 50/50 blends along with the spectra of pure PEEK and PEI.

bands exhibited by the composite difference spectra are rather random and small compared to those appeared in the blend difference spectra. In addition, the difference spectra of the 75/25 and 50/50 blends are almost identical. These provide the reliability of the difference spectra shown in Fig. 2.18. Comparing the difference spectra with the spectra of pure PEEK and PEI, it is found that in addition to the bands at 1725 and 1357 cm^{-1} associated with PEI, there are five bands: 1599, 1491, 1227, 1189, and 1160 cm^{-1} , which are associated with PEEK. The 1599 and 1491 cm^{-1} are due to the skeletal in-plane vibration of the phenyl rings; the 1227 and 1189 cm^{-1} are due to the antisymmetric stretching of the diphenyl ether groups; and the 1160 cm^{-1} is due to the in-plane vibrations of the aromatic hydrogen.³² An IR spectroscopic study of PEEK has been reported by Nguyen and Ishida.³² The difference spectra between the PEEK annealed at 380 °C and that annealed at 400 °C have been obtained in their study. It is interesting to note that this difference spectra is identical to the interaction spectra associated with PEEK in Fig. 2.18. These observations indicate that the structures of the diphenyl ether of PEEK are sensitive to both the melt annealing temperature and the blending with PEI.

Fig. 2.19 displays the interaction spectra of 30/70 blend. In contrast to the interaction spectra shown in Fig. 2.18, the bands of this interaction spectra show negative absorptions. Several residual bands associated with PEI not seen clearly in Fig. 2.18 appear in Fig. 2.19. The residual bands located in the frequency region of 1200 to 1300 cm^{-1} are also due to the vibrations of the imide rings.²⁶⁻²⁷ The residual bands associated with PEEK seen in Fig. 2.18 cannot be distinguished clearly in Fig. 2.19 due to low PEEK concentration and the overlaps with the extra residual bands of PEI.

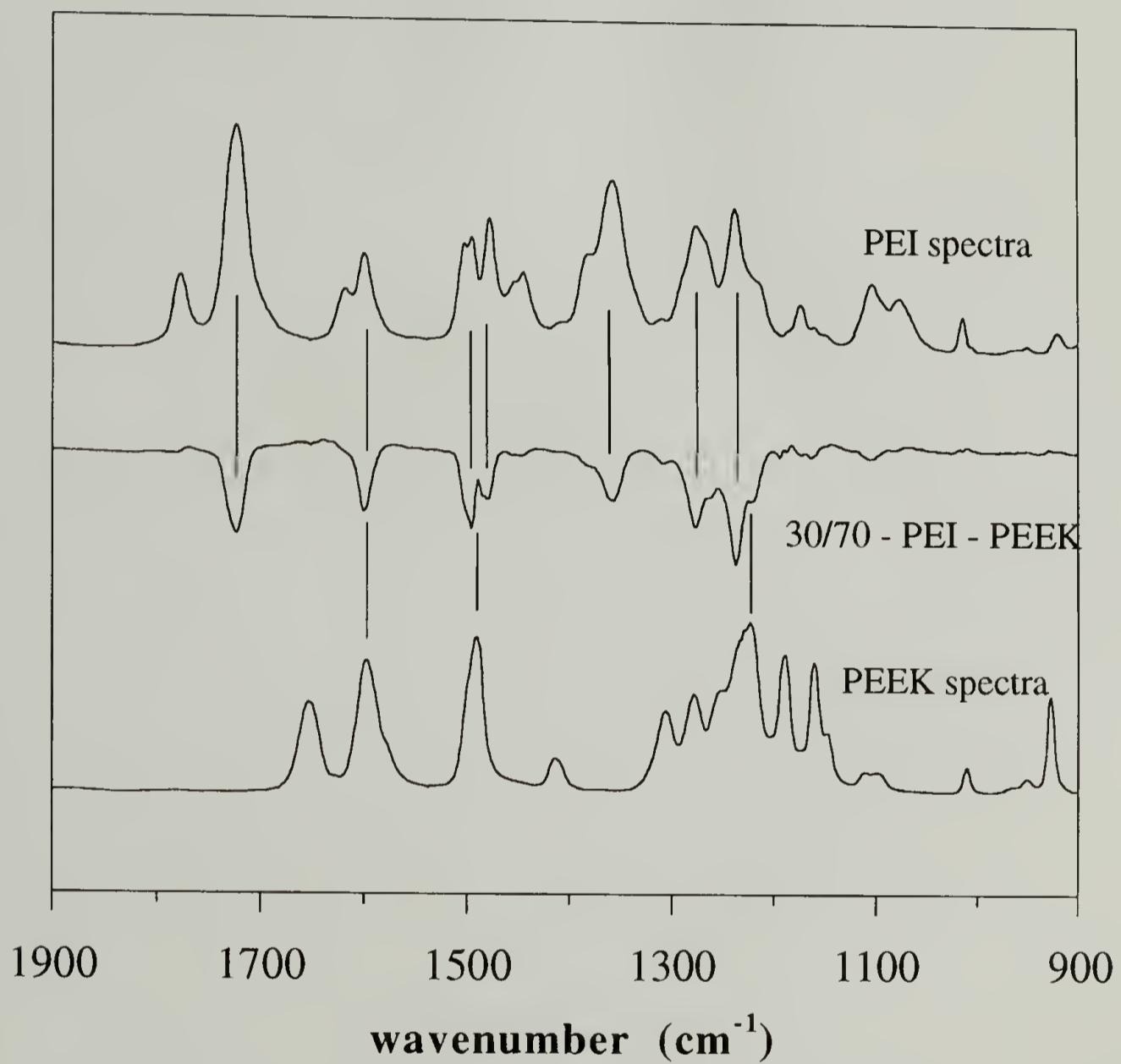


Fig. 2.19 The interaction spectra of PEEK/PEI 30/70 blend along with the spectra of pure PEEK and PEI.

Based on Fig. 2.18 and 2.19, it is suggested that the group in PEEK contributing to the favorable intermolecular interaction with the imide rings in PEI is the diphenyl ether moiety. It is therefore proposed that the oxygen lone-pair electrons of the ether groups in PEEK interact favorably with the electron-deficient imide rings in PEI. The proposed specific interaction is shown schematically in Fig. 2.20. Unlike some strong intermolecular interactions such as hydrogen bonding, the interaction mode shown in Fig. 2.20 is not strong enough to perturb the frequencies of the IR bands significantly, but it is strong enough to affect the band intensities considerably. It is interesting to note that in the 30/70 blend, which shows the minimum C=O out-of-phase stretching intensity, one ether group in PEEK interacts with about one imide ring in PEI.

The interactions between the oxygen lone-pair electrons and the electron-deficient groups have also been observed in the polymer electrolytes containing poly(ethylene oxide) (PEO) and salts.³⁴ For example, the oxygen lone-pair electrons in PEO interact with the lithium cations in the salts, and consequently a miscible solution of PEO and the lithium salt was formed.

2.4 Conclusions

The phase behavior of PEEK/PEI blends in the amorphous state has been investigated. In contrast to the melt blending used in previous studies, a solution blending, using dichloroacetic acid as the solvent, is employed to blend PEEK and PEI. A single T_g is observed over the whole composition range, indicating the miscibility between these two polymers in the melt. The composition variation of T_g of this binary blend can be described satisfactorily by the simple Fox equation and the

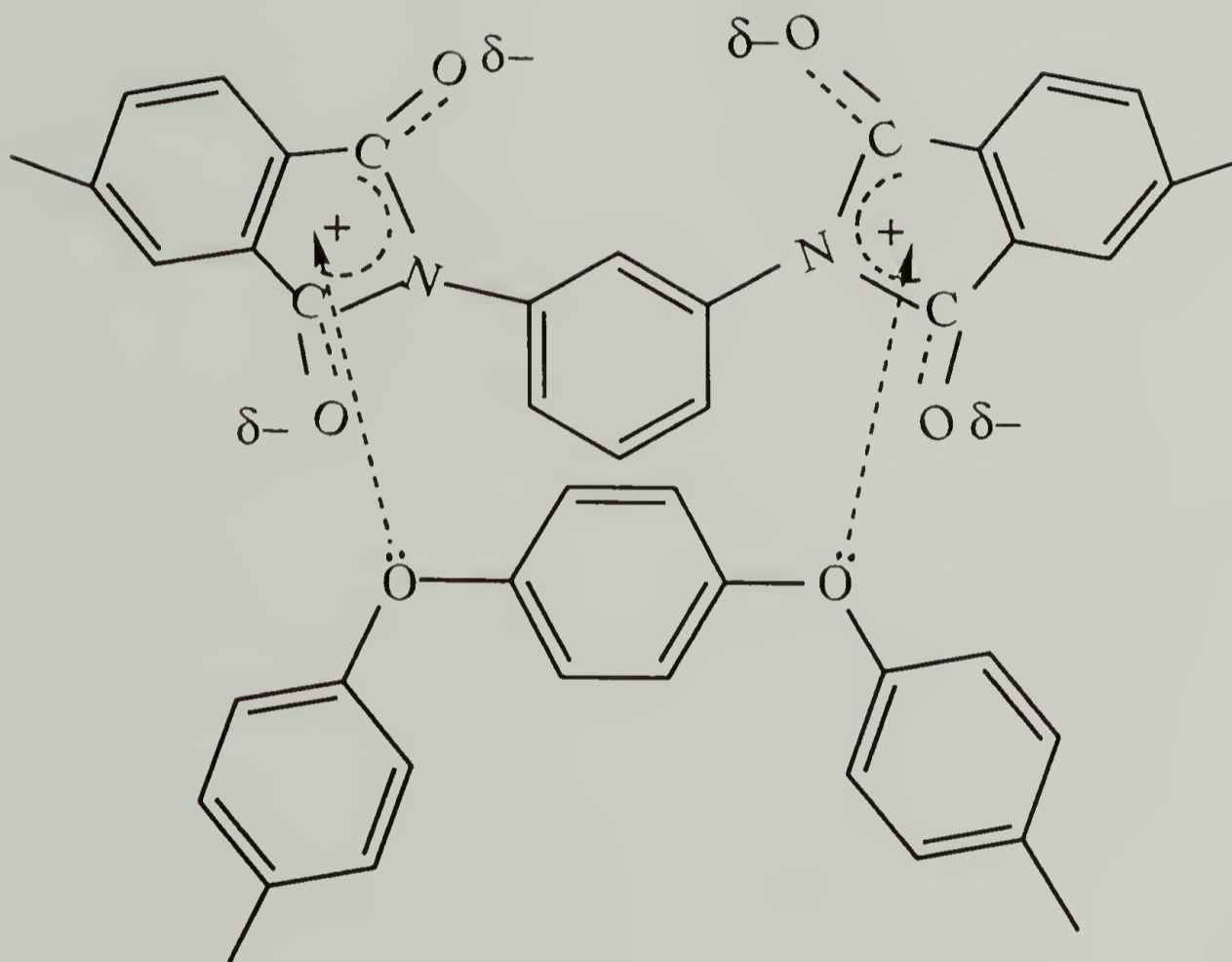


Fig. 2.20 The proposed specific interaction between PEEK and PEI. The oxygen lone-pair electrons of the ether groups in PEEK interact favorably with the electron-deficient imide rings in PEI.

Gordon-Taylor's equation. The specific volume measurement and the melting point depression analysis have shown the existence of favorable interaction between PEEK and PEI. The equilibrium M.P. analysis gives the interaction density $B = -1.2$ cal/cm³, and $\chi = -0.4$ at 400 °C.

Infrared spectroscopy appears to be a powerful method for studying the specific interaction and conformational change in PEEK/PEI blends. From the composition variation of the PEI C=O stretching intensity, it is concluded that blending with PEEK changes the coplanarity of the two imide rings bridged by the phenylene group. The difference spectra (blend - PEEK - PEI) reveal that the bands associated with the diphenyl ether groups in PEEK are modified by blending with PEI. It is proposed that the specific interaction takes place between the oxygen lone-pair electrons of the ether groups in PEEK and the electron-deficient imide rings in PEI.

References

1. Olabisi, O.; Robeson, L. M.; Shaw, M. T. *Polymer-Polymer Miscibility* Academic Press: New York, **1979**.
2. Nishi, T.; Wang, T. T. *Macromolecules* **1975**, 8, 909.
3. Koningsveld, R., private communication.
4. Lu, F. J.; Benedetti, E.; Hsu, S. L. *Macromolecules* **1983**, 16, 1525.
5. Parmer, J. F., Ph. D. Thesis, Univ. of Mass., Amherst, Mass., **1987**.
6. Karcha, R. J., Ph. D. Thesis, Univ. of Mass., Amherst, Mass., **1990**.
7. Harris, J. E.; Robeson, L. M. *J. Appl. Polym. Sci.* **1989**, 35, 1877.
8. Grevecocur, G.; Groeninckx, G. *Macromolecules* **1991**, 24, 1190.
9. Hsiao, B. S.; Sauer, B. B. *J. Polym. Sci. Polym. Phys. Ed.* **1993**, 31, 901.
10. Nguyen, H. X.; Ishida, H. *Polymer* **1986**, 27, 1400.
11. Musto, P.; Karasz, F. E.; MacKnight, W. J. *Macromolecules* **1991**, 24, 4762.
12. Lee, Y., Ph.D. Thesis, Univ. of Mass., Amherst, Mass., **1988**.
13. Fox, T. G. *Bull. Am. Phys. Soc.* **1956**, 1, 123.
14. Gordon, M.; Taylor, J. S. *J. Appl. Chem.* **1952**, 2, 495.
15. Aubin, M.; Prud'homme, R. E. *Macromolecules*, **1990**, 13, 365.
16. Sun, J.; Cabasso, I. *Macromolecules* **1991**, 24, 3603.
17. MacKnight, W. J.; Karasz, F. E.; Fried, J. R. in *Polymer Blends*, Vol. 1; Paul, D. R.; Newman, S. Eds.; Academic Press: New York, **1978**; Chap. 5.
18. Buchdahl, R.; Nielsen, L. E. *J. Polym. Sci., Polym. Phys. Ed.*, **1989**, 27, 2153.
19. Hoffman, J. D.; Davis, G. T.; Lauritzen, Jr., J. I. In *Treatise on Solid State Chemistry*; Hanny, N. B., Ed.; Plenum Press: New York, **1976**; Chap. 7.
20. Blundell, D. J.; Osborn, B. N. *Polymer* **1983**, 24, 953.
21. Cheng, S. Z. D.; Cao, M.-Y.; Wunderlich, B. *Macromolecules* **1986**, 19, 1868.
22. Rim; P. B.; Runt, J. P. *Macromolecules* **1983**, 16, 762.
23. Wunderlich, B.; Cormier, C. M. *J. Polym. Sci. Polym. Phys. Ed.* **1967**, 5, 987.

24. Matsuo, T. *Bull. Chem. Soc. Japan* **1964**, 37, 1844.
25. Dine-Hart, R. A.; Wright, W. W. *Makromol. Chem.* **1971**, 143, 189.
26. Ishida, H.; Wellinghoff, T.; Baer, E.; Koenig, J. L. *Macromolecules* **1980**, 13, 826.
27. Silverman, B. D. *Macromolecules* **1989**, 22, 3768.
28. Gribov, L. A. *Intensity Theory for Infrared Spectra of Polyatomic Molecules*; Academy of Sciences of U.S.S.R. Press: Moscow, **1963**.
29. Higuchi, S.; Nakamori, K.; Tanaka, S.; Kamada, H. *J. Chem. Soc. Jpn. Pure Chem. Sec.* **1968**, 89, 565.
30. Goda, Y.; Higuchi, S.; Tanaka, S.; Kamada, H. *J. Chem. Soc. Jpn. Pure Chem. Sec.* **1971**, 92, 21.
31. Higuchi, S.; Tsuyama, H.; Tanaka, S.; Kamada, H. *Spectrochimica Acta*, **1974**, 30A, 463.
32. Nguyen, H. X.; Ishida, H. *Polymer*, **1986**, 27, 1400.
33. Matsuo, T. *Bull. Chem. Soc. Jpn.* **1965**, 38, 557.
34. Owen, J. in *Comprehensive Polymer Science*; Pergamon: New York, **1989**; Vol. 2.

CHAPTER 3

TWO-STAGE CRYSTALLIZATION BEHAVIOR OF PEEK AND PEEK/PEI BLENDS

3.1 Introduction

The studies of the crystallization behavior of PEEK have been largely motivated by the two melting endotherms observed in the DSC scans.¹⁻⁷ Based on the electron micrographs, two crystal populations of different thickness have been identified in crystalline PEEK.^{2,4} In addition to the thicker primary crystals, a set of thinner secondary crystals have been found to grow in between the primary crystals. This double lamellar morphology has been considered to give rise to the two melting endotherms observed by DSC.^{2,4} Recently, Marand et al.³ have observed the aggregation of the secondary crystals inside PEEK spherulites using optical microscopy at crystallization temperatures (T_c) > 295 °C. However, at a T_c < 295 °C, these secondary crystals were not seen by optical microscopy, despite that two melting endotherms were still observed by DSC.

Although these studies have shown the existences of two crystal populations in PEEK, the origin of this two-stage crystallization phenomenon is still an open question. Since this two-stage crystallization pattern has not been observed in the conventional aliphatic polymers, the stiff nature of PEEK molecules has been suggested to relate to this behavior.⁷ Similar two-stage crystallization has also been reported for poly(phenylene sulfide) (PPS) which is also an aromatic polymer.⁸ Therefore, it is likely that there are some intrinsic differences in the crystallization

patterns between the aromatic polymers and the more studied aliphatic polymers. In order to explore these differences, more detailed studies are necessary. One of the most important investigations is the crystallization kinetics of these two crystallization stages. The crystallization kinetics study requires real-time observation, and DSC appears to be a suitable tool for such investigation. However, it will be shown that DSC is indeed not sensitive enough to resolve the two PEEK crystallization stages, which are distinguishable by another technique, thermal mechanical analysis (TMA).

In the first part of this chapter, the application of thermal mechanical analysis (TMA) to study the two-stage crystallization behavior of PEEK is reported. This simple and convenient technique is a one-dimensional dilatometry, measuring the variation of film thickness with time during isothermal crystallization. It will be shown that, as PEEK undergoes isothermal crystallization, two crystallization stages can be distinguished by TMA, while they are not resolvable by DSC. This technique provides a simple method for monitoring the two PEEK crystallization stages in real-time, and hence the respective kinetic behavior of these two stages can be obtained.

The second part of this chapter describes the application of TMA to study the crystallization kinetics of PEEK/PEI blends. The effect of blending with PEI on the two-stage crystallization behavior of PEEK is discussed. It is known that blending with a miscible polymer may have significant effects on the crystallization behavior of the crystalline polymer.⁹⁻¹⁴ These include changes in thermodynamic driving force and molecular mobility associated with crystallization. Since blending with PEI may provide an important method to systematically control the crystallization rate of PEEK. The investigation of the effect of PEI on the crystallization behavior of PEEK is thus of interest.

3.2 Experimental

3.2.1 Materials and Sample Preparations

PEEK/PEI blends were prepared by dissolving these two polymers in dichloroacetic acid followed by precipitation in methanol/water mixture. The precipitates were filtered, washed with a large amount of water, and then dried in a vacuum oven at 95 °C to constant weight.

Fully amorphous films of PEEK and PEEK/PEI blends for TMA investigation were prepared by compression molding at 400 °C for 5 mins under vacuum followed by quenching in cold water.

3.2.2 Thermal Mechanical Analysis and DSC Measurement

A Perkin-Elmer TMS-2 Thermomechanical Analyzer was used to detect the thickness change of PEEK and PEEK/PEI blend films during isothermal crystallization at 162 to 258 °C. A schematic representation of TMA is shown in Fig. 3.1. A PEEK or PEEK/PEI blend film of about 0.1 mm thick was placed on the platform of the sample tube and the probe placed in contact with the film. An oil bath was equilibrated at the desired crystallization temperature with the control of $\pm 1^\circ\text{C}$. The oil bath was then quickly moved to immerse the sample, and the change of the specimen thickness with respect to time was recorded.

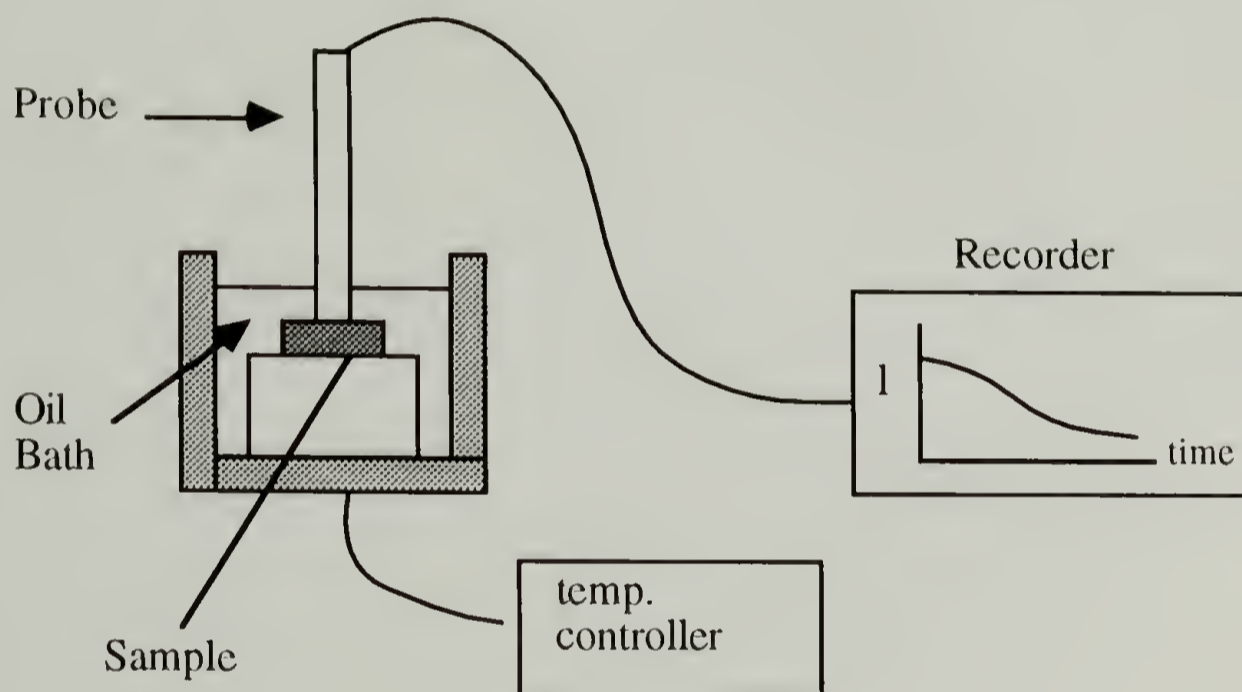


Fig. 3.1 Schematic plot of the thermal mechanical analyzer for studying the isothermal crystallization of PEEK/PEI blends.

Crystallizations at high T_c (from 290 to 310 °C) of PEEK and PEEK/PEI blends were monitored by a Perkin-Elmer DSC-4. The sample was heated from 100 °C to 400 °C at 100 °C/min, and was held at this temperature for 3 mins. The sample was then quickly cooled at ~ 200 °C/min to the desired T_c , and the isothermal crystallization exotherm was recorded.

3.3 Results and Discussion

3.3.1 Two-Stage Crystallization of PEEK

Fig. 3.2 shows the direct recorded TMA traces of amorphous PEEK films during isothermal crystallization at three temperatures. It can be seen that two crystallization stages are distinguished: an initial drop of specimen thickness corresponds to the first stage (primary) crystallization, a subsequent plateau indicates an induction period, and a final drop of the specimen thickness corresponds to the second stage (secondary) crystallization. The clear distinction of these two crystallization stages for PEEK is unusual among the semicrystalline polymers for which generally only one crystallization curve has been observed.¹⁵ The secondary crystallization of PEEK appears to start after or shortly before the conclusion of the primary crystallization.

Primary crystallization has normally been attributed to the formation of spherulites, and secondary crystallization has been attributed to the crystallization taking place inside the spherulites (intraspherulitic crystallization).¹⁵ For most polymers, intraspherulitic crystallization proceeded before the conclusion of spherulite

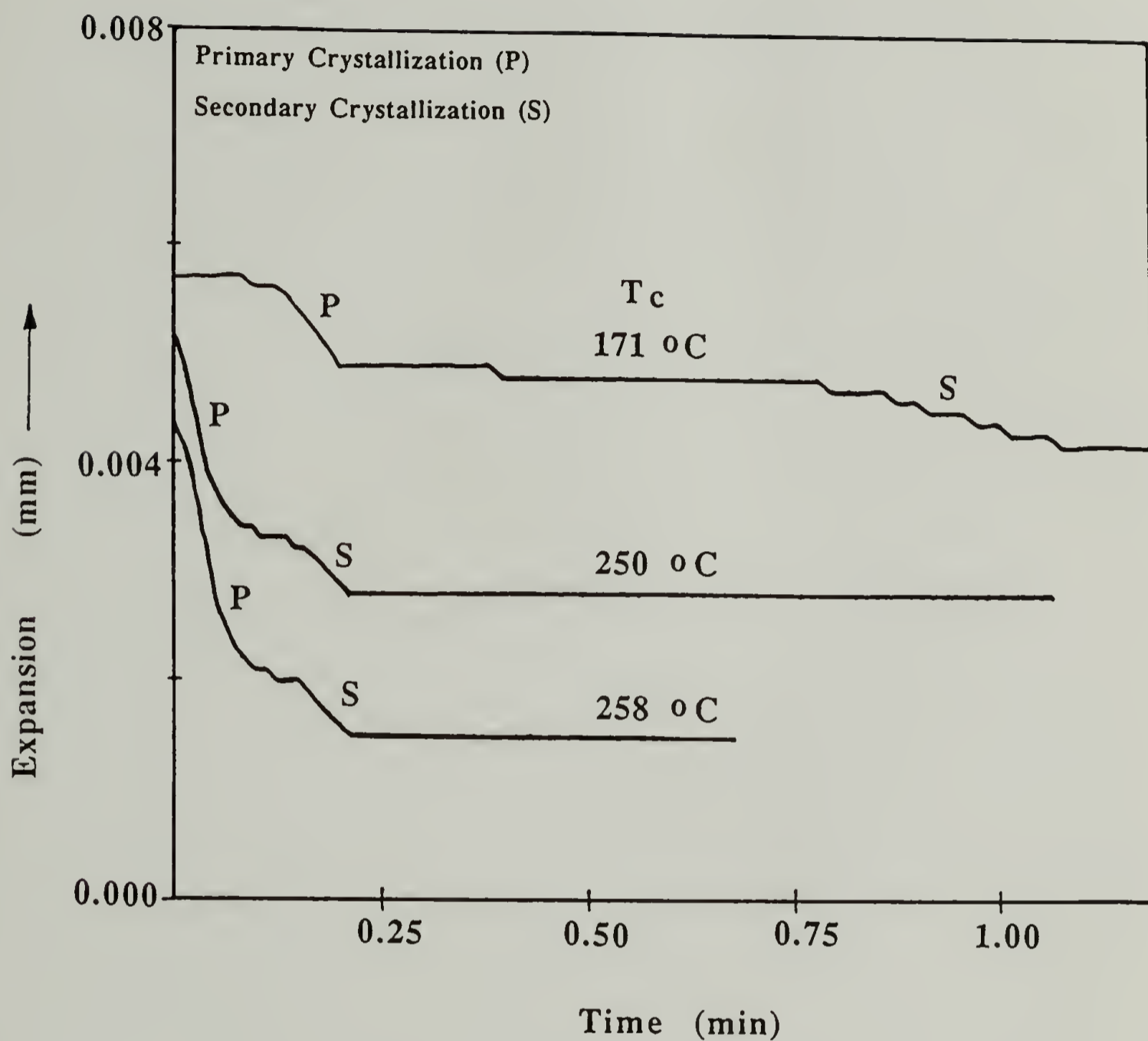


Fig. 3.2 Direct recorded TMA traces of PEEK during isothermal crystallization at T_c indicated. In the crystallization curves, the primary crystallization is denoted by "P", and the secondary crystallization is denoted by "S".

formation. Therefore, these two crystallization stages can not be distinguished due to overlap. However, for PEEK, the intraspherulitic crystallization started after or shortly before the impingement of spherulites, so that two crystallization stages are clearly distinguished. In principle, it is possible to test if the time where the primary crystallization concluded corresponds to the time where the impingement of PEEK spherulites occurred. Nevertheless, such observation by optical microscopy is very difficult at low T_c due to very high nucleation density (and hence very small size) of PEEK spherulites.¹

Fig. 3.2 also shows that as T_c is increased, the plateau between the primary and the secondary crystallization becomes shorter. This indicates the gradual overlap of these two stages with increasing T_c . It is also noted that as T_c is increased from 250 to 258 °C, the crystallization rate is actually decreased (this can be judged from the time at which the primary and the secondary crystallization concluded). Nevertheless, the plateau between these two crystallization stages still shortens with increasing T_c . This may imply that the PEEK chains participating in the secondary crystallization are more sensitive to temperature change than those participating in the primary crystallization. These two crystallization stages may overlap significantly at high T_c , such that they are not experimentally distinguishable.

The relative crystallinity can be evaluated from the TMA traces in Fig. 3.2. It is reasonable to assume that the crystallization proceeded isotropically in the film. Therefore, the relative crystallinity can be calculated from the change of the specimen thickness by

$$X_c = \frac{1 - (l/l_0)^3}{1 - (l_\infty/l_0)^3} \quad (3.1)$$

where l_0 is the initial specimen thickness, and l_∞ is the specimen thickness after the conclusion of the crystallization. Assuming that the two crystallization stages do not overlap, the secondary crystallinities of the three T_c s are evaluated directly from Fig. 3.2. The amount of the secondary crystals is found to be 37 %, 20%, and 16% of the total crystallinity for $T_c = 171$ °C, 250 °C, and 258 °C, respectively. This suggests that the secondary crystallinity decreases with increasing T_c . However, this disagrees with the conclusions derived from the Transmission Electron Microscopy (TEM)² and DSC⁵⁻⁶ showing that the secondary crystallinity indeed increased with T_c . In Fig. 3.2, it can be seen that the plateaus between the primary and the secondary crystallization are not really flat for the curves of $T_c = 250$ and 258 °C, indicating the overlap of these two crystallization stages. Thus, the secondary crystallinities calculated above for these two T_c s are underestimated. From the DSC study of the melting behavior of PEEK, it has been shown that the total crystallinity of PEEK ranged from ca. 30 to 40%.^{1,5-6} In addition, the enthalpy of fusion of the lower melting endotherm has been found to account for about 10% of the total enthalpy of fusion,⁵⁻⁶ which is lower than the relative crystallinity calculated above. This is due to that the secondary crystals underwent reorganization and recrystallization during DSC heating.⁵⁻⁶ The melting endotherm of these reorganized crystals merged with that of the primary crystals, so that the amount of the secondary crystals determined from the lower-melting endotherm was underestimated. Therefore, the amount of the secondary crystals determined by DSC should be less than that determined by TMA.

DSC is the most commonly used technique in studying the crystallization kinetics of polymers. It is thus instructive to compare the crystallization curves detected by DSC with that obtained by TMA. Fig. 3.3 are the DSC crystallization curves of PEEK during isothermal crystallization at T_c indicated in the figure. It can be seen that

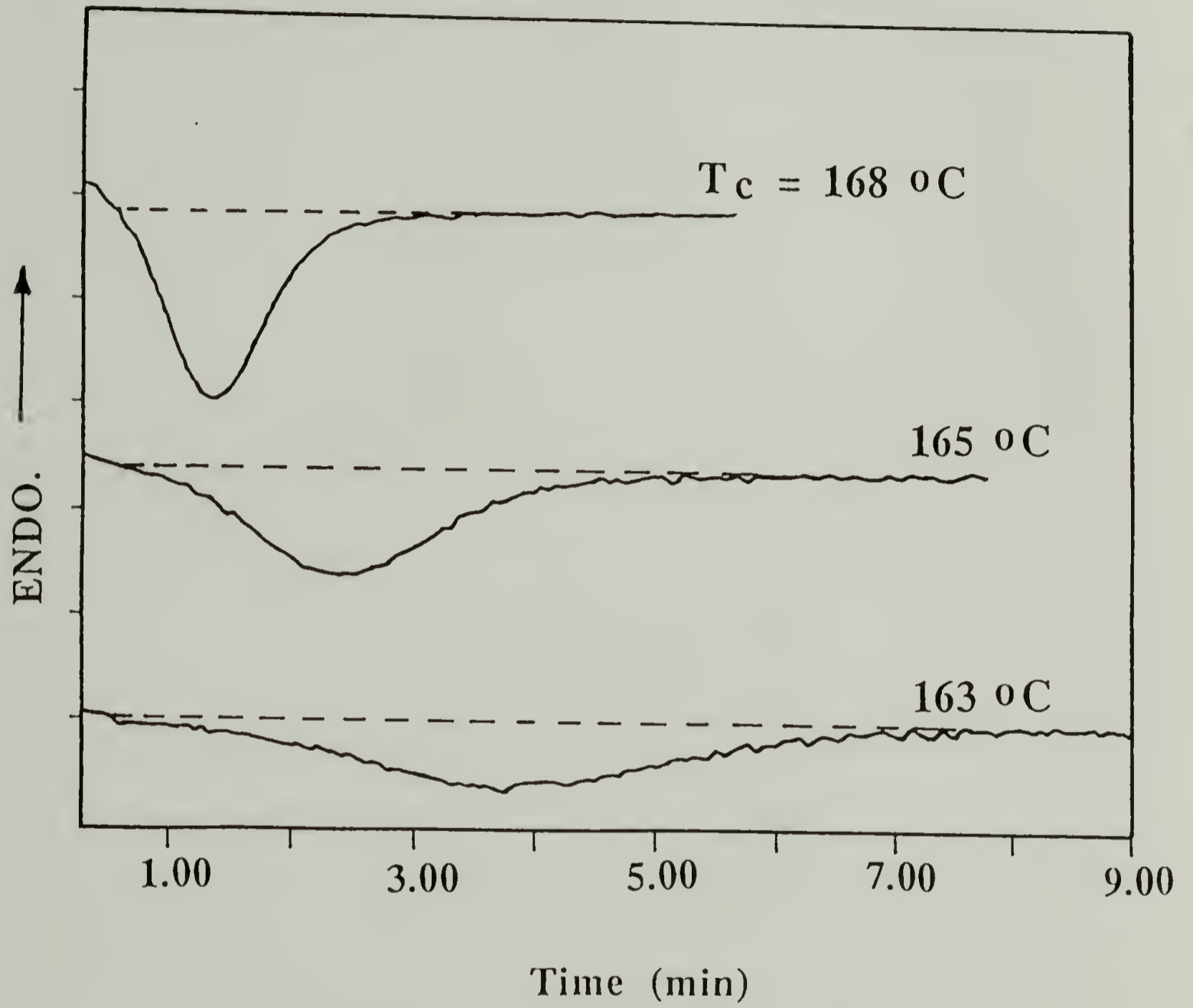


Fig. 3.3 DSC isothermal crystallization exotherms of PEEK at 163, 165, and 168 °C.

there is only one rather than two crystallization exotherms, in contrast to the TMA results. Fig. 3.3 shows that DSC is indeed not sensitive enough to resolve the two crystallization stages for PEEK. Nevertheless, for high T_c at which the primary and the secondary crystallization overlap significantly, the crystallization curve detected by DSC should be more reliable and close to the real crystallization curve.

3.3.2 Two-Stage Crystallization of PEEK in PEEK/PEI Blends

Before applying TMA to study the crystallization behavior of PEEK in PEEK/PEI blends, the DSC scans of the isothermally crystallized blends were recorded to gain the first glance on the crystallization of PEEK in the blends. Fig. 3.4 and 3.5 show the DSC thermograms of PEEK/PEI 90/10 and 50/50 blends scanned after isothermal crystallization at 270 °C for different times (t_c), respectively. Two melting endotherms still appear in the DSC thermograms, indicating that the two-stage crystallization behavior of PEEK does not disappear upon blending with PEI. A very interesting phenomenon in Fig. 3.5 has to be noted. It can be seen in the 50/50 blend that the lower melting endotherm does not appear in the thermogram for the crystallization time of 5 mins, while the higher melting endotherm has already existed. With increasing crystallization time, the lower melting endotherm gradually develops. This is an evidence showing that the lower-melting secondary crystals develops after the formation of the higher-melting primary crystals. Such clear distinction is not observed for 90/10 blend, since the lower melting endotherm has already developed at $t_c = 5$ mins.

Fig. 3.6 displays the direct recorded TMA traces of amorphous PEEK and PEEK/PEI blend films during isothermal crystallization at 191 °C. It is seen that the

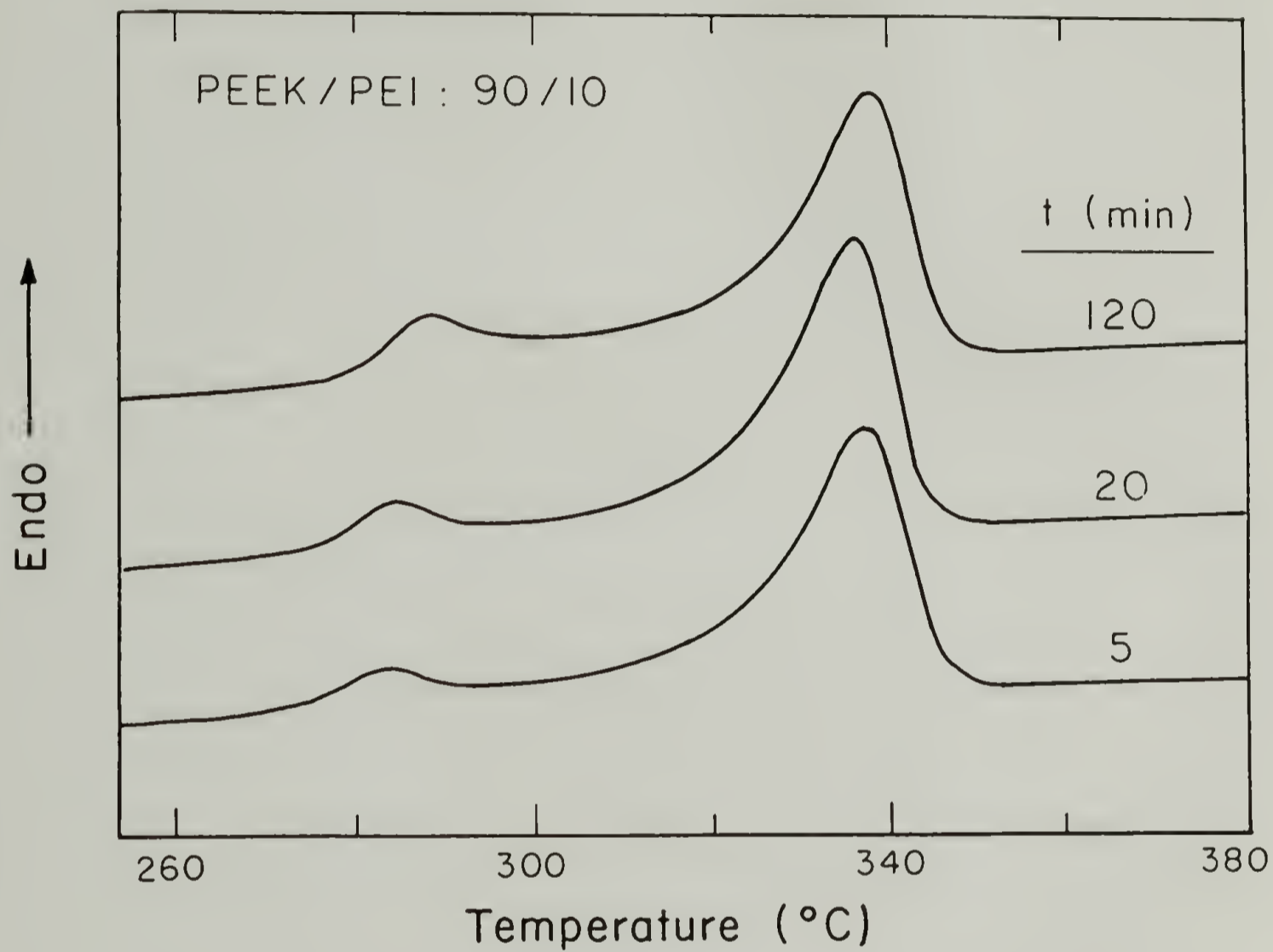


Fig. 3.4 DSC scans of PEEK/PEI 90/10 blend after crystallization at 270 °C for different times indicated.

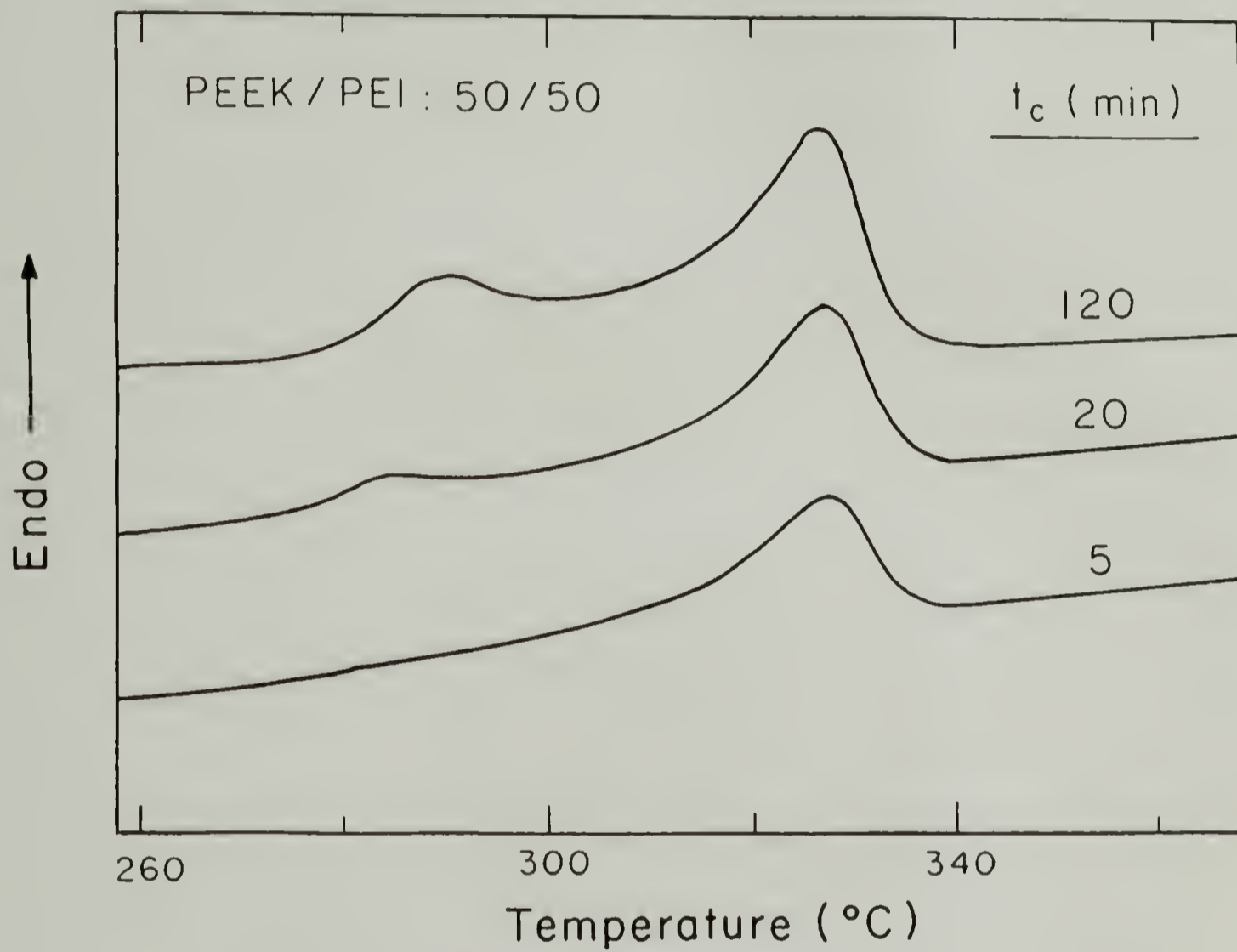


Fig. 3.5 DSC scans of PEEK/PEI 50/50 blend after crystallization at 270 °C for different times indicated.

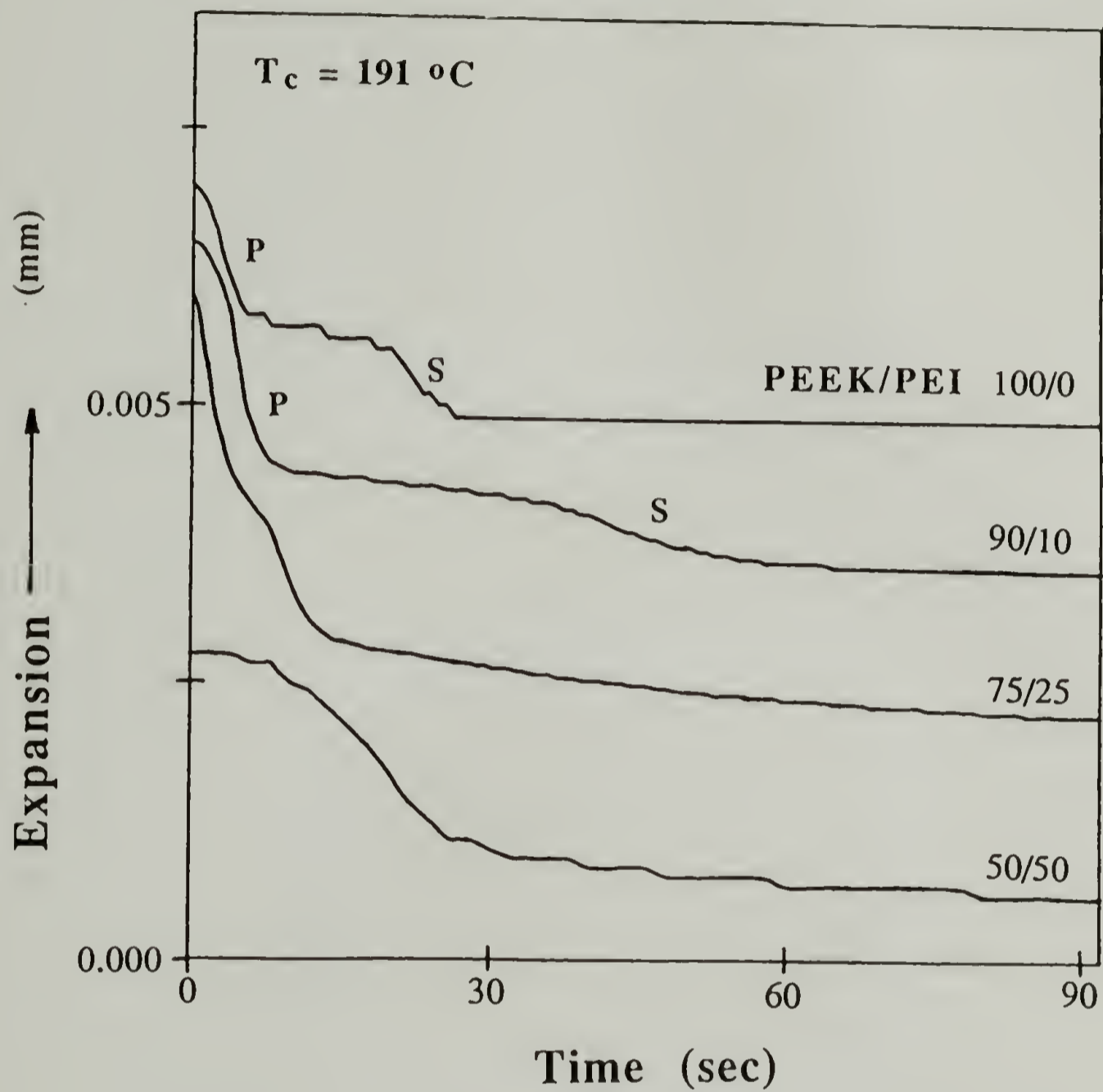


Fig. 3.6 Direct recorded TMA traces of PEEK/PEI blends during isothermal crystallization at $191\text{ }^\circ\text{C}$.

TMA crystallization curves of the blends are different from that of the pure PEEK. The distinction between the first and the second stage crystallization becomes obscure in the blends. As PEI concentration in the blends was increased to 50 wt%, the two crystallization stages become indistinguishable. This indicates the significant overlap of these two stages in the crystallization curves. Unlike in pure PEEK, the secondary crystallization in the blends appears to proceed longer before the conclusion of the primary crystallization.

The overlap of the two crystallization stages in the blends shows that the intraspherulitic crystallization took place before the impingement of PEEK spherulites. This phenomenon can be attributed to the depressions in both the PEEK nucleation density and the spherulite growth rate upon blending with PEI. Fig. 3.7 shows the optical micrographs of PEEK spherulites grown from pure PEEK and PEEK/PEI 75/25 blend at $T_c = 250$ °C. The average size of the spherulites grown from the blends is larger than that grown from the pure PEEK. This shows that blending with PEI decreases the nucleation density of PEEK crystallization. In addition, the spherulite growth studies, which will be described in Chapter 4, have shown that the spherulite growth rate of PEEK is also depressed by blending with PEI. These two observations indicate that the time required for the spherulites to impinge is longer in the blends. Therefore, for pure PEEK crystallized at 191 °C in Fig. 3.6, intraspherulitic crystallization actually took place after the impingement of the spherulites, so that the two crystallization stages can be distinguished. On the other hand, for the blends, intraspherulitic crystallization proceeded before the impingement of the spherulites. Therefore, an overlap of the primary and the secondary crystallization occurred making these two crystallization stages indistinguishable by TMA. These descriptions are concluded schematically in Fig. 3.8.



(a)



(b)

100 μm

Fig. 3.7 The optical micrographs of PEEK spherulites grown from (a) pure melt and (b) PEEK/PEI 75/25 blend.

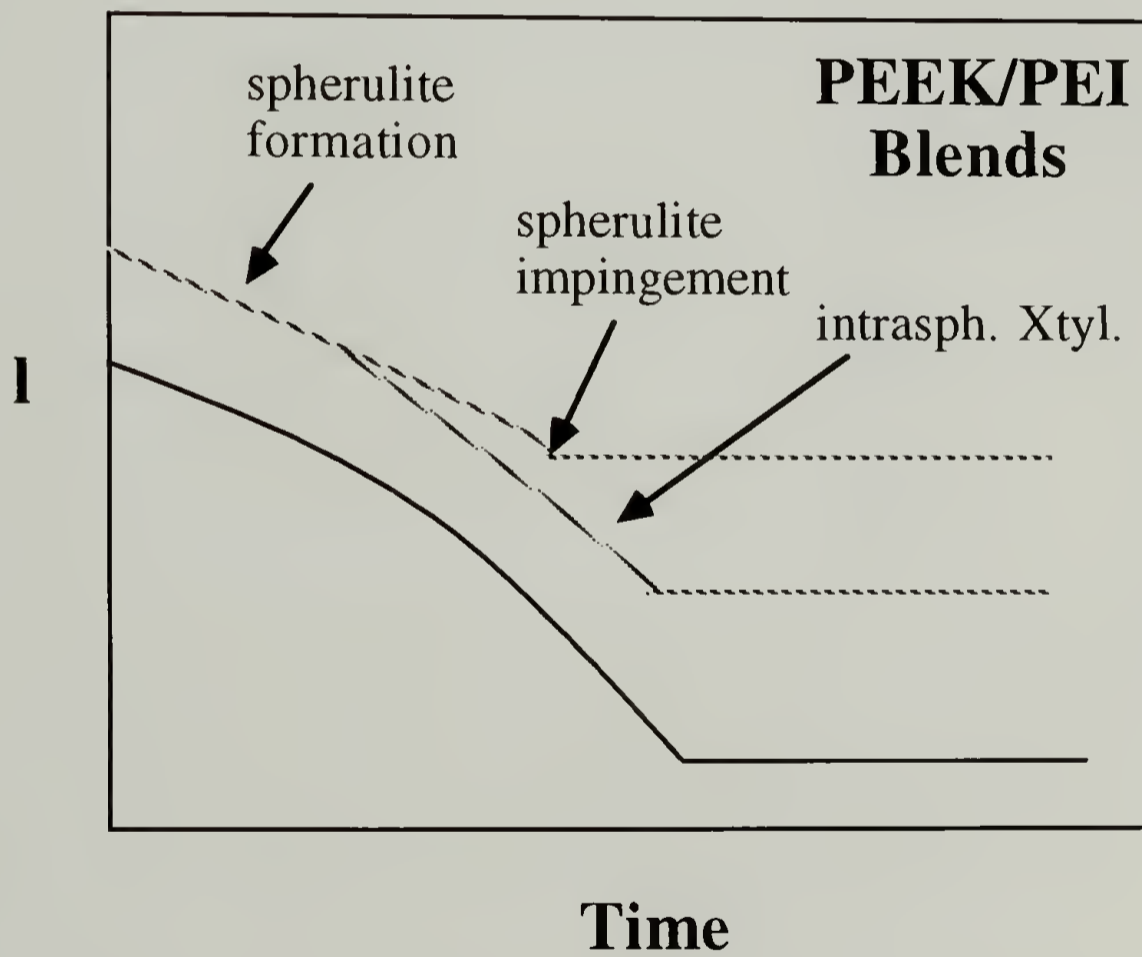
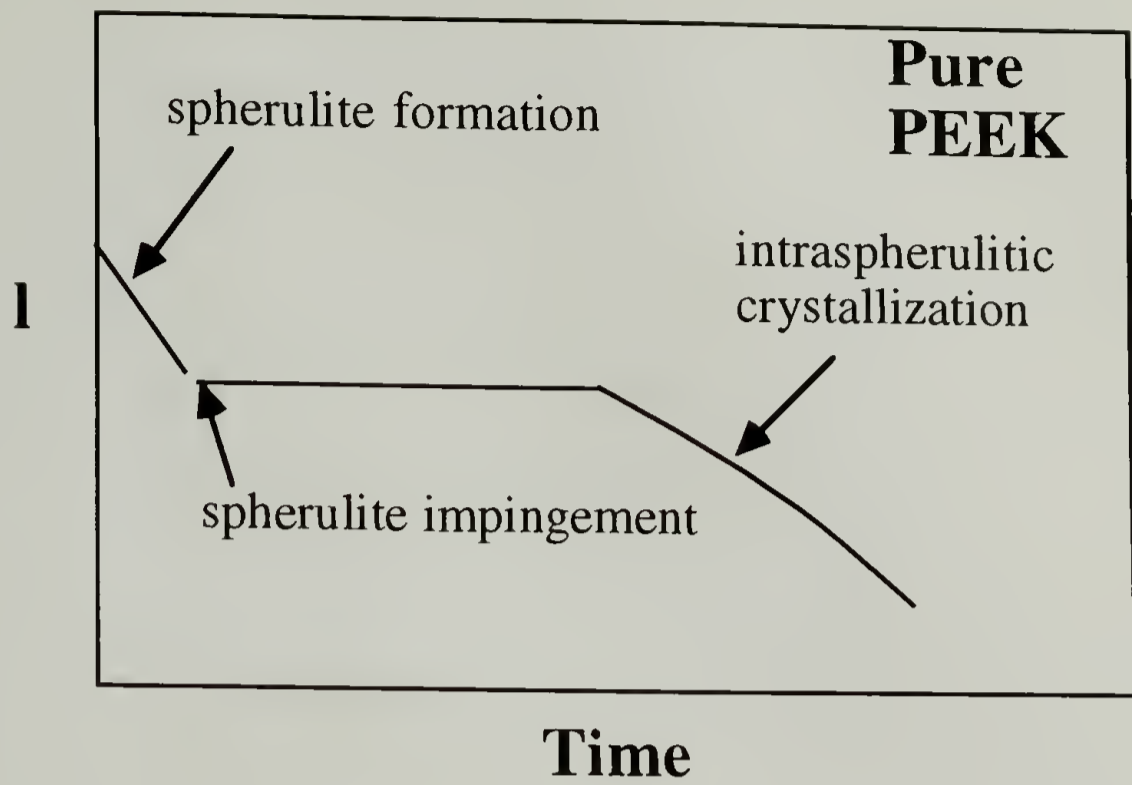


Fig. 3.8 The simulated TMA curves depicting the crystallization of PEEK in the pure melt and in its blends with PEI.

3.3.3 Two-Stage Crystallization Kinetics

Assuming that the crystallization proceeded isotropically in the film, the evolution of the relative degree of crystallinity can then be calculated by Eq. (3.1). Due to the limitation in obtaining high temperature by the oil bath, the T_c range studied by TMA was limited to 162 to 225 °C. The crystallization at high T_c (from 290 to 310 °C) was instead monitored by DSC. Although DSC is not sensitive enough to resolve the two PEEK crystallization stages at low T_c , the crystallization curves detected by DSC at high T_c should be close to the real crystallization curve due to the significant overlap of these two crystallization stages.

A crystallization model proposed by Price¹⁵ is adopted here for the data analysis. This model is an Avrami theory modified by considering the secondary crystallization. Spherulite formation is regarded as the primary crystallization, and the intraspherulitic crystallization is regarded as the secondary crystallization. In the original Price model the relative crystallinity at time t is given by

$$X(t) = \int_0^t [1 - ce^{-k_i^m(t-\tau)^m}] nk_s^n \tau^{n-1} e^{-k_s^n \tau^n} d\tau \quad (3.2)$$

where c is the total relative crystallinity developed in the secondary crystallization, k_i and k_s are the rate constants of the intraspherulitic crystallization and spherulite formation respectively, m and n are the exponents of the intraspherulitic crystallization and the spherulite formation, respectively. Eq. (3.2) assumed that the intraspherulitic crystallization took place immediately after the spherulite was formed. This is apparently not the case encountered in PEEK and PEEK/PEI blends. As shown in Fig. 3.2, there is an induction time before the occurrence of the secondary crystallization. A slight modification is therefore required to account for this induction

time, t_i . Since only primary crystallization takes place at time $t < t_i$, the crystallinity development is simply given by the Avrami equation as:

$$X(t) = 1 - ce^{-k_s^n t^n} \quad (3.3)$$

At time $t > t_i$, the total crystallinity is given by Eq. (3.3) plus Eq. (3.2), but note that the lower integration limit in Eq. (3.2) should be changed from 0 to t_i :

$$X(t) = 1 - ce^{-k_s^n t_i^n} + \int_{t_i}^t [1 - ce^{-k_i^m (t-\tau)^m}] nk_s^n \tau^{n-1} e^{-k_s^n \tau^n} d\tau \quad (3.4)$$

The parameters representing the rates of the primary and the secondary crystallization are k_s and k_i , respectively, which are obtained by curve fitting of Eq. (3.3) and (3.4) to the data. The curve fittings were performed by the least square method. The values of n chosen for the fit were estimated from the initial slopes of the Avrami plot. It was found that $n = 2.8 \pm 0.5$ for the crystallization at 290 to 310 °C. Thus, $n = 3$ was chosen for this T_c range, which signifies a thermodynamically-controlled crystallization with heterogeneous nucleation and spherical growth geometry. This value of n also agrees with the prior studies on the crystallization kinetics of PEEK by Avrami analysis.^{6,16-17} For the crystallization at 162 to 225 °C, n was found to be 1.7 ± 0.5 from the Avrami plot. Since the crystallization is diffusion controlled in this T_c range,¹⁶ $n = 1.5$ was chosen to signify a diffusion-controlled crystallization with heterogeneous nucleation and spherical growth geometry. For the values of m , because of the spatial restrictions imposed by the primary crystals, the dimensionality of the growth is reduced.¹⁸ Here $m = 2$ (thermodynamically-controlled with heterogeneous nucleation and disk growth geometry) was chosen for the T_c range of 290 to 310 °C, and $m = 1$ (diffusion-controlled) was chosen for the T_c range of 160 to 225 °C. The initial guesses of the

rate constants k_s and k_i have been recommended to be obtained from the two intercepts in the Avrami plot.¹⁹

Typical fits of the Price model to the data are shown in Fig. 3.9. It can be seen that the Price model does give a better fit to the data than the conventional Avrami equation. The k_s and k_i are plotted against T_c for different blend compositions in Fig. 3.10 to 3.13. Fig. 3.10 and 3.11 display the plot in the T_c range of 162 to 225 °C. Both k_s and k_i increase with increasing T_c , indicating a diffusion-controlled crystallization. Fig. 3.12 and 3.13 show the plot in the T_c range of 290 to 310 °C. Both k_s and k_i decrease with increasing T_c , depicting a thermodynamically-controlled crystallization. From Fig. 3.10 to 3.13, it can also be seen that, in general, the intraspherulitic crystallization proceeded slower than the spherulite formation at a given T_c . It has to be noted that sometimes curve fitting may not give meaningful values of k_s and k_i , and hence it is necessary to justify the obtained values of k_s and k_i to see if they are meaningful.¹⁹ This can be achieved by comparing the values of k_s and k_i obtained for different T_c , as suggested by Hsiao.¹⁹ We believe that the k_s and k_i shown in Fig. 3.10 to 3.13 are meaningful since (1) they exhibit normal temperature dependence, i.e., they increase with T_c in the diffusion-controlled crystallization and decrease with T_c in the thermodynamically-controlled crystallization, (2) the order of magnitude of k_s agrees with that reported in the prior studies by Avrami analysis,⁶ and (3) they decrease with increasing PEI concentration in the blends. Therefore, the values of k_s and k_i obtained here are meaningful.

Fig. 3.14 is an overlay plot of logarithmic rate constants vs. T_c for PEEK and 75/25 blend. It can be seen that in the thermodynamically controlled T_c range, k_i is close to k_s for both PEEK and the blend at a given T_c . However, in the diffusion controlled T_c range the difference between k_i and k_s becomes clear. The difference

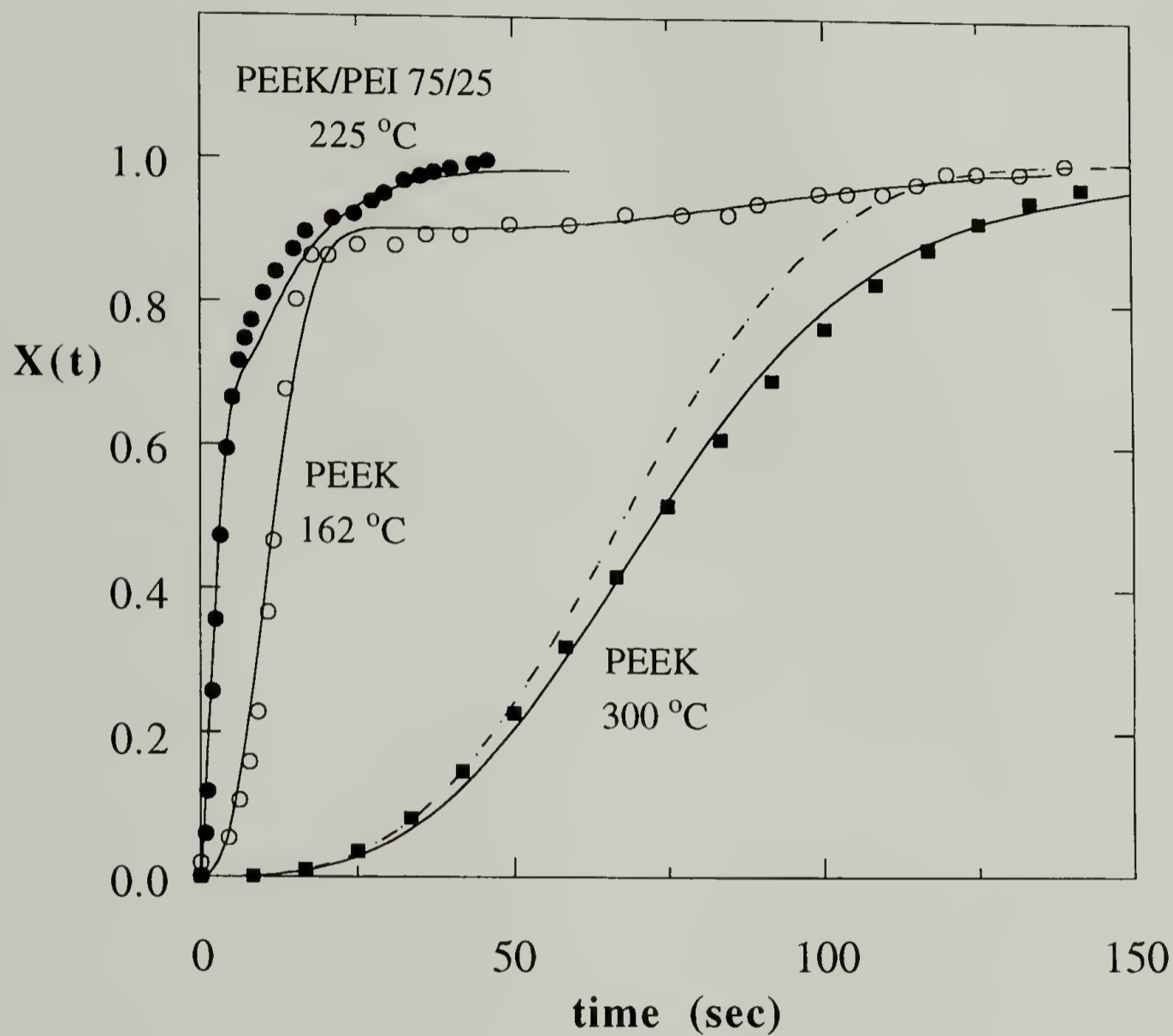


Fig. 3.9 Relative degree of crystallinity vs. time plot of PEEK/PEI blends. The composition and the T_c are indicated in the figure. The solid lines are the results obtained by Price model fit. For PEEK at $T_c = 300$ °C the dash line is the fit by the Avrami equation.

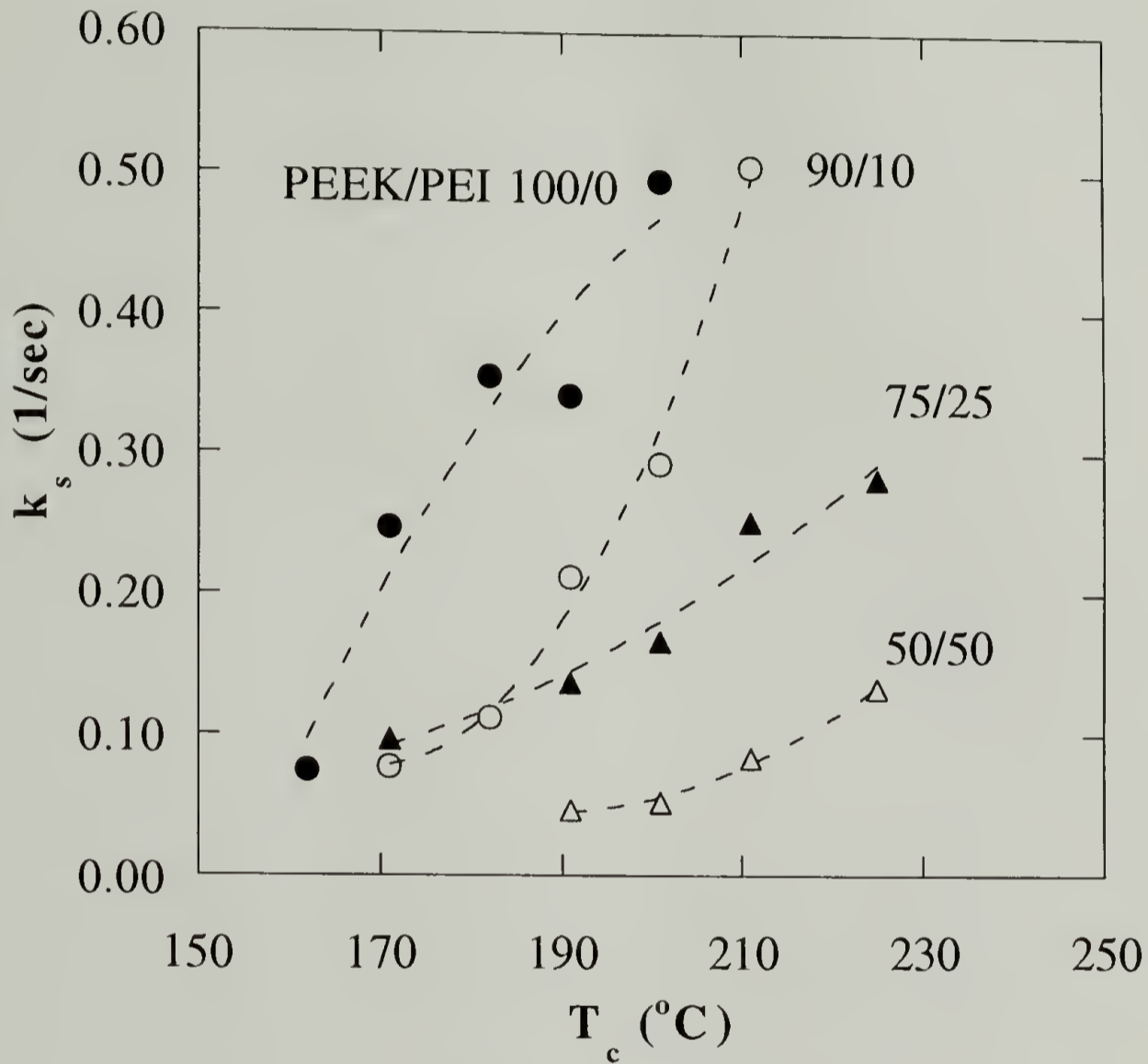


Fig. 3.10 Variations of k_s with T_c for PEEK/PEI blends in the temperature range between 162 and 225 °C.

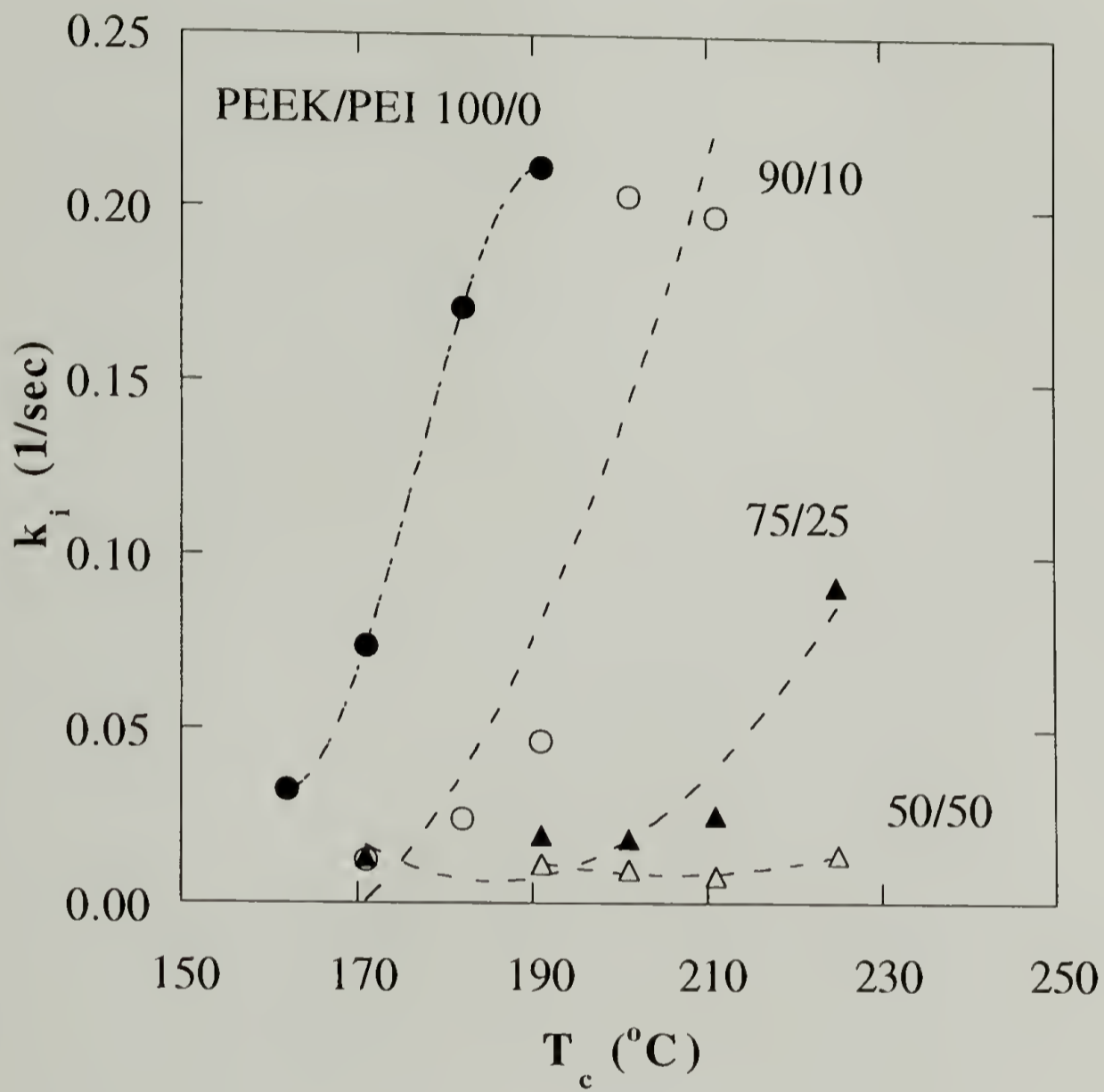


Fig. 3.11 Variations of k_i with T_c for PEEK/PEI blends in the temperature range between 162 and 225 °C.

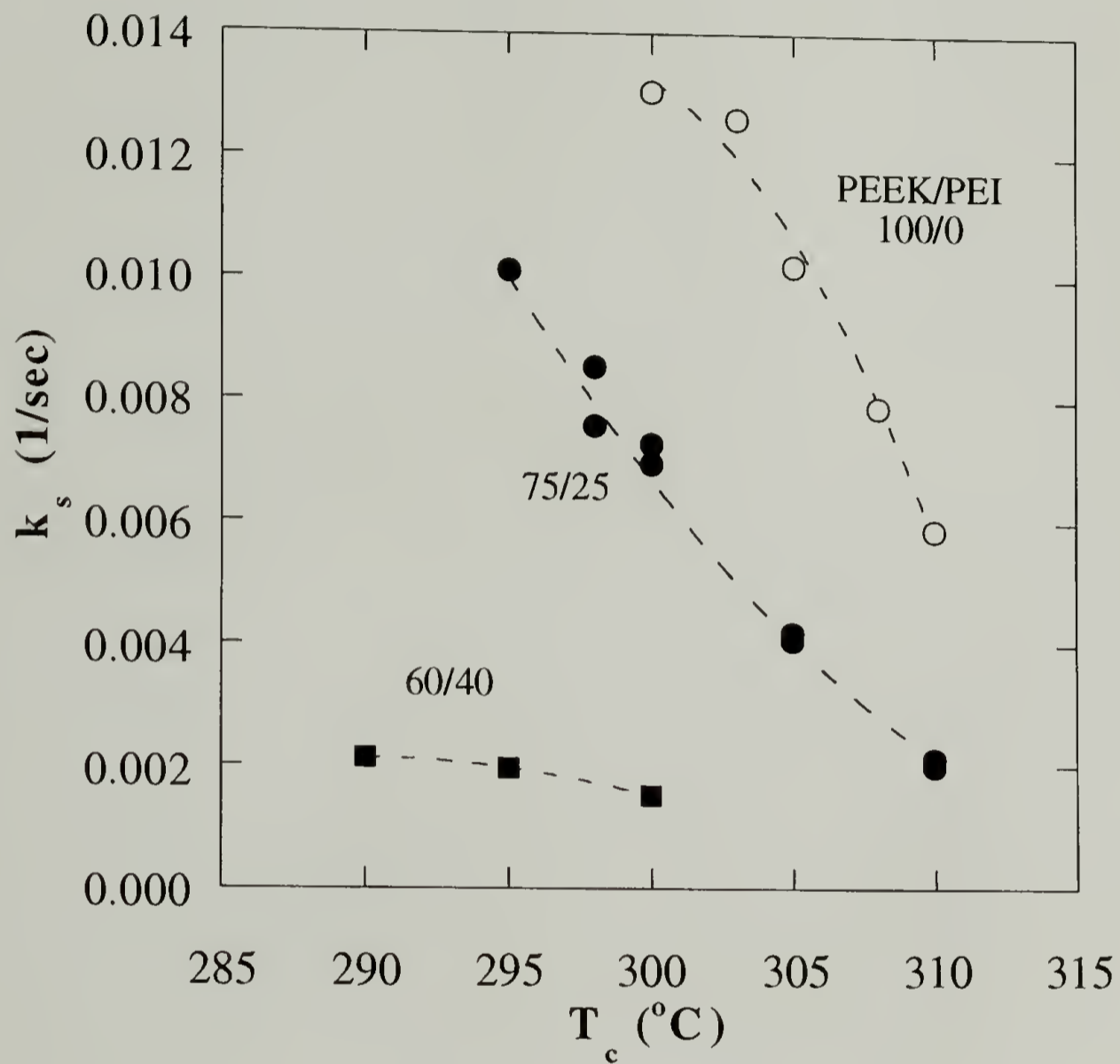


Fig. 3.12 Variations of k_s with T_c for PEEK/PEI blends in the temperature range between 290 and 310 $^{\circ}\text{C}$.

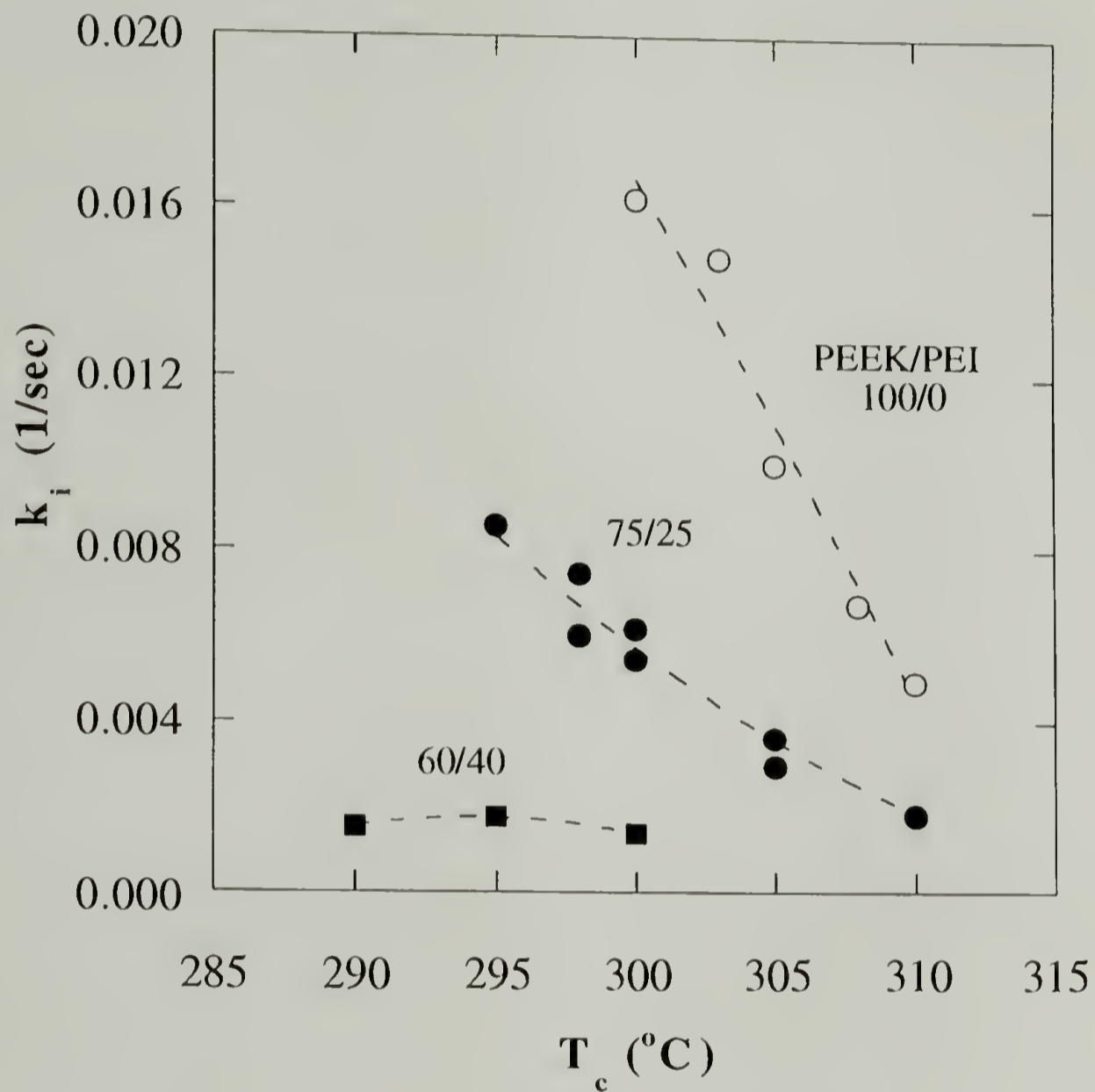


Fig. 3.13 Variations of k_i with T_c of PEEK/PEI blends in the temperature range between 290 and 310 °C.

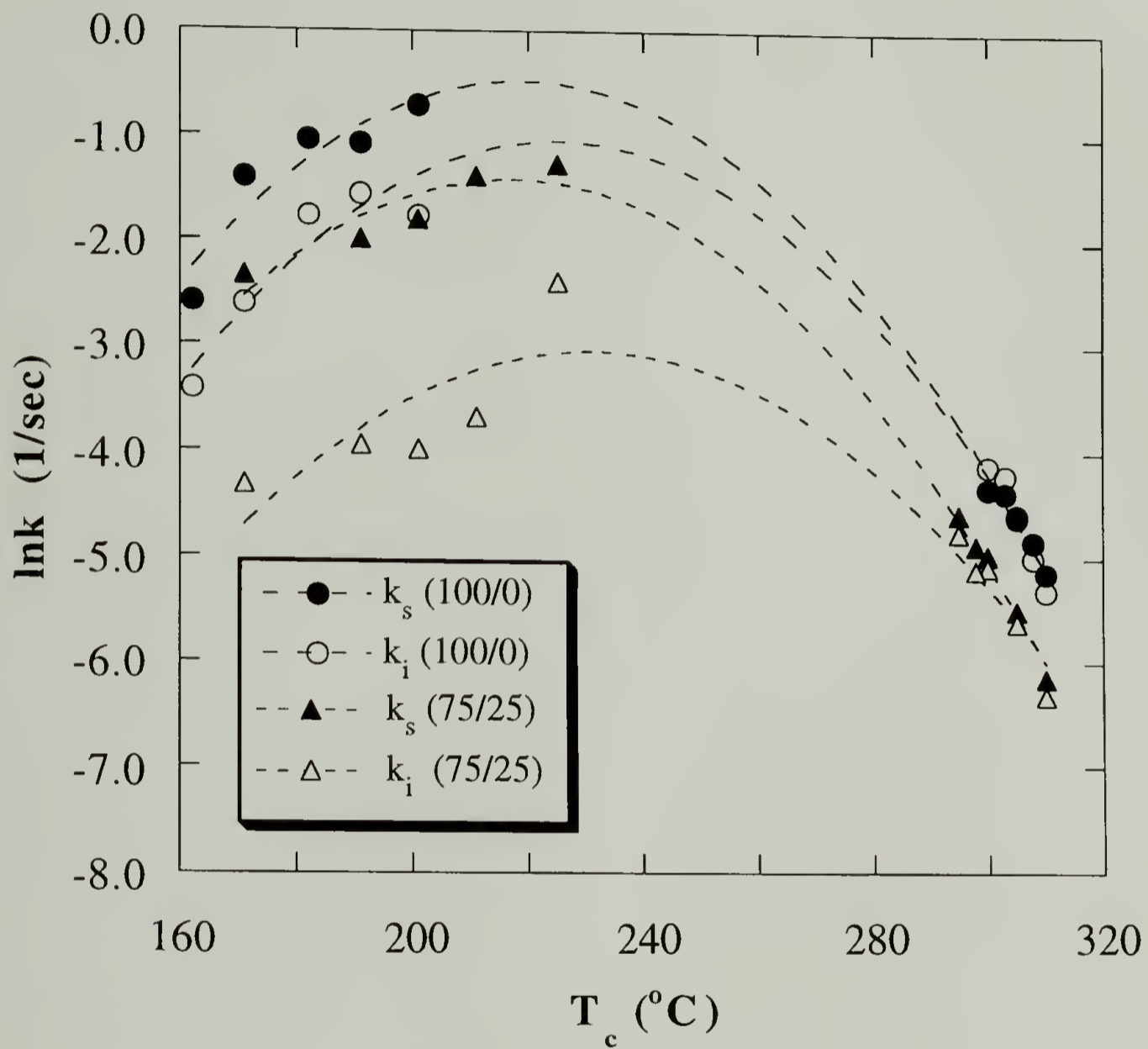


Fig. 3.14 Overlay plot of logarithmic rate constants vs. T_c of PEEK/PEI blends.

between k_i and k_s is larger for the blend than that for pure PEEK in this T_c range. A parameter β has been defined in the Price model to signify the relative rate of the intraspherulitic crystallization to the spherulite formation, $\beta = k_i / k_s$.¹⁵ The average value of β of PEEK in the T_c range of 162 to 201 °C is about 0.44, whereas that of PEEK in the T_c range of 300 to 310 °C is about 1.0. Comparing these values of β , it can be seen that the intraspherulitic crystallization proceeded about two times slower than the spherulite formation in the diffusion-controlled crystallization. On the other hand, these two crystallization stages proceeded nearly as fast as each other in the thermodynamically-controlled crystallization.

The schematic descriptions of the two-stage crystallization behavior of pure PEEK is shown in Fig. 3.15(a). It can be seen that the secondary crystallization of PEEK is restricted by the constraints imposed by the primary crystals. Therefore, the diffusion of the chain segments participating in the secondary crystallization is more difficult than those participating in the primary crystallization. In the diffusion-controlled crystallization, the chain mobility is the dominant role in determining the overall crystallization rate. The secondary crystallization is hence slower than the primary crystallization at low T_c . On the other hand, in the thermodynamically-controlled crystallization, the thermal energy imparted on the chains can easily overcome the diffusion barrier. Therefore, the rate of the secondary crystallization is comparable to that of the primary crystallization.

The relative rate of the secondary crystallization to the primary crystallization in the 75/25 blend is even smaller than that in pure PEEK. This can also be reflected by the value of β of the blend. The average value of β of 75/25 blend in the T_c range of 171 to 225 °C is about 0.15, and that in the T_c range of 295 to 310 °C is about 0.85. Comparing the values of β of 75/25 blend with that of PEEK, it can be seen that β of

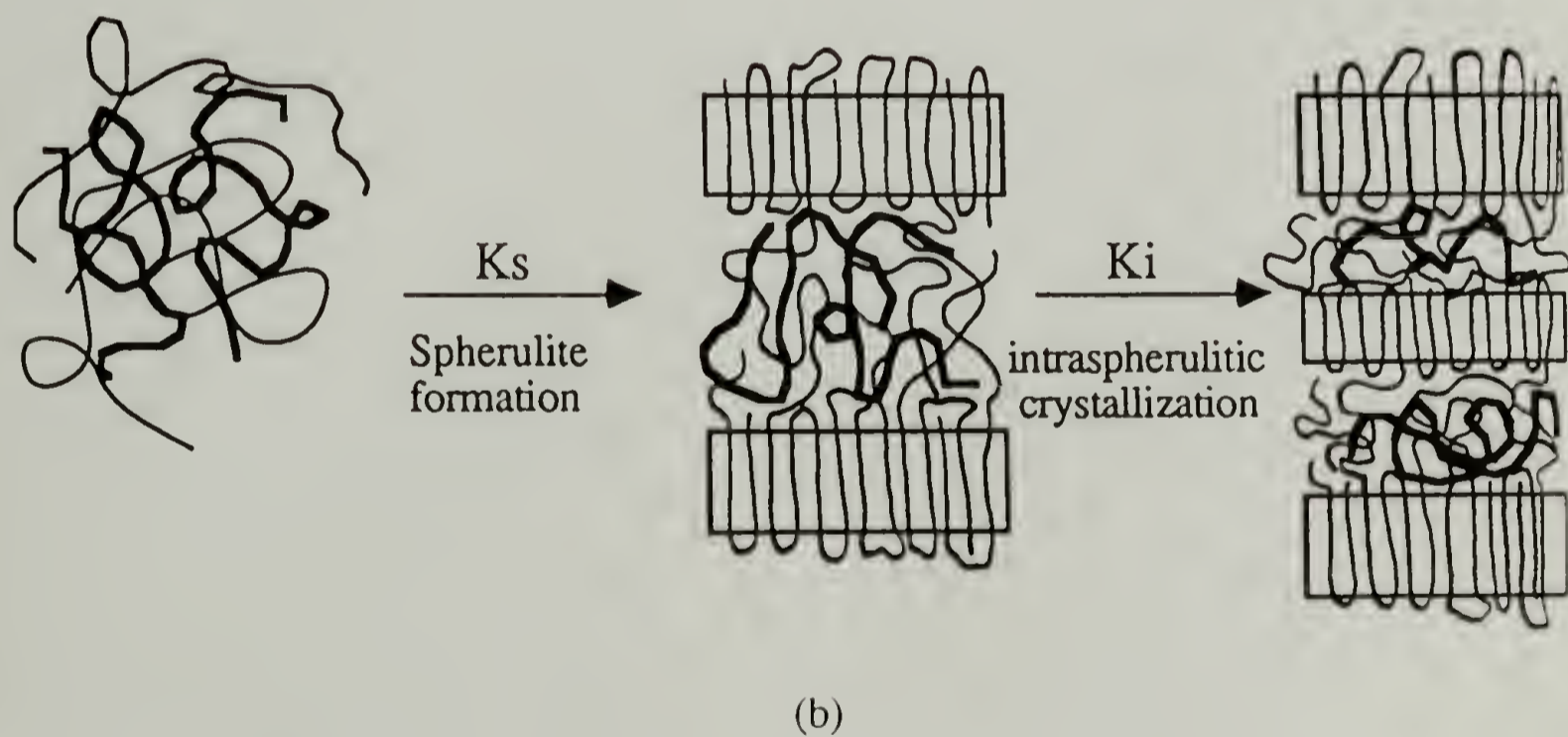
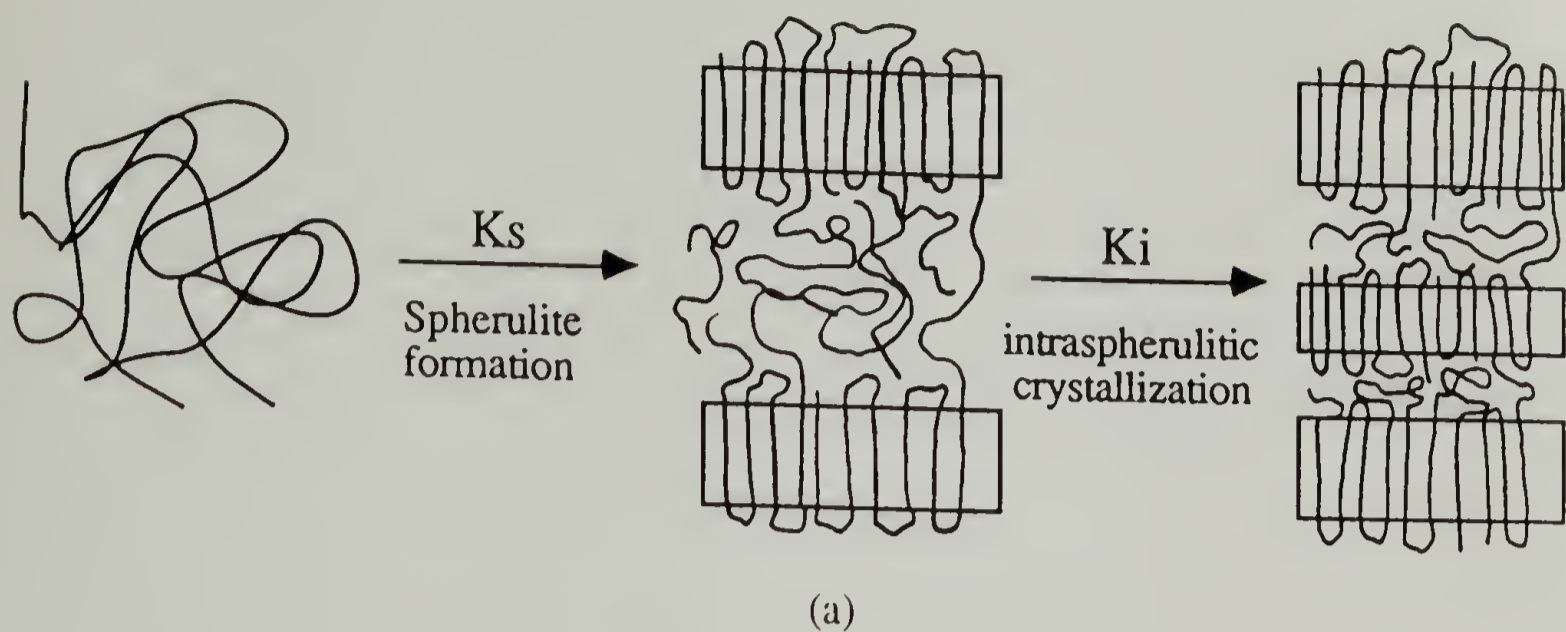


Fig. 3.15 Schematic descriptions of the two-stage crystallization behavior of PEEK in (a) the pure state, and in (b) the blends with PEI.

the 75/25 blend is about three times smaller than that of pure PEEK in the diffusion-controlled crystallization. On the other hand, β of the blend is close to that of pure PEEK in the thermodynamically-controlled crystallization. This indicates that blending with PEI has induced a stronger depression in the secondary crystallization rate than in the primary crystallization rate.

This observation can be rationalized from Fig. 3.15(b) which displays the two-stage crystallization of PEEK in the blends. The morphological study which will be described in Chapter 5 indicates that full segregation of PEI from the interlamellar regions of PEEK crystals did not occur, and some PEI molecules were still trapped in the interlamellar regions after PEEK crystallization. Therefore, the amorphous phase from which the secondary crystallization took place was a miscible amorphous phase. The crystallization in the miscible blends requires a mutual diffusion to transport the crystallizable component to the growth front and reject the amorphous component away.¹⁴ The PEEK primary crystals imposed a spatial restriction making this mutual diffusion in the interlamellar regions more difficult than in the fully amorphous phase. In addition, depending on the distance of segregation, the gradual rejection of PEI during PEEK crystallization could induce an accumulation of PEI in the crystal growth front. Consequently, the concentration of PEI in the interlamellar regions could be higher than that of the initial concentration. Due to this accumulation effect and the increased difficulty in mutual diffusion imposed by the primary crystals, the diffusion barrier in the secondary crystallization in the blend was increased by an even larger extent comparing to that in pure PEEK. Therefore, lower value of β is observed in the blend in the diffusion-controlled crystallization.

3.4 Conclusions

The two-stage crystallization behavior of PEEK and PEEK/PEI blends has been studied by TMA. The two crystallization stages of PEEK are clearly distinguished by measuring the variation of film thickness with time during isothermal crystallization. These two crystallization stages can not be readily distinguished by DSC. Blending with PEI obscures the distinction of these two crystallization stages by TMA, due to the depressions in both nucleation density and spherulite growth rate.

The crystallization kinetics of these two crystallization stages have also been studied. The results indicate that the PEEK chains participating in the secondary crystallization is more sensitive to mobility change. In the diffusion controlled T_c range, the secondary crystallization proceeds slower than the primary crystallization, due to the increased difficulty in diffusion as a result of the spatial constraint imposed by the primary crystals. In the thermodynamically controlled T_c range, the secondary crystallization rate is comparable to the primary crystallization rate. Blending with PEI induces a stronger depression in the secondary crystallization rate than in the primary crystallization rate. This is ascribed to the hindrance in mutual diffusion due to the spatial restriction imposed by the PEEK primary crystals and likely the accumulation of PEI in the amorphous phase during PEEK crystallization.

References

1. Blundell, D. J.; Osborn, B. N. *Polymer* **1983**, 24, 953.
2. Bassett, D. C.; Olley, R. H.; Al Raheil, I. A. M. *Polymer* **1988**, 29, 1745.
3. Marand, H.; Prasad, A. *Macromolecules* **1992**, 25, 1731.
4. Lovinger, A. J.; Hudson, S. D.; Davis, D. D. *Macromolecules* **1992**, 25, 1752.
5. Cheng, S. Z. D.; Cao, M.-Y.; Wunderlich, B. *Macromolecules* **1986**, 19, 1868.
6. Lee, Y., Ph.D. Thesis, Univ. of Mass., Amherst, Mass., **1988**.
7. Mdedllin-Rodriguez, F. J.; Philips, P. J. *Polym. Eng. Sci.* **1990**, 30, 860.
8. Cheng, S. Z. D.; Wu, A. Q.; Wunderlich, B. *Macromolecules* **1987**, 20, 2802.
9. Boon, J.; Azcue, J. M. *J. Polym. Sci., Part A* **1968**, 6, 885.
10. Wang, T. T.; Nishi, T. *Macromolecules* **1977**, 10, 421.
11. Calahorra, E.; Cortazar, M.; Guzman, G. M. *Polymer* **1982**, 23, 1322.
12. Alfonso, G. C.; Russell, T. P. *Macromolecules* **1986**, 19, 1143.
13. Chow, T. S. *Macromolecules* **1990**, 23, 333.
14. Saito, H.; Okada, T.; Hamane, T.; Inoue, T. *Macromolecules* **1991**, 24, 4446.
15. Price, F. P. *J. Polym. Sci., Part A* **1965**, 3, 3079.
16. Cebe, P.; Hong, S.-D. *Polymer* **1986**, 27, 1183.
17. Day, M.; Deslandes, Y.; Roovers, J.; Suprunchuk, T. *Polymer* **1991**, 32, 1258.
18. Hsiao, B. *J. Polym. Sci., Polym. Phys. Ed.* **1993**, 31, 237.

CHAPTER 4

SPHERULITE GROWTH KINETICS IN PEEK/PEI BLENDS

4.1 Introduction

The crystallization kinetics described in Chapter 3 is the macroscopic kinetics. The obtained rate constants contain both the nucleation rate and crystal growth rate.¹⁻² In this chapter, the crystal growth kinetics of PEEK from both the pure melt and PEEK/PEI blends are isolated by monitoring the spherulite development using cross-polarized optical microscopy. The investigation of crystal growth is of great interest, since it can provide the information on the crystallization mechanism and the molecular parameters such as the fold surface free energy and the work of chain folding.³ In this chapter, the study of the spherulite growth kinetics of PEEK/PEI blends is reported. The spherulite growth rates are analyzed by a modified Lauritzen-Hoffman theory which considers the effect of diluent on the crystal growth.⁴ Crystallization regime behavior and the obtained molecular parameters are discussed.

4.2 Background

4.2.1 General Considerations

The addition of an amorphous polymer to a crystalline polymer can have dramatic effects on the thermodynamic and kinetic parameters governing the crystal growth.

First, the presence of the specific interaction lowers the equilibrium M.P., which leads to a change in the free energy for formation of secondary nuclei.⁴⁻⁸ Furthermore, depending on the T_g s of the pure components, crystal growth of the crystalline component may either be enhanced or be hindered due to the change in molecular mobility.⁴⁻⁸

The theory of crystal growth kinetics for pure homopolymers has been developed by Lauritzen and Hoffman.³ The growth kinetics for crystalline/amorphous polymer blends have also been formulated with minor modification by taking account of the equilibrium M.P. depression and the change in T_g .^{5,7} More considerations on the diffusion mechanism have also been proposed.^{6,8} During the crystallization of the crystalline component, the amorphous component should diffuse away from the crystal growth front, i.e., exclusion should take place at least in an order of the lamellar size. This diffusion effect on the crystal growth in crystalline/amorphous polymer blends has been considered by Alfonso and Russell.⁶

Recently, Saito et al.⁸ have considered the diffusion mechanism in the crystal growth in crystalline/amorphous blends. According to the Lauritzen-Hoffman theory,³ the crystal growth is governed by two elementary steps: (1) secondary nucleation, formation of the secondary nuclei by depositing the first stem on the crystal growth front and (2) surface spreading, spread of the following stems on the existing crystal surface after the secondary nuclei have formed. A simple scheme of the crystal growth in crystalline/amorphous blends is shown in Fig. 4.1. In the secondary nucleation, the crystalline segments must diffuse into the nucleation sites, and the amorphous component must diffuse away from the crystal growth front to accommodate the secondary nucleation. This type of diffusion is a mutual diffusion.⁸

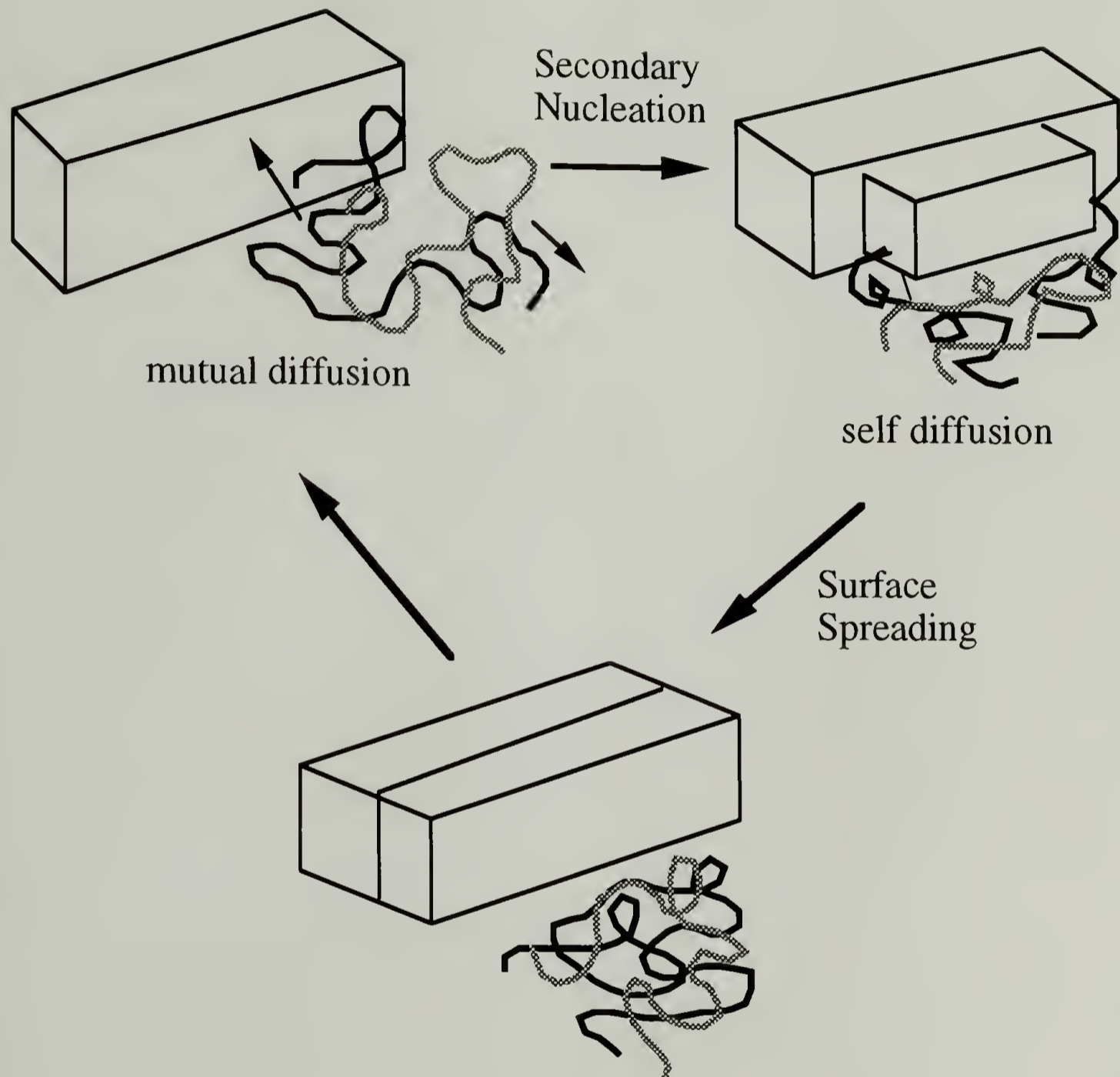


Fig. 4.1 Crystal growth in crystalline/amorphous polymer blends.

In the surface spreading, the segments attached on the crystal surface should pull out the residual segments remained in the melt, and this is a self-diffusion process.⁸ These two types of diffusion have been considered by Saito et al. in formulating the growth rate for the crystalline/amorphous polymer blends.⁸

Although there are complicated diffusions involved in the crystal growth in crystalline/amorphous blends, the consideration of T_g change is normally sufficient to provide a satisfactory description for mobility term of the crystal growth rate. This is because in most cases, the crystallization temperatures of interest are located in the thermodynamically-controlled region in which the mobility is of secondary importance. In the diffusion-controlled crystallization region, the spherulite growth is normally too difficult to follow due to high nucleation density (and hence small spherulite size).

4.2.2 Crystal Growth Rate and Growth Regimes

The crystal growth rate of a homopolymer is given by³

$$G = G_0 \exp\left[-\frac{U^*}{R(T_c - T_0)}\right] \exp\left[-\frac{K_g}{T_c(T_m^0 - T_c)f}\right] \quad (4.1)$$

The first exponential term is the mobility term, and the second exponential term is the thermodynamic term governed by the thermodynamic driving force of secondary nucleation. In Eq. (4.1), U^* is the activation energy required to transport the chain segments across the solid-liquid interface, T_0 is the temperature at which such transport ceases, f is a correction factor for the temperature dependence of Δh_f^0 , $f = 2T_c/(T_m^0 + T_c)$, and K_g is a nucleation constant given by

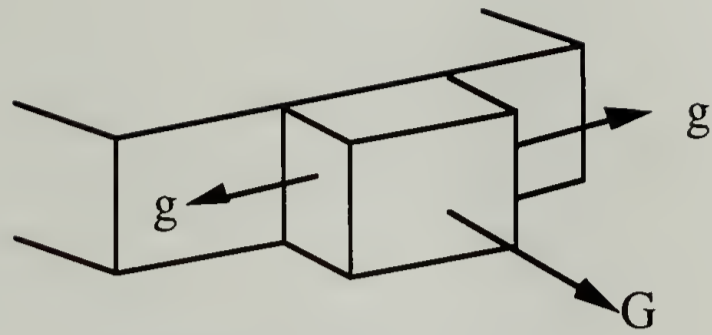
$$K_g = \frac{\alpha b_0 \sigma \sigma_e T_m^0}{k_B \Delta h_f^0} \quad (4.2)$$

where σ and σ_e are the side and fold surface free energy, respectively, b_0 is the monomolecular thickness, and α is a constant depending on the growth regime. It can be seen that K_g contains the surface free energies. Therefore, the analysis of the crystal growth rate is able to determine the crystal surface free energies.

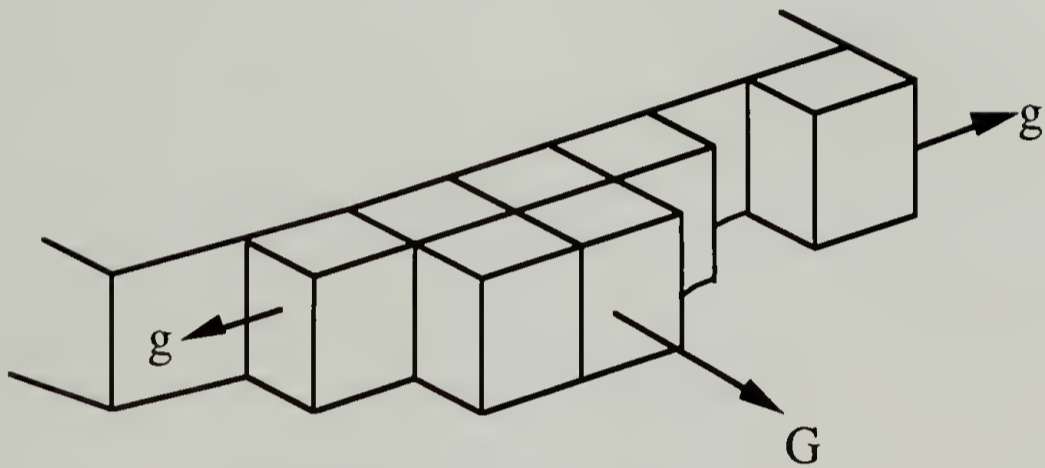
Depending on the crystallization temperatures (T_c) (and hence the degree of supercooling), crystal growth in polymers can be separated into three regimes.^{3,9} The three different regimes are shown in Fig. 4.2. At high T_c , the degree of supercooling is low, therefore the driving force for crystallization is small. In this case, the secondary nucleation (i) proceeds much slower than the surface spreading (g), and hence the overall growth rate is controlled by i, i.e., $G \sim i$. This is called regime I, and α in Eq. (4.2) for regime I is 4.

At medium degree of supercooling, the secondary nucleation can proceed at a comparable rate to the surface spreading, i.e., $i \approx g$. The growth rate is therefore proportional to $(ig)^{1/2}$.¹ This is called regime II, and α in Eq. (4.2) for regime II is 2.

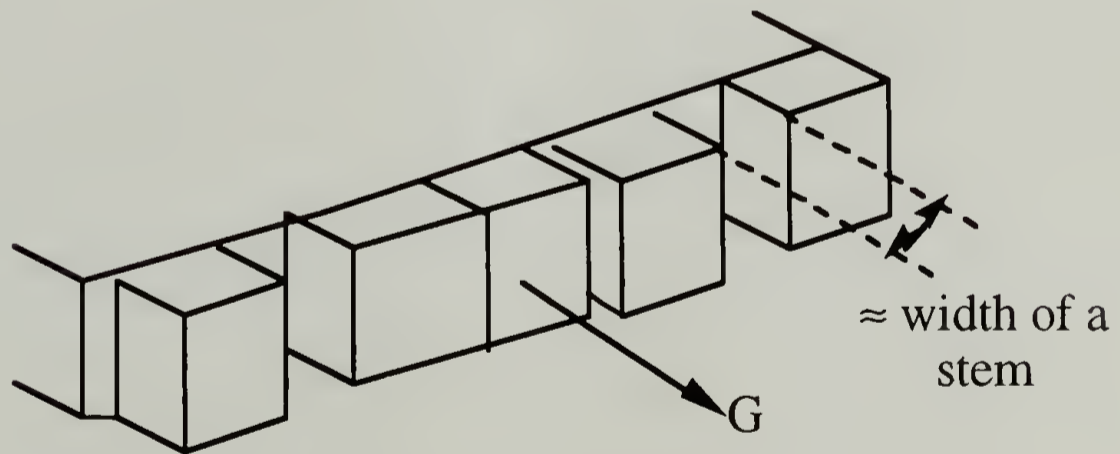
At high degree of supercooling, since the secondary nucleation can proceed very fast, which in turn leads to very high nucleation density. As the separation between two nearest secondary nuclei is close to the width of a stem, the surface spreading can not proceed.⁹ Therefore, the overall growth rate is governed by the secondary nucleation again, i.e., $G \sim i$. This is called regime III, and α in Eq. (4.2) for this regime is 4.



Regime I (low ΔT)



Regime II (medium ΔT)



Regime III (high ΔT)

Fig. 4.2 Three regimes of crystal growth.

The transition from one regime to another can be resolved by a plot shown in Fig. 4.3. The slope of Fig. 4.3 is given by K_g which is proportional to α . Thus, the slopes of regime I and regime III are identical, and are two times that of regime II.⁹

4.3 Experimental

PEEK spherulite growth was monitored by a Carl Zeiss cross-polarized optical microscopy. PEEK and PEEK/PEI blend powders were sandwiched between two glass slides. The sample under study was first melted on a Thomas Model 40 Micro hot stage at 400 °C for 1 min followed by quickly moving to a Mettler FP2 hot stage equilibrated at the desired crystallization temperature (T_c). Spherulite diameters were measured by the micrometer attached on the lens. The growth of at least three spherulites were measured at each T_c . The growth rate of each measurement agreed well with each other.

4.4 Results and Discussion

It has already been indicated in Chapter 3 that the first stage crystallization is associated with the formation of the spherulites, and the second stage crystallization is associated with the intraspherulitic crystallization. Therefore, the growth kinetics monitored by the spherulite size development is due to the growth of the primary crystals. Unfortunately, the growth rate of the secondary crystals can not be determined by optical microscopy. Therefore, the molecular parameters obtained in this chapter are only associated with the primary crystals.

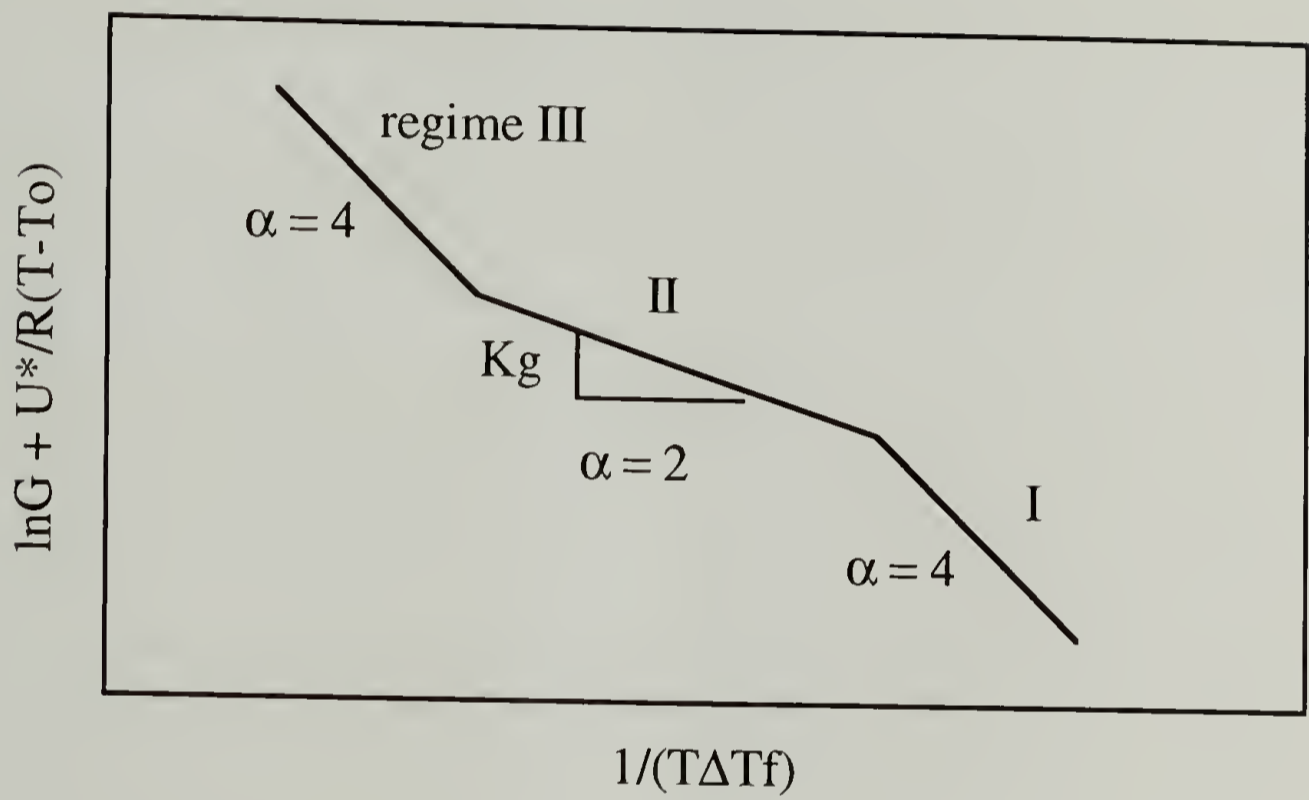


Fig. 4.3 The plot for distinguishing the three growth regimes.

4.4.1 Nucleation Density

Fig. 4.4 displays the optical micrographs of PEEK spherulite growth from the pure melt and 75/25 blend. A plot of the spherulite size vs. time for different PEEK/PEI blend compositions at $T_c = 270$ °C is shown in Fig. 4.5. The growth rate given by the slope of Fig. 4.5 decreases with increasing PEI content, which can also be seen in Fig. 4.6 showing the plot of the growth rate vs. composition. It is noted that in addition to the depression in growth rate, the nucleation density of PEEK is also decreased by blending with PEI, which has also been indicated in 3.3.2.

Previous studies of the crystallization kinetics in polymer blends have focused mainly on either the overall crystallization kinetics or the spherulite growth rate, very little attention has been paid to the influence of blending on the nucleation density. The nucleation density observed by optical microscopy is a consequence of the competition between the nucleation and the subsequent crystal growth. The faster the former process, the higher the nucleation density, and vice versa. Reduction in nucleation density upon blending with PEI indicates that dilution has induced a stronger depression in the PEEK nucleation rate than in the crystal growth rate.

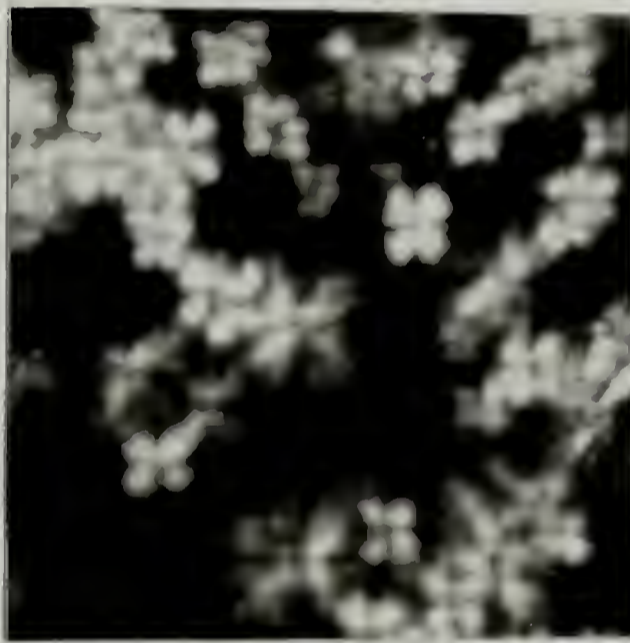
A calculation can be performed to demonstrate the effect of PEI on the nucleation density of PEEK crystals. For the sake of simplicity, the nucleation process is approximated as a homogeneous primary nucleation. Consider $T_c = 250$ °C, it has been shown in Chapter 3 that this T_c is in the thermodynamically controlled crystallization region. Thus the rate of the primary nucleation can be approximated as¹⁰



90 sec



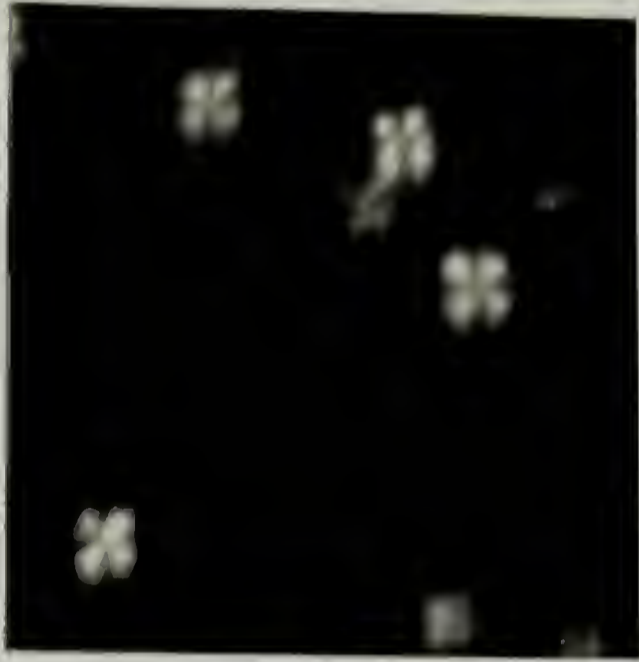
300 sec



150 sec

(a)

Fig. 4.4 Optical micrographs of PEEK spherulites grown from (a) pure PEEK and (b) PEEK/PEI 75/25 blend at 250 °C (continued next page).



60 sec



180 sec



120 sec



360 sec

(b)

Fig. 4.4 continued

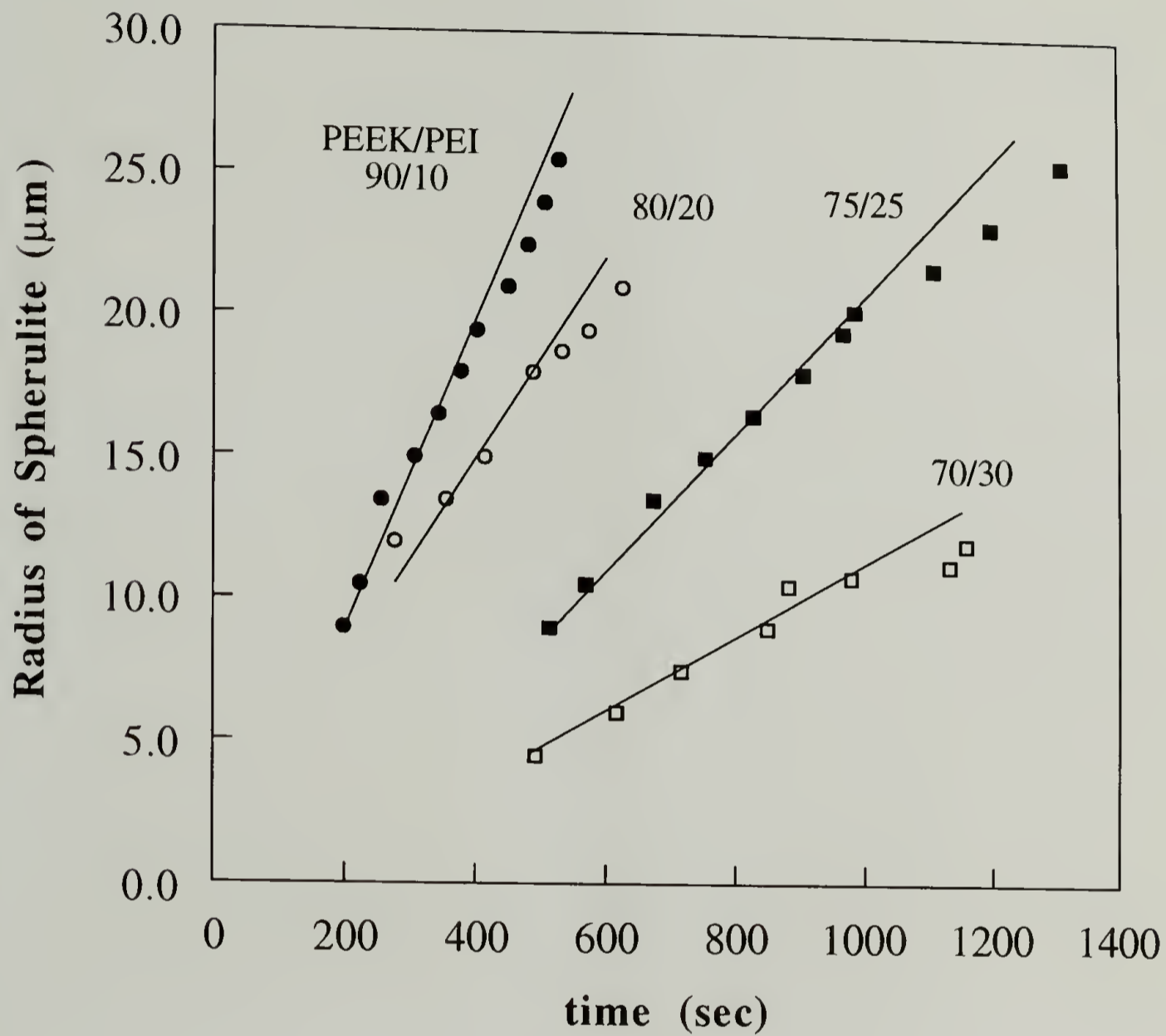


Fig. 4.5 Radii of PEEK spherulites vs. time plot for growth rate determination; $T_c = 270^\circ\text{C}$.

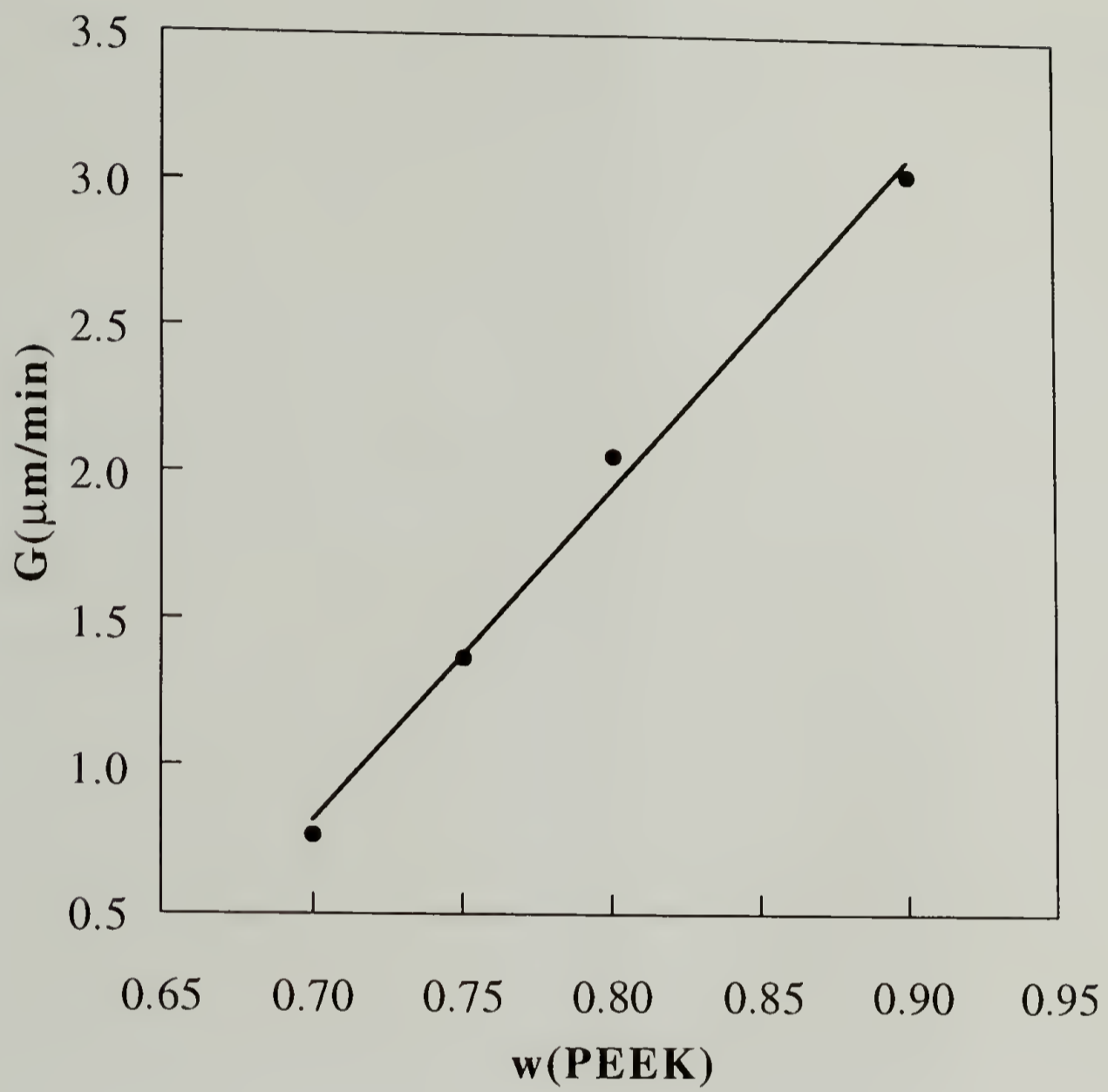


Fig. 4.6 Composition variation of PEEK spherulite growth rate at 270 °C.

$$i_p \propto \exp \left[\frac{-32\sigma^2 \sigma_c T_m^0}{k_B T_c \Delta h_f^0 (T_m^0 - T_c)^2} \right] \quad (4.3)$$

For the crystal growth rate, it will be shown later that at $T_c = 250$ °C, the crystal growth is in regime III in which the overall growth rate is controlled by the secondary nucleation. Therefore the crystal growth rate can be approximated as⁹

$$G \propto \exp \left[\frac{-4\sigma \sigma_c b_0 T_m^0}{k_B T_c \Delta h_f^0 (T_m^0 - T_c)} \right] \quad (4.4)$$

It can be seen from Eq. (4.3) and (4.4) that the nucleation rate varies with $\exp(-1/\Delta T^2)$ and the growth rate varies with $\exp(-1/\Delta T)$; therefore, the nucleation is more sensitive to the change in degree of supercooling than the crystal growth. Blending can certainly change the degree of supercooling as a result of equilibrium melting point depression. From Eq. (4.3) and (4.4), the ratios i_0/i_b and G_0/G_b for PEEK/PEI blends are calculated; where the subscripts 0 and b denote pure PEEK and PEEK/PEI blends, respectively. These ratios reflect the blending effect on the rates of primary nucleation and crystal growth, respectively. The values of the parameters used in this calculation will be indicated in the later discussion. The result indicates that as the equilibrium M.P. of PEEK is depressed by 1 °C due to blending with PEI, $i_0/i_b \approx 2.78$ and $G_0/G_b \approx 1.15$. This shows that depression of M.P. by 1 °C reduces the primary nucleation rate by ca. 1.78 times; however, this M.P. depression reduces the crystal growth rate by only ca. 0.15 time. Depression of equilibrium M.P. by 2 °C decreases the primary nucleation rate by ca. 6.89 times, whereas the crystal growth rate is only reduced by ca. 0.33 time. This calculation clearly indicates that dilution by PEI has decreased the primary nucleation rate more than the crystal growth rate of

PEEK. This explains the decrease in nucleation density of PEEK crystallization upon blending with PEI.

4.4.2 Regimes of Growth

For the growth rate analysis of PEEK/PEI blends, only the modification on the thermodynamic term in Eq. (4.1) will be considered. For the mobility term, only the effect of blending on T_g will be considered, since the T_c range under study is in the thermodynamically controlled region. For the thermodynamic term, a modification proposed by Boon and Azcue is adopted here.⁴ In addition to the equilibrium M.P. depression, this modification considers the effect of the probability of selecting a crystallizable sequence from the mixture on the free energy of formation of a two-dimensional nucleus. This gives the crystal growth rate⁴

$$G = G_0 \exp\left[-\frac{U^*}{R(T_c - T_0)}\right] \exp\left[-\frac{K_g}{T_c(T_{mb}^0 - T_c)f}\right] \exp\left[\frac{\lambda \sigma T_{mb}^0 \ln \phi_2}{b_0 \Delta h_{fb}^0 (T_{mb}^0 - T_c)f}\right] \quad (4.5)$$

K_g is now given by

$$K_g = \frac{\alpha b_0 \sigma \sigma_e T_{mb}^0}{k_B \Delta h_{fb}^0} \quad (4.6)$$

where $\lambda = 2$ for regime I and III growth and $\lambda = 1$ for regime II growth, ϕ_2 is the volume fraction of the crystalline component in the melt, T_{mb}^0 and Δh_{fb}^0 are the equilibrium melting point and bulk enthalpy of melting of the blend, and both depend on the magnitude of interaction (χ) in the blend. The ratio $T_{mb}^0/\Delta h_{fb}^0$ is equal to the inverse of the entropy of melting of the blend. If the entropic contribution to the free

energy of mixing is negligible, the entropy of melting of the blend can be approximated by that of the pure homopolymer. Thus, $T_{mb}^0/\Delta h_{fb}^0$ in Eq. (4.5) and (4.6) can then be replaced by $T_m^0/\Delta h_f^0$. Expressing Eq. (4.5) in logarithmic form and rearranging terms:

$$\ln G + \frac{U^*}{R(T_c - T_0)} - \frac{\lambda \sigma T_m^0 \ln \phi_2}{b_0 \Delta h_f^0 (T_{mb}^0 - T_c) f} = \ln G_0 - \frac{K_g}{T_c (T_{mb}^0 - T_c) f} \quad (4.7)$$

A plot of the left-side terms in Eq. (4.7) vs. $1/[T_c(T_{mb}^0 - T_c)f]$ yields a straight line with the slope given by K_g . Therefore, if the regime of growth can be identified, σ_e of the crystal can be calculated by Eq. (4.6).

The following parameters of PEEK and PEEK/PEI blends are used for the growth rate analysis by Eq. (4.6) and (4.7): $\Delta h_f^0 = 44 \text{ cal/cm}^3$,⁹ $T_m^0 = 384 \text{ }^\circ\text{C}$, T_{mb}^0 of the blends have been extrapolated by the Hoffman-Weeks plot in Chapter 2, the densities $\rho(\text{PEEK}) = 1.2639 \text{ g/cm}^3$ and $\rho(\text{PEI}) = 1.2889 \text{ g/cm}^3$ are used to convert the weight fraction to volume fraction assuming the volume of mixing is negligible. The value of a_0 which is the width of a molecule is obtained from the lattice parameter to be 3.875 \AA .¹² The value of the monomolecular thickness b_0 depends on the growth direction. PEEK lamellae have been found to grow predominantly along the b-axis,¹³ therefore for the (010) growth plane b_0 is 5.86 \AA .¹²

Analysis of the growth rate data based on Eq. (4.7) also requires the values of U^* and T_0 . From the WLF relationship, it can be derived that $U^* = 4120 \text{ cal/mol}$ and $T_0 = T_g - 51.6$.^{3,7} It has been found that $U^* = 1500 \text{ cal/mol}$ and $T_0 = T_g - 30$ give better fits to the experimental data for several polymers.³ Nevertheless, it is found here that

WLF values of U^* and T_0 give better fits to the experimental data. This is consistent with a prior investigation of PEEK spherulite growth by Deslandes et al.¹⁴

A plot of the left-side terms in Eq. (4.7) vs. $1/[T_c(T_{mb}^0 - T_c)f]$ is shown in Fig. 4.7. It is seen that regime III-II transition can be identified for PEEK and the blends. The slopes which are given by K_g for different blend compositions are tabulated in Table 4.1. The ratio of K_g of these two regimes is about 2, in agreement with the theoretical prediction.⁹

The spherulite growth rates recalculated by Eq. (4.5) are plotted against T_c in Fig. 4.8. The regime III-II transition temperatures are plotted against the blend composition in Fig. 4.9. It can be seen that the regime III-II transition temperature decreases with increasing PEI content in the blends. Regime III growth is identified as the separation between two secondary nuclei is close to the width of a crystalline stem, such that the surface spreading cannot proceed.⁹ This occurs at large degree of supercooling as the secondary nucleation proceeds more rapidly than the surface spreading and hence gives rise to high nucleation density. Therefore, a shift in regime III-II transition to lower temperature with increasing PEI content indicates that blending with PEI has a stronger effect in depressing the secondary nucleation rate than in reducing the surface spreading rate.

4.4.3 Crystal Surface Free Energies

To calculate the fold surface free energy by Eq. (4.6), the side surface free energy, σ , should be evaluated first. A theoretical treatment by Hoffman et al.¹⁵ has related σ to the characteristic ratio of the molecule. Although this theory has been

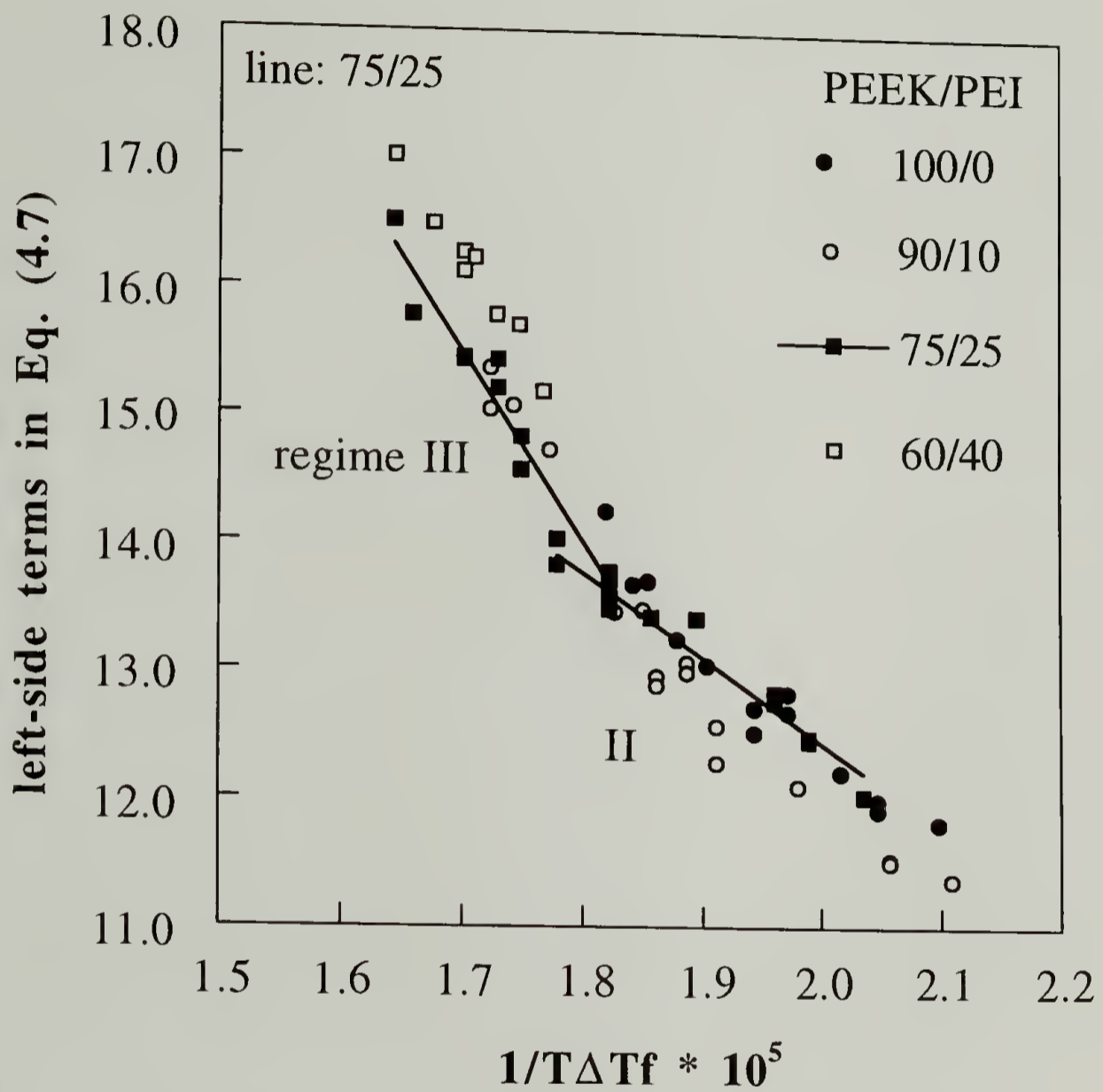


Fig. 4.7 The modified Lauritzen-Hoffman plot (Eq. (4.7)) for PEEK/PEI blends.

Table 4.1 K_g , σ_e and work of chain folding q determined from Fig. 4.7.

w(PEEK)	$K_g * 10^{-5}$		σ_e (erg/cm ²)		q (kcal/mol)	
	III	II	III	II	III	II
1.00	12.11	6.67	166.75	183.59	10.90	12.00
0.90	14.86	6.60	204.54	181.79	13.37	11.88
0.75	14.88	6.56	204.89	180.65	13.39	11.81
0.60	13.97		192.34		12.57	

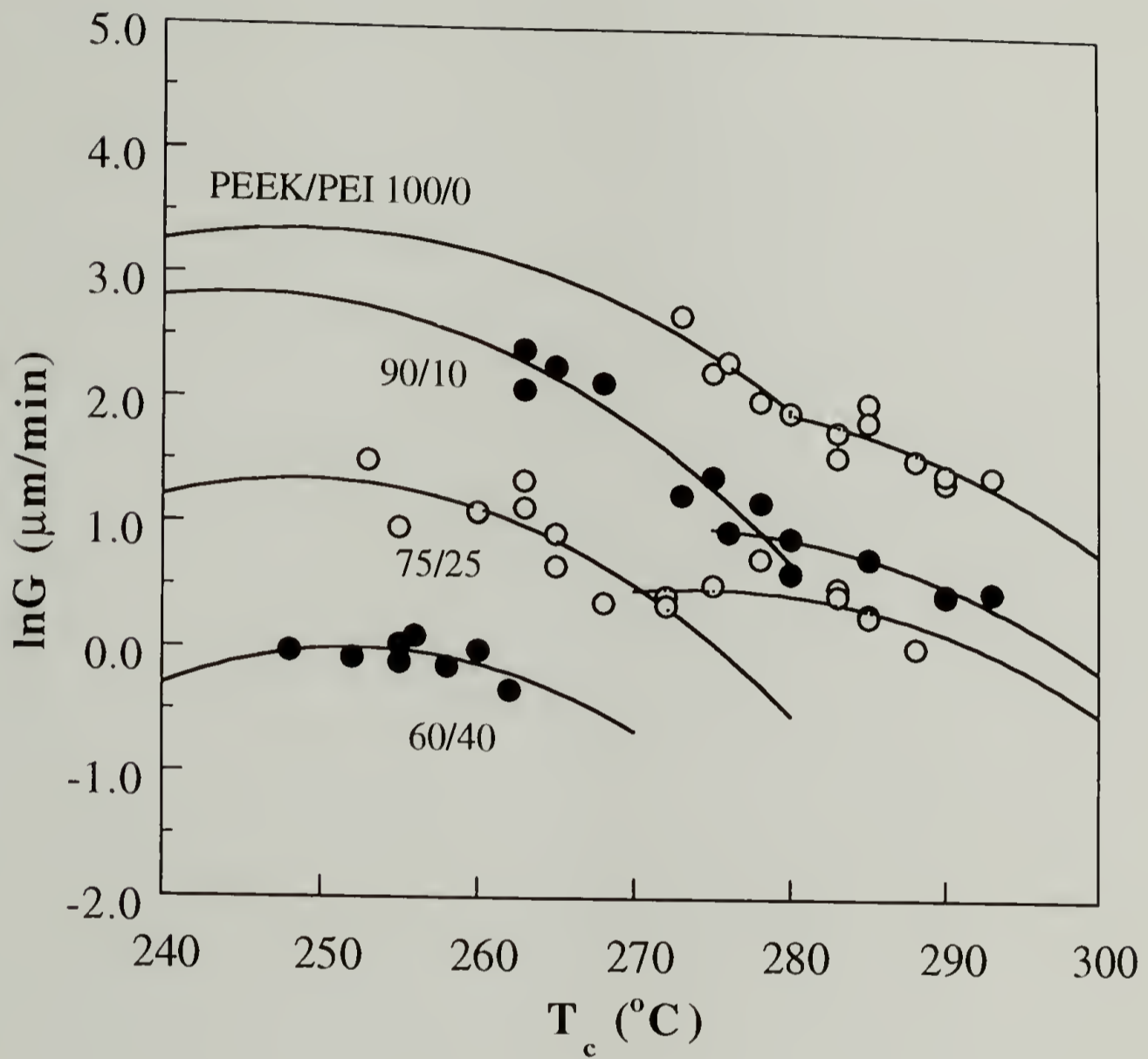


Fig. 4.8 Logarithmic growth rate vs. the crystallization temperature plot for PEEK/PEI blends. The lines are the results calculated by Eq. (4.5).

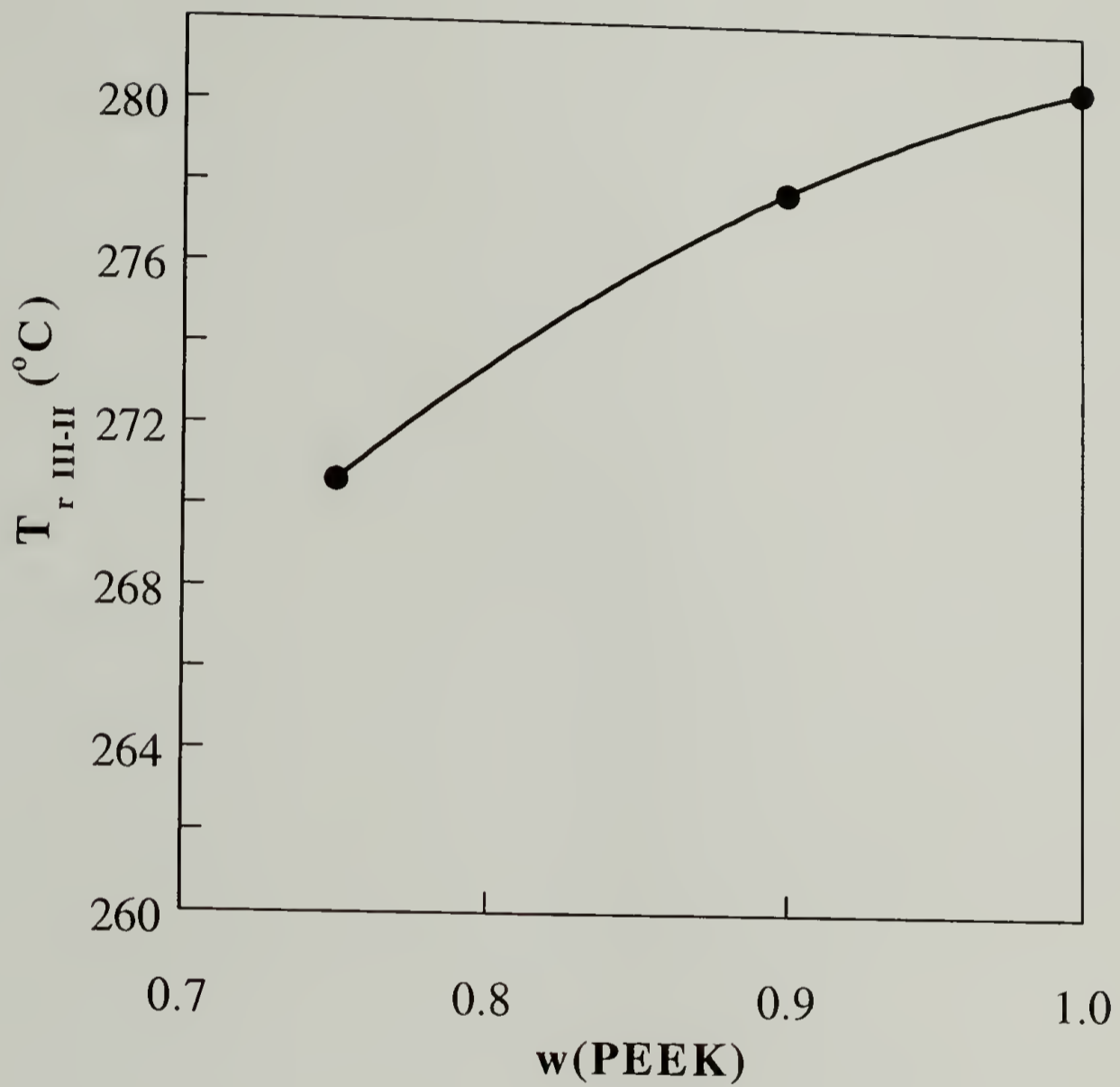
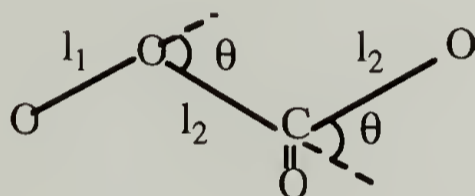


Fig. 4.9 Composition variation of regime III-II transition temperature of PEEK/PEI blends.

questioned recently,¹⁶ it has been shown to give good predictions for the σ of several polymers. Besides, this is the only available theory allowing direct evaluation of σ . Therefore, it will be adopted here. The σ of non-vinyl polymers is given by¹⁵

$$\sigma = \Delta h_f^0 \left(\frac{a_0}{2} \right) C_\infty \quad (4.8)$$

where C_∞ is the characteristic ratio. The characteristic ratio of a non-vinyl polymer is given by $C_\infty = \langle r^2 \rangle_0 / (nl_v^2)$, where $\langle r^2 \rangle_0$ is the end-to-end distance of the polymer in the unperturbed state, l_v is the length of a virtual bond, and n is the number of such bond. The PEEK chain can be represented as a succession of two types of virtual bonds,¹⁷ as shown below



For polymers with structure similar to PEEK, for example, poly(2,6-disubstituted-1,4-phenylene oxides), and bisphenol A polycarbonate, both theoretical calculations of the conformational energies of rotational isomers¹⁸ and experimental results on the unperturbed dimensions in solution¹⁹⁻²¹ have shown that representation of these polymers as freely rotating chains of virtual bonds provides a reasonable description of their equilibrium properties in the unperturbed state. The characteristic ratio of PEEK is thus estimated by assuming free rotation of the virtual bonds, this gives

$$C_\infty = 1 + \frac{2\cos\theta}{3(x_1 l_1^2 + x_2 l_2^2)(1 - \cos^3\theta)} [(1 + \cos\theta)(l_1^2 + 2l_1 l_2) + \cos^2\theta(l_1^2 + 2l_2^2)] \quad (4.9)$$

where x_1 and x_2 are the number fraction of virtual bond 1 and 2 in a repeating unit, respectively, l_1 and l_2 are the respective bond length, and θ is the bond angle supplement. For PEEK, $x_1 = 1/3$, $x_2 = 2/3$, $l_1 = 5.50 \text{ \AA}$, $l_2 = 5.62 \text{ \AA}$, and $\theta = 55^\circ$ are taken for the calculation.¹⁷ The calculated C_∞ is 2.97, and the side surface free energy is then calculated by Eq. (4.8) to be 12.0 erg/cm^2 .

The calculated fold surface free energies from Eq. (4.6) are listed in Table 4.1. The value of σ_e calculated from the growth data of pure PEEK is 175.2 erg/cm^2 , and that calculated from the data of the blends is about 10% higher than this value. Not much reliable information can be inferred from this observation due to the inherent error in the data analysis and the experimental uncertainties. The average value of σ_e calculated from pure PEEK and the blends is 188 erg/cm^2 . This value is considerably higher than 49 erg/cm^2 obtained by the Thomson-Gibbs plot.¹¹ Similar observation has also been reported for the selenium crystals,²² for which the σ_e obtained by the crystal growth rate was 337 erg/cm^2 , whereas that obtained by the Thomson-Gibbs plot was only 31.5 erg/cm^2 . It has been suggested that σ_e determined by the crystal growth rate is a "kinetic" surface free energy, whereas that obtained by the Thomson-Gibbs plot is a "thermodynamic" one. The melting points used in the Thomson-Gibbs plot are normally measured after the crystals have been annealed for a long time, i.e., after they have reached the metastable equilibrium state. In the annealing process, the PEEK crystal surfaces perhaps reorganized significantly to reduce the fold surface free energy. On the other hand, the σ_e obtained by the spherulite growth rate is the surface free energy of the crystals just formed during the crystallization process. In the crystal growth process, PEEK chains perhaps assumed larger folding loops due to the inherent difficulty to form a small fold immediately.

The fold surface free energy does not give much information on the stiffness of the molecule, another parameter, the work of chain folding, q , is the parameter that closely related to the chain stiffness. q can be calculated from σ_e by³

$$q = 2a_0b_0\sigma_e \quad (4.10)$$

The calculated values of q for PEEK are also listed in Table 1. The average value of q is 12.3 Kcal/mol. For other polymers, q of more flexible chains such as poly(ethylene oxide),³ polyethylene,¹⁵ and *i*-polypropylene¹⁵ are 2.3, 4.90, and 5.75 Kcal/mol, respectively. The work of chain folding for stiffer chains such as Nylon 6,³ *i*-polystyrene,³ and poly(ethylene terephthalate)²³ are 6, 6.97, and 10 Kcal/mol, respectively. The magnitude of q has been suggested to be proportional to the energy difference between the *trans* and *gauche* conformational states and the number of *gauche* conformation in a fold.³ The value of q obtained for PEEK is reasonable in view of its molecular bulkiness. Due to the bulky phenylene groups in the backbone, PEEK chains probably have to assume large loops in the fold surface in the crystallization process. Therefore, q of PEEK is higher than that of other polymers indicated above.

4.5 Conclusions

The spherulite growth kinetics of PEEK and PEEK/PEI blends have been studied. The decrease in PEEK nucleation density upon blending with PEI has been attributed to be a result of the equilibrium melting point depression. Regime III-II transitions are identified for PEEK and PEEK/PEI blends. The regime transition temperature decreases with increasing PEI content in the blend. The side surface free

energy of PEEK has been calculated from the characteristic ratio assuming free rotations of the virtual bonds. The calculated σ is 12 erg/cm². The "kinetic" fold surface free energy evaluated from the growth rate data is 188 erg/cm². This gives the work of chain folding of PEEK, $q = 12.3$ Kcal/mol.

References

1. Schultz, J. M. *Polymer Materials Science*, Prentice-Hall: Englewood Cliffs, **1974**, Chap. 9.
2. Avrami, M. *J. Chem. Phys.* **1939**, 7, 1103.
3. Hoffman, J. D.; Davis, G. T.; Lauritzen, Jr., J. I. in *Treatise on Solid State Chemistry* Hanny, N. B. Ed; Plenum Press: New York, **1976**, Chap. 7.
4. Boon, J.; Azcue, J. M. *J. Polym. Sci., Part A* **1968**, 6, 885.
5. Wang, T. T. and Nishi, T. *Macromolecules* **1977**, 10, 421.
6. Alfonso, G. C.; Russell, T. P. *Macromolecules* **1986**, 19, 1143.
7. Chow, T. S. *Macromolecules* **1990**, 23, 333.
8. Saito, H.; Okada, T.; Hamane, T.; Inoue, T. *Macromolecules* **1991**, 24, 4446.
9. Hoffman, J. D. *Polymer* **1983**, 24, 3.
10. Wunderlich, B. *Macromolecular Physics*; Academic Press: New York, **1977**, Vol. 2, Chap. 7.
11. Blundell, D. J.; Osborn, B. N. *Polymer* **1983**, 24, 953.
12. Dawson, P. C.; Blundell, D. J. *Polymer* **1980**, 21, 577.
13. Lovinger, A. J.; Hudson, S. D.; Davis, D. D. *Macromolecules* **1992**, 25, 1752.
14. Deslandes, Y.; Sabir, F-N; Roovers, J. *Polymer* **1991**, 32, 1267.
15. Hoffman, J. D.; Miller, R. L.; Marand, H.; Roitman, D. B. *Macromolecules* **1992**, 25, 2221.
16. Tonelli, A. E. *Macromolecules* **1992**, 25, 7199.
17. Bishop, M. T.; Karasz, F. E.; Russo, P. S.; Langley, K. H. *Macromolecules* **1985**, 18, 86.
18. Tonelli, A. E. *Macromolecules* **1972**, 5, 558; **1973**, 6, 503.
19. Barrales-Rienda, J. M.; Pepper, D. C. *J. Polym. Sci., Part B* **1966**, 939.
20. Akers, P. J.; Allen, G.; Bethell, M. J. *Polymer* **1968**, 9, 575.
21. Schultz, A. R. *J. Poly. Sci., Part A-2* **1970**, 8, 883.
22. Crystal, R. G. *J. Polym. Sci. Part A-2* **1970**, 8, 1755.

23. Runt, J.; Miley, D. M.; Zhang, X., Gallagher; K. P., MaFeaters; K.; Fishburn,
J. Macromolecules **1992**, 25, 1929.

CHAPTER 5

MELTING BEHAVIOR AND MORPHOLOGY OF PEEK AND PEEK/PEI BLENDS

5.1 Introduction

Bulk crystallized PEEK normally exhibits two melting endotherms in the DSC scans. It has been indicated in Chapter 3 that this double melting behavior is associated with the meltings of two crystal populations formed by the two crystallization stages, i.e., the lower- and the higher-melting endotherms are associated with the meltings of the thinner secondary crystals and the thicker primary crystals, respectively. In spite of the evidence for the presences of two lamellar populations in PEEK, studies by thermal analysis have also showed that PEEK crystals exhibited significant simultaneous melting, recrystallization, and remelting in the melting region.¹⁻² This phenomenon would also contribute to the double melting behavior of PEEK. Therefore, the interpretation of the melting behavior of PEEK should combine two phenomena, i.e., crystals with two different perfections and recrystallization during heating.

In the previous investigations of the melting behavior of PEEK, only bulk-crystallized PEEK has been studied. There has been no reported study on the melting behavior of PEEK crystallized from its solution with a low molecular weight solvent. The study of the melting behavior of solution-crystallized PEEK is of interest, since the crystallization behavior of PEEK in the bulk may be different from that in the solution. This study may provide important clues for exploring the origin of the

unique two-stage crystallization behavior of PEEK. Therefore, in the first part of this chapter, the melting behavior of PEEK crystallized from its solution with dichloroacetic acid is reported. The melting of this solution-crystallized PEEK will be compared with that of the melt-crystallized PEEK.

In the second part of this chapter, the morphology and the melting behavior of semicrystalline PEEK/PEI blends are discussed. Since morphology is directly related to the polymer properties, it is very important to study the morphology of PEEK/PEI blends. There is a controversy in the literature over the existence of the interlamellar segregation morphology in PEEK/PEI blends.³⁻⁴ From the small-angle X-ray scattering (SAXS), Grevecoeur and Groeninckx showed the relative constancy of the long period with the blend composition.³ Consequently, they concluded that PEI was not trapped in the PEEK crystalline interlamellar regions. On the other hand, based on the SAXS and mutual diffusion coefficient measurement, Hsiao et al. have indicated that PEI should be trapped in the PEEK crystalline interlamellar zones over a wide range of crystallization temperatures.⁴ In this chapter, a method based on the investigation of PEEK crystal reorganization in PEEK/PEI blends is reported to resolve if PEI is trapped in the interlamellar zones.

5.2 Background

In the crystalline/amorphous polymer blends, upon crystallization of the crystalline component, the amorphous component should be segregated away from the crystal growth front. Depending upon the extent of segregation, and hence the location of the amorphous component, three types of morphology can be distinguished, as shown in Fig. 5.1:⁵

(a) interlamellar segregation (Fig. 5.1 (a)):

The segregation of the amorphous component occurred at the lamellar level, such that the amorphous component is trapped in the crystalline interlamellar zones. Examples of polymer blends exhibiting this morphology include PVC/PCL,⁶ PPO/i-PS,⁷ and PVF₂/PVP.⁸

(b) interfibrillar segregation (Fig. 5.1 (b)):

The amorphous component is segregated by a larger distance to the regions between the branches of the spherulites. Examples include a-PS/PP,⁹ i-PS/a-PS with a-PS < 30 wt%.¹⁰

(c) interspherulitic segregation (Fig. 5.1 (c)):

The amorphous component is segregated by the largest distance such that it is not within the spherulites. An example is the PCL/poly(hydroxy ether of bisphenol A) blend.¹¹

From pure thermodynamic viewpoint, since the equilibrium M.P. depression is very small for polymer blends, the crystallization driving force can easily supersede the interaction between two polymers at temperatures below the equilibrium M.P. As a consequence, a nearly complete phase separation is the most thermodynamically favorable. Nevertheless, such complete phase separation has never taken place. This indicates that the morphology of the crystalline/amorphous blends is determined by the



Fig. 5.1 Three possible morphologies for crystalline/amorphous polymer blends: (a) interlamellar segregation, (b) interfibrillar segregation, and (c) interspherulitic segregation.

kinetics such as the diffusions of the two components during the crystallization of the crystalline polymer.

Keith and Padden have proposed a parameter δ , to characterize the morphology of polymer blends:⁹

$$\delta = D/G \quad (5.1)$$

where D is the diffusion coefficient of the amorphous component and G is the growth rate of the crystalline component. Eq. (5.1) suggests that the morphology of the blends is controlled by the competition between the growth rate of the crystalline component and the diffusion rate of the amorphous component away from the growth front. Since δ has the unit of length, the larger this parameter is, the farther the amorphous component is rejected. Therefore, Fig. 5.1 is characterized by an increase in δ from Fig. 5.1(a) to 5.1(c).

5.3 Experimental

5.3.1 Solution Crystallization of PEEK

The crystallization of PEEK from its solution with dichloroacetic acid is studied. PEEK powder was dissolved in dichloroacetic acid to the concentration of 4% (w/v) at 150 °C. The resulting solution was quickly moved to an oil bath preheated to the desired crystallization temperatures (30 and 40 °C). The temperature control was within the accuracy of ± 1 °C. Crystallization was allowed to proceed for three days.

The resulting crystalline PEEK was then filtered, heated on a hot plate at 50 °C for 24 hrs to remove most of the solvent, and finally dried in vacuo at 95 °C for 72 hrs for complete removal of the residual solvent.

5.3.2 Optical Microscopy Study

PEEK and PEEK/PEI blend powders were sandwiched between two glass slides. The sample under study was first melted on a Thomas Model 40 Micro hot stage at 400 °C for 1 min followed by quickly moving to a Mettler FP2 hot stage equilibrated at 270 °C. The micrographs of PEEK spherulites were taken after no further spherulite growth was observed.

5.3.3 Thermal Analysis

All thermal analyses were carried out in a Perkin-Elmer DSC-4. The weight of the sample under study was controlled to be in the range of 5 to 6 mg.

5.4 Results and Discussion

5.4.1 Melting Behavior of Solution-Crystallized PEEK

Previous studies on the double melting behavior of PEEK have noted two characteristics: (a) the lower melting endotherm is strongly dependent on the

crystallization temperature (T_c), and (b) the higher melting endotherm is weakly dependent on T_c .¹⁻² An interesting experiment was performed here to demonstrate the effect of thermal history on the melting behavior of PEEK. Here a stepwise annealing experiment was performed. PEEK was melt crystallized at 310 °C for 30 mins, followed by successive annealing at 300, 290, 270, 220 and 190 °C for 30 mins at each of these temperatures. The sample was then scanned by DSC, and the result is shown in Fig. 5.2. It can be seen that multiple melting endotherms are created by this annealing experiment. Except for the highest melting endotherm, each melting endotherm represents a mark for its corresponding annealing temperature. The peak temperatures of the endotherms are about 10 °C higher than their corresponding annealing temperatures. The double melting behavior of PEEK is due to the meltings of two crystal populations of different thickness. Therefore, each melting endotherm shown in Fig. 5.2 signifies the melting of one crystalline lamellar thickness. Multiple melting endotherms has also been observed for ethylene-butene copolymers after a multistage annealing.¹²

Fig. 5.3 displays the melting curves of the solution-crystallized PEEK and the melt-crystallized PEEK at 300 °C. In contrast to the melt-crystallized PEEK, the solution-crystallized PEEK shows only one melting endotherm located at 339.7 °C. The degree of crystallinity is determined from the enthalpy of melting by taking 130 J/g as the enthalpy of melting of 100% crystalline PEEK.¹³ The measured degree of crystallinity is 41.6% for the solution-crystallized PEEK, about 5% higher than that of PEEK crystallized at 300 °C.

To be certain that the difference in the melting behavior between these two samples is not due to the difference in crystal structure, the wide-angle X-ray diffraction (WAXD) patterns are examined. The results are shown in Fig. 5.4. The

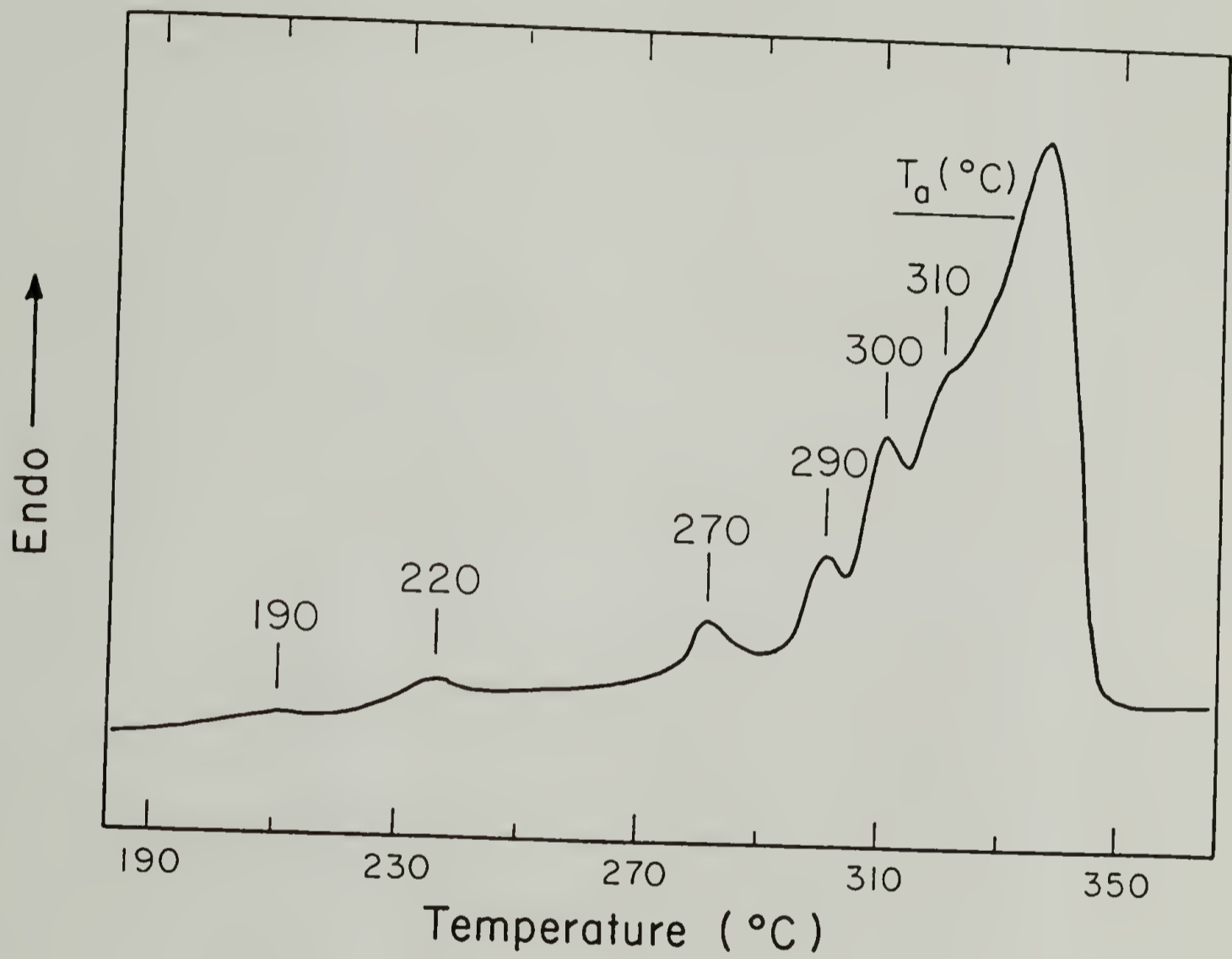


Fig. 5.2 The DSC traces of PEEK after a stepwise annealing. The annealing temperatures are indicated in the figure.

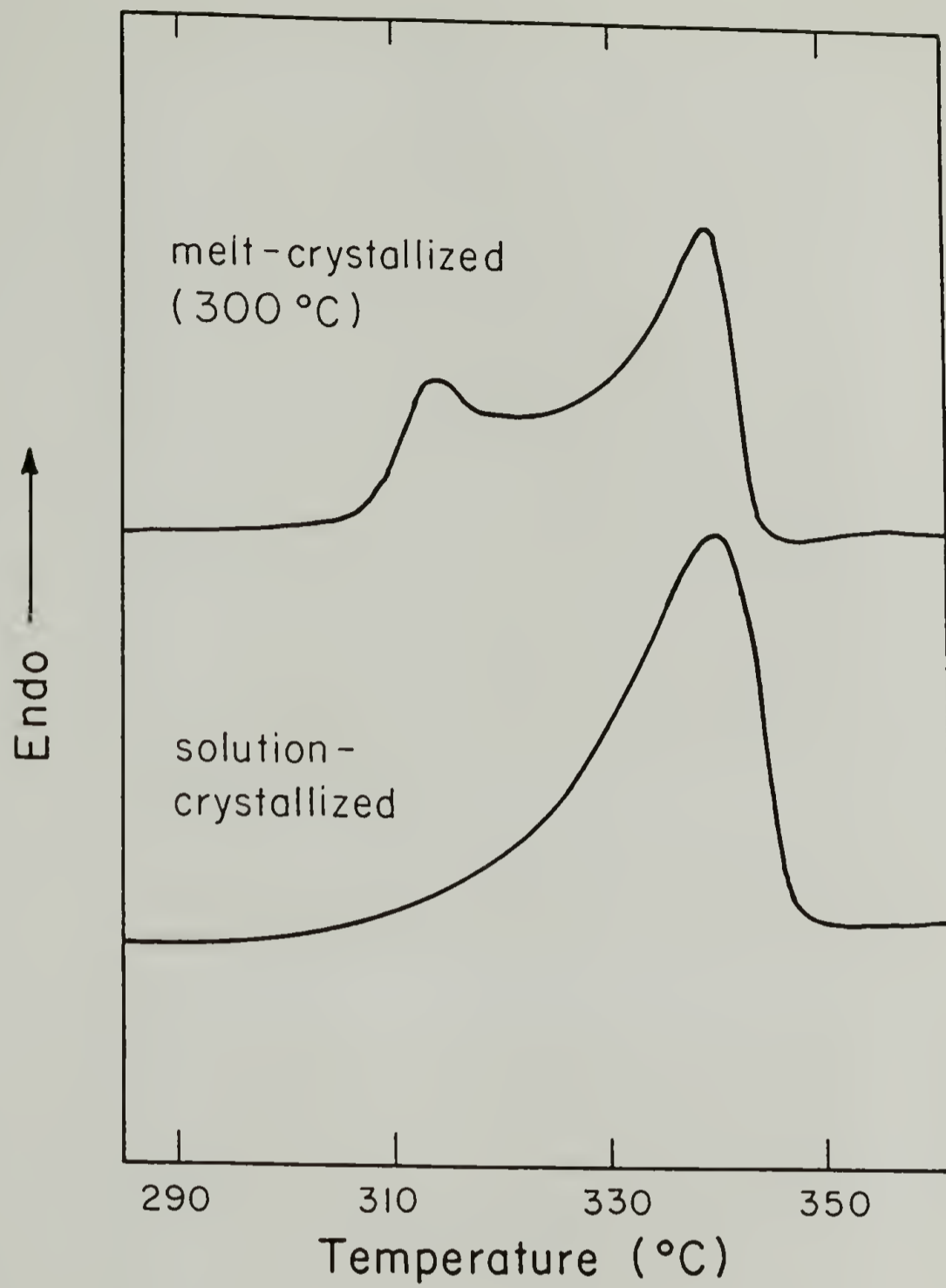
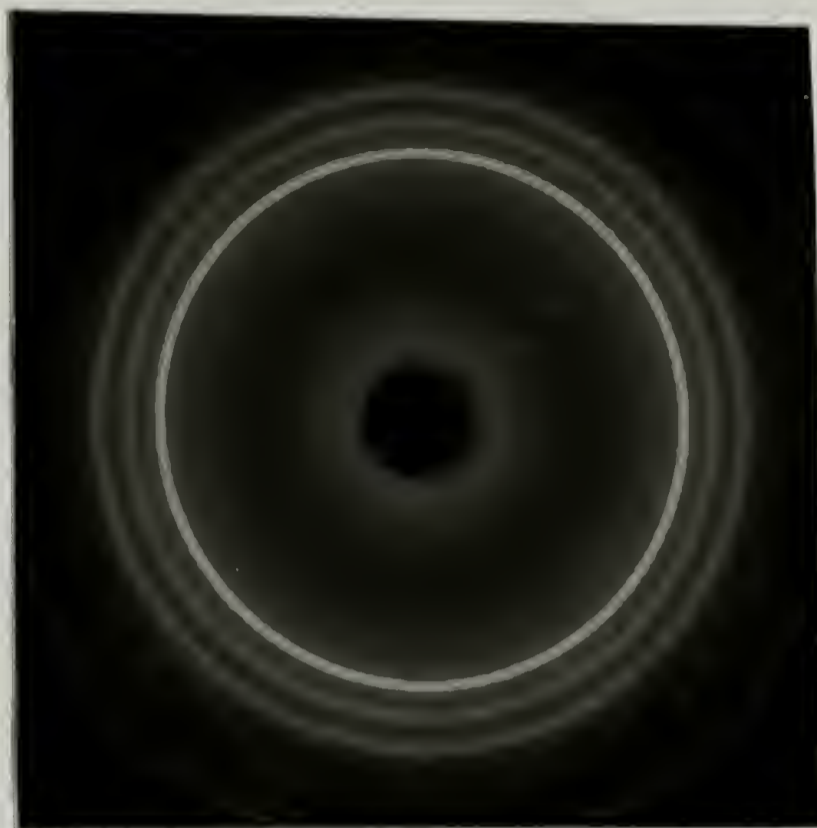
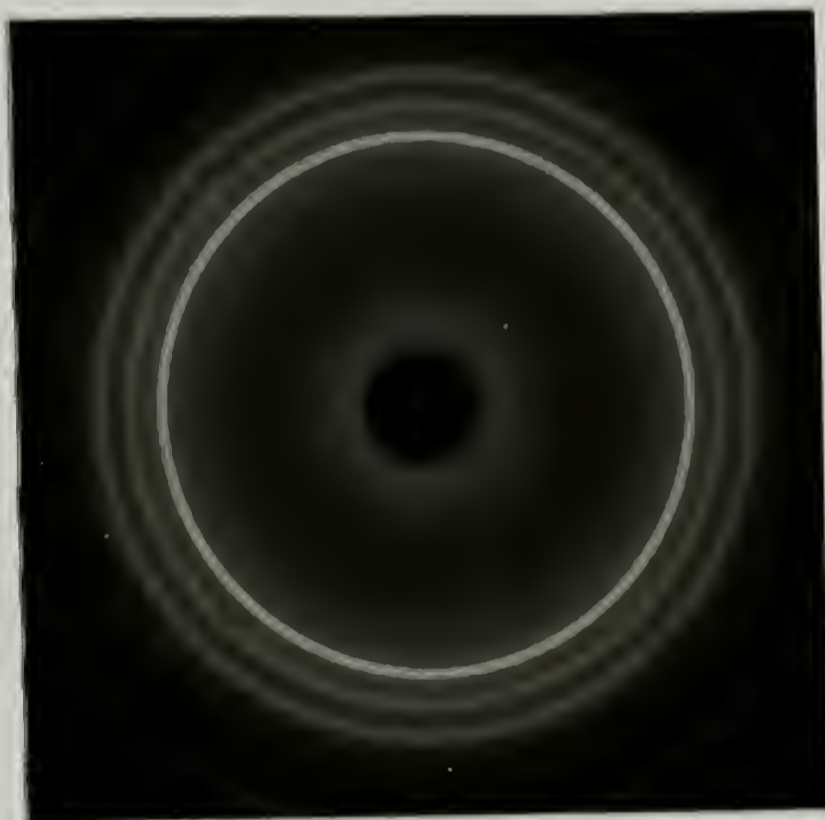


Fig. 5.3 DSC traces of solution-crystallized PEEK and melt-crystallized PEEK at 300 °C.



(a)



(b)

Fig. 5.4 The WAXD patterns of (a) melt-crystallized PEEK, and (b) solution-crystallized PEEK.

WAXD patterns of both crystalline PEEK are identical, indicating that the different melting behavior observed in Fig.5.3 does not arise from the difference in crystal structure. Therefore, it should be a result of change in crystallization behavior when PEEK was crystallized from the solution with dichloroacetic acid. In Fig. 5.3, it can also be seen that the melting onset temperature of the solution-crystallized PEEK is comparable to that of the melt-crystallized PEEK. However, unlike melt-crystallized PEEK, the crystal size distribution of solution-crystallized PEEK is not bimodal.

Since there is only one melting endotherm observed, the growth of the infilling secondary lamellae in between the primary lamellae through second-stage crystallization, which occurred in the PEEK melt crystallization, did not occur in the solution crystallization. Of course, the possibility of secondary crystallization which produces the crystals of smaller sizes is not precluded in the solution crystallization of PEEK. However, this secondary crystallization is different in nature from that in the PEEK melt crystallization, where the secondary crystallization in the later produces another distribution of crystal size.

The heating rate dependence of the melting of solution-crystallized PEEK is also investigated. The melting onset temperature (T_b), the melting peak temperature (T_p), as well as the melting end temperature (T_e) are plotted against logarithmic heating rate in Fig. 5.5. The plot for melt-crystallized PEEK is shown in Fig. 5.6. The melting onset temperature of solution-crystallized PEEK decreases with increasing heating rate up to 30 °C/min. This is ascribed to the hindrance in annealing of PEEK crystals with increasing heating rate. The melting onset temperature increases with increasing heating rate for heating rate > 30 °C/min, which is attributable to the effect of superheating. For both samples, the melting end shows the strongest superheating.

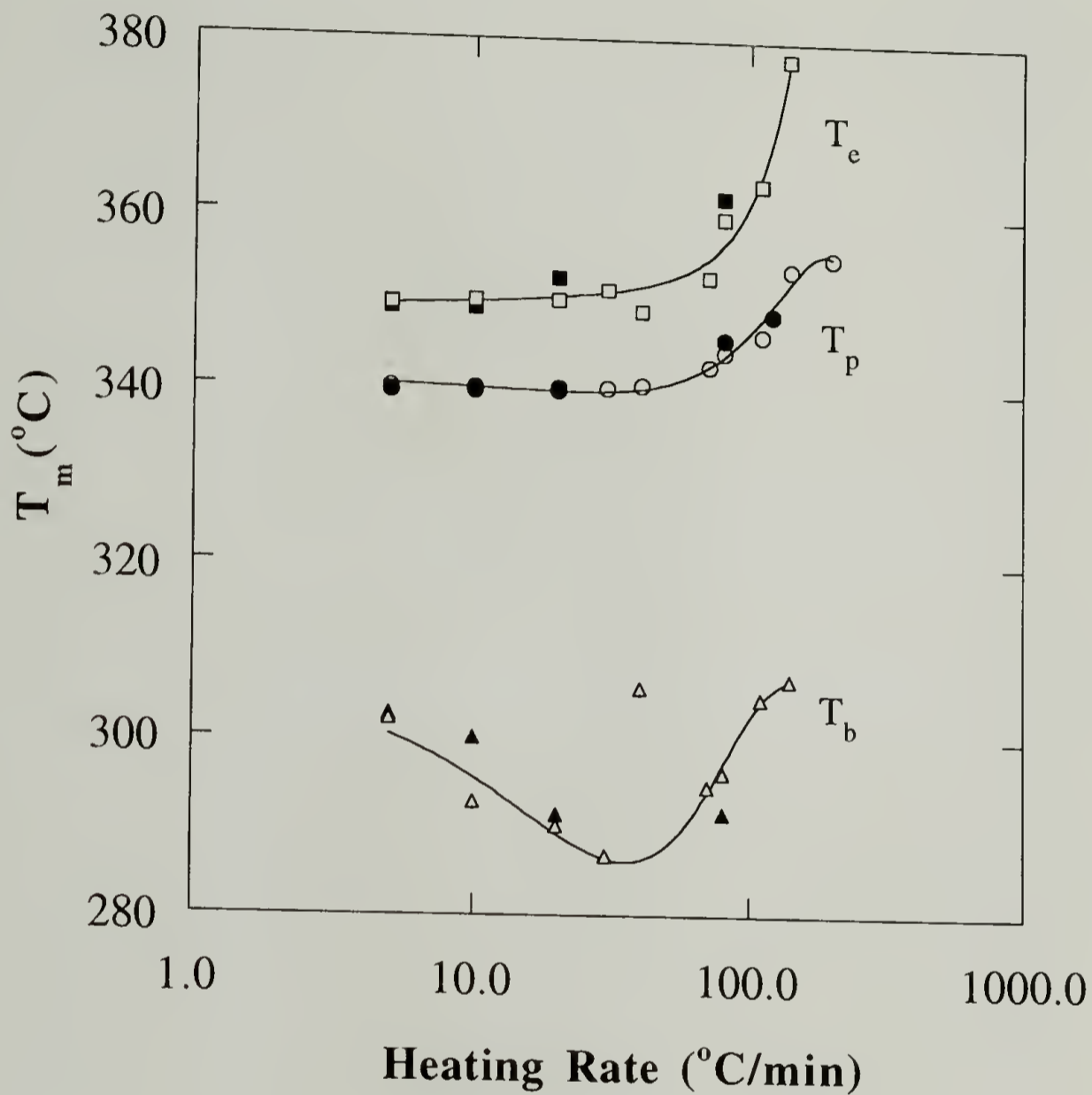


Fig. 5.5 Heating rate dependence of the melting onset temperature (T_b), melting peak temperature (T_p), and melting end temperature (T_e) of solution-crystallized PEEK.

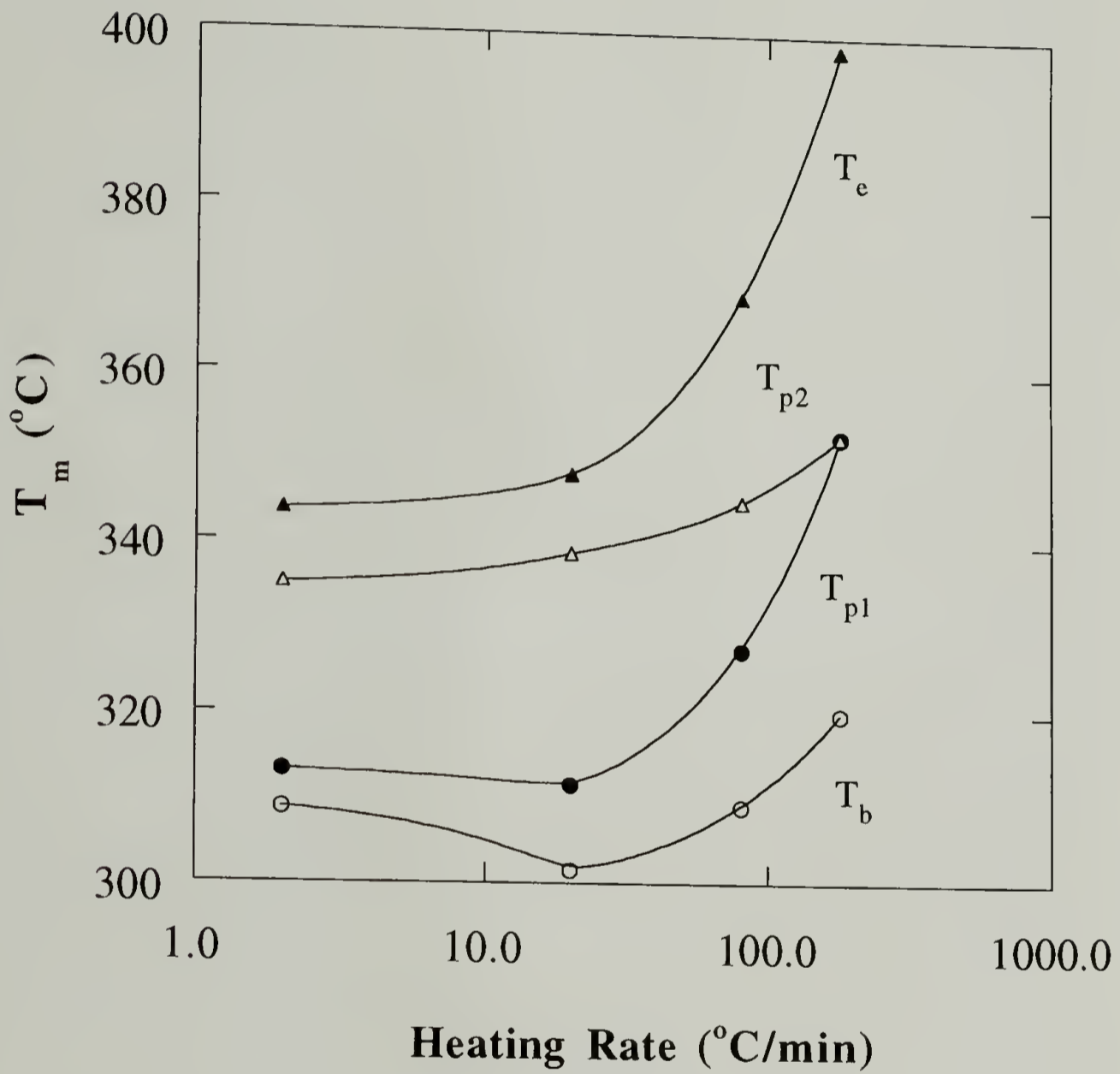


Fig. 5.6 Heating rate dependence of the melting onset temperature (T_b), melting peak temperatures (T_{p1} and T_{p2}), and melting end temperature (T_e) of melt-crystallized PEEK ($T_c = 300$ °C).

One interesting observation in Fig. 5.6 should be indicated. In Fig. 5.6, it can be seen that the lower melting peak temperature (T_{m1}) shows stronger superheating than the higher melting peak temperature (T_{m2}). This has not been noticed in the previous studies of melt-crystallized PEEK. From the viewpoint of the crystal size associated with melting, the thinner crystals should be superheated less than the thicker crystals. The observed discrepancy might indicate that the lamellar morphology, such as the structure of the crystal-amorphous interphase, of the lower-melting PEEK crystals is different from that of the higher-melting PEEK crystals. The superheating phenomena have been correlated to the chain conformations in the crystal surface by Zahmann.¹⁴

5.4.2 Morphology of Semicrystalline PEEK/PEI Blends

In Chapter 4, Fig. 4.5 shows that the average radii of the PEEK spherulites grew linearly with time at 270°C for all the blend compositions studied. Such linear spherulite growth has been observed for many crystalline/amorphous polymer blends. If the crystallization mechanism in the blends is considered in detail, it will be seen that such observation could post an interesting implication for the morphology of the crystalline/amorphous blends. As has been indicated, during the crystal growth of PEEK, PEI must diffuse away from the growth front to accommodate lamellar growth. Consequently, this would lead to an accumulation of PEI in the growth front, and hence a shift in the amorphous phase composition. Due to the buildup of PEI, the melting point will be depressed further decreasing the thermodynamic driving force for crystallization. Moreover, the T_g of the remaining amorphous phase will increase as the crystallization proceeds. These two factors tend to retard growth rate with time, and hence a nonlinear growth should be observed.

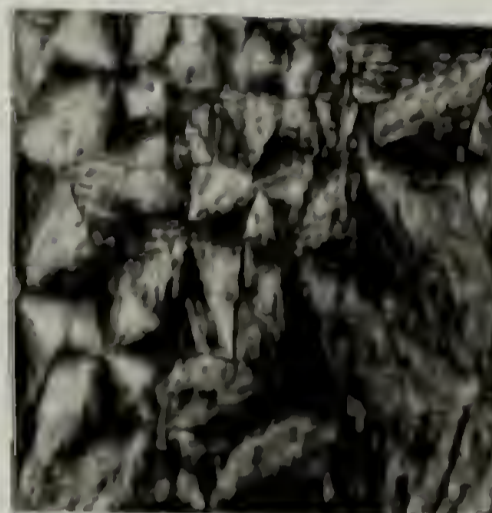
The linear growth observed for PEEK/PEI blends may imply that the growing PEEK crystals are exposed to a nearly constant concentration layer. The average concentration of PEI in this layer increases with increasing initial PEI concentration. If this is true, the continuous rejection and buildup of PEI is forbidden in the growth direction. As a consequence, PEI must diffuse in a direction normal to the growth direction or being trapped in the interlamellar regions.^{6,15-16}

From this discussion, it might be expected that PEI was totally trapped in the interlamellar regions during the crystallization of PEEK. The optical micrographs of the final spherulite morphology are shown in Figure 5.7. It can be seen that as the concentration of PEI was increased, the texture of PEEK spherulites grown from the melt becomes coarse. At 50/50 blend composition, the branches of the spherulites are clear. Fig. 5.7 shows that the interfibrillar segregation is apparently occurring during the crystallization of PEEK. In other words, not all the PEI are trapped in the interlamellar region, in contradiction to the observed linear spherulite growth. This may be due to that the macroscopic observation of the spherulite growth may not be sensitive enough to reflect the detailed mechanisms of the microscopic crystal growth. Therefore, an approximate linear growth can still be observed even though there is an accumulation of PEI in the growth front.

Although the interfibrillar morphology is apparent, the possibility that some PEI may locate in the interlamellar regions is not precluded. It is possible that the segregation of PEI, especially the high molecular weight fractions, out of the PEEK crystalline interlamellar regions is not complete. It has been indicated that there is a controversy over the existence of interlamellar segregation in PEEK/PEI blends.³⁻⁴ A method based on the investigation of PEEK crystal reorganization is established here to resolve this controversy, and this is the subject of discussion in 5.4.3.



PEEK



PEEK/PEI 75/25



50/50



25/75

—
100 μm

Fig. 5.7 Optical micrographs of PEEK spherulites grown from pure melt and PEEK/PEI blends.

5.4.3 Melting Behavior of PEEK in PEEK/PEI Blends

In 2.3.2, it was indicated that the higher melting PEEK crystals formed at $T_c < 305\text{ }^\circ\text{C}$ reorganized significantly on heating at $20\text{ }^\circ\text{C}/\text{min}$, and hence gave rise to constant T_{m2} with increasing T_c . If a complete rejection of PEI from the PEEK interlamellar zones occurs, the reorganization of PEEK crystals before melting should be identical to that of pure PEEK, since the crystals are exposed to a pure PEEK amorphous matrix. On the other hand, if PEI is contained in the interlamellar regions, the PEEK crystal reorganization should be changed. First, the crystals are surrounded by a miscible PEEK/PEI amorphous matrix. This miscible amorphous matrix has a higher T_g than the pure PEEK amorphous matrix, therefore the lamellar thickening during reorganization is more difficult. Furthermore, the structure of the crystal-amorphous interphase, whose thickness depends on chain flexibility, also plays a role in the crystal reorganization. The crystal-amorphous interphase in crystalline/amorphous blends has been discussed theoretically by Kumar and Yoon.¹⁷⁻¹⁸ This interphase in blends was predicted to contain segments of the amorphous component. The concentration profile along the interphase depends on the magnitude of interaction between these two components. Therefore, if PEI is contained in the PEEK crystalline interlamellar regions, the mixing (entanglements) of the chain segments of PEI with the segments of PEEK in the interphase can restrict the cooperative motion of the crystalline chains in the subsequent lamellar thickening during reorganization. As a consequence, hindrance of crystal reorganization is expected.

The effect of PEI on PEEK crystal reorganization has been evaluated by thermal analysis. Figure 5.8 and 5.9 are the DSC melting curves of PEEK and PEEK/PEI blends scanned after crystallized at 297 and $320\text{ }^\circ\text{C}$, respectively. Fig. 5.8 compares the melting behavior of pure PEEK with that of PEEK in PEEK/PEI blends at $T_c <$

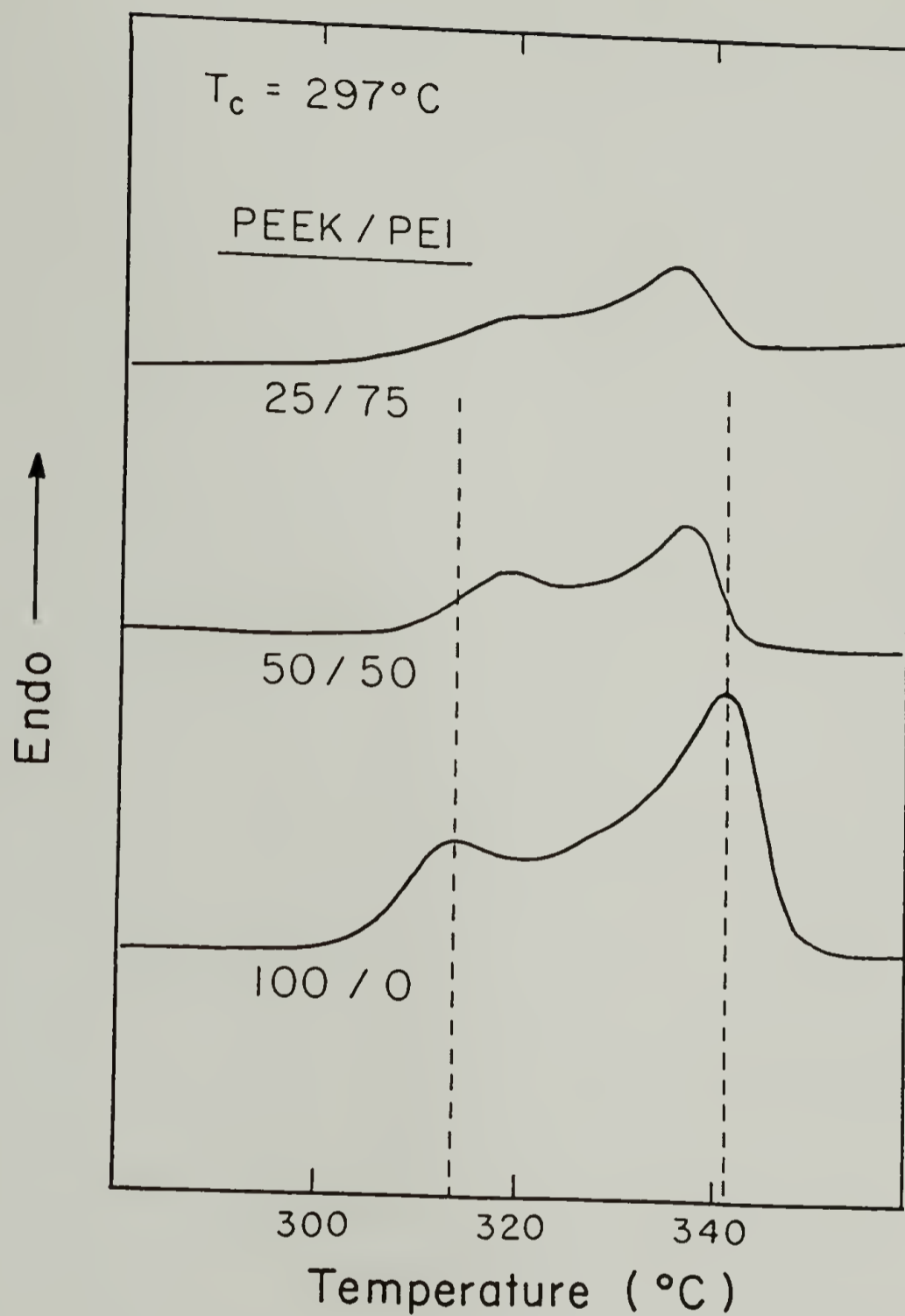


Fig. 5.8 The DSC traces of PEEK/PEI blends crystallized at 297°C for 12 hrs.

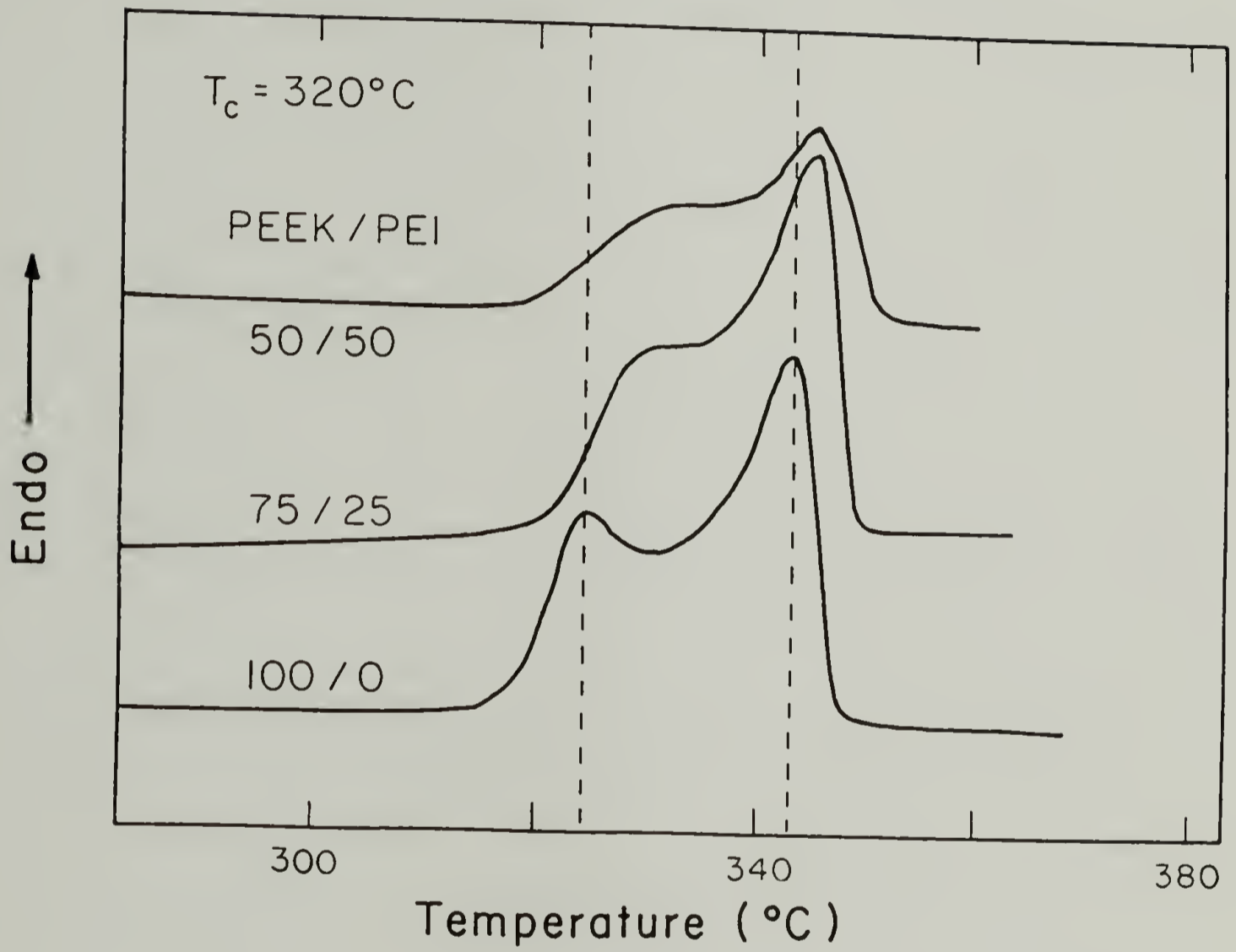


Fig. 5.9 The DSC traces of PEEK/PEI blends crystallized at 320 °C for 12 hrs.

305 °C. It can be seen that T_{m1} of the blends is ~ 5 °C higher than that of pure PEEK. T_{m2} of the blends, on the other hand, is ~ 4 °C lower than that of pure PEEK. As T_c is increased to 320 °C, the situation changes as shown in Fig. 5.9. Here T_{m1} of the blends is ~ 2 °C higher than that of pure PEEK. However, in contrast to the case of $T_c = 297$ °C, T_{m2} of the blends is ~ 2.5 °C higher than that of PEEK.

Fig. 5.10 and 5.11 display the DSC melting curves of PEEK and PEEK/PEI 75/25 blend scanned after crystallized at different T_c indicated. As expected, T_{m1} of both samples decreases with decreasing T_c . The T_{m2} of PEEK remains approximately constant for $T_c < 305$ °C due to crystal reorganization. However, it is interesting that T_{m2} of 75/25 blend still decreases with decreasing T_c at $T_c < 305$ °C, as can be seen in Fig. 5.11.

The above observations can be summarized by plotting the observed T_{m1} and T_{m2} of different PEEK/PEI blend compositions against the corresponding T_c , as shown in Fig. 5.12 and 5.13. Over the T_c range investigated (Fig. 5.12), T_{m1} of the blends is higher than that of pure PEEK at the same T_c . Fig. 5.13 is the T_{m2} vs. T_c plot, it can be seen that T_{m2} of the blends is higher than that of pure PEEK at $T_c > \text{ca. } 303$ °C. However, T_{m2} of the blends becomes lower than that of pure PEEK at $T_c < \text{ca. } 303$ °C. In addition, in this region, T_{m2} of all the blends decrease with decreasing T_c , while T_{m2} of PEEK remains approximately constant with T_c . This indicates that the reorganization of PEEK crystals in the blends is hindered. Consequently, this suggests that PEI is located in the interlamellar zones of PEEK lamellae. Although interfibrillar segregation has been observed for PEEK/PEI blends, the segregation of PEI from the interlamellar zones is not complete so that these regions do not contain exclusively pure PEEK chain segments. Indeed, PEEK is bulkier and stiffer than other flexible macromolecules such as polyethylene and poly(vinylidene fluoride). As

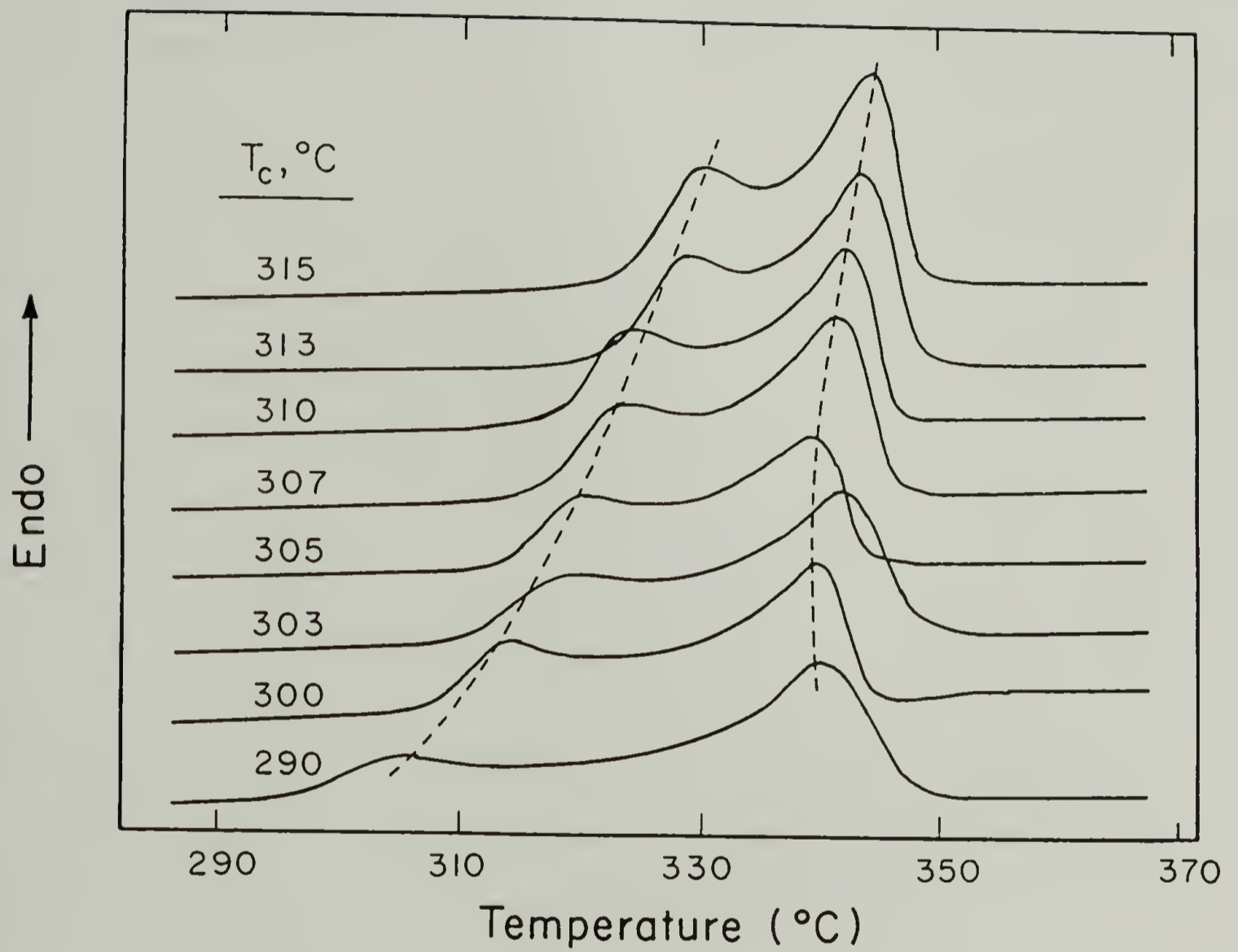


Fig. 5.10 The DSC traces of PEEK crystallized at different temperatures for 12 hrs.

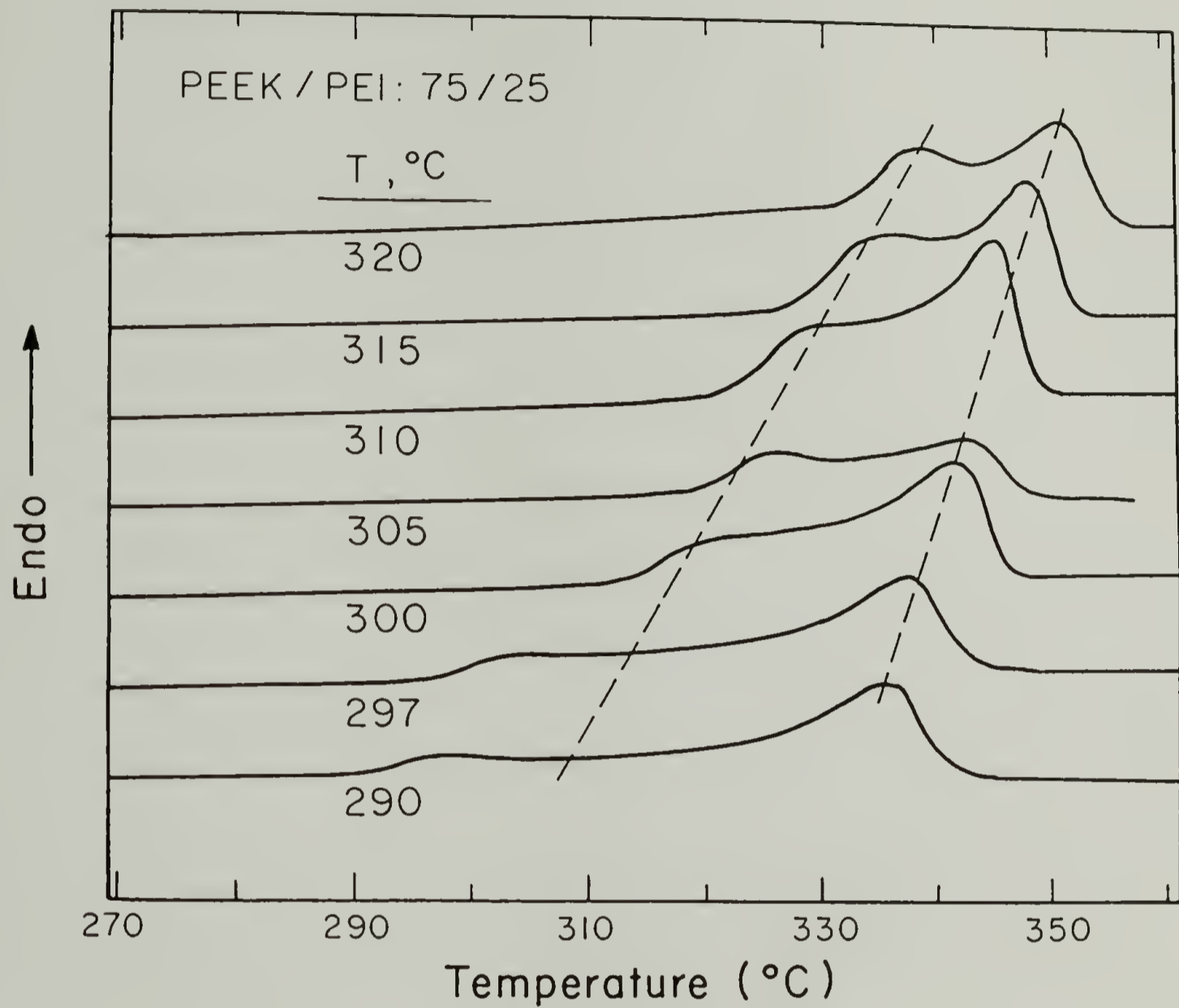


Fig. 5.11 The DSC traces of PEEK/PEI 75/25 blend crystallized at different temperatures for 12 hrs.

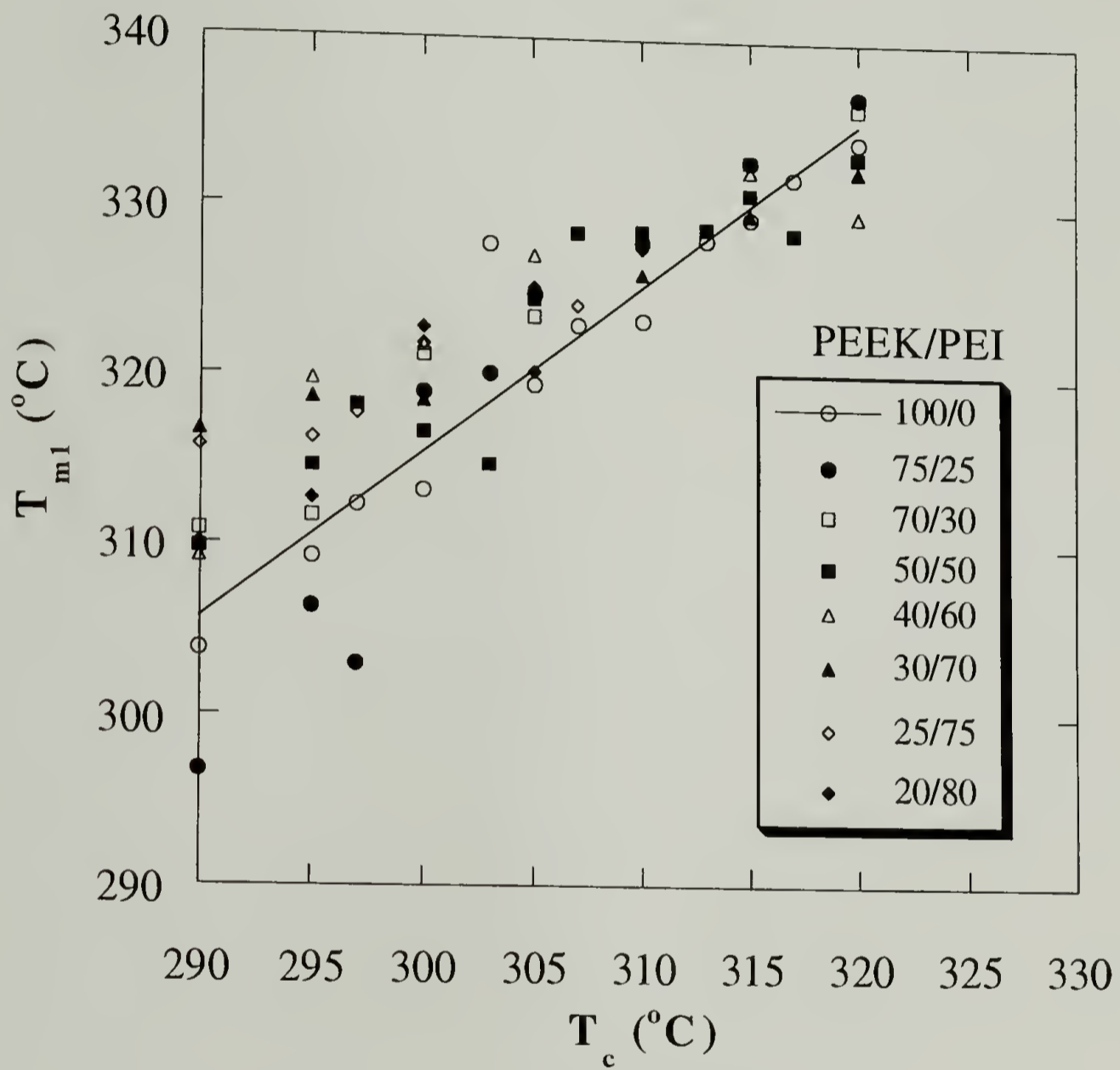


Fig. 5.12 T_{m1} vs. T_c plot of PEEK/PEI blends.

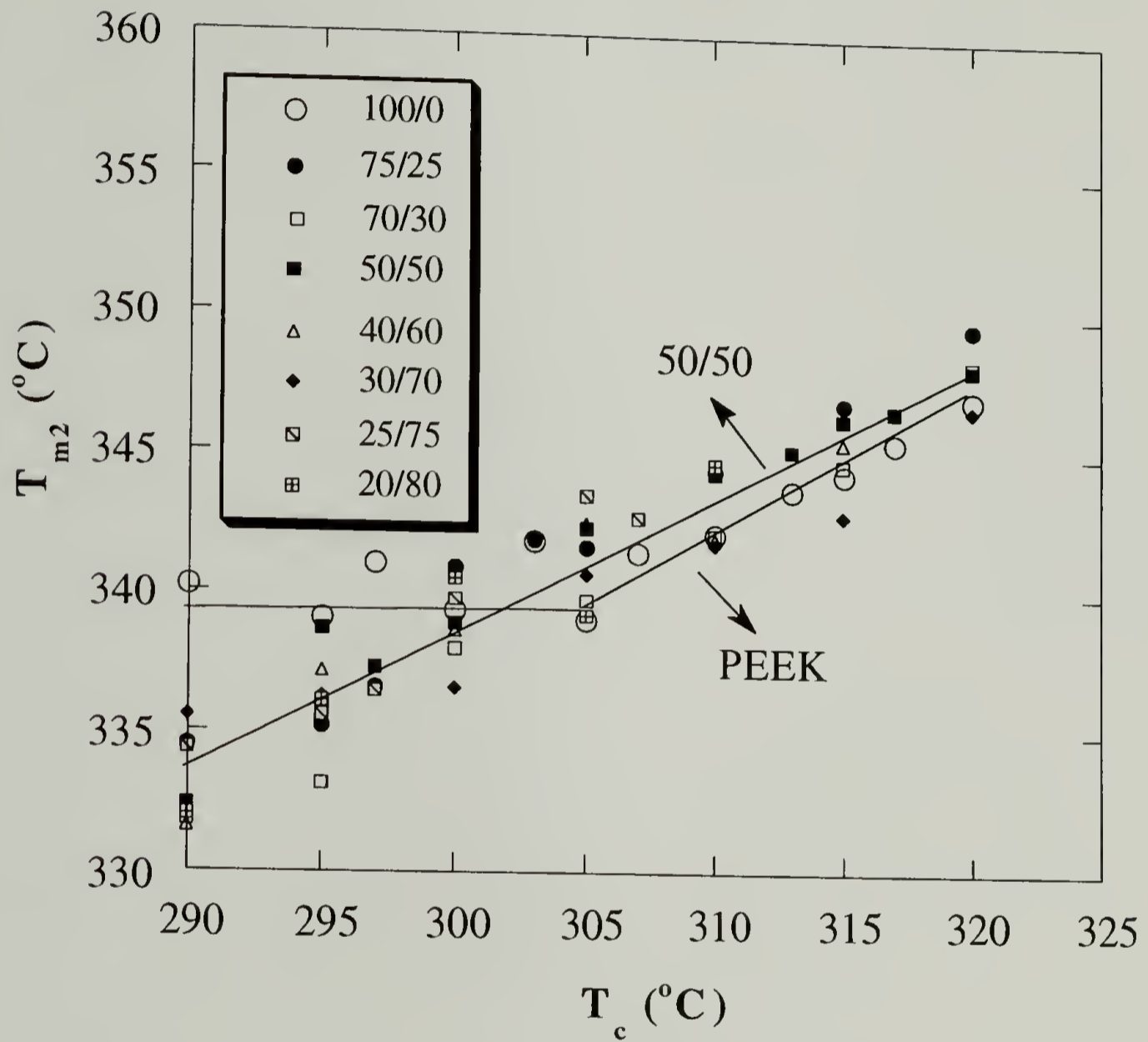


Fig. 5.13 T_{m2} vs. T_c plot of PEEK/PEI blends.

a consequence, the thickness of the crystal-amorphous interphase of PEEK is expected to be larger. The larger crystal-amorphous interphase facilitates the penetration of PEI segments into this region, which as a result hinders PEEK crystal reorganization.

5.5 Conclusions

The melting behavior of a solution-crystallized PEEK is investigated. PEEK was crystallized from the solution with dichloroacetic acid at 30 and 40 °C. The DSC scans of this solution-crystallized PEEK shows only one melting endotherm, in contrast to the two melting endotherms observed for the melt-crystallized PEEK. This indicates that the growth of the infilling secondary lamellae between the primary crystals did not occur in the solution crystallization. The semicrystalline morphology of PEEK/PEI blends has been studied by optical microscopy and DSC. The optical micrographs show that the branches of the spherulites become more clear for PEEK spherulites formed from the blend than that grown from pure PEEK melt. Therefore, a significant amount of PEI has been rejected to the interfibrillar regions of PEEK spherulites during PEEK crystallization. From the examination of PEEK crystal reorganization by DSC, it is found that the crystal reorganization is hindered in the blends. This has been attributed to the incorporation of PEI in the PEEK crystalline interlamellar regions.

References

1. Cheng, S. Z. D.; Cao, M.-Y.; Wunderlich, B. *Macromolecules* **1986**, 19, 1868.
2. Lee, Y., Ph.D. Thesis, Univ. of Mass., Amherst, Mass., **1988**.
3. Grevecoeur, G.; Groeninckx, G. *Macromolecules* **1991**, 24, 1190.
4. Hsiao, B. S.; Sauer, B. B. *J. Polym. Sci. Polym. Phys. Ed.* **1993**, 31, 901.
5. Stein, R. S.; Khambatta, F. B.; Warner, F. P.; Russell, T.; Escala, A.; Balizer, E. *J. Polym. Sci. Polym. Symp.* **1978**, 63, 313.
6. Russell, T.; Stein, R. S. *J. Polym. Sci., Polym. Phys. Ed.* **1983**, 21, 999.
7. Wenig, W.; Karasz, F. E.; MacKnight, W. J. *J. Appl. Phys.* **1975**, 46(10), 4194.
8. Russell, T. *ACS Polym. Prepr.* **1989**, 30(2), 282.
9. Keith, H. D.; Padden, F. J. *J. Appl. Phys.* **1964**, 35(4), 1270.
10. Warner, F. P.; MacKnight, W. J.; Stein, R. S. *J. Polym. Sci., Polym. Phys. Ed.* **1977**, 15, 2113.
11. Defiew, G.; Groeninckx, G.; Reynaers, H. *Polymer* **1989**, 30, 2160.
12. Gray, A. P.; Casey, K. *J. Polym. Sci. Polym. Lett. Ed.* **1964**, 2, 381.
13. Blundell, D. J.; Osborn, B. N. *Polymer* **1983**, 24, 953.
14. Zachman, H. G. *Kolloid Z.* **1969**, 231, 504.
15. Morra, B. S., Ph.D. Thesis, Univ. of Mass., Amherst, Mass., **1980**.
16. Alfonso, G. C.; Russell, T. *Macromolecules* **1986**, 19, 1143.
17. Kumar, S. K.; Yoon, D. Y. *Macromolecules* **1989**, 22, 4098.
18. Kumar, S. K.; Yoon, D. Y. *Macromolecules* **1991**, 24, 5414.

CHAPTER 6

UNIAXIAL DEFORMATION OF PEEK/PEI BLENDS BY SOLID-STATE COEXTRUSION

6.1 Introduction

It is known that the tensile moduli of polymers can be increased by uniaxial draw.¹ This process may create oriented, extended, and more densely packed chains, such that the stiffness and strength of the sample along the draw direction is improved. Solid-state coextrusion is a uniaxial drawing technique developed in this laboratory, and is superior for producing high-modulus polymers.² For instance, high density polyethylene (HDPE) has been drawn by this technique to change its modulus from 1 GPa to almost the theoretical modulus of 240 GPa.³ A prior drawing study of PEEK by solid-state coextrusion has been reported by Lee and Porter.⁴

There is an abundant literature on the uniaxially draw of homopolymers; however, such studies on polymer blends are rare. There has been no prior study on the deformation behavior of PEEK/PEI blends. As has been shown in the previous chapters, PEEK and PEI are miscible in the amorphous state, and PEEK can undergo crystallization at temperatures above T_g . It will thus be interesting to explore the effect of uniaxial deformation on the physical properties of PEEK/PEI blends, such as glass transition, crystallization behavior and the orientations of PEEK and PEI in the blends. In this chapter, the uniaxial draw of PEEK/PEI blends by solid-state coextrusion is described. Both amorphous and crystalline PEEK/PEI blends have been drawn by solid-state coextrusion at two temperatures: 125 °C which is below the T_g and 225 °C

which is above the T_g of the blends. The glass transition behavior, density, crystallization, and the orientations of PEEK and PEI in the drawn blends will be discussed.

6.2 Experimental

6.2.1 Sample Preparation

Fully amorphous films of PEEK and PEEK/PEI blends for solid-state coextrusion were prepared by compression molding at 400 °C under vacuum for 3 mins followed by quenching in cold water. The crystalline films were obtained by annealing the initial amorphous films at 265 °C for 3.5 hrs.

Isotactic polypropylene (PP) rods were used as coextrudates for uniaxial draw of PEEK/PEI blend films by solid-state coextrusion at 125 °C, and Nylon 6, 6 rods were used for the draw at 225 °C. The PEEK films were inserted as a ribbon within the PP or Nylon split billet and then press fitted into the barrel of an Instron capillary rheometer. The billet assemblies were then extruded through a conical brass die of 20° entrance angle. The extrusion draw ratio (EDR) was determined from the displacement of lateral ink marks placed initially on the film surface before (l_0) and measured after extrusion (l_t), viz., $EDR = l_t/l_0$.

6.2.2 Thermal Analysis

The glass transition and the crystallization behavior of drawn PEEK/PEI blends were studied by a Perkin-Elmer DSC-4. The DSC scans were all recorded at a heating or cooling rate of 20 °C/min. The DSC thermograms were normalized to 1 mg of the sample.

6.2.3 Density Measurement

The densities of the uniaxially drawn PEEK/PEI blends were measured by a density gradient column at 23 °C. Calcium nitrate aqueous solution was used to establish the density gradient ranging from 1.2400 to 1.4000 g/cm³. The sensitivity of the column was about 0.0001 g/cm³.

6.2.4 Infrared Dichroism

The orientations of PEEK and PEI in the drawn blends were determined by infrared dichroism. The infrared dichroic ratios of drawn PEEK/PEI films were measured by an IBM IR/32 Fourier-Transform infrared spectrometer with a resolution of 2 cm⁻¹ after computer-averaging 256 scans. The polarization of the incident beam was realized by the use of a Perkin-Elmer gold wire-gride polarizer. To eliminate the inherent polarizations of the instrument, parallel and perpendicular polarized spectra were used as reference. For the two perpendicular polarization measurements, the polarizer rather than the sample was rotated. This can avoid the error arising from the

nonuniform film thickness. Infrared dichroic ratio was calculated as $D = A_{\text{par}} / A_{\text{per}}$ with A_{par} and A_{per} being the optical densities at the absorption maximum.⁵

6.3 Results and Discussion

6.3.1 Uniaxial Draw of Amorphous PEEK/PEI Blends

The drawing experiments of amorphous PEEK by solid-state coextrusion have been reported.⁴ However, the previous drawing of amorphous PEEK was conducted at 154 °C, which is above the T_g of PEEK, and hence PEEK crystallized during draw. In the present study, amorphous PEEK and PEEK/PEI blends were drawn at 125 °C, which is below the T_g (cold drawing). Since there is no thermally-induced crystallization during cold drawing, the structural change of amorphous PEEK/PEI blends are induced solely by drawing.

The effect of drawing on the glass transition behavior of amorphous PEEK/PEI blends has been studied. Fig. 6.1 and 6.2 show the T_g regions of amorphous drawn PEEK and 50/50 blend, respectively. The exotherms observed in the DSC traces are due to the cold crystallization of PEEK. It can be seen that the T_g of both PEEK and the blend are depressed by drawing. The T_g of amorphous PEEK is decreased by 7 °C as the EDR reaches 2.8. Fig. 6.3 displays the T_g vs. EDR plot. The T_g depression by drawing is seen to occur over the whole composition range. It is also noted that, in contrast to T_g , the heat capacity increment at the glass transition (ΔC_p) is increased by drawing, as can be seen in Fig. 6.1 and 6.2. The ΔC_p vs. EDR plots for PEEK and 50/50 blend are shown in Fig. 6.4 and 6.5, respectively. The increase

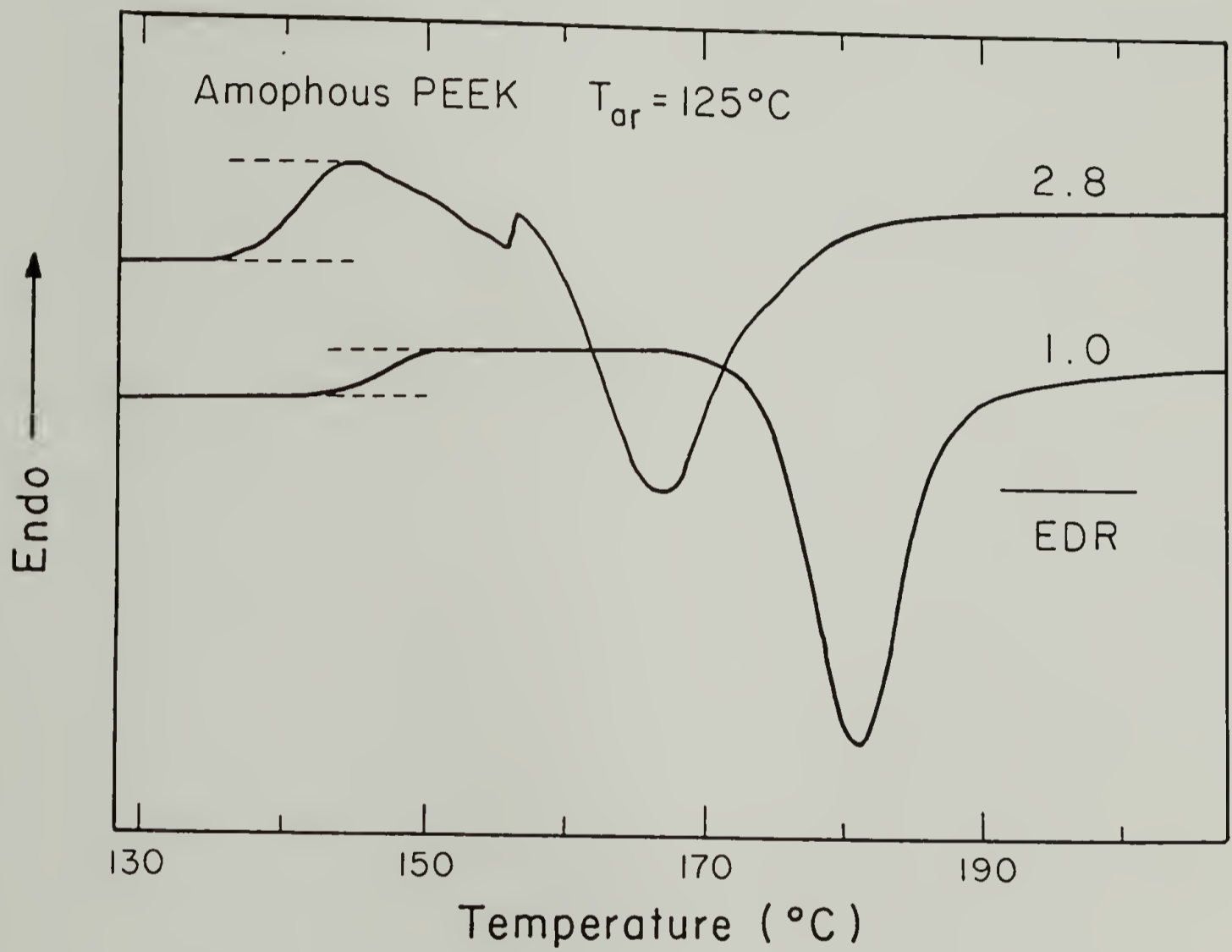


Fig. 6.1 The DSC traces of amorphous PEEK drawn at 125°C .

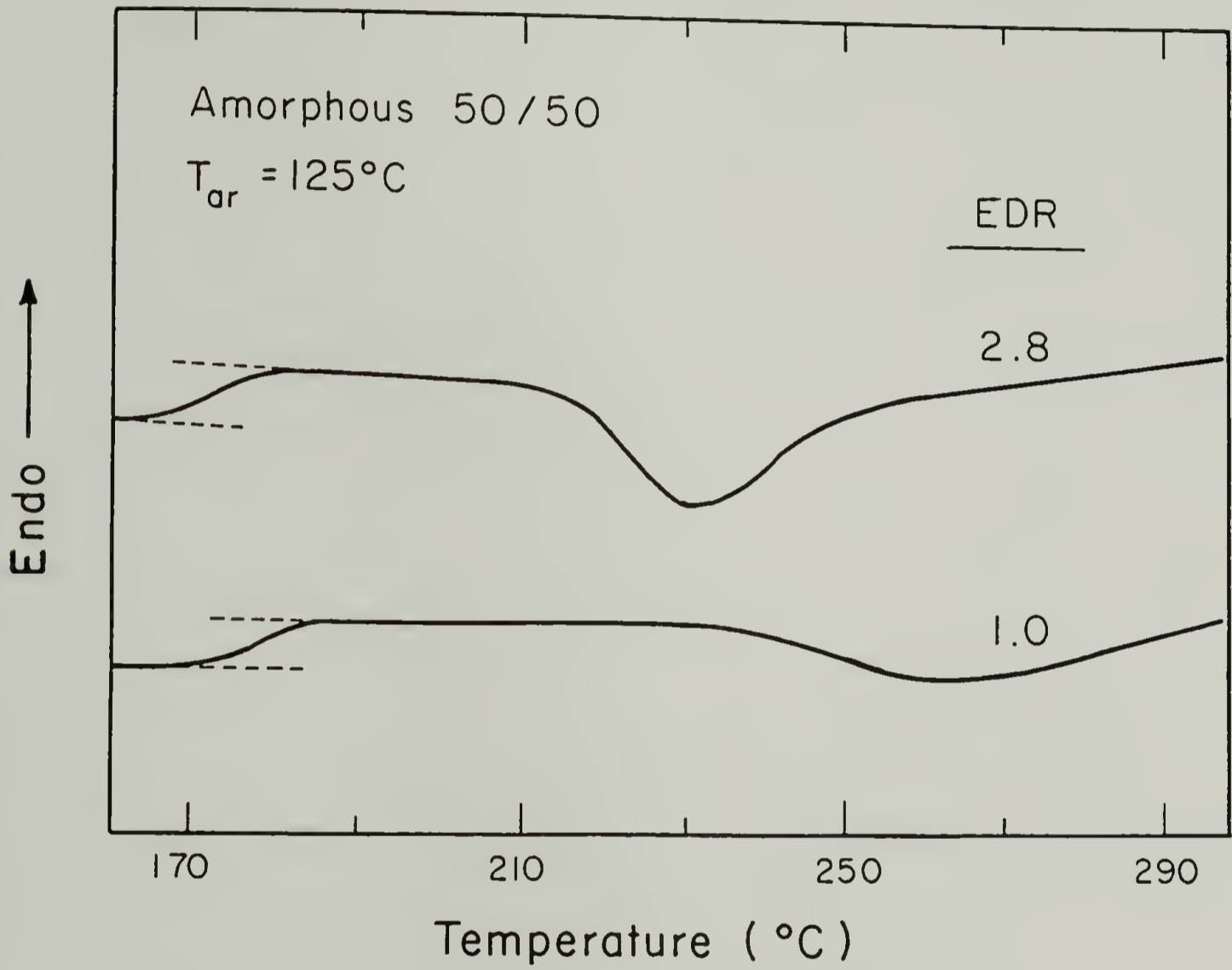


Fig. 6.2 The DSC traces of amorphous 50/50 blend drawn at 125 °C.

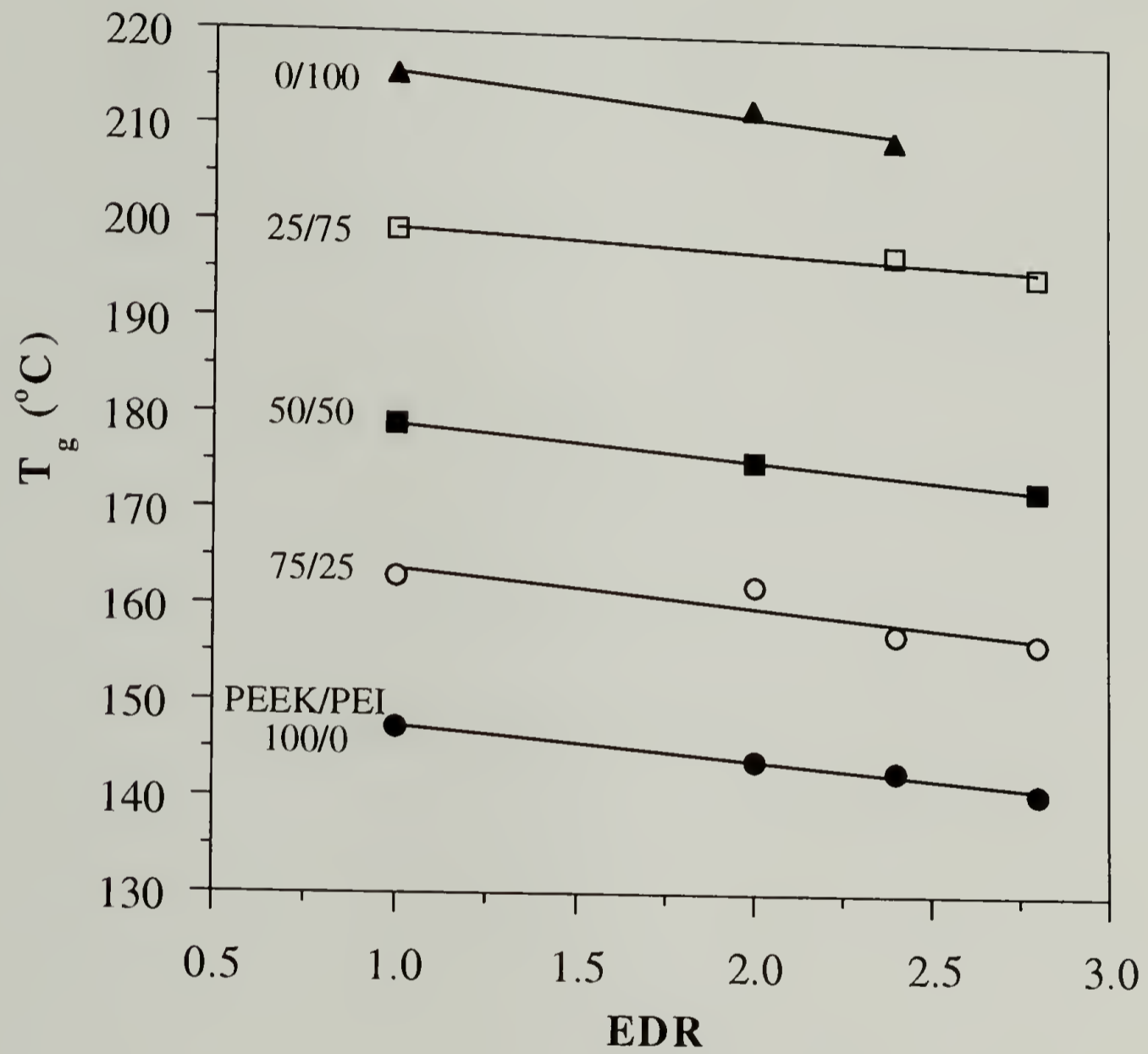


Fig. 6.3 The variations of T_g with EDR for amorphous PEEK/PEI blends drawn at 125 °C.

in ΔC_p may be expected from the Simha-Boyer rule, which suggested that the product $T_g \Delta C_p$ is a constant.⁶

It has been established that tensile stretching may lower the T_g of a polymer.⁷⁻¹² The decrease in T_g with increasing tensile stress has been ascribed to the increase in free volume with increasing applied stress.^{8,12} The increase in free volume upon tensile stretching is visualized by the experimental observation that tensile stretching is normally a dilation process (the Poisson's ratio of a glassy polymer is normally less than 1/2, and hence the volume is increased by elongation).⁸⁻¹⁰ The theoretical treatment by Chow has provided a quantitative prediction for the tensile stress dependence of T_g .¹² Robertson has proposed that it is the shear component of the tensile stress that causes the T_g depression.¹¹

To test if the volume of amorphous PEEK/PEI blends was increased by drawing (so that the conventional free volume concept can be applied to explain the observed T_g depression by drawing), the densities of the drawn samples were measured. Fig. 6.6 is the plot of the measured density vs. EDR for the drawn amorphous PEEK/PEI blends. Over the whole composition range, the density increases with increasing EDR. Therefore, the conventional free volume concept does not apply in this case.

The X-ray scattering studies on the structural change accompanying volume change in polystyrene have been reported by Song and Roe.¹³ The results suggested that the specific volume alone is not sufficient to characterize the glassy state. The local segmental packing or the free volume distribution is another parameter that should be considered. Therefore, it is likely that cold drawing of PEEK/PEI blends

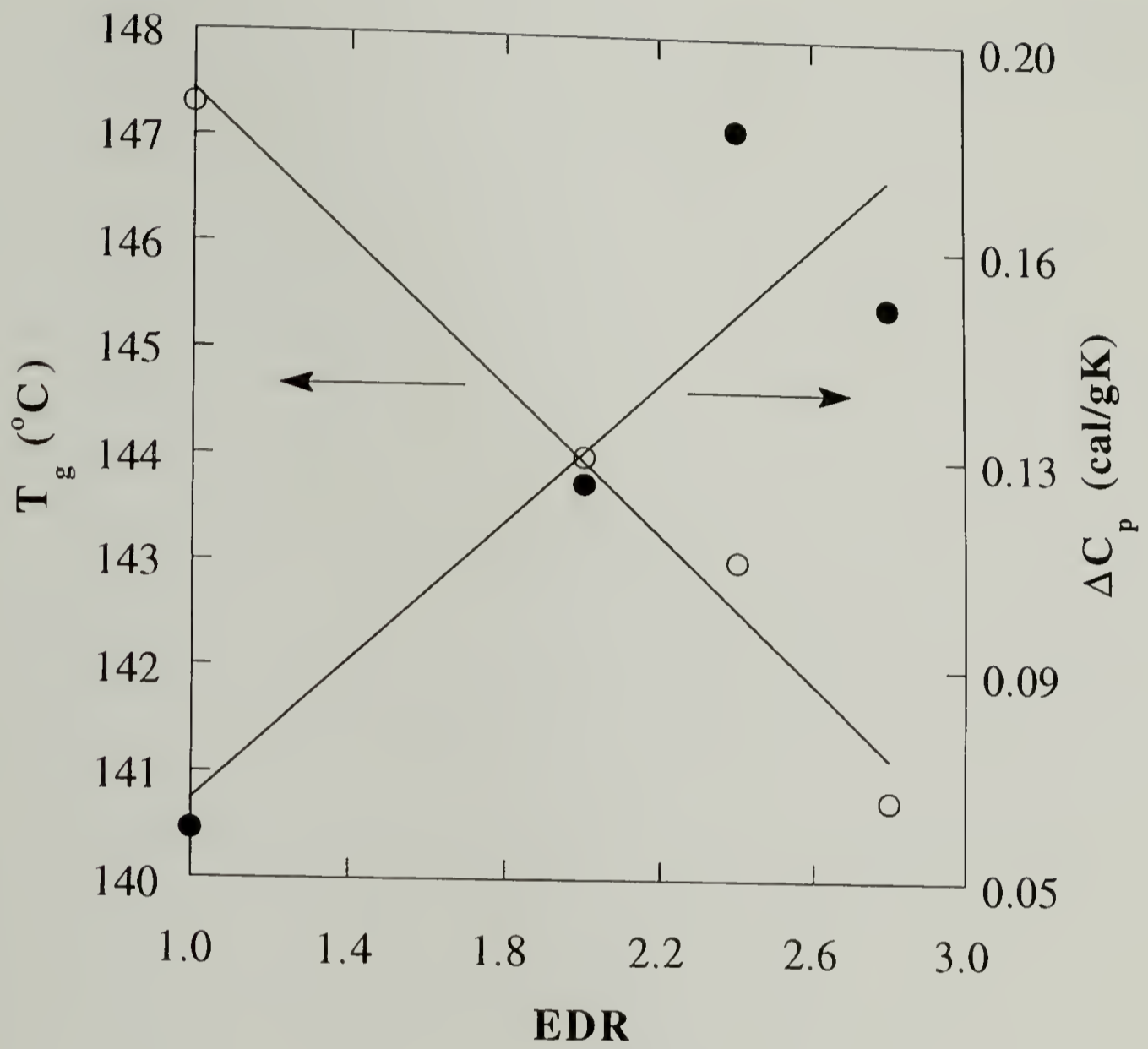


Fig. 6.4 T_g and ΔC_p vs. EDR of amorphous PEEK drawn at 125 °C.

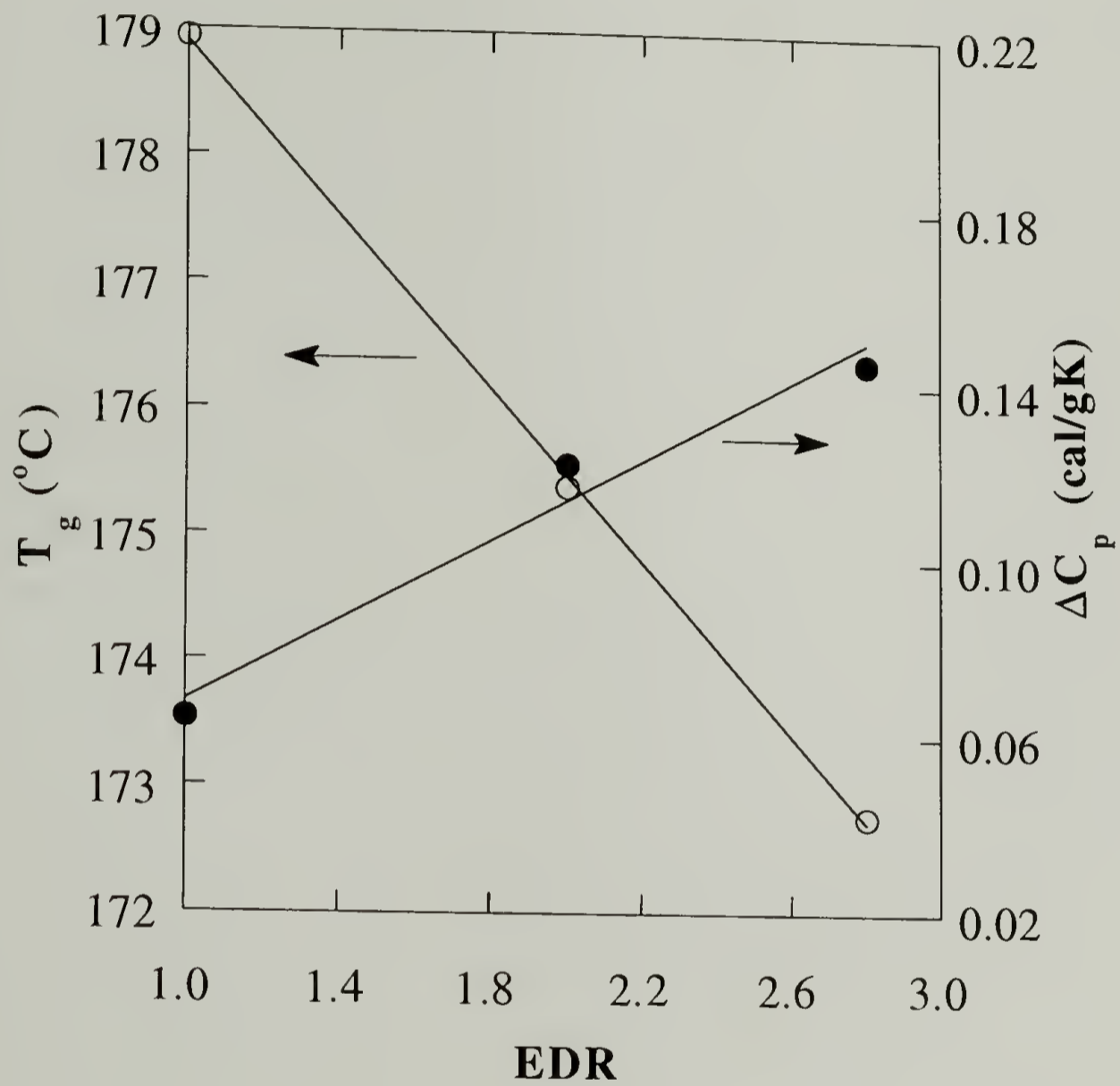


Fig. 6.5 T_g and ΔC_p vs. EDR of amorphous 50/50 blend drawn at 125 $^{\circ}\text{C}$.

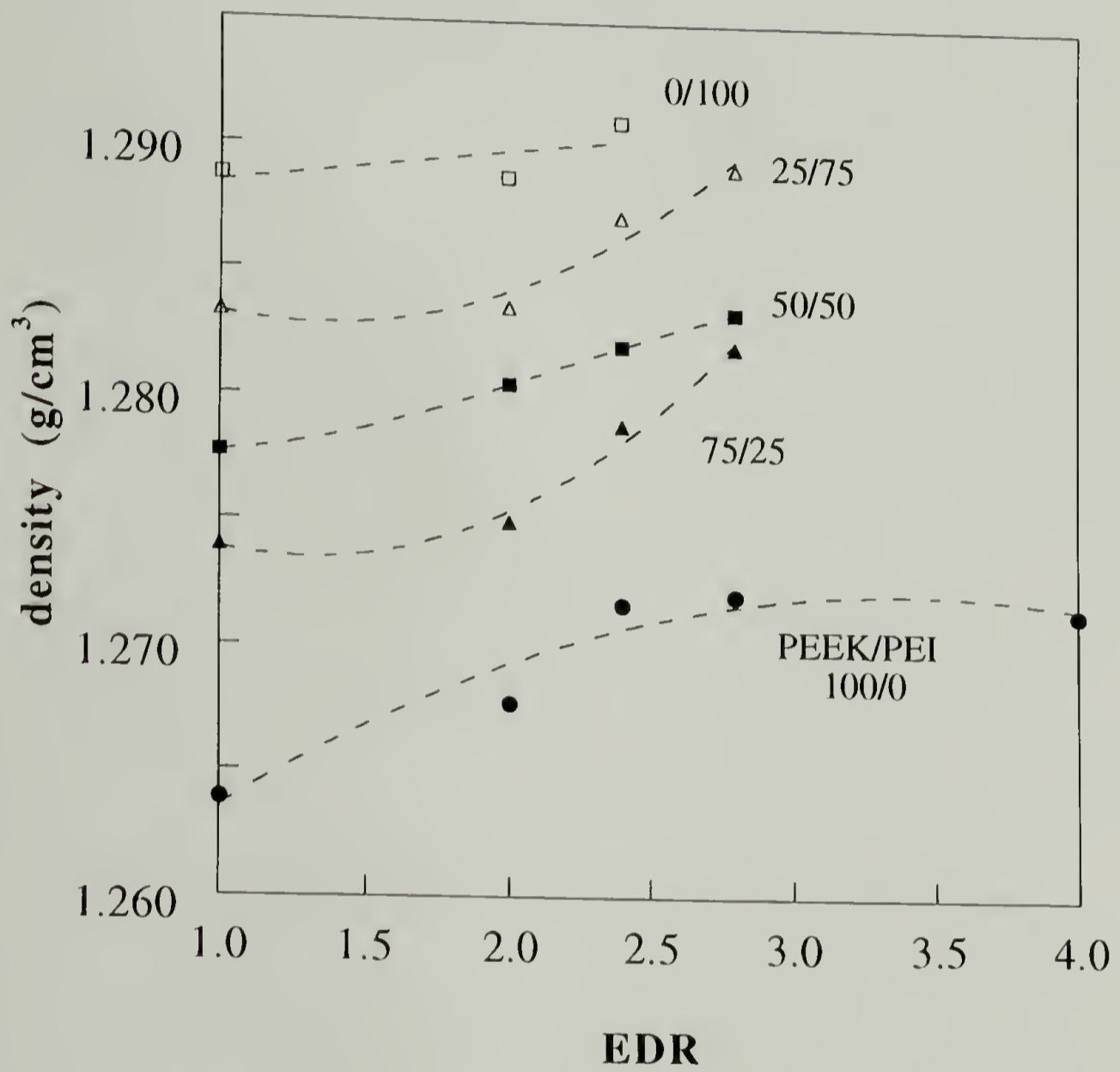


Fig. 6.6 The densities of amorphous PEEK/PEI blends drawn at 125 °C.

has altered the segmental packing and the distribution of free volume to such an extent that it induced the depression in T_g , despite the density was increased.

In this study, the maximum obtained draw ratio for PEEK film is 4, and this was achieved by two-stage solid-state coextrusion. This draw ratio could not be achieved for the blends. For pure PEI, the maximum draw ratio was only 2.4, and further increase in drawing temperature to 230 °C did not increase the drawability of PEI. A strain-induced crystallization is observed for PEEK at EDR = 4.0, as evidenced in Fig. 6.7. Fig. 6.7 displays the DSC scans of PEEK drawn from the amorphous state at 125 °C. It can be seen that the cold crystallization exotherm on heating is not observed for PEEK at EDR = 4.0. This shows that crystallization of PEEK has been induced by drawing at EDR = 4.0.

6.3.2 Density Changes of Crystalline Drawn PEEK/PEI Blends

The density changes of the crystalline PEEK/PEI blends on drawing have been investigated. Fig. 6.8 displays the density vs. EDR plot of crystalline PEEK drawn at two temperatures. It can be seen that for the higher drawing temperature (T_{dr}) of 225 °C, the density stays approximately constant or with a shallow minimum in the region of EDR < 2.8, and the density increases monotonically with increasing EDR for EDR > 2.8. On the other hand, for $T_{dr} = 125$ °C, the density vs. EDR shows a minimum at EDR = 2.0. The density minimum has also been reported by Lee and Porter for PEEK drawn from the amorphous state at 154 °C.⁴ In their study, the minimum was observed at EDR = 3.0, which is higher than that shown in Fig. 6.8. This may be due to the occurrence of thermally-induced crystallization in their study, and such effect also contributed to the change in density on drawing, which consequently shifted the

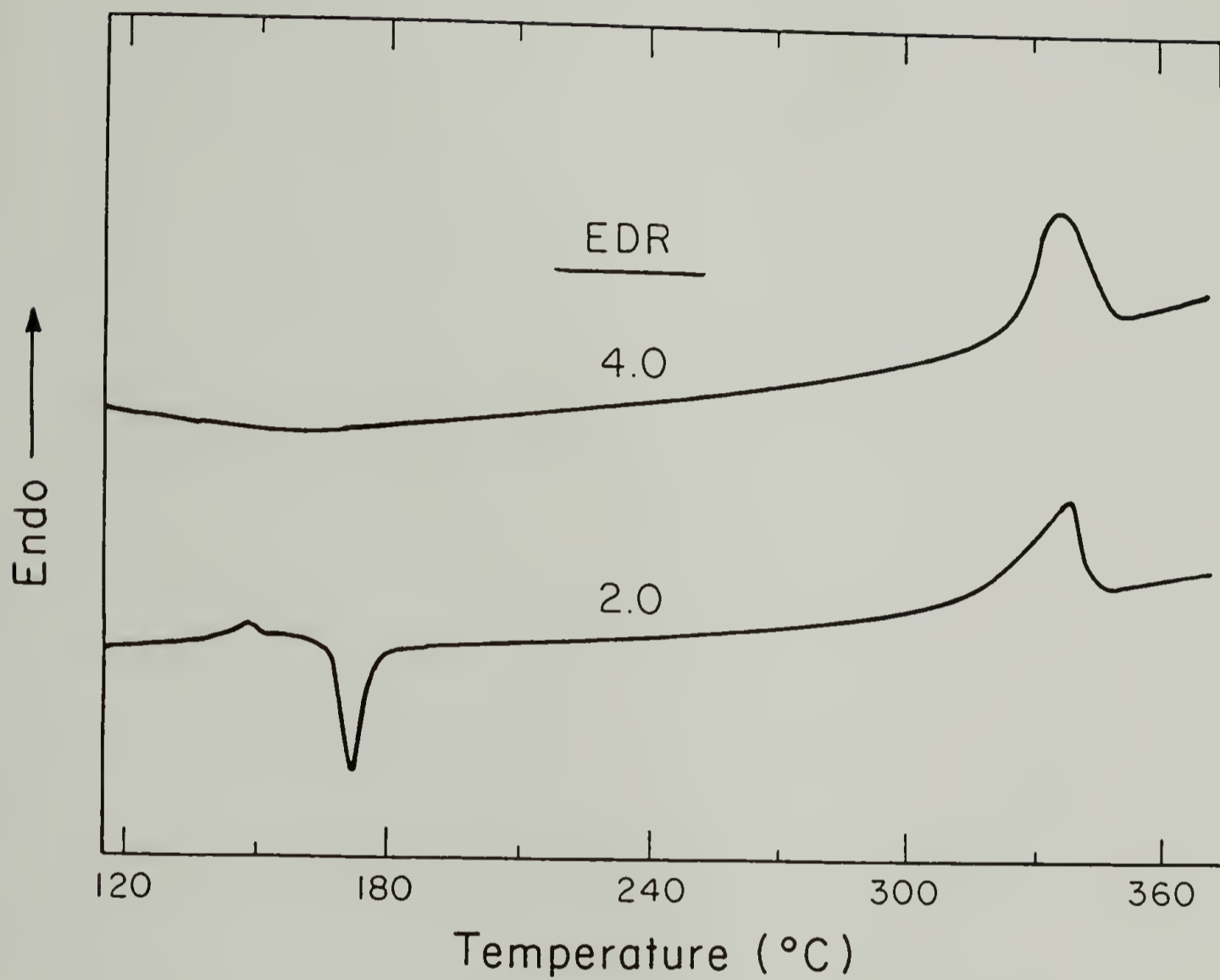


Fig. 6.7 The DSC traces of amorphous PEEK drawn at 125 °C. The cold crystallization exotherm is not observed at EDR = 4.0, indicating a strain-induced crystallization.

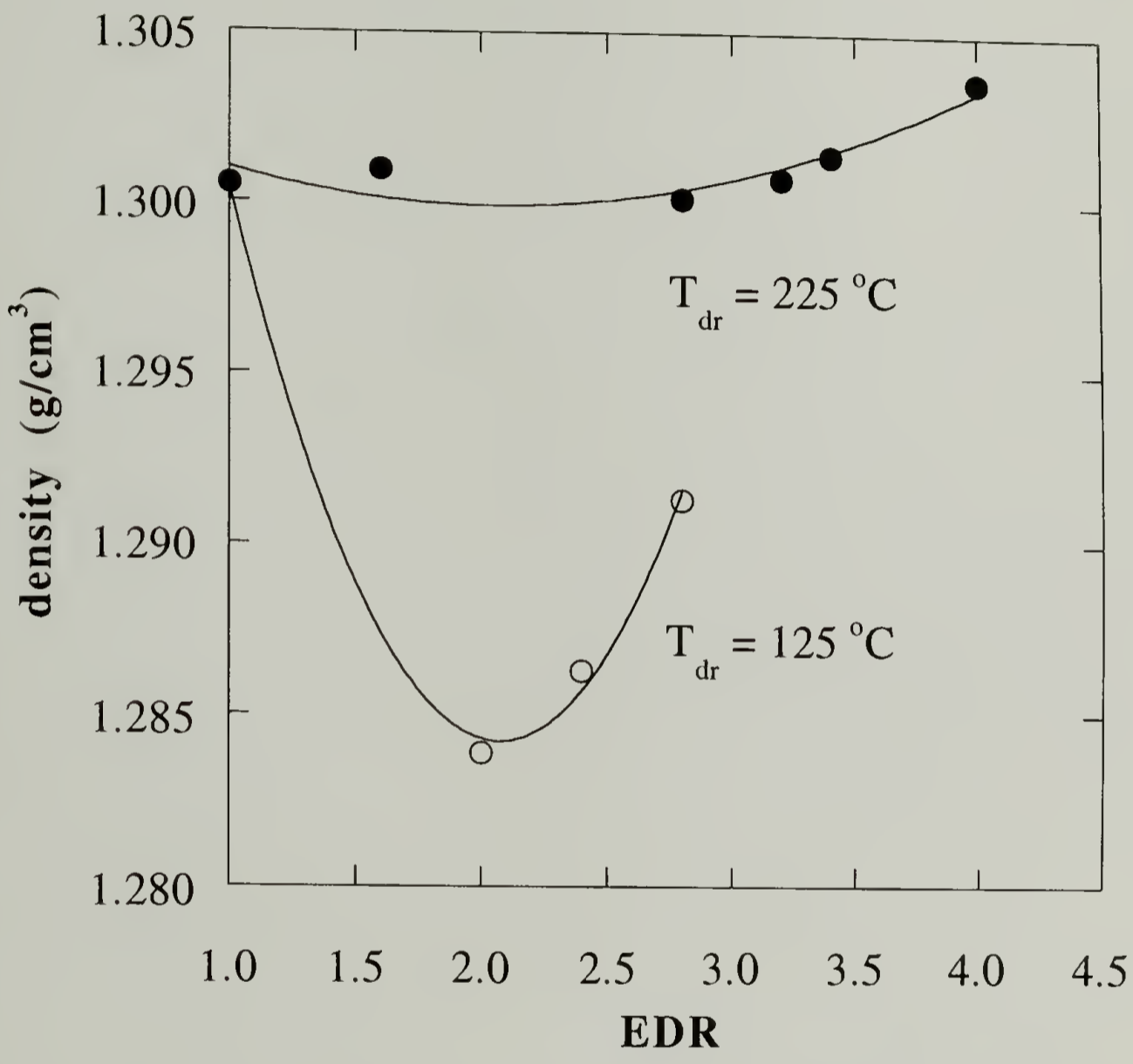


Fig. 6.8 The densities of crystalline PEEK drawn at 225 and 125 °C.

minimum to higher EDR. The density minima have also been observed at EDR of 3 for solid-state extruded poly(ethylene terephthalate) (PET),¹⁴ and at EDR of 5-10 for HDPE.¹⁵

The density changes of crystalline PEEK/PEI 75/25 blend on drawing are shown in Fig. 6.9. In contrast to PEEK, the densities decrease monotonically with increasing EDR for both blend samples drawn at two temperatures. In Fig. 6.8 and 6.9, it is also noted that the densities of the samples drawn at 225 °C are higher than that drawn at 125 °C.

The decrease in density with EDR in some semicrystalline polymers has been suggested to result from the partial distortion and subsequent destruction of the original crystals on transformation into fibril structure.¹⁶ During this process some oriented interfibrillar voids are created. At high EDR, the chains in the amorphous regions are extended to pack more closely and extended chain crystals are formed. This transformation increases the density and the combination of these two opposing effects may generate a minimum in the density vs. EDR plot, as observed for PEEK. For the blends, the decrystallization by drawing dominated over the densification in the amorphous regions, and hence the density decreases monotonically with increasing EDR. This would also imply that the densification in the amorphous regions is more difficult in the blends.

The destruction of PEEK crystals upon drawing is supported by the DSC study. Fig. 6.10 and 6.11 show the DSC traces of the crystalline drawn PEEK and PEEK/PEI 75/25 blend, respectively. It can be seen that the lower melting endotherm observed at ca. 273 °C for the undrawn samples is not observed in the traces of the drawn samples. This indicates that the lower-melting PEEK crystals were disrupted

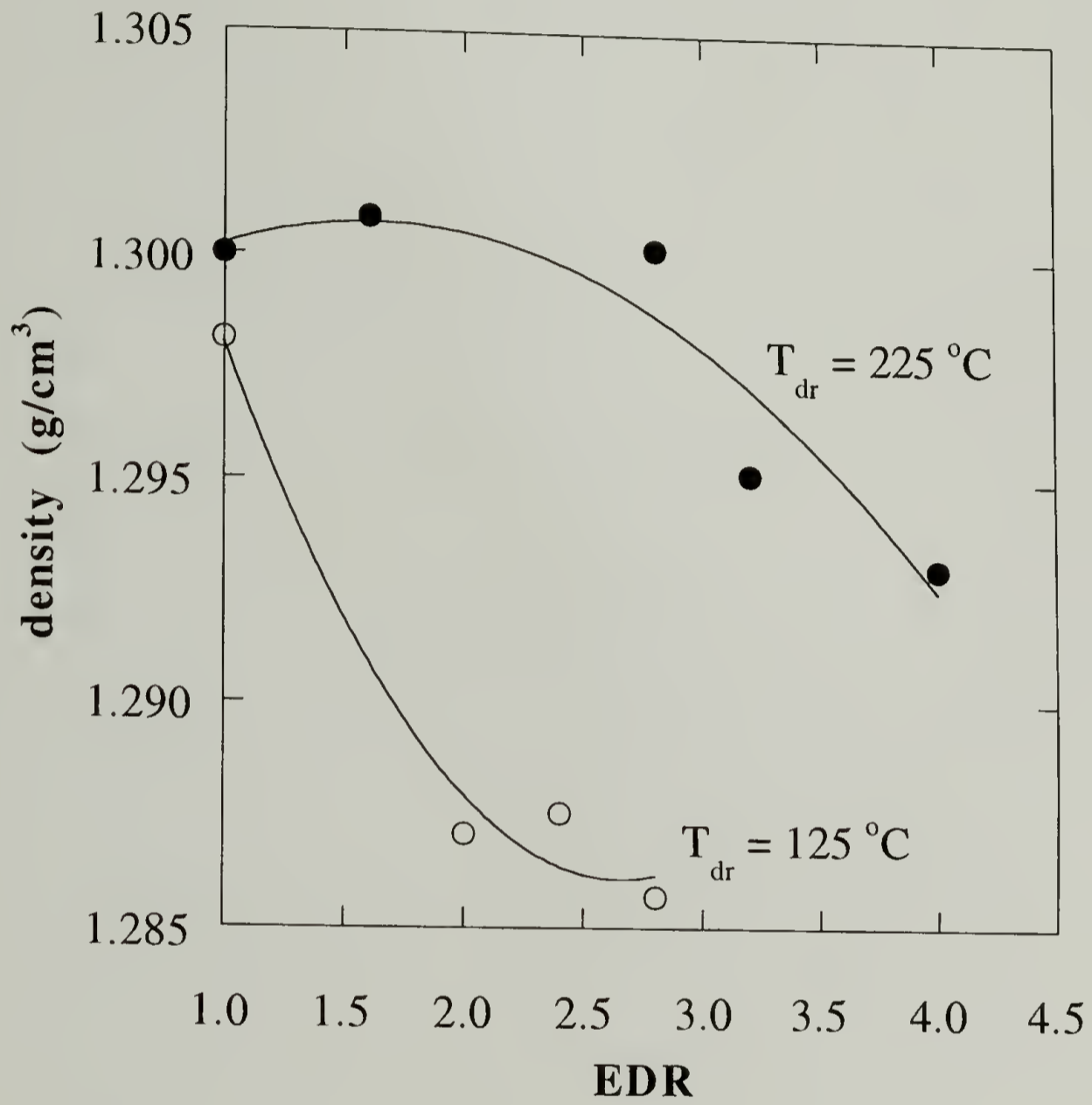


Fig. 6.9 The densities of crystalline 75/25 blend drawn at 225 and 125 °C.

by drawing. The degree of crystallinity determined from the enthalpy of melting is plotted against the EDR in Fig. 6.12. It can be seen that the DSC crystallinity decreases with increasing EDR for all compositions investigated.

Assuming an ideal crystalline and amorphous two-phase model, the density of the amorphous phase can be calculated from the overall density and the DSC crystallinity. The density of 1.415 g/cm^3 was adopted as the density of 100 % crystalline PEEK.⁴ The calculated density of the amorphous phase is plotted against EDR in Fig. 6.13. The absolute values of the calculated densities may be subject to some error, since there are still controversies over the density of 100% crystalline PEEK (reported between 1.378 and 1.415 g/cm^3).¹⁷⁻¹⁸ Nevertheless, the variation of the density with EDR is the primary interest here. Fig. 6.13 shows that for both PEEK and the blends, the densities of the amorphous phase exhibit a minimum at $\text{EDR} = 2$. This implies that on the initial drawing, the destructions of the lower-melting PEEK crystals occurred predominantly. The decrease in PEEK crystallinity loosened the amorphous regions consistent with a drop in density occurred on initial drawing. As the EDR was further increased, the orientations of the chains in the amorphous regions induced closer packing as the density increased.

For pure PEEK drawn at $225 \text{ }^\circ\text{C}$, the density minimum is not clearly observed (Fig. 6.8). Since $225 \text{ }^\circ\text{C}$ is $80 \text{ }^\circ\text{C}$ above the T_g of PEEK, after the destruction of the lower-melting PEEK crystals by drawing, the recrystallization in the amorphous regions can occur. This effect would increase the density of the sample. Therefore, no minimum is observed for $T_{dr} = 225 \text{ }^\circ\text{C}$. For PEEK rods drawn at $310 \text{ }^\circ\text{C}$, the density has been found to increase monotonically with EDR.⁴

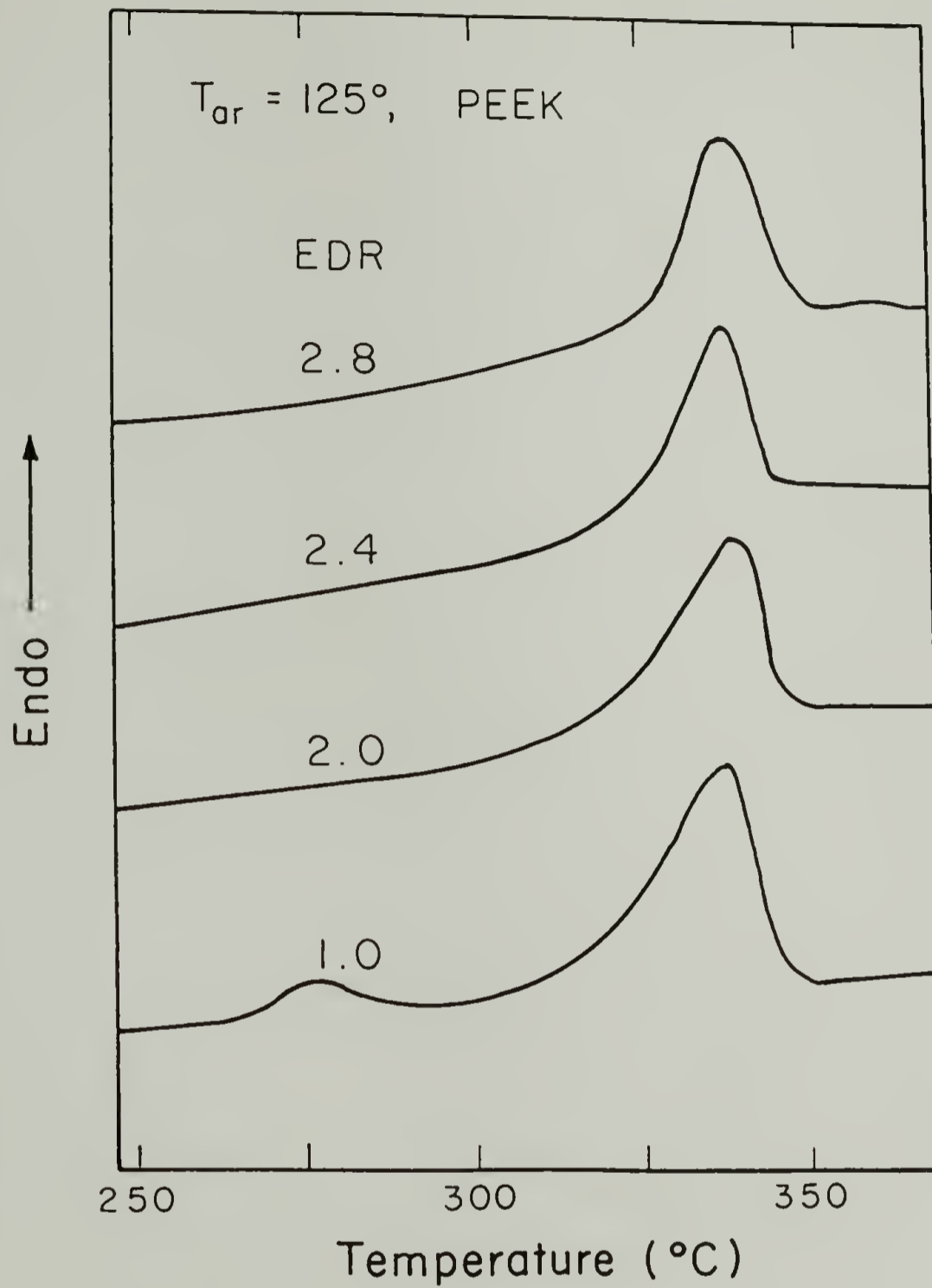


Fig. 6.10 The DSC traces of crystalline PEEK drawn at 125 °C.

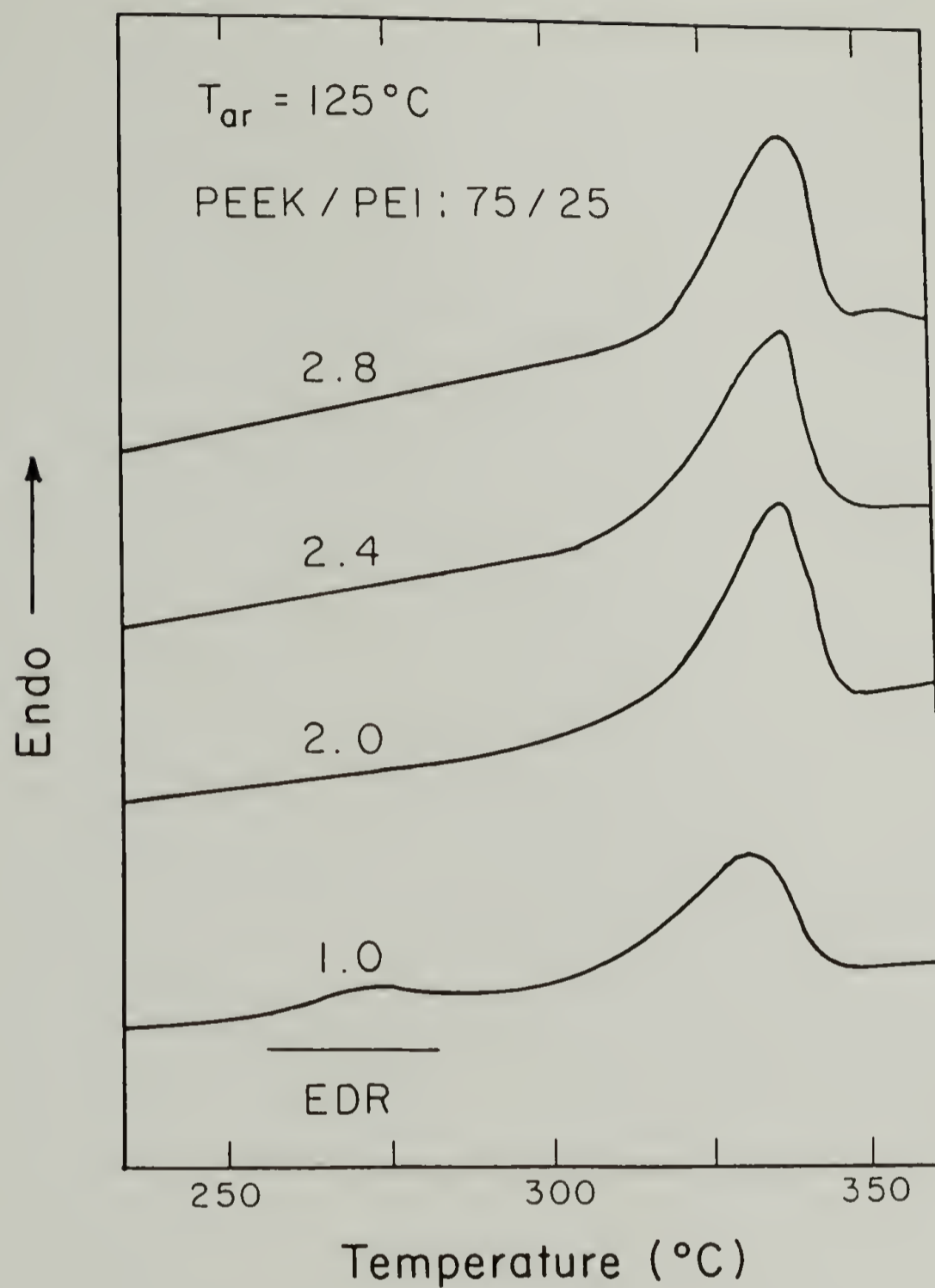


Fig. 6.11 The DSC traces of crystalline PEEK/PEI 75/25 blend drawn at 125 °C.

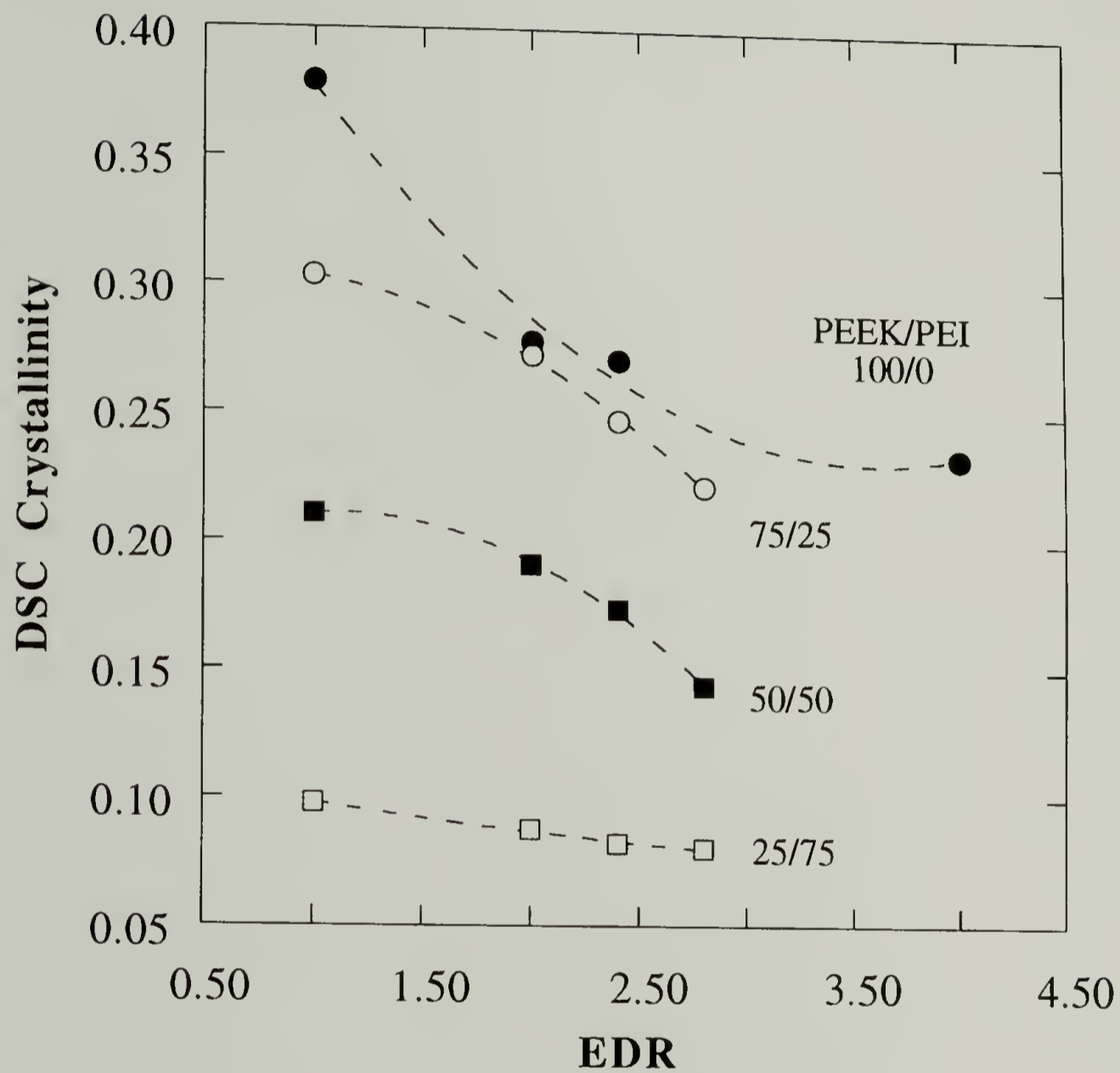


Fig. 6.12 The fractional crystallinity measured by DSC vs. EDR of crystalline PEEK/PEI blends drawn at 125 °C.

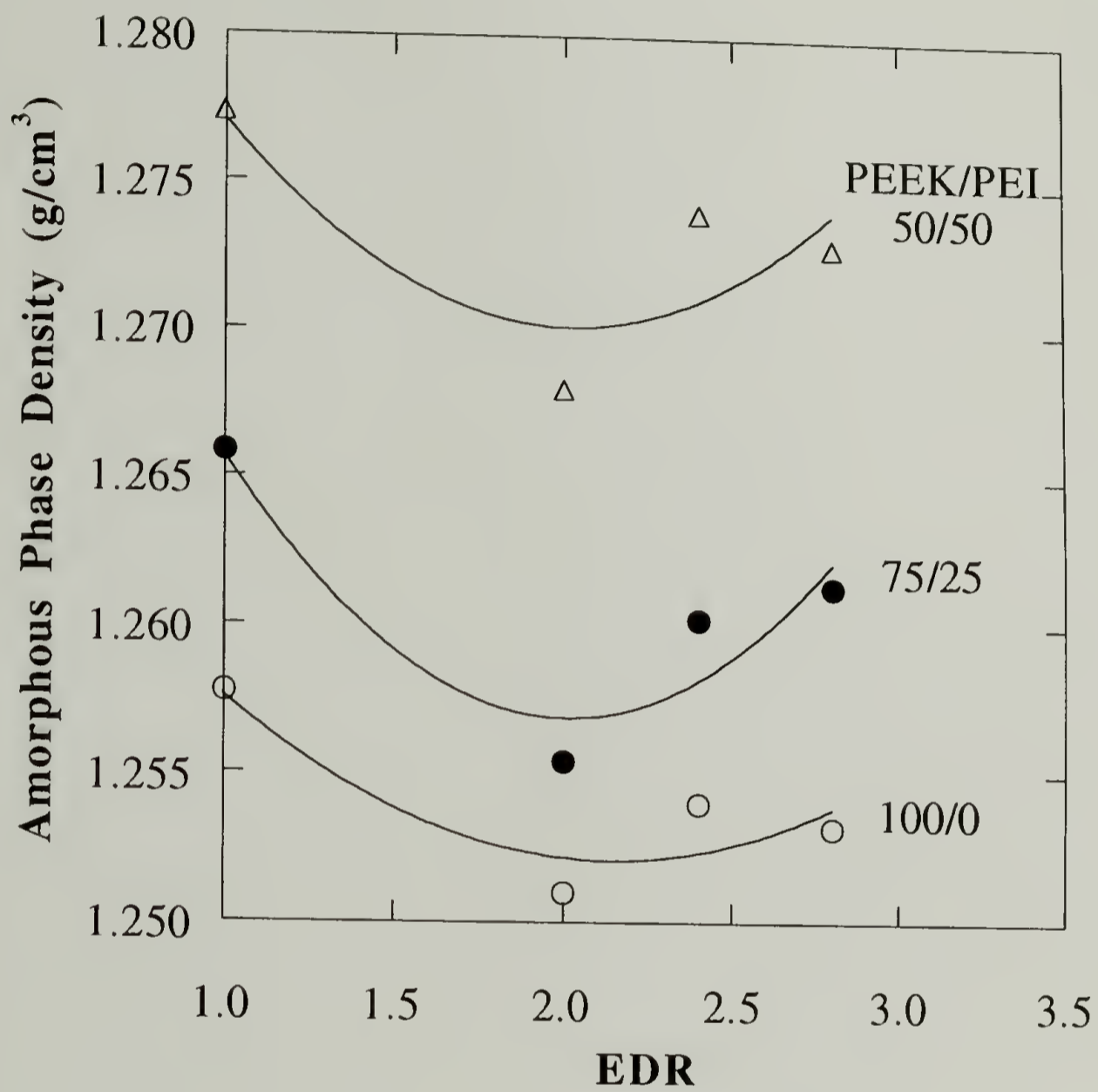


Fig. 6.13 The density of the amorphous phase calculated by the two-phase model for crystalline drawn PEEK/PEI blends; $T_{dr} = 125$ °C.

6.3.3 Crystallization Behavior

It is known that crystallization rate can be promoted by orientation. Molecular orientation decreases the entropy, and hence increases the degree of supercooling at a given crystallization temperature.¹⁹⁻²⁰ In addition, the conformations of the oriented molecules are closer to the conformation in the crystalline state; therefore, the chain packing during crystallization can be facilitated by orientation.

In Fig. 6.1 and 6.2, it can be seen that the cold crystallization exotherms of amorphous drawn PEEK/PEI blends shift to lower temperatures upon drawing. Fig. 6.14 displays the peak temperature of the cold crystallization exotherm (T_c) vs. EDR plot. For all compositions investigated, T_c decreases with increasing EDR, indicating that the cold crystallization is promoted by drawing.

It should be noted that in addition to crystallization, the relaxation (disorientation) of the oriented chains can also take place above T_g . Therefore, there should be a competition between the relaxation and the crystallization of the oriented chains. For PET, crystallization and relaxation have been found to occur simultaneously.²¹⁻²³ It has been demonstrated in Chapter 3 that TMA is a powerful technique for studying the crystallization of PEEK. TMA may also be used to investigate the crystallization and relaxation in oriented PEEK. When the film thickness normal to the draw direction is measured, the relaxation of the oriented chains will result in a thickness increase, opposing a decrease arising from crystallization.

Fig. 6.15 shows the direct recorded TMA traces of amorphous drawn PEEK films (EDR = 2.0) during isothermal crystallization. It can be seen that the film

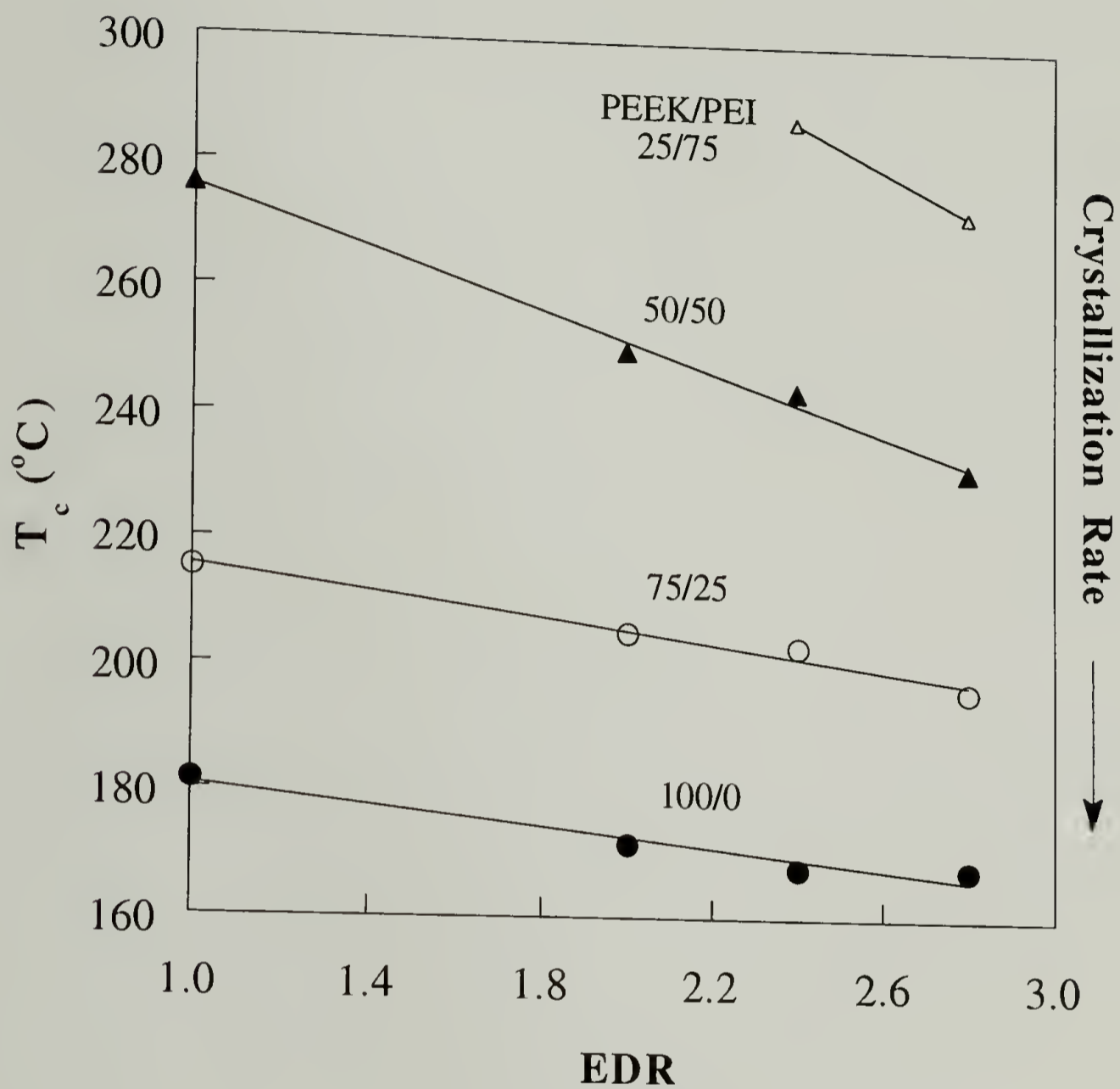


Fig. 6.14 The peak temperature of the cold crystallization exotherm vs. EDR plot of amorphous PEEK/PEI blends drawn at 125 °C.

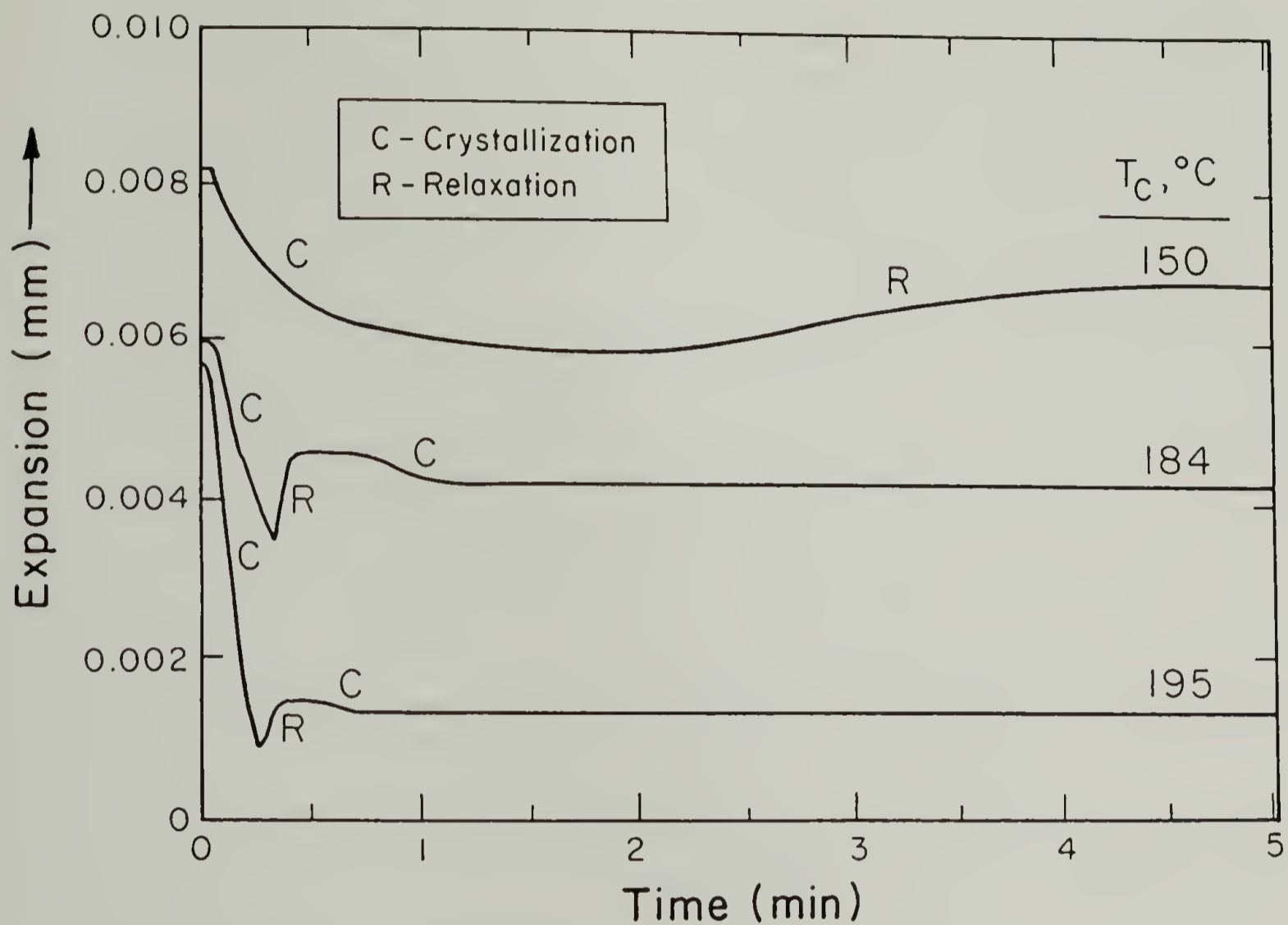


Fig. 6.15 Directed recorded TMA traces of the isothermal crystallization of amorphous drawn PEEK (EDR = 2.0, $T_{dr} = 125$ °C). The crystallization temperatures are indicated in the figure.

thickness drops initially followed by an increase. Fig. 6.15 indicates that the crystallization started prior to the relaxation in the cold crystallization of oriented PEEK. Since the cold crystallization in drawn PEEK is faster than in the undrawn state, if the crystallization had to start after the completion of chain relaxation, the crystallization in the drawn PEEK should have been slower.

In addition to cold crystallization, the crystallization following annealing the drawn PEEK/PEI blends in the melt is also of interest. A previous study on such crystallization of drawn PEEK by Lee and Porter has shown some interesting results.⁴ In their study, the drawn PEEK was annealed at 370 °C for 5 mins followed by DSC cooling scan at 10 °C/min. This showed that after melt annealing, the drawn PEEK actually crystallized slower than the undrawn PEEK. It was proposed that the drawn PEEK chains had to relax first before crystallization. In the present study, similar but more thorough melt annealing experiments are carried out for both drawn PEEK and PEEK/PEI blends.

Fig. 6.16 shows the DSC cooling scans of amorphous drawn PEEK after annealing at 370 °C for 5 mins. The crystallization exotherms of the drawn PEEK are located at lower temperatures, confirming that the melt crystallization in the drawn PEEK is slower than in the undrawn PEEK. Fig. 6.17 is a plot of the exothermic peak temperature vs. EDR. It can be seen that the melt crystallization of the crystalline drawn PEEK crystallizes faster than the amorphous drawn PEEK. This may be due to the ample presence of unmelted residual crystals that serve as the nuclei for the subsequent crystallization.⁴ Note in Fig. 6.17 that the T_c vs. EDR plot shows a minimum at EDR = 3.2 for both PEEK samples. As can be seen in the figure, the melt crystallization of EDR = 4.0 is faster than that of EDR = 3.0. This minimum behavior has also been observed in the previous study by Lee and Porter.⁴ This can

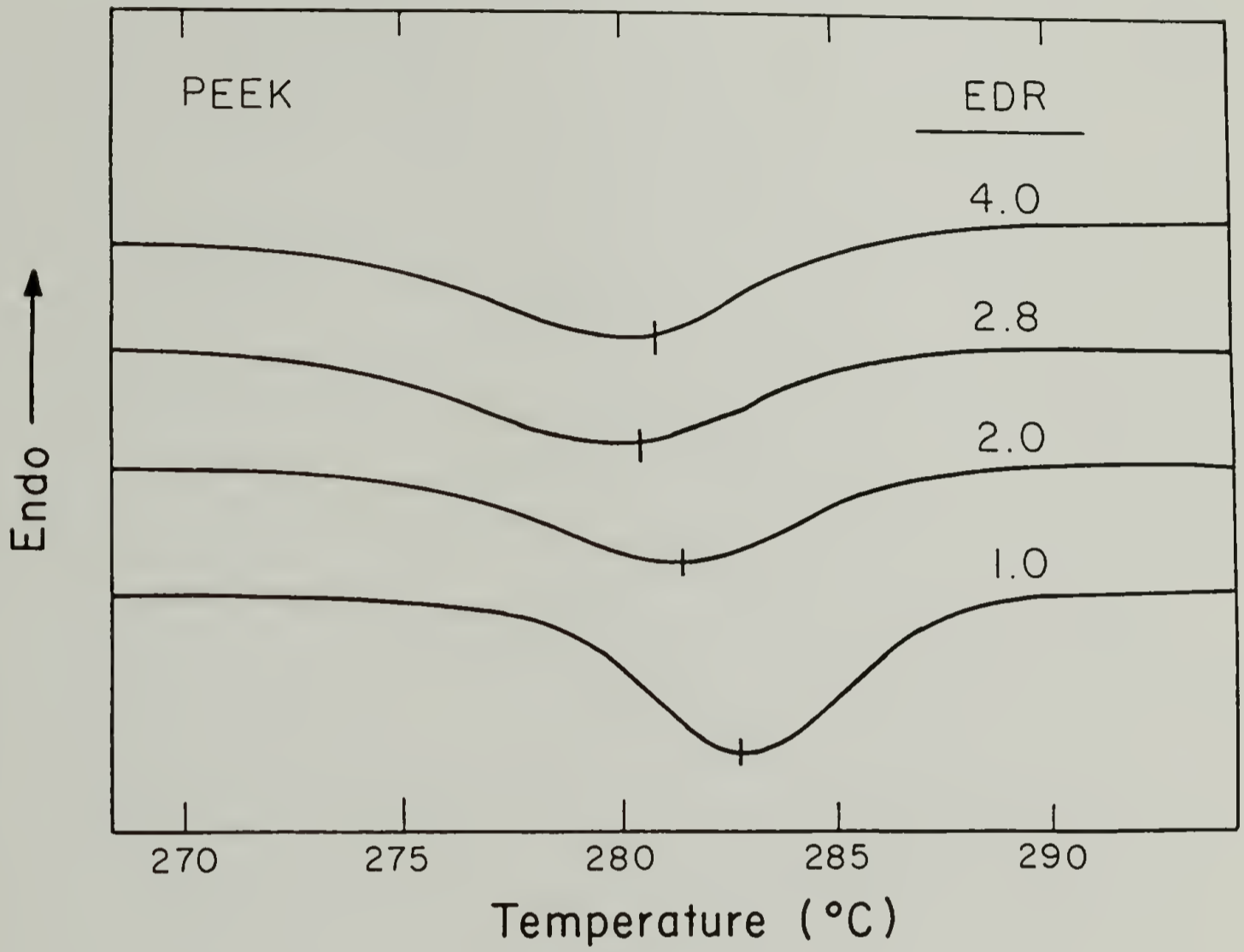


Fig. 6.16 The DSC cooling curves of amorphous drawn PEEK after annealing at 370 °C for 5 mins.

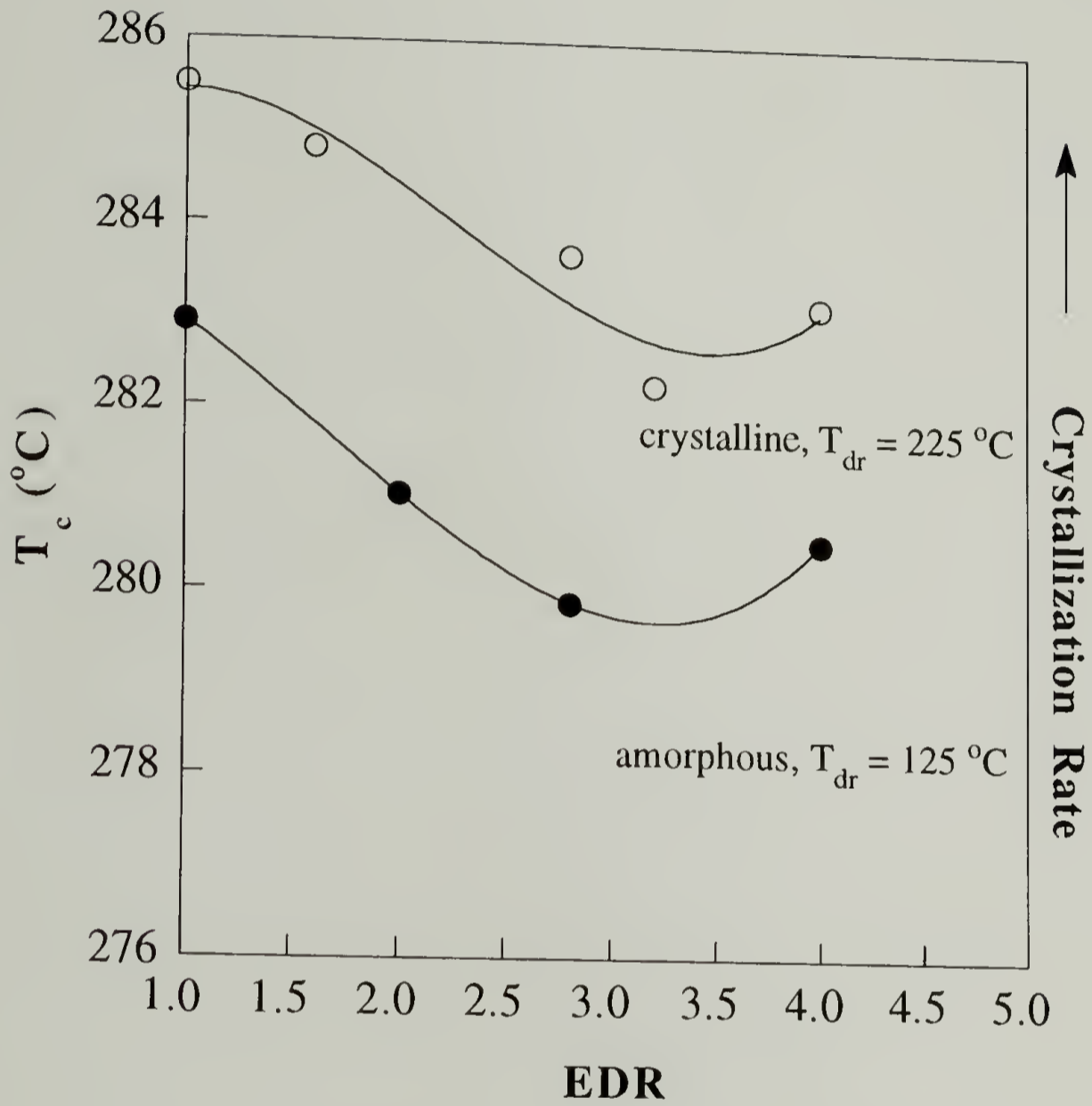


Fig. 6.17 The peak temperature of the crystallization exotherm during cooling vs. EDR of crystalline and amorphous drawn PEEK.

be explained by the strain-induced crystallization shown in 6.3.1. It has been indicated that at $EDR = 4.0$, crystallization of PEEK was induced by drawing. Consequently, some of these strain-induced PEEK crystals may remain unmelted after the melt annealing and serve as the nuclei for subsequent crystallization.

The same melt annealing experiment has also been performed for drawn PEEK/PEI 75/25 blend. Fig. 6.18 displays the DSC cooling scans of this blend. It can be seen that the crystallization exotherm actually moves up to higher temperature with increasing EDR. Fig. 6.19 is the plot of the exothermic peak temperature vs. EDR for the drawn 75/25 blends. Like PEEK, the crystalline drawn blend crystallizes faster than the amorphous drawn blend. However, the melt crystallization rate in the blend is increased by drawing, in opposite to that found for PEEK.

According to the previous study, the reduction in the melt crystallization rate of PEEK by drawing is due to the necessity of molecular relaxation before the occurrence of crystallization.⁴ But this model seems to post a question, "why didn't this occur in the cold crystallization?". To test the previous relaxation model, the melt annealing of amorphous drawn PEEK was carried out for various annealing times. If the annealing time is longer, then PEEK chains should relax more, and hence the subsequent crystallization should be faster according to the proposed model. Fig. 6.20 displays the plot of cooling exothermic peak temperature vs. logarithmic annealing time. It can be seen that the crystallization rate is indeed reduced by increasing the melt annealing time, which is opposite to what should be observed based on the proposed relaxation model. This suggests that the previous relaxation model is insufficient to describe the melt crystallization of drawn PEEK, and the melt crystallization in drawn PEEK is complicated.

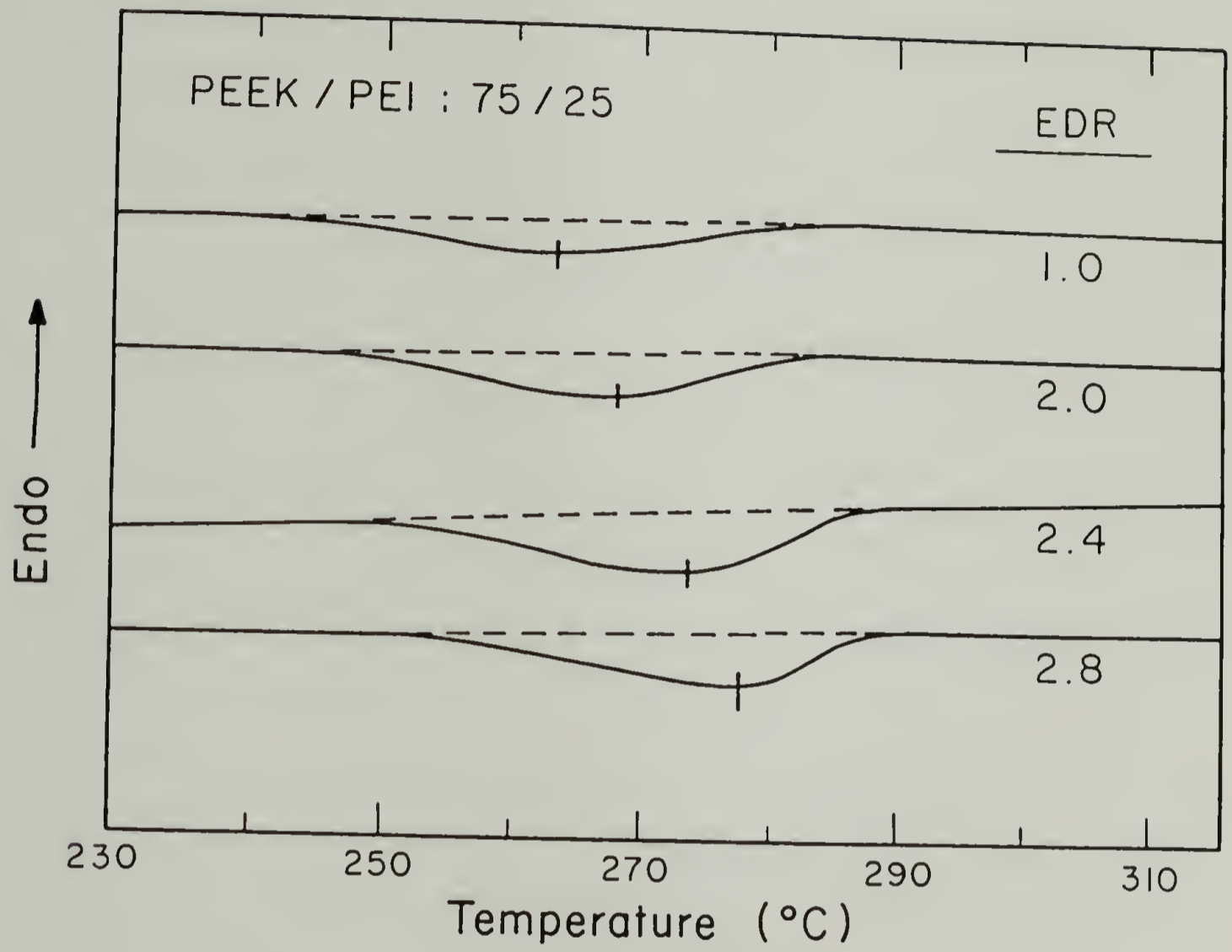


Fig. 6.18 The DSC cooling curves of amorphous drawn PEEK/PEI 75/25 blend after annealing at 370 °C for 5 mins.

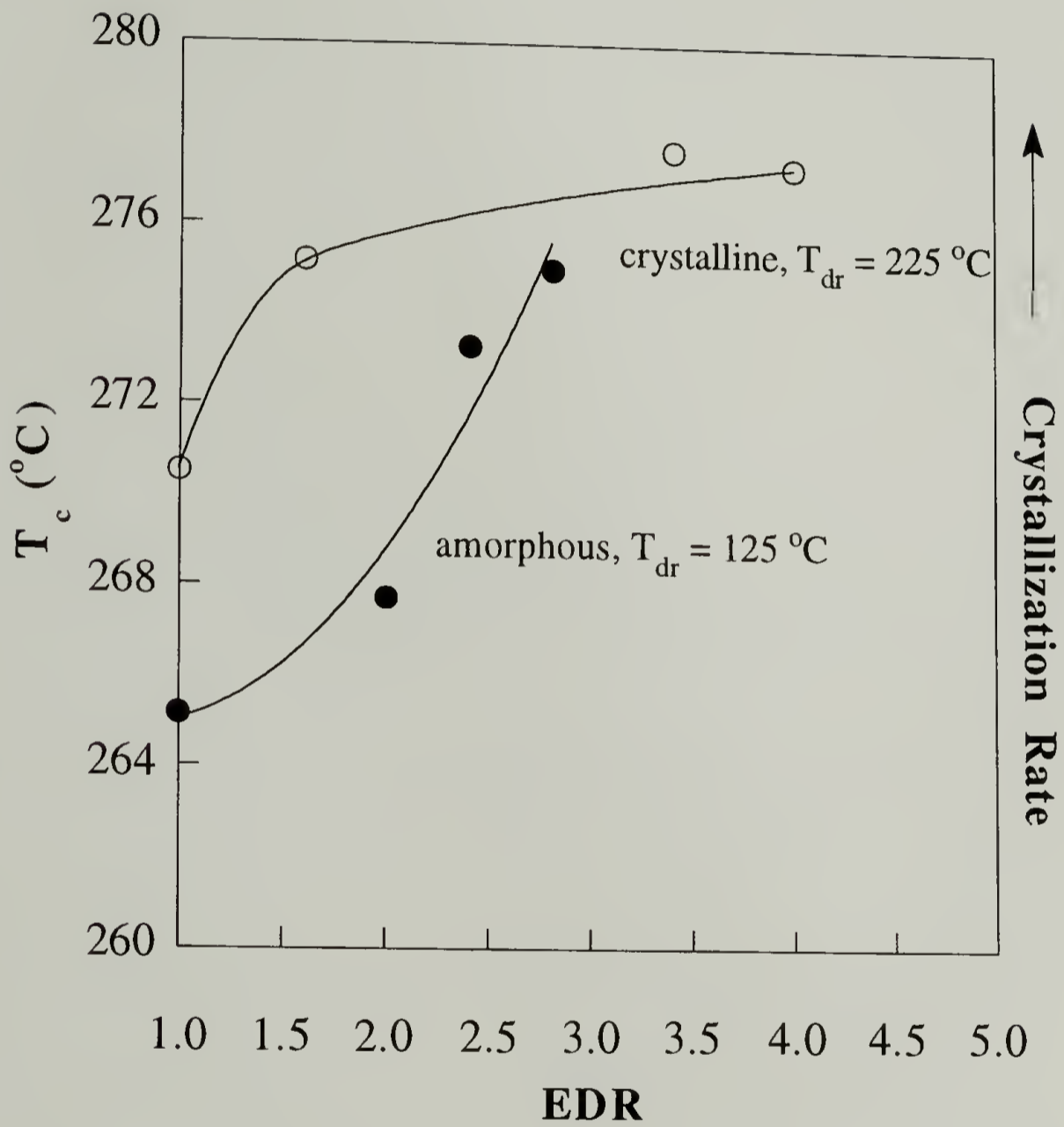


Fig. 6.19 The peak temperature of the crystallization exotherm during cooling vs. EDR of crystalline and amorphous drawn PEEK/PEI 75/25 blend.

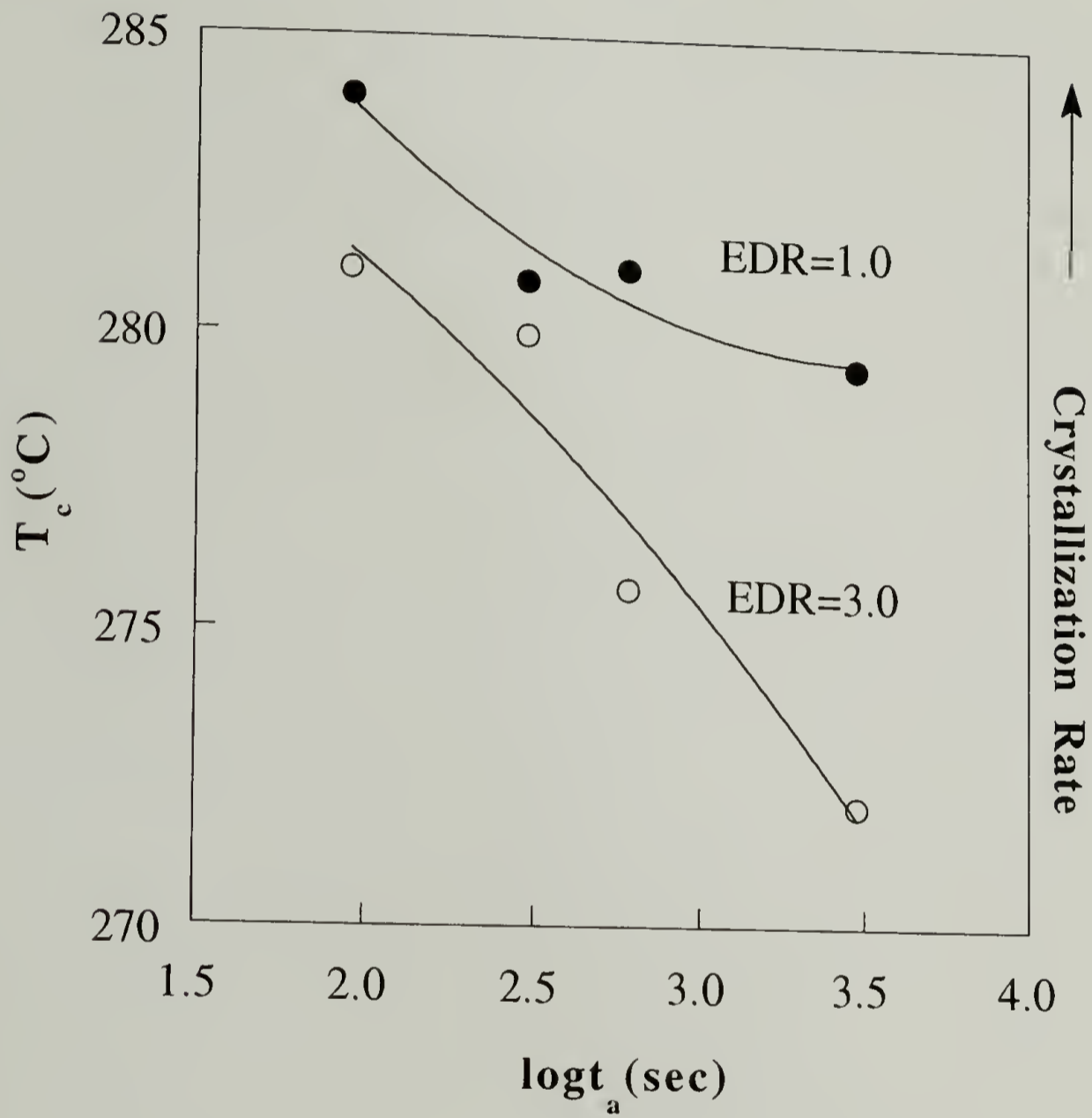


Fig. 6.20 The peak temperature of the crystallization exotherm during cooling vs. annealing time at 370 °C of undrawn and drawn PEEK.

6.3.4 Orientations of PEEK and PEI in Drawn PEEK/PEI Blends

The respective orientations of the polymers in a drawn blend is an interesting subject. Due to the effect of miscibility, the orientation of a polymer at a given draw ratio can be affected by blending.²⁴⁻²⁷ Several studies on the orientations in polymer blends have been reported.²⁴⁻²⁷ It is also of interest to see if the orientations of PEEK and PEI at a given draw ratio are affected by blending. Infrared dichroism can be used for such an investigation.

Fig. 6.21 shows the polarized IR spectra of PEEK drawn from the amorphous state at 125 °C. Fig. 6.22 displays the variations of the measured dichroic ratios with EDR. The dichroic ratio increases with EDR for the bands of $D > 1$, and decreases with increasing EDR for the bands of $D < 1$, indicating an increase in PEEK orientation with draw ratio.

Since the angles between the transition moments and the chain axis have not been determined for the various bands of PEEK and PEI, the absolute orientations of these two polymers cannot be determined at this stage. However, it is still valuable to consider the relative orientations of these two polymers in the blends, and this can be evaluated from the dichroic ratios. To examine the orientation of PEEK in the blends, the overtone band at 2426 cm^{-1} is used, since it overlaps weakly with the bands of PEI as shown in Fig. 6.23. For the orientation of PEI in the blends, the aliphatic C-H stretching at 2965 cm^{-1} overlaps weakly with the bands of PEEK (Fig. 6.24), and hence it can be used for evaluating PEI orientation in the blends. Due to the relatively weak absorptions, the absorbances of these two bands are easily below unity, and hence the Beer's law is applicable.

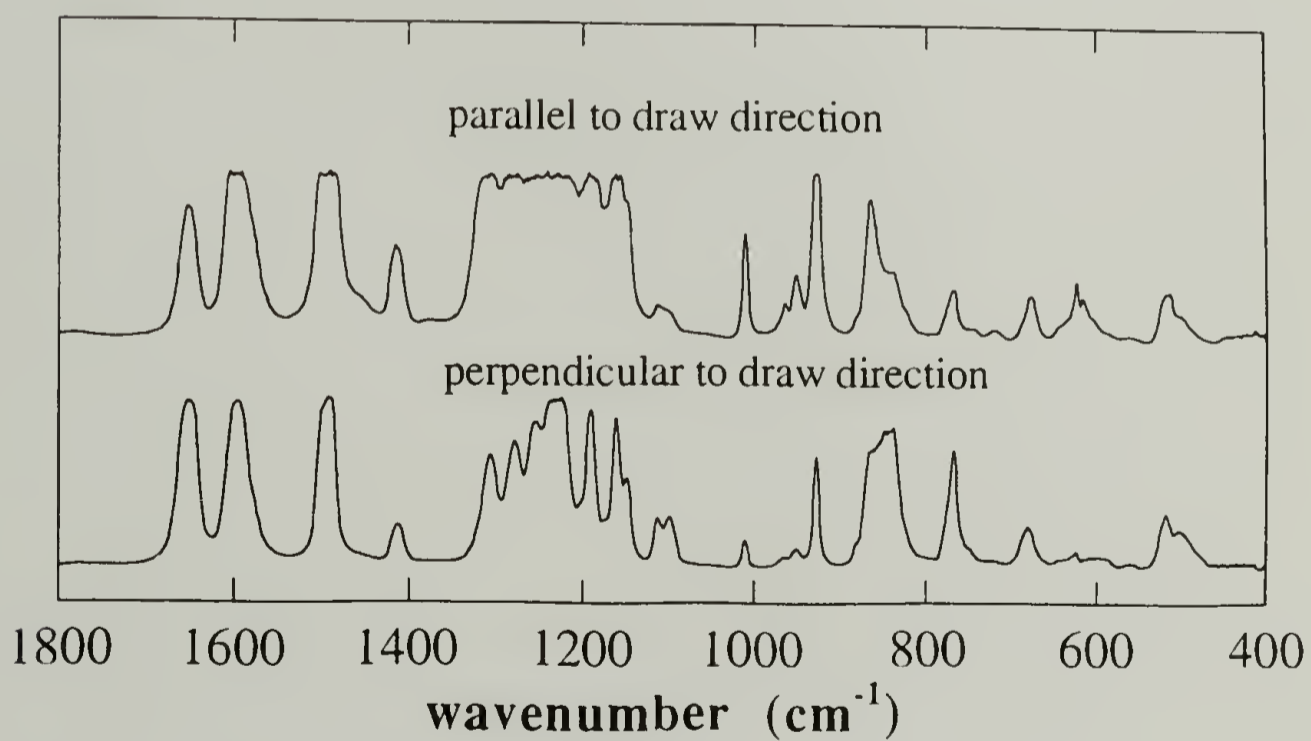
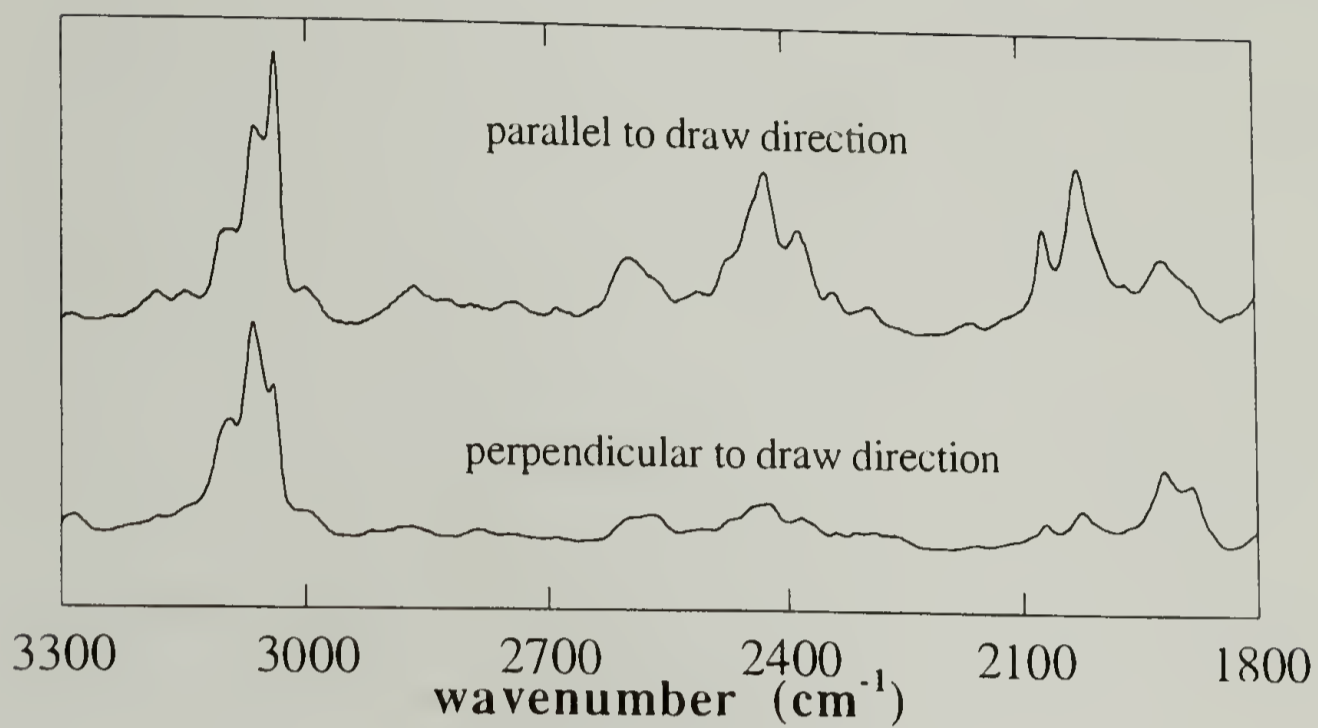


Fig. 6.21 Polarized infrared spectra of PEEK drawn from the amorphous state at 125 °C (EDR = 4.0).

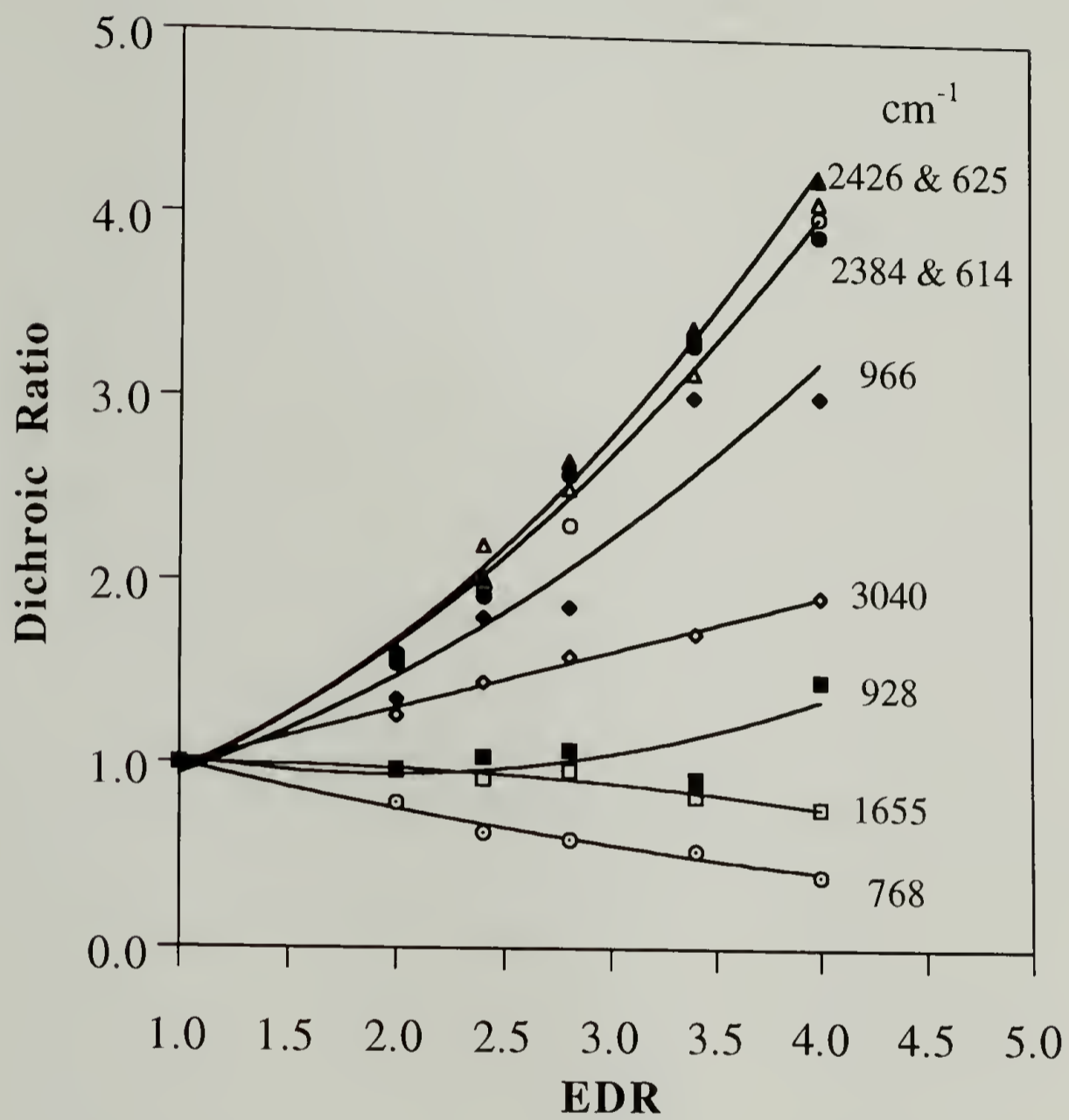


Fig. 6.22 Dichroic ratios of various IR bands of amorphous drawn PEEK vs. EDR.

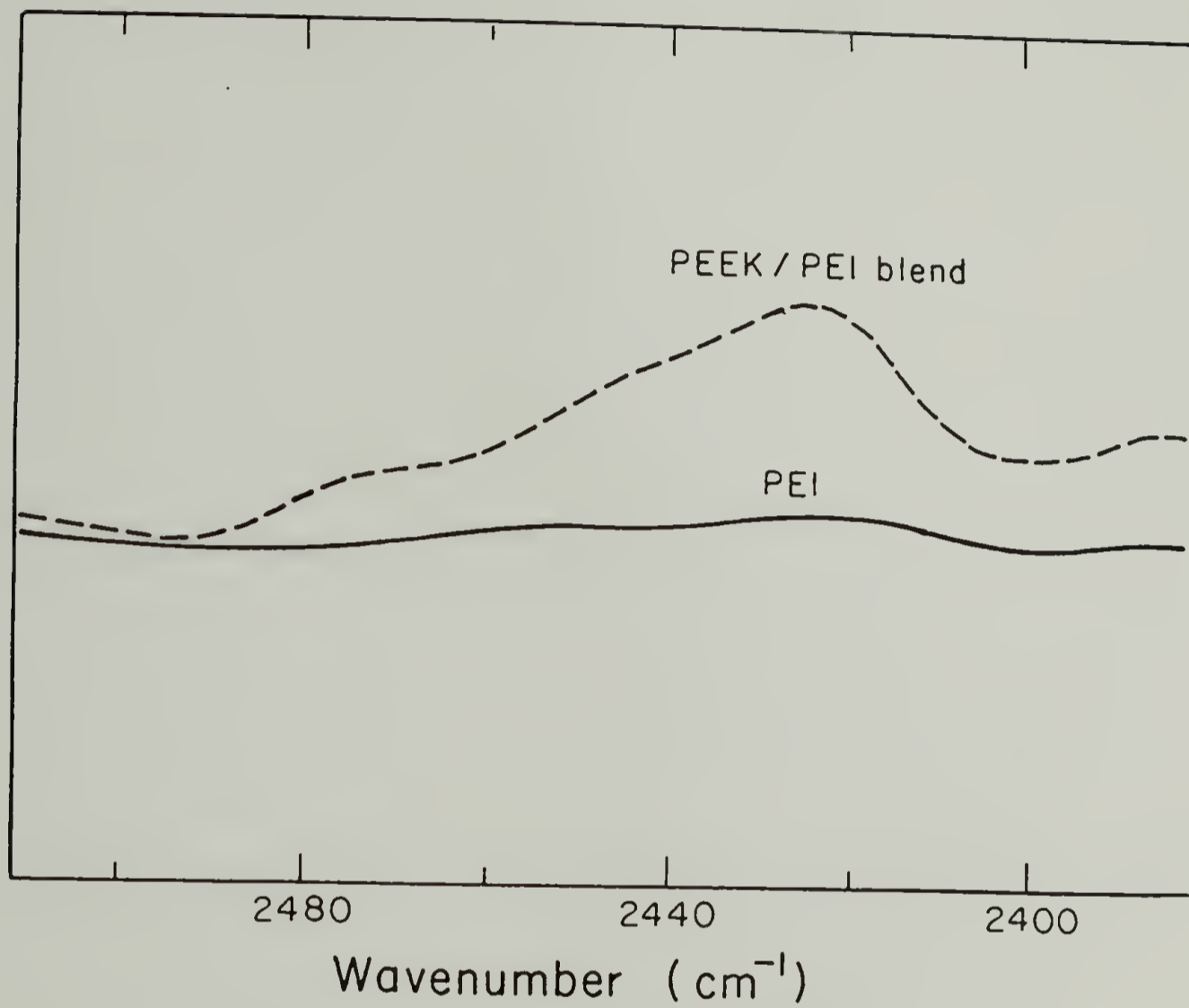


Fig. 6.23 The 2426 cm⁻¹ band of PEEK. It can be seen that this band overlaps weakly with the bands of PEI.

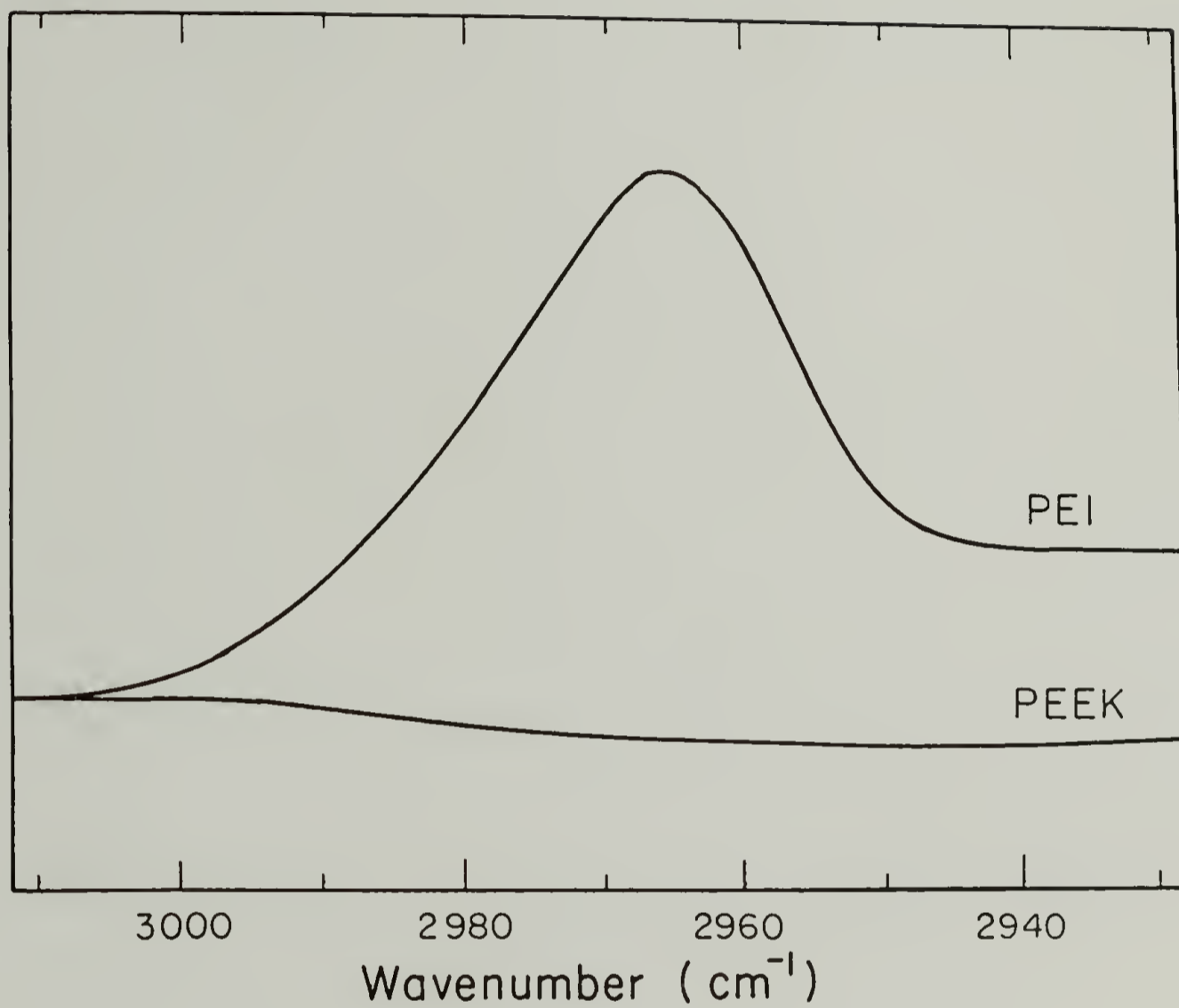


Fig. 6.24 The 2965 cm⁻¹ band of PEI. It can be seen that this band overlaps weakly with the bands of PEEK

Fig. 6.25 displays the composition variations of PEEK and PEI orientations in amorphous drawn blends at a given draw ratio. It can be seen that the orientations of both PEEK and PEI are decreased by increasing the PEI content in the blends. In other words, the orientation of PEEK is decreased by blending with PEI, but that of PEI is increased by blending with PEEK. In PS/PPO blends, it has been found that the orientations of both polymers were also decreased by increasing PPO content in the blends.²⁵

PEEK is a crystallizable polymer, and it has been shown in 6.3.1 that drawing of PEEK tends to pack the PEEK chains to form crystals. On blending with PEI, the miscibility between these two polymers hinders strain induced crystallization of PEEK, since such crystallization can not occur without phase separation between these two polymers. Therefore, it is expected that the conformations of PEEK chains in the drawn blends are not as extended as in the pure state at a given draw ratio. As a consequence, the orientation of PEEK chains is decreased by blending.

6.4 Conclusions

The uniaxial draw of amorphous and crystalline PEEK/PEI blends has been studied. The T_g s of the amorphous drawn PEEK/PEI blends are depressed by draw, whereas the densities of these samples are increased. This demonstrates that a higher density sample can have lower T_g . The density of crystalline PEEK drawn at 125 °C shows a minimum at EDR = 2.0, whereas that of the crystalline blends decrease monotonically with EDR. This is due to the interplay between the destruction of the lower-melting PEEK crystals and the densification in the amorphous regions. The TMA curves for the cold crystallization of drawn PEEK indicates that the

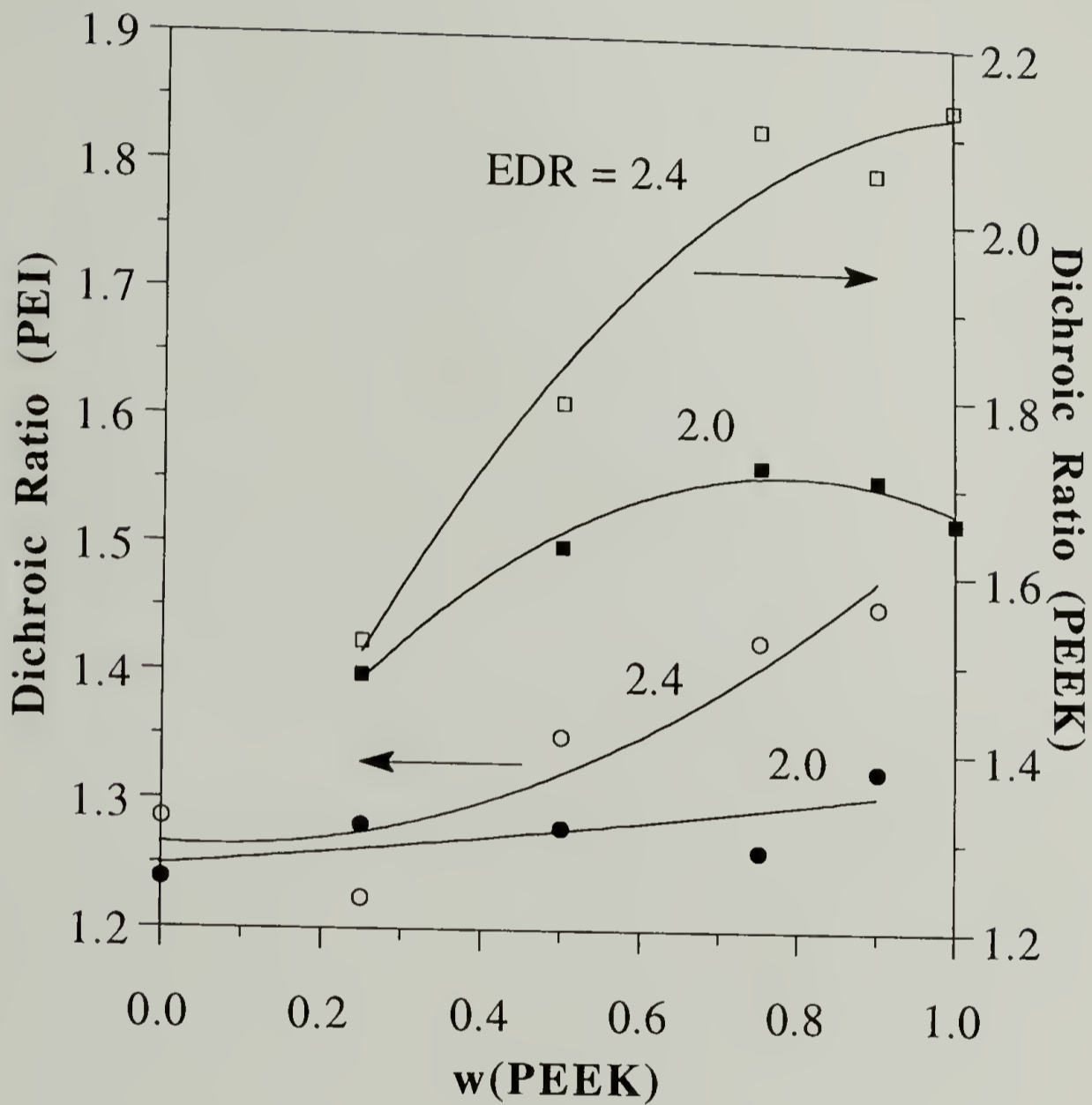


Fig. 6.25 The orientations of PEEK and PEI in amorphous drawn PEEK/PEI blends.

crystallization proceeds prior to chain relaxation. Therefore, the cold crystallization is promoted by drawing. On the other hand, when PEEK is annealed in the melt followed by crystallization, the crystallization is slower in the drawn PEEK. The opposite trend is observed for the blend, where the melt crystallization is faster in the drawn blends. The orientations of PEEK and PEI in the amorphous drawn blends have been studied by infrared dichroism. It is found that the orientations of both PEEK and PEI at a given draw ratio are decreased by decreasing the PEEK content in the blends.

References

1. Vincent, P. I. *Polymer* **1968**, 1, 7.
2. Porter, R. S.; Southern, J. H.; Capiati, N. J.; Kanamoto, T.; Zachariades, A. E. in *Encyclopedia Polym. Sci. Eng.*; John Wiley & Sons: New York **1989**, 15, 346; 2nd Ed.
3. Zachariades, A. E.; Porter, R. S. *The Strength and Stiffness of Polymers*; Marcel Dekker: New York, **1983**.
4. Lee, Y., Ph.D. Thesis, Univ. of Mass., Amherst, Mass., **1988**.
5. Zbinden, R. *Infrared Spectroscopy of High Polymers*; Academic Press: New York, **1964**; Chap. 5.
6. Boyer, R. F. *J. Macromol. Sci. (Phys.)* **1973**, B7(3), 487.
7. Lazurkin, J. S. *J. Polym. Sci.* **1958**, 30, 595.
8. Ferry, J. D.; Stratton, R.A. *Kolloid Z.* **1960**, 171, 107.
9. Robertson, R. E. *J. Appl. Polym. Sci.* **1963**, 7, 443.
10. Newman, S.; Strella, S. *J. Appl. Polym. Sci.* **1965**, 9, 2297.
11. Robertson, R. E. *J. Chem. Phys.* **1966**, 44, 3950.
12. Chow, T. S. *Polym. Eng. Sci.* **1984**, 24, 915.
13. Song, H.-H.; Roe, R.-J. *Macromolecules* **1987**, 20, 2723.
14. Pereira, J. R. C.; Porter, R. S. *J. Polym. Sci. Polym. Phys. Ed.* **1983**, 21, 1147.
15. Chuah, H. H.; DeMicheli, R. E.; Porter, R. S. *J. Polym. Sci. Polym. Lett. Ed.* **1983**, 21, 791.
16. Peterlin, A. *J. Mater. Sci.* **1971**, 6, 490.
17. Rueda, D. R.; Ania, F.; Richardson, A.; Ward, I. M.; Balta-Calleja, F. J. *Polym. Commun.* **1983**, 24, 258.
18. Hay, J. N.; Kemmish, D. J.; Langford, J. I.; Rae, A. I. M. *Polym. Commun.* **1984**, 25, 175.
19. Wunderlich, B. *Macromolecular Physics*; Academic Press: New York, **1977**; Vol. 2.
20. Keller, A.; Machin, M. J. *J. Macromol. Sci. (Phys.)* **1967**, B1, 41.

21. Nobbs, J. H.; Bower, D. I.; Ward, I. M. *Polymer* **1976**, 17, 25.
22. Statton, W. O.; Koenig, J. L.; Hannon, M. J. *J. Appl. Phys.* **1970**, 41, 4290.
23. Gupta, V. B.; Radhakrishnan, J.; Sett, S. K. *Polymer* **1993**, 34, 3814.
24. Lefebvre, D.; Jasse, B.; Monnerie, L. *Polymer* **1981**, 22, 1616.
25. Wang, L. H.; Porter, R. S. *J. Polym. Sci. Polym. Phys. Ed.* **1983**, 21, 1815.
26. Zhao, Y.; Prud'homme, R. E.; Bazuin, C. G. *Macromolecules* **1991**, 24, 1261.
27. Zamel, I. S.; Ronald, C. M. *Polymer* **1992**, 33, 4522.

CHAPTER 7

SUGGESTIONS FOR FUTURE WORK

In this dissertation, both the thermodynamic and the kinetic aspects of PEEK/PEI blends have been studied. Several interesting areas of further research can be derived from this study.

In Chapter 2, the specific interaction between PEEK and PEI has been established by density measurement, DSC, and FTIR. The interaction parameter determined by the equilibrium M.P. depression can only serve as an approximation for the strength of interaction. To obtain the interaction parameter accurately for PEEK/PEI blends, small-angle neutron scattering (SANS) can be performed as deuterated PEEK or PEI is available. The interaction parameter of this binary blend can be obtained by analyzing the scattering intensity using the random phase approximation (RPA). The NMR spectroscopy can also provide useful and more quantitative information on the specific interaction between PEEK and PEI. From the NMR band shift and the areas of the bands, the magnitude of interaction and the concentration of the interacting groups can be elucidated.

In Chapter 2, it was also indicated that the glass transition regions of amorphous PEEK/PEI blends were broader than that of pure PEEK and PEI. This broadening phenomenon may be due to the change in molecular mobility and relaxation spectrum upon blending. Therefore, it will be interesting to investigate the molecular motions and relaxations in PEEK/PEI blends. To our knowledge, there is no reported attempt to correlate the T_g broadening in polymer blends with the relaxation behavior. Useful

techniques for such study include dynamic mechanical analysis, dielectric relaxation spectroscopy, and NMR spectroscopy. The NMR relaxation study may be particularly useful to reveal the local molecular dynamics in the blends.

In Chapter 3, the two-stage crystallization behavior of PEEK was first time revealed clearly by TMA. However, one question remained unanswered is the origin of this two-stage crystallization behavior for PEEK. Similar two-stage behavior has also be suggested for another aromatic polymer, poly(phenylene sulfide) (PPS). Therefore, it will be interesting to see if this two-stage crystallization phenomenon is a unique feature for the aromatic crystalline polymers. TMA will still be a powerful technique for studying the crystallization of these aromatic crystalline polymers such as PEK, PEKK, poly(phenylene oxide), PPS, etc. This study will be useful in unifying the crystallization behavior of the crystalline aromatic polymers and reveals the differences in the crystallization patterns between these polymers and the more studied aliphatic polymers.

In Chapter 5, the hindrance in PEEK crystal reorganization during heating was observed in the blends, and was ascribed to the incorporation of PEI in the interlamellar regions of PEEK crystals. This is a new supposition. Therefore, it will be interesting to study the melting behavior for some model blend systems which are known to have interlamellar segregation morphology unambiguously, to see if the crystal reorganizations are also hindered in these systems. For example, PCL/PVC blends are known to have interlamellar segregation morphology.

Since the morphology is controlled by the diffusion of the two polymers, molecular weight (MW) may play an important role in determining the morphology of the blends. There is no systematic study in the literature for the MW effect on the

morphology of crystalline/amorphous blends. Therefore, if a wide range of molecular weight (from oligomer to very high $M_n > 100,000$) of PEEK or PEI is available, it will be of fundamental interest to investigate the MW dependence of blend morphology by microscopies and small-angle X-ray scattering (SAXS).

In this thesis and other previous studies, PEEK has been drawn in the amorphous and the crystalline states. The maximum reached draw ratio was 4 for the coextruded PEEK films, and this was achieved by two-stage solid-state coextrusion. The low drawability of PEEK compared to other crystalline polymers may be attributed to the morphology inherent in the bulk crystallized PEEK. The limited drawability of a crystalline polymer has been ascribed to the entanglements of chain segments in the crystalline interphase. Therefore, it will be interesting to draw PEEK of different morphologies which may be created by solution crystallization and pressure crystallization, to see if the drawability of PEEK can be improved.

The T_g s of amorphous PEEK/PEI blends were depressed by drawing, whereas the densities were increased by drawing. It has been indicated in Chapter 6 that such conflict with the conventional free volume theory of T_g may be due to the change in segmental packing or free volume distribution upon drawing. Therefore, it will be interesting to investigate the change in segmental packing upon drawing for PEEK/PEI blends by SAXS or intermediate angle X-ray scattering. The change in segmental packing can be deduced by obtaining the radial distribution function using Fourier-Transform of the scattering intensity profile.

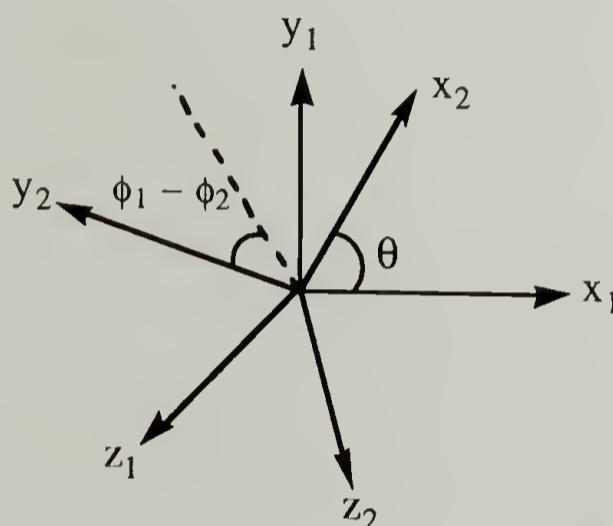
In addition to PEEK, there are other poly(aryl ether ketone)s such as PEK, PEKK, PEEKK, etc. It will be interesting to carry out a systematic study of the blends of the poly(aryl ether ketone) family with PEI. This study can provide the

information such as the effect of chemical structures of the poly(aryl ether ketone)s on the miscibility with PEI. In Chapter 2, it was proposed that the oxygen lone-pair electrons of the ether groups in PEEK interact favorably with the electron-deficient imide rings in PEI. Since each polymer in the poly(aryl ether ketone) family has different number fraction of the ether group in a repeating unit, it will thus be interesting to study the correlation between the ether group concentration and the miscibility with PEI. For example, polyketone (PK) does not contain the ether linkage, it will be interesting to see if PK/PEI blends are still miscible. In addition, it has been observed in Chapter 2 that the IR intensity of the PEI C=O out-of-phase stretching reached the minimum at 70 wt% PEI, perhaps due to that one ether group in PEEK interacted with one imide ring in PEI. It will thus be interesting to see if the minimum of PEI C=O intensity occurs at different compositions for the blends of PEI and other poly(aryl ether ketone)s.

APPENDIX

DERIVATION OF THE PEI C=O STRETCHING INTENSITIES BY VALENCE-OPTICAL THEORY

In Fig.2.15, the two imide rings in a PEI unit can be described by two sets of Cartesian coordinate, i.e., $\mathbf{Q}_1 = (x_1, y_1, z_1)$ for imide ring 1, and $\mathbf{Q}_2 = (x_2, y_2, z_2)$ for imide ring 2. These two sets of coordinate are shown below:



In order to perform the summation of the vectors $\alpha_k \mathbf{h}_k$ in Eq. (2.7), it is necessary to transform the dipole moment vector defined by \mathbf{Q}_2 to \mathbf{Q}_1 , i.e.,

$$\mathbf{h}_2 = h_{2x} \mathbf{x}_2 + h_{2y} \mathbf{y}_2 + h_{2z} \mathbf{z}_2 = h_{2x'} \mathbf{x}_1 + h_{2y'} \mathbf{y}_1 + h_{2z'} \mathbf{z}_1 \quad (\text{A.1})$$

This can be done easily by using the transformation matrix, i.e.,

$$[\mathbf{h}_2'] = [\mathbf{T}][\mathbf{h}_2] \quad (\text{A.2})$$

where $[\mathbf{T}]$ is

$$[\mathbf{T}] = \begin{bmatrix} \cos\theta & -\sin\theta\cos(\phi_1-\phi_2) & \sin\theta\sin(\phi_1-\phi_2) \\ \sin\theta & \cos\theta\cos(\phi_1-\phi_2) & -\cos\theta\sin(\phi_1-\phi_2) \\ 0 & \sin(\phi_1-\phi_2) & \cos(\phi_1-\phi_2) \end{bmatrix} \quad (\text{A.3})$$

From the geometric analysis, it is shown that $\theta \approx 60^\circ$.

Consider the C=O in-phase stretching shown in Fig. 2.12 (a), since the transition dipole moment in each imide ring aligns along the x axis, $\mathbf{h}_1 = \mathbf{x}_1$, and $\mathbf{h}_2 = \mathbf{x}_2$, and $\alpha_1 = \alpha_2 = 1$ (both dipole moments direct to the positive x axis). From Eq. (A.2) and Eq. (2.7), the intensity of this C=O stretching mode is thus derived to be Eq. (2.8).

For the C=O out-of-phase stretching shown in Fig. 2.12 (b), the transition dipole moment in each imide ring aligns along the y axis, i.e., $\mathbf{h}_1 = \mathbf{y}_1$, and $\mathbf{h}_2 = \mathbf{y}_2$, and $\alpha_1 = \alpha_2 = 1$. From Eq. (A.2) and Eq. (2.7), the intensity of this C=O stretching mode is derived to be Eq. (2.9).

BIBLIOGRAPHY

- Akers, P. J.; Allen, G.; Bethell, M. J. *Polymer* **1968**, 9, 575.
- Alfonso, G. C.; Russell, T. P. *Macromolecules* **1986**, 19, 1143.
- Aubin, M.; Prud'homme, R. E. *Macromolecules*, **1990**, 13, 365.
- Avrami, M. *J. Chem. Phys.* **1939**, 7, 1103.
- Bailly, C.; Williams, D. J.; Karasz, F. E.; MacKnight, W. J. *Polymer* **1987**, 28, 1009.
- Barrales-Rienda, J. M.; Pepper, D. C. *J. Polym. Sci., Part B* **1966**, 939.
- Bassett, D. C.; Olley, R. H.; Al Raheil, I. A. M. *Polymer* **1988**, 29, 1745.
- Bishop, M. T.; Karasz, F. E.; Russo, P. S.; Langley, K. H. *Macromolecules* **1985**, 18, 86.
- Blundell, D. J.; D'Mello, J. *Polymer* **1991**, 32, 304.
- Blundell, D. J.; Newton, A. B. *Polymer* **1991**, 32, 308.
- Blundell, D. J.; Osborn, B. N. *Polymer* **1983**, 24, 953.
- Boon, J.; Azcue, J. M. *J. Polym. Sci., Part A* **1968**, 6, 885.
- Boyer, R. F. *J. Macromol. Sci. (Phys.)* **1973**, B7(3), 487.
- Buchdahl, R.; Nielsen, L. E. *J. Polym. Sci., Polym. Phys. Ed.*, **1989**, 27, 2153.
- Calahorra, E.; Cortazar, M.; Guzman, G. M. *Polymer* **1982**, 23, 1322.
- Cebe, P.; Hong, S.-D. *Polymer* **1986**, 27, 1183.
- Cheng, S. Z. D.; Cao, M.-Y.; Wunderlich, B. *Macromolecules* **1986**, 19, 1868.
- Cheng, S. Z. D.; Wu, A. Q.; Wunderlich, B. *Macromolecules* **1987**, 20, 2802.
- Chow, T. S. *Polym. Eng. Sci.* **1984**, 24, 915.
- Chow, T. S. *Macromolecules* **1990**, 23, 333.
- Chuah, H. H.; DeMicheli, R. E.; Porter, R. S. *J. Polym. Sci. Polym. Lett. Ed.* **1983**, 21, 791.
- Crystal, R. G. *J. Polym. Sci. Part A-2* **1970**, 8, 1755.
- Dawson, P. C.; Blundell, D. J. *Polymer* **1980**, 21, 577.

- Day, M.; Deslandes, Y.; Roovers, J.; Suprunchuk, T. *Polymer* **1991**, 32, 1258.
- Defiew, G.; Groeninckx, G.; Reynaers, H. *Polymer* **1989**, 30, 2160.
- Deslandes, Y.; Sabir, F-N; Roovers, J. *Polymer* **1991**, 32, 1267.
- Dine-Hart, R. A.; Wright, W. W. *Makromol. Chem.* **1971**, 143, 189.
- Ferry, J. D.; Stratton, R.A. *Kolloid Z.* **1960**, 171, 107.
- Fox, T. G. *Bull. Am. Phys. Soc.* **1956**, 1, 123.
- Franchina, N. L.; McCarthy, T. J. *Macromolecules* **1991**, 24, 3045.
- Goda, Y.; Higuchi, S.; Tanaka, S.; Kamada, H. *J. Chem. Soc. Jpn. Pure Chem. Sec.* **1971**, 92, 21.
- Gordon, M.; Taylor, J. S. *J. Appl. Chem.* **1952**, 2, 495.
- Gray, A. P.; Casey, K. *J. Polym. Sci. Polym. Lett. Ed.* **1964**, 2, 381.
- Grevecocour, G.; Groeninckx, G. *Macromolecules* **1991**, 24, 1190.
- Gribov, L. A. *Intensity Theory for Infrared Spectra of Polyatomic Molecules*; Academy of Sciences of U.S.S.R. Press: Moscow, **1963**.
- Gupta, V. B.; Radhakrishnan, J.; Sett, S. K. *Polymer* **1993**, 34, 3814.
- Harris, J. E.; Robeson, L. M. *J. Appl. Polym. Sci.* **1989**, 35, 1877.
- Hay, J. N.; Kemmish, D. J. *Polymer Commun.* **1989**, 30, 77.
- Hay, J. N.; Kemmish, D. J.; Langford, J. I.; Rae, A. I. M. *Polym. Commun.* **1984**, 25, 175.
- Hay, J. N.; Langford, J. I.; Lloyd, J. R. *Polymer* **1989**, 30, 489.
- Hedrick, J. C.; Arnold, C. A.; Zumburum, M. A.; Ward, Y. C.; McGrath, J. E. *35th Int. SAMPE Symp.* **1990**, 382.
- Higuchi, S.; Nakamori, K.; Tanaka, S.; Kamada, H. *J. Chem. Soc. Jpn. Pure Chem. Sec.* **1968**, 89, 565.
- Higuchi, S.; Tsuyama, H.; Tanaka, S.; Kamada, H. *Spectrochimica Acta*, **1974**, 30A, 463.
- Hoffman, J. D. *Polymer* **1983**, 24, 3.
- Hoffman, J. D.; Davis, G. T.; Lauritzen, Jr., J. I. In *Treatise on Solid State Chemistry*; Hanny, N. B., Ed.; Plenum Press: New York, **1976**; Chap. 7.
- Hoffman, J. D.; Miller, R. L.; Marand, H.; Roitman, D. B. *Macromolecules* **1992**, 25, 2221.

- Hsiao, B. *J. Polym. Sci., Polym. Phys. Ed.* **1993**, 31, 237.
- Hsiao, B. S.; Sauer, B. B. *J. Polym. Sci. Polym. Phys. Ed.* **1993**, 31, 901.
- Hudson, S. D.; Davis, D. D.; Lovinger, A. J. *Macromolecules* **1992**, 25, 1759.
- Ishida, H.; Wellinghoff, T.; Baer, E.; Koenig, J. L. *Macromolecules* **1980**, 13, 826.
- Jonas, A.; Legras, R.; Issi, J.-P. *Polymer* **1991**, 32, 3364.
- Jones, J. P.; Leach, D. C.; Moore, D. R. *Polymer* **1985**, 26, 1385.
- Karcha, R. J., Ph. D. Thesis, Univ. of Mass., Amherst, Mass., **1990**.
- Keith; H. D.; Padden, F. J. *J. Appl. Phys.* **1964**, 35(4), 1270.
- Keller, A.; Machin, M. J. *J. Macromol. Sci. (Phys.)* **1967**, B1, 41.
- Kumar, S.; Anderson, D. D.; Adams, W. W. *Polymer* **1986**, 27, 329.
- Kumar, S. K.; Yoon, D. Y. *Macromolecules* **1989**, 22, 4098.
- Kumar, S. K.; Yoon, D. Y. *Macromolecules* **1991**, 24, 5414.
- Lazurkin, J. S. *J. Polym. Sci.* **1958**, 30, 595.
- Lee, Y., Ph.D. Thesis, Univ. of Mass., Amherst, Mass., **1988**.
- Lefebvre, D.; Jasse, B.; Monnerie, L. *Polymer* **1981**, 22, 1616.
- Lovinger, A. J.; Davis, D. D. *J. Appl. Phys.* **1985**, 58, 2843.
- Lovinger, A. J.; Hudson, S. D.; Davis, D. D. *Macromolecules* **1992**, 25, 1752.
- Lu, F. J.; Benedetti, E.; Hsu, S. L. *Macromolecules* **1983**, 16, 1525.
- MacKnight, W. J.; Karasz, F. E.; Fried, J. R. in *Polymer Blends*, Vol. 1; Paul, D. R.; Newman, S. Eds.; Academic Press: New York, **1978**; Chap. 5.
- Marand, H.; Prasad, A. *Macromolecules* **1992**, 25, 1731.
- Matsuo, T. *Bull. Chem. Soc. Japan* **1964**, 37, 1844.
- Matsuo, T. *Bull. Chem. Soc. Jpn.* **1965**, 38, 557.
- Mededllin-Rodriguez, F. J.; Philips, P. J. *Polym. Eng. Sci.* **1990**, 30, 860.
- Mittal, M. L., *Polyimides*, Vol.1, Plenum Press: New York , **1984**.
- Morra, B. S., Ph.D. Thesis, Univ. of Mass., Amherst, Mass., **1980**.
- Musto, P.; Karasz, F. E.; MacKnight, W. J. *Macromolecules* **1991**, 24, 4762.
- Newman, S.; Strella, S. *J. Appl. Polym. Sci.* **1965**, 9, 2297.

- Nguyen, H. X.; Ishida, H. *Polymer* **1986**, 27, 1400.
- Nishi, T.; Wang, T. T. *Macromolecules* **1975**, 8, 909.
- Nobbs, J. H.; Bower, D. I.; Ward, I. M. *Polymer* **1976**, 17, 25.
- Olabisi, O.; Robeson, L. M.; Shaw, M. T. *Polymer-Polymer Miscibility*, Academic Press: New York, **1979**.
- Owen, J. in *Comprehensive Polymer Science*; Pergamon: New York, **1989**; Vol. 2.
- Parmer, J. F., Ph. D. Thesis, Univ. of Mass., Amherst, Mass., **1987**.
- Pereira, J. R. C.; Porter, R. S. *J. Polym. Sci. Polym. Phys. Ed.* **1983**, 21, 1147.
- Peterlin, A. *J. Mater. Sci.* **1971**, 6, 490.
- Porter, R. S.; Southern, J. H.; Capiati, N. J.; Kanamoto, T.; Zachariades, A. E. in *Encyclopedia Polym. Sci. Eng.*; John Wiley & Sons: New York **1989**, 15, 346; 2nd Ed.
- Prasad, A.; Marand, H. *Bull. Amer. Phys. Soc.* **1991**, 36(3), 632.
- Price, F. P. *J. Polym. Sci., Part A* **1965**, 3, 3079.
- Rim; P. B.; Runt, J. P. *Macromolecules* **1983**, 16, 762.
- Robertson, R. E. *J. Appl. Polym. Sci.* **1963**, 7, 443.
- Robertson, R. E. *J. Chem. Phys.* **1966**, 44, 3950.
- Rose, J. B. *Am. Chem. Soc., Polym. Prepr.* **1986**, 27(1), 480.
- Rueda, D. R.; Ania, F.; Richardson, A.; Ward, I. M.; Balta-Calleja, F. J. *Polym. Commun.* **1983**, 24, 258.
- Runt, J.; Miley, D. M.; Zhang, X., Gallagher; K. P., MaFeaters; K.; Fishburn, J. *Macromolecules* **1992**, 25, 1929.
- Russell, T. *ACS Polym. Prepr.* **1989**, 30(2), 282.
- Russell, T.; Stein, R. S. *J. Polym. Sci., Polym. Phys. Ed.* **1983**, 21, 999.
- Saito, H.; Okada, T.; Hamane, T.; Inoue, T. *Macromolecules* **1991**, 24, 4446.
- Schultz, A. R. *J. Poly. Sci., Part A-2* **1970**, 8, 883.
- Schultz, J. M. *Polymer Materials Science*, Prentice-Hall: Englewood Cliffs, **1974**, Chap. 9.
- Silverman, B. D. *Macromolecules* **1989**, 22, 3768.
- Song, H.-H.; Roe, R.-J. *Macromolecules* **1987**, 20, 2723.

- Statton, W. O.; Koenig, J. L.; Hannon, M. J. *J. Appl. Phys.* **1970**, 41, 4290.
- Stein, R. S.; Khambatta, F. B.; Warner, F. P.; Russell, T.; Escala, A.; Balizer, E.J. *Polym. Sci. Polym. Symp.* **1978**, 63, 313.
- Sun, J.; Cabasso, I. *Macromolecules* **1991**, 24, 3603.
- Tonelli, A. E. *Macromolecules* **1972**, 5, 558.
- Tonelli, A. E. *Macromolecules* **1973**, 6, 503.
- Tonelli, A. E. *Macromolecules* **1992**, 25, 7199.
- Vincent, P. I. *Polymer* **1968**, 1, 7.
- Wang, L. H.; Porter, R. S. *J. Polym. Sci. Polym. Phys. Ed.* **1983**, 21, 1815.
- Wang, T. T.; Nishi, T. *Macromolecules* **1977**, 10, 421.
- Warner, F. P.; MacKnight, W. J.; Stein, R. S. *J. Polym. Sci., Polym. Phys. Ed.* **1977**, 15, 2113.
- Wenig, W.; Karasz, F. E.; MacKnight, W. J. *J. Appl. Phys.* **1975**, 46(10), 4194.
- Wunderlich, B. *Macromolecular Physics*; Academic Press: New York, **1977**; Vol. 2.
- Wunderlich, B.; Cormier, C. M. *J. Polym. Sci. Polym. Phys. Ed.* **1967**, 5, 987.
- Zachariades, A. E.; Porter, R. S. *The Strength and Stiffness of Polymers*; Marcel Dekker: New York, **1983**.
- Zachman, H. G. *Kolloid Z.* **1969**, 231, 504.
- Zamel, I. S.; Ronald, C. M. *Polymer* **1992**, 33, 4522.
- Zbinden, R. *Infrared Spectroscopy of High Polymers*; Academic Press: New York, **1964**; Chap. 5.
- Zhao, Y.; Prud'homme, R. E.; Bazuin, C. G. *Macromolecules* **1991**, 24, 1261.

